Fakultät für Maschinenwesen
Lehrstuhl für Carbon Composites

Ultrasonic Mixing Head for Resin Transfer Molding: The Interaction between Sonication, Process Characteristics and Resin System Properties

Maximilian Kunibert Schäfer

Vollständiger Abdruck der von der Fakultät für Maschinenwesen der Technischen Universität München zur Erlangung des akademischen Grades eines

Doktor-Ingenieurs

genehmigten Dissertation.

Vorsitzender:

Prof. Dr. rer. nat. Oliver Lieleg

Prüfer der Dissertation:

1. Prof. Dr.-Ing. Klaus Drechsler
2. Prof. Dr. mont. Gerald Pinter

Die Dissertation wurde am 09.01.2018 bei der Technischen Universität München eingereicht und durch die Fakultät für Maschinenwesen am 07.05.2018 angenommen.

Technische Universität München
Fakultät für Maschinenwesen
Lehrstuhl für Carbon Composites
Boltzmannstraße 15
D-85748 Garching bei München

Tel.: +49 (0) 89 / 289 – 15092
Fax.: +49 (0) 89 / 289 – 15097
Email: info@lcc.mw.tum.de
Web: www.lcc.mw.tum.de

Declaration

Ich erkläre hiermit ehrenwörtlich, dass ich die vorliegende Arbeit selbstständig und ohne Benutzung anderer als der angegebenen Hilfsmittel angefertigt habe; die aus fremden Quellen (einschließlich elektronischer Quellen) direkt oder indirekt übernommenen Gedanken sind ausnahmslos als solche kenntlich gemacht.

Die Arbeit wurde in gleicher oder ähnlicher Form noch keiner anderen Prüfungsbehörde vorgelegt.

....

Ort, Datum Unterschrift

Acknowledgement

I would like to express my gratitude to my supervisor Prof. Klaus Drechsler, who enabled me to write my PhD thesis at the Institute for Carbon Composite. Further, I would like to thank him for several hours of discussion and his valuable suggestions. I gratefully acknowledge Prof. Gerald Pinter's time and interest to review my thesis and to be my second advisor.

I express my deepest thanks to my group leader Swen Zaremba, who contributed valuable technical input to my thesis and who also gave me confidence in my own work.

Further, I would like to thank Prof. Pierre Mertiny for being my host during my final elaboration at the University of Alberta in Edmonton, Canada.

My research was made possible by the financial support of the German Federal Ministry for Economic Affairs and Energy (BMWi) (contract numbers: KF2939503SL2, ZF4004304TA5) within a central innovation program for small and medium-sized enterprises.

My experience also originated from my colleagues at the Institute of Carbon Composites. Their technical and personal support within many discussions, conversations and chats challenged my research and added useful ideas. My closest collaborators were Peter Kuhn, Ludwig Eberl, Philipp Kammerhofer, Andreas Mierzwa, Jan Krollmann, Reinhold Meier, Andreas Altmann, David Schultheiß, Daniel Teufl, Luciano Avila Gray and Sebastian Gruber. Thank you for your support.

During my work at the Institute, I supervised several students during their theses. I thank them for their technical support: Mateusz Griner, Julian Hornung, Michael Borgmann, Maximilian Gößl, Thomas Zimmermann, Christian Aigner, Andreas Dietrich, Stefan Ehrenreich, Johanna Wiethaler, Simon Wittman, Christof Rauch and Maximilian Freudenstein.

I also want to thank my colleagues and friends for reviewing my thesis: Elisabeth Ladstätter, Reinhold Meier, Peter Kuhn, Wolfgang Raffelt, Frederik Wilhelms and Sandra Wisgalla.

This thesis wouldn't have been possible without my friends' and family's love and support. Mum, Dad and Christoph, there has never been a day when you didn't believe in me. I am very grateful that I could always count on you. Thank you, Theresa, for supporting me in all aspects of life and for being such a wonderful girlfriend. Thank you, Robert, for sharing the everyday life with me and to always be up for a nice chat. This journey would not have been possible without them and I dedicate this milestone to them.

Abstract

The mixing heads which are currently used to activate resin systems in Resin Transfer Molding (RTM) processes are incapable of ensuring an environmentally friendly and cost-effective production. Low pressure mixing heads are based on friction at shear elements. High pressure mixing heads are based on impingement. Whereas the first requires an expensive, environmentally harmful solvent flushing, the latter requires a high pressure resistance, which is material and cost intensive. The aim of this thesis is to investigate how acoustic cavitation caused by sonication can be utilized to activate resin systems in RTM.

The laboratory investigations show that higher amplitudes come along with a higher expansion of the cavitation zone, a faster increase of the viscosity and a higher glass transition temperature of an epoxy resin system. The results of the laboratory investigation are the foundation of the Ultrasonic Mixing Head design. Altschuller's Theory of Inventive Problem Solving is used to analyze a low pressure Static Mixing Head and to develop the Ultrasonic Mixing Head. The single functions mixing, heating and cleaning of the resin system are cumulatively attributed to the sonication effect. Further, the ultrasonic parameters amplitude and power are utilized for the online quality control of the mixing process.

The process characteristics of the Ultrasonic Mixing Head are screened by a Design of Experiment procedure. Hereby, the amplitude, the volume flow and the injection pressure are identified as the dominating factors of the process. The Resin Transfer Molding characteristic is determined by the production of fiber reinforced plates and of neat resin plates. By processing a slow and a fast curing epoxy resin system, a UMH process window is derived. It is limited by a lower amplitude threshold. If this threshold is undercut, no sufficient mixing occurs. An upper threshold of the power is detected. By exceeding this threshold, a curing of the resin system occurs before the cavity is completely filled. Tensile tests and in plane shear tests of samples produced within these thresholds show a similar mechanical performance to samples produced with a low pressure Static Mixing Head.

The technology transfer of acoustic cavitation to the injection technique is completed by integrating the UMH in a fully automated RTM injection process to build a generic part. For the first time, the use of sonication enables a solvent free production at low injection pressures.

Übersicht

Mischköpfe, welche aktuell zur Verarbeitung von Harzsystemen im Resin Transfer Molding Verfahren (RTM) eingesetzt werden, verfehlen das Ziel einer umweltfreundlichen und kosteneffizienten Fertigung. Niederdruck-Mischköpfe nutzen die Reibung an Scherelementen zur Homogenisierung. In Hochdruck-Mischköpfen werden die Komponenten des Harzsystems unter hohem Druck und hoher Geschwindigkeit im Gegenstromprinzip eingespritzt und homogenisiert. Während bei Ersteren die Reinigung durch eine Lösungsmittelspülung einen hohen Aufwand darstellt, ist bei Letzteren die Umsetzung der notwendigen Druckstabilität der Injektionsanlage Material- und Kostenintensiv. In dieser Arbeit wird untersucht wie akustische Kavitation, hervorgerufen durch Ultraschall, zur Verarbeitung von Harzsystemen im RTM Prozess eingesetzt werden kann.

Die Laboruntersuchungen zeigen, dass höhere Amplituden mit einer größeren Kavitationszone, einem schnelleren Viskositätsanstieg und einer höheren Glasübergangstemperatur eines Epoxidharzsystems einhergehen. Diese Ergebnisse bilden die Grundlage für die Entwicklung eines Ultraschall-Mischkopfs. Altschullers Theorie der Erfinderischen Problemlösung wird zur Analyse des Niederdruck-Mischkopfs und Konzeptionierung des Ultraschall-Mischkopf genutzt. Die Einzelfunktionen, Mischen, Heizen und Reinigen des Harzsystems, werden im Ultraschall-Mischkopf kumulativ der akustischen Kavitation zugewiesen. Zudem sollen die Ultraschall Parameter Amplitude und Leistung zur Online-Qualitätsüberwachung des Mischprozesses herangezogen werden.

Die Prozesscharakteristika des Ultraschall-Mischkopfs werden durch eine nach Design of Experiment aufgestellte Versuchsmatrix untersucht. Hierbei werden die Amplitude, der Volumenfluss und der Injektionsdruck als den Prozess dominierende Parameter identifiziert. Die Resin Transfer Molding Charakteristika werden durch die Herstellung von Reinharzplatten und Faserverbundplatten bestimmt. Die Verarbeitung eines langsam- und eines schnellhärtenden Epoxidharzsystems ermöglicht ein Prozessfenster abzuleiten. Dieses weist einen unteren Grenzwert für die Amplitude auf. Wird dieser Grenzwert unterschritten, ist keine ausreichende Durchmischung gewährleistet. Für die Leistung wird ein oberer Grenzwert detektiert. Wird dieser Grenzwert überschritten, härtet das Harzsystem bevor die Kavität vollständig gefüllt ist. Zug- und Scherproben von Platten die innerhalb dieses Prozessfensters hergestellt wurden, zeigen vergleichbare mechanische Kennwerte zu Proben, die mit einem Niederdruck-Mischkopf hergestellt wurden.

Der Technologietransfer der akustischen Kavitation zur Injektionstechnik wird komplettiert durch die Integration des Ultraschall-Mischkopfs in einen vollautomatisierten RTM Injektionsprozess zur Herstellung eines generischen Bauteils. Hierbei ermöglicht die Ultraschalltechnik erstmals eine lösungsmittelfreie Fertigung eines Faserverbundbauteils im Niederdruck-Injektionsprozess.

Table of Contents

Glossary

Symbol	Unit	Short term
γ_{12}	%	Engineering shear strain
$\dot{\gamma}$	1/s	Shear rate
ε	%	Engineering axial strain
η	Pa s	Dynamic viscosity
η^*	Pa s	Complex viscosity
η'	Pa s	Viscose part of the viscosity
η''	Pa s	Elastic part of the viscosity
$\eta_{initial}$	Pa s	Initial dynamic viscosity
$\eta_{initial\ com}$	Pa s	Initial complex viscosity
ρ	kg/m³	Density
ρ_E	W s/cm³	Energy density
ρ_{fluid}	kg/m³	Fluid density
σ	Pa	Stress
σ_{max}	Pa	Tensile strength
τ	Pa	Shear stress
A	µm	Amplitude
A_{cross}	m²	Cross sectional area
c	m/s	Speed of sound
d	mm	Diameter
E	Pa	Young's modulus
F	N	Axial force

Symbol	Unit	Short term
f	1/s	Frequency
G	Pa	Shear modulus
G^*	Pa	Complex shear modulus
G'	Pa	Storage modulus
G''	Pa	Loss modulus
ΔH_{res}	J/g	Residual enthalpy
K	m²	Permeability
L_0	m	Initial specimen length
L	m	Cavity length
M	Ns	Momentum
m	kg	Mass
p	Pa	Pressure
p_{ac}	Pa	Acoustic pressure
Pw	W	Power
Q	-	Indicator for the variation
$\dot{Q}$	W	Heat flow
r	m	Radius
R^2	-	Fraction of the variation
T	°C	Temperature
T_{curing}	°C	Curing temperature
t	s	Time
t_{exp}	s	Exposure time

Symbol	Unit	Short term
t_{gel}	s	Gel time
$T_{g\ final}$	°C	Final glass transition temperature
$T_{g\ initial}$	°C	Initial glass transition temperature
T_{guide}	°C	Preset temperature
u	m/s	Superficial flow velocity
Va	-	Valve
$V_{chamber}$	m³	Chamber volume
v_{max}	m/s	Maximum fluid element velocity
$\dot{V}$	m³/s	Volume flow
x	m	Displacement
Δx	m	Distance
Z	m	Characteristic linear dimension

List of Abbreviations

Abbreviation	Description
ABB	Abbreviation
AM	Arithmetic mean value
B	Binder
CAD	Computer-aided design
CCF	Central Composite Face Design
CI	Confidence interval
DoE	Design of Experiment
FEM	Finite element method
FRP	Fiber reinforced plate
HS	Hielscher sonotrode
LES	Large eddy simulation
LMV	Large mixing vessel
NN	Not necessary
NRP	Neat resin plate
PTFE	Polytetrafluoroethylene
RTM	Resin Transfer Molding
SD	Standard deviation based on a sample
SMH	Static Mixing Head
SMV	Small mixing vessel
SRIM	Structural Reaction Injection Molding
TRIZ	Theory of inventive problem solving

Abbreviation	Description
TTT	Time temperature transition
UMH	Ultrasonic Mixing Head
UMHS	Ultrasonic mixing head sonotrode
VBA	Visual basic for applications
VC	Volume control system

List of Figures

List of Tables

1 Introduction

1.1 Recent development in the composite industry

Global trends toward CO_2 reduction and resource efficiency have significantly increased the importance of composite materials as lightweight material over the last years [1]. Nowadays, these materials are most important in the aviation, wind power and automotive sector due to their high potential for weight reduction, high specific mechanical properties, fatigue and corrosion resistance [2]. In particular, the vehicle manufacturers are confronted with a proposed CO_2 limit per car passed by the European commission [3]. For this, the environmental footprint of the production process gains more and more attention, besides from the performance of a composite part. Further, the innovations concerning the overall process development are connected to a potential of 40 % cost reduction per part within the next ten years [4].

The Resin Transfer Molding (RTM) process is utilized for the high volume production of composite parts. This injection process is based on the impregnation of dry fibers which are shaped to the final contour inside a rigid mold. Recent process improvements target an efficiency increase of different process steps [5]:

The preforming, describing the stacking and draping of the dry fibers to the final part contour, is currently automated by autonomous cutting and handling systems. These improvements target a faster, more precise handling of the fiber structures, enabling waste and time reduction. [6]

The innovation in the mold design targets various aims: New mold concepts enable the injection and curing of metal composite hybrids, saving an additional joining process step [7]. For a more robust process guidance, features like motion concepts of the mold halves, resin traps and process control sensors are integrated [8].

The improvement of resin systems, which are used as matrix in the composite, is challenging. Apart from its processability, the performance of the resin system embedding the fibers is critical [2]. So called ‘snap cure’ resin systems [9–13] are formulated to shorten cycle times. These resin systems show low viscosities during the injection and a rapid solidification during the cure. To process these resin systems two online mixing techniques are distinguished by their mixing pressure: First, low pressure mixing heads use shear elements to divide and merge the resin components [14, 15]. Song and Han [16] describe an average pressure drop of approximately 15 bar in low pressure mixing heads. The relatively low pressure drop is accompanied by low investment costs. On

the contrary, the mixing chamber has to be flushed with a solvent or has to be replaced after each injection. This leads to high operational costs due to the high waste production. Second, high pressure injection heads, injecting the resin components at a pressure of approximately 120 bar in the mixing head, are utilized [17–19] . Since the equipment has to withstand a high mixing pressure in addition to the injection pressure, high investment costs occur. Chaudhari et al. [20] emphasized a low waste production as their main advantage since a piston movement ensures the cleaning of the mixing chamber. This is known as self cleaning method and leads to comparable low operational costs.

1.2 Recent development in the sonochemical industry

In recent years, the field of green chemistry and engineering has been growing rapidly. This technology focuses on approaches to reduce the energy consumption and waste production of production processes. Nowadays, the usage of ultrasound contributes more and more to this area, opening up the field of sonochemistry [21]. The hereby occurring physical phenomenon of cavitation was first detected at the inspection of damaged pumps and propellers. Acoustic cavitation describes the phenomenon, if it is generated by ultrasonic waves. An explication of its success in green aspects is the similarity between the principles of green chemistry/engineering and the benefits brought by ultrasound in chemistry: Change of reactivity, improvement of yields and selectivity, reduction of reaction time, energy consumption and waste production, use of water as solvent instead of organic solvents [21] and mixing [22]. To sonicate high volumes, the process materials are pumped through sonochemical chambers. This operation is based on the release of a high amount of energy from ultrasonic irradiations, namely sonication. The potential of theses chambers are still limited due to the lack of understanding about their design, operational and performance characteristics [23]. Therefore, chambers at pilot and production scale are currently developed [24].

1.3 Motivation and objectives of the thesis

The composite industry and sonochemical industry have in common that their current optimization of processes targets a reduction of the environmental footprint by reducing energy consumption and waste production.

The motivation of this thesis is to transfer the ultrasound technology to the injection technology for resin systems. For this, the physical phenomenon of acoustic cavitation is created in a mixing head. The scientifical and technological work of this thesis aims at the investigation of the following research questions:

- Effect of acoustic cavitation on a resin system:
  - How does a resin system respond to sonication?
  - How does the acoustic cavitation affect the process capability and material properties of a resin system?
- Technology transfer:
  - How can the ultrasound technique be integrated in a discontinuous process like the RTM injection?
  - What are the dominating process parameters?
  - What is the process capability of ultrasound in RTM injections?

1.4 Thesis outline

The thesis is structured in form and content as follows (see Fig. 1-1):

The current chapter introduces the development in the composite and sonochemical industry. They target more efficient processes by ensuring an environmental friendly production. Thereof, the motivation and objectives of the thesis are derived. In chapter 2 current research subjects regarding the ultrasound and injection technology are introduced. Hereby, the equipment, the handling thereof and its process principles are revealed. Finally, the purpose and principle of the measurement methods utilized in this thesis are outlined. In chapter 3, the laboratory investigations are pointed out. Hereby, resin systems are sonicated and inspected with reference to three aspects: the extent of the cavitation zone within the resin system, the effect on the rheology of the resin system and the effect on the thermal properties of the resin system. In chapter 4, the development of the Ultrasonic Mixing Head (UMH), based on these investigations, is described. For this, the Theory of Inventive Problem Solving (TRIZ) is used. Further, main constructional features of the UMH are discussed. For the investigation of the UMH, the complexity of the process is put forward throughout the next three chapters. In chapter 5, the process characteristics of the UMH are given. For this purpose, the UMH is connected to a metering device. The process parameter and the thermal properties of the sonicated resin system are inspected. In chapter 6, the RTM characteristics of the UMH is revealed. Hereby, the performances of the UMH and a Static Mixing Head (SMH) are compared. Apart from the process parameter, the mechanical properties of neat resin plates and fiber reinforced plates are revealed. Chapter 7 shows the integration of the UMH into a fully automated RTM injection process to manufacture a generic part. In chapter 8, a summary of the previous chapters is given and main findings are highlighted. In chapter 9 an overview of potential future research areas is given.

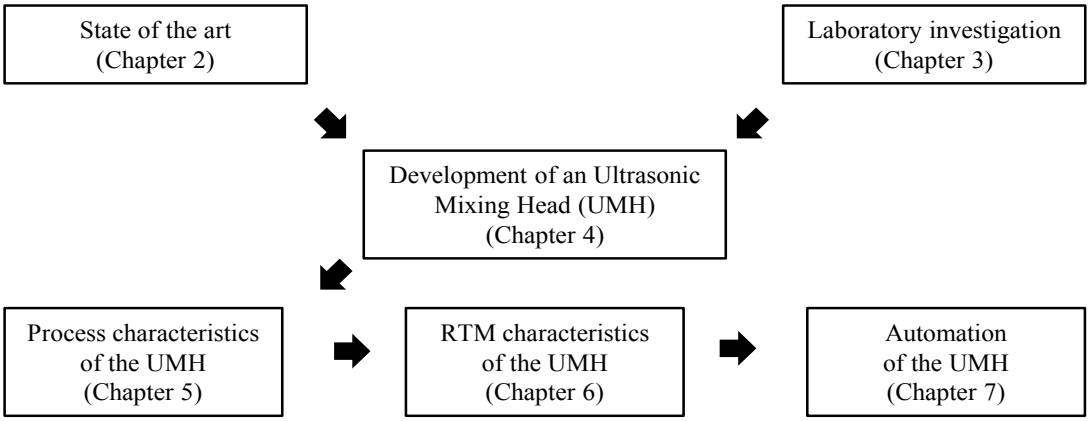

Fig. 1-1 Outline of the thesis

2 State of the art

This chapter gives an overview of the use and research state of injection technologies. To classify this thesis within the research context, the following fields are described:

- Ultrasonic technology (see chapter 2.1): The principles of the cavitation effect and design aspects of the equipment for sonication are given.
- Injection technology (see chapter 2.2): The process materials and the process parameters are introduced. Strategies for RTM injections are revealed.
- Materials specifications (see chapter 2.3): The materials and the equipment utilized in this thesis are set in the context of the state of the art technologies introduced in chapter 2.1 and chapter 2.2.
- Measurement methods (see chapter 2.4): The principles and formulas of the measurement methods are introduced. Further the use of these methods for the resin system characteristics is outlined as found in the literature.

2.1 Ultrasonic technology

The effects investigated and utilized in this thesis are based on the sonication of fluids. For this, the creation of sonication, the occurrence of cavitation and the equipment to sonicate liquids are described.

2.1.1 Creation of sonication

To create ultrasonic oscillation, namely sonication, either mechanical or electrical energy is used as a source. Mechanical systems use the energy within a flowing medium. The Galton whistle uses air that flows through a small circular hole onto a sharp blade. This results in periodic whirls on the surface and they move the air periodically [22]. Most of the electrical sources are either magnetostrictive or piezoelectric transducers. A magnetostrictive transducer utilizes the form changing of ferromagnetic materials when applying a magnetic field. An external magnetic field causes the rotation of magnetic domains, which result in a length change. This phenomenon is called Joule effect [25]. The piezoelectric transducer is based on materials of crystal lattices with electrical loaded modules. This leads to a deformation when an electrical signal is applied. The effect is called inverse piezoelectric [26]. Since the magnetostrictive transducers are limited to frequencies between 70 kHz and 100 kHz mainly piezoelectric transducers are utilized, today. These devices enable an animation in the spectrum from 20 kHz to more than 5 MHz [27]. To transfer the ultrasonic oscillation to the fluid, two options are possible: The ultrasonic oscillating element, called sonotrode, is

either in direct contact to the fluid or stimulates the board of a structure which contains the fluid. The coupling between the sonotrode and the fluid or the sonicated structure is critical, since already small gaps disturb the transfer of the ultrasonic waves [28].

2.1.2 Formation, development and collapse of cavitation bubbles

If sound waves are coupled in a fluid, the acoustic waves flow longitudinally through the medium dependent on pressure and density variations. If an infinitesimal fluid element is considered, the acoustic pressure variation is described by Monnier et al. as follows [29]:

$$p_{ac} = \rho_{fluid}\, c\, v_{max}\, \cos\left[2\pi f\, (t - x/c)\right] \qquad \text{Eq. 2-1}$$

The acoustic pressure in the fluid p_{ac} is hereby dependent on the fluid density ρ_{fluid}, the speed of sound in the fluid c and the maximum velocity of the fluid element v_{max}. The oscillation is described by the cosine term consisting of the frequency f, the time t and displacement of the fluid element x referred to the speed of sound in the fluid. Acoustic cavitation occurs if the pressure forces exceed the inter-particular cohesion forces: a cavitation bubble occurs and the fluid rips off locally. The bubble grows during the rarefaction phases $\cos\left[2\pi f\, (t - x/c)\right] > 0$ and shrinks during the compression phases $\cos\left[2\pi f\, (t - x/c)\right] < 0$.

At acoustic intensities of 1 to 3 W/cm² the bubbles vibrate around an equilibrium called stable cavitation [29, 30]. The effect is used for the degassing in liquids. Hereby, the diffusion of gas occurs solely from the liquid to the bubble since during the rarefaction phase the surface of the bubbles are larger than during the compressed phase. For this, the amount of gas entering the bubbles during rarefaction is higher than the amount of gas leaving the bubbles during its compression. It leads to an accumulation of the entrapped air which supplies the degassing effect [31].

If the acoustic intensity is greater than 10 W/cm² [29, 32] respective 50 W/cm² [30], the bubbles collapse after a few oscillations during a compression phase [29, 30, 33]. The collapses result in locally extreme conditions of temperature (> 2000 K) and pressure (> 500 bar) on a microsecond timescale [34, 35]. If a collapsing bubble is surrounded by fluid, a symmetrical collapse will occur. If a phase boundary is next to the bubble, the collapse will be asymmetrically directed to the boundary layer [28, 36, 37]. Hereby a jet stream (see Fig. 2-1) breaks through the bubble and causes streams in the fluid. The phenomenon of collapsing bubbles is called transient cavitation and is used in applications as ultrasonic cleaning or homogenization processes.

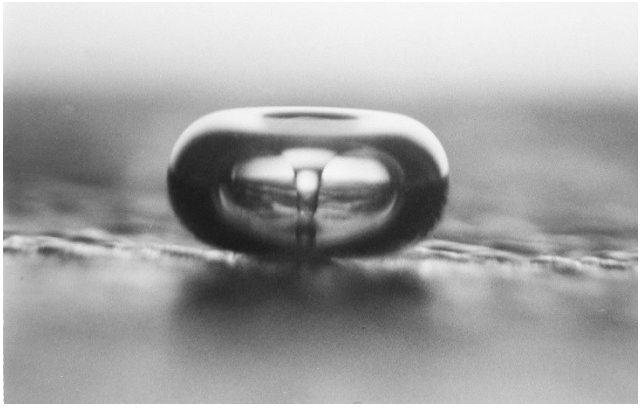

Fig. 2-1 Asymmetric collapse of a cavitation bubble at a boundary layer; occurrence of a jet stream [38]

Apart from the comparatively simple equation by Monnier et al. [29], a variety of mathematical descriptions exist [39–41] which take additional fluid parameters into account. These descriptions can be found even though the mechanisms for bubble growth and collapse in a sonicated fluid are a very complex phenomena and not completely understood today [22]. Considering the content of the cavitation bubbles, three types are distinguished: First, the true cavitation bubbles represent idealized conditions, with no matter inside the bubbles. Second, the vapor cavitation bubbles consist of vaporized fluid and third the gas cavitation bubbles consist of entrapped gas particles [22]. Whereas the true cavitation bubbles are rare in reality [28], the vapor and gas cavitation bubbles, or a mixture thereof [28] exist rather often. They emerge at suspended solids, entrapped air or boundary phases far before the pressure variation mandatory for true cavitation is reached [31]. For most applications of ultrasonic devices transient cavitation is required [29].

Parameters possessing properties that influence the cavitation effect are described in the following: [22, 27, 28]

- Frequency: The effect of this parameter is still an active field of research. The spectrum of frequencies is divided in two sections: Low frequencies ranging from 16 to 100 kHz are mainly used in heterogeneous systems for micromixing and cleaning. The reason is that these frequencies support the occurrence of transient cavitation, which means larger bubbles with higher energy. Higher frequencies support the creation of smaller bubbles with lower energy.
- Fluid pressure: This parameter alters the threshold value for the creation of cavitation bubbles. Provided that the energy in the bubbles is given, higher fluid pressure leads to smaller bubbles. At higher fluid pressure, the vapor pressure of the liquid decreases and the creation of a cavitation bubble is rarer [42]. By further increasing the fluid pressure, the generation of cavitation bubbles can be entirely prevented.

- Fluid viscosity: This parameter determines the degree of damping of the ultrasonic waves spreading through the fluid. Here, it influences the volumetric size of the cavitation zone inside the fluid. It determines, where the conditions to create cavitation bubbles are fulfilled. Generally spoken, higher viscosities correspond with a higher damping of the wave propagation.
- Vapor pressure: This parameter influences the intensity of the transient bubble collapse. High vapor pressure can, similar to a high gas content, cushion the bubble collapse to nearly zero. Vapor can be condensed within the compression cycle and lead to higher cavitation intensities than it would be the case in gas filled bubbles.
- Power: The effect of the power delivered by the ultrasonic device is complex. A higher power value leads to more and larger bubbles. On the one side, the collapse of these large bubbles is more violent compared to smaller bubbles. On the other side, the large bubbles can coalescent and lead to less transient occurrences. The optimum power for each application is often found in experiments.

To classify mixing processes, Baldyga and Bourne [43] define three categories according to the scale of the movement:

- Macromixing describes macroscopic streaming. Hereby, the concentration and velocity differences are in the range of centimeter and larger.
- Mesomixing is in the scale of millimeter and occurs during the homogenization of components in a mixture. Hereby, the fluid elements disperse due to inertial forces until the viscose forces are higher than the inertial forces.
- Micromixing is in the scale of micrometer and smaller. The mixing takes part on a molecular level.

According to these categories, the ultrasonic treatment leads to mixing effects on two scales: First, a fluid streaming on a mesomixing level takes place by the movement of the sonotrode in the sonicated fluid. Second, the collapse of the transient cavitation bubbles entails a streaming on a micromixing level. In the following, the term cavitation is used synonymously to acoustic cavitation, in particular transient cavitation.

2.1.3 Sonochemical effect

In most cases, the effects of ultrasound on chemical reactions are secondary effects caused by cavitation. Hereby, five groups are distinguished [22]:

- Reactions inside the cavitation bubble at high temperatures and high pressures
- Reactions at the gas to liquid interface of the bubbles
- Reactions in the surrounding liquid due to high pressures
- Effects caused by non symmetrical bubble collapses near boundaries
- Enhanced mass and heat transfer due to macro and micro mixing

Various theories are developed to describe the phenomenon of the sonication effect. An extensive description of them is given by Peuker et al. [22]. Here, the focus is laid on the theories most relevant for mixing, tempering and cleaning effects:

Hot spot theory: High temperatures and pressures occur as a result of the collapse of cavitation bubbles. During the experiment with metal carbonyls temperatures of 5000 K in the bubble and 2000 K in the liquid surrounding the bubble are detected by ultraviolet spectroscopy at pressures of $50*10^6$ Pa [44]. High temperature reactions can be initiated in a liquid remaining at ambient temperatures. This is confirmed by the presence of pyrolysis products in the sonicated liquids. These are the homolytic cleavage of water, the cleavage of carbon-halogen bonds or the production of radical products from organic liquids. The heating and cooling rates of about 10^5 K/s are similar to the freezing of molten metal when poured onto a plate with a temperature of -270 °C. [22, 45]

Shock wave theory: The compression of transient cavitation bubbles leads to an increasing bubble wall velocity. Thus, the speed of sound can be reached in the liquid during the collapse. In true cavitation, the bubble vanishes after the collapse, creating a shock wave. Particles are accelerated in the steep pressure gradient and are shock fragmented. High speed particles collide and undergo mechanical damage. [22]

Promotion of electron transfer: Ionic bimolecular nucleophilic substitution reactions are interpreted as a radical mechanism with radical formation by the transfer of a single electron according to $RX + Y^- \rightarrow RX^{\cdot -} + Y$. Ultrasound accelerates such a single-electron transfer reaction. If reactions occur in parallel, the reaction path can be altered. Different products are formed. [22, 46]

Surface cleaning: The jet streams, microstreaming, and shock waves lead to an effective cleaning in the vicinity of solid surfaces [47]. Insoluble layers like inorganic salts, polymers, or liquids can be removed by sonication. In heterogeneous systems, higher reaction rates can be achieved due to the lack of these layers. [22]

Mechanical activation: Transient cavitation is not only able to remove passivating layers on solids, but to break solids like salts and metals. This enables the activation of the solids for chemical reactions. Some examples of the activation are the surface renewal by pitting on solid surfaces [48], the agglomeration of particles coming from a melting during their collision [49], and particle disruption enabling the breakage of solids to the range of micrometer. [22]

2.1.4 Chamber design

For the type and distribution of the cavitation bubbles, the geometry of the mixing chamber and the flow conditions within the fluid are important design parameters [50].

Two types of mixing chambers are differenced (see Fig. 2-2):

- Batch chamber: The entire fluid is sonicated at once. This type is mostly used for cleaning applications and for laboratory applications with small fluid volumes.
- Flow through chamber: The fluid is sonicated while flowing through a mixing chamber. This type is mostly integrated in a closed circulatory system to enable a repetitive sonication of the fluid. Hence, large fluid volumes can be sonicated.

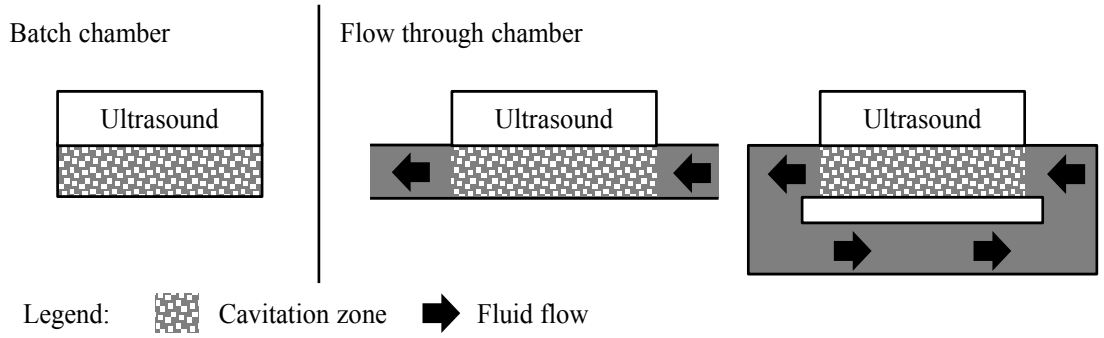

Fig. 2-2 Design of chambers for sonication: Batch chamber (left) and flow through chamber (right)

The flow through chambers are used for fluids requiring a short exposure time in the cavitation zone [28]. Hereby, the focus of the research is in particular the design of the mixing chamber. Pohl. et al [51] investigated the synthesis of nanoparticles by precipitation. Two conical chamber geometries are compared. The results show an improvement of the synthesis in a chamber geometry imitating the mesoscopic shape of the cavitation zone. Hereby, the target is to avoid areas of reflux and without cavitation bubbles. Machunsky and Peuker [52] analyzed the agglomeration of nanoparticles in water. In their investigation cylindrical chamber geometries are examined. The results are similar to the ones of Pohl. et al [51]. They also claim an improvement of the nanoparticle dispersion by avoiding reflux in the chamber.

2.1.5 Sonotrode design

The sonotrode design is, besides the chamber design, the most crucial part for an efficient sonication. This item transfers the high frequency movement generated in the transducer to the fluid. For this, the sonotrode is designed to perform a movement at a natural frequency identical to the transducer frequency (see chapter 2.1.1). Dependent on the purpose, the sonotrode moves in longitudinal, torsional or flexural modes [32].

Four sonotrode designs are distinguished by their influence on the height of the sonotrodes' end-to-end movement. Latter is termed amplitude [27] (see Fig. 2-3):

- Cylindric sonotrodes do not vary the amplitude.
- Linear taper sonotrodes increase the amplitude roughly by the factor of the back plane diameter divided by the front plane diameter.
- Exponential taper sonotrodes increase the amplitude highest by a small tip diameter of a few millimeter.
- Stepped sonotrodes enable an amplification of the amplitude within the range of linear and exponential taper sonotrodes.

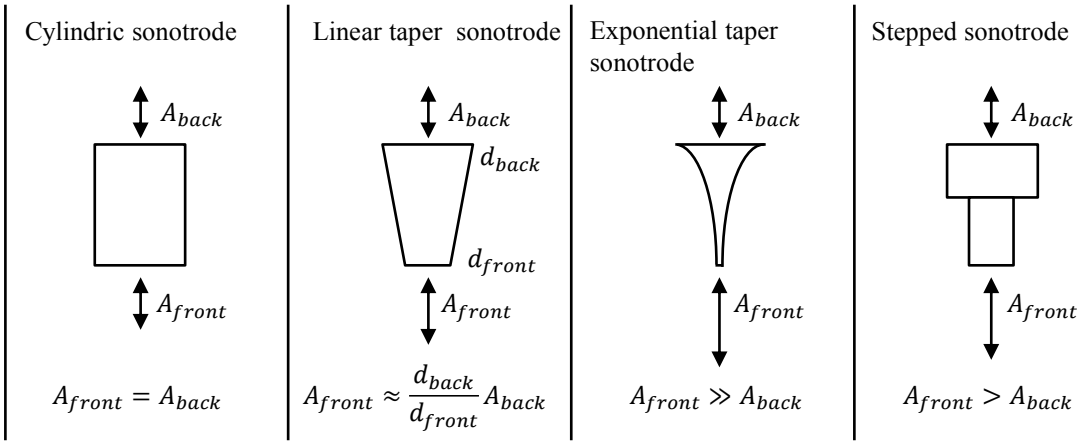

Fig. 2-3 Sonotrode designs and their influence on the amplitude

A range of amplitudes can be produced with a sonotrode by adjusting the power supply of the transducer. If this range is not sufficient, a so called booster can be utilized. The booster is shaped similar to a linear taper sonotrode or a stepped sonotrode and is mounted between transducer and sonotrode. The amplitude increase or reduction caused by the booster is multiplied with the amplitude of the sonotrode. For the integration of the sonotrode in a rig or a chamber, its nodal point is used. This point occurs in between the maximum amplitudes at the end planes. Flanges can be added to enforce the nodal point to a predefined location. The measurement of the amplitudes can be done by a Laser Doppler Vibrometer [53, 54]. Hereby, a laser is focused on the sonotrode. Due to the Doppler Effect, the movement of the sonotrode changes the frequency of the laser beam response. The deviation of the frequency is traced back to the amplitude of the sonotrode.

2.1.6 Frequencies for fluid sonication

In the last decades, researchers started to work across a series of different ultrasonic frequencies in the range of 20 kHz to 1 MHz. The importance of the frequency for both physical and chemical effects was realized. Mason et al. [55] summarized that the mechanical effect decreases and the chemical effect increases with increasing frequen-

cies for aqueous systems. Peuker et al. [22] investigated the occurrence of transient and stable cavitation dependent on the frequency. Hereby, a lower frequency leads to larger bubbles with higher energy content whereas a higher frequency leads to smaller bubbles with less energy. The power describes the electrical effort of the ultrasonic device to move the sonotrode at a selected amplitude and its natural frequency. Mostly the power is given in reference to the area of the sonotrode front end plane. Today, the so called low power ultrasound is usually applied in frequencies above 100 kHz with a power intensity ranging from 0.1 – 0.5 W/cm². This is used in non-destructive testing and medical diagnostic applications. The high power ultrasound describes sonication at a frequency range of 20 kHz to 100 kHz, and power intensity higher than 10 W/cm² [29, 32]. The ultrasonic equipment for mixing applications is mostly designed for sonication at a frequency of 20 kHz. At this frequency, the occurrence of transient cavitation is promoted even though transient and stable cavitation occurs in parallel at low and high frequencies [33].

2.2 Injection technology

The following chapter focuses on the injection technology in particular the Resin Transfer Molding (RTM) technology, to gain an overview of the reinforcement and matrix materials as well as their processing. The process parameters are defined and their influence on the process conditions and part quality is discussed. Further, the strategies of and differences between techniques to process resin systems for Resin Transfer Molding are pointed out.

2.2.1 Reinforcement materials for Resin Transfer Molding

A composite material consists of a minimum of two main components: the reinforcement structure and the matrix system. Mainly glass, carbon and aramid fibers are utilized as reinforcement. Glass fibers are most common due to their desirable price to performance ratio [17]. The use of carbon fibers is less spread due to higher costs. They have a high tensile strength and comparable low density. Therefore, they are used for structural aerospace composites [56]. Aramid fibers offer a high toughness compared to glass or carbon fibers. They are used for applications like protective jackets, where high energy absorption rates are required. All these fibers are processed in different forms: chopped fibers, continuous rovings or various fabrics. RTM procedures are characterized by two main steps: First these fibers are stacked and draped in a near end part geometry by various preforming technologies. Second, the matrix system is added. Details on preforming technologies are given in the literature [56–58].

2.2.2 Matrix materials for Resin Transfer Molding

In general different materials are utilized for the matrix system: polymer, carbon, ceramic or metal [59]. In RTM processes mainly polymers, in particular thermoset resin systems, are used. However, at the moment the market of composites with thermoplastic matrix systems shows a higher grow rate [59]. A thermoset resin system consists of two main components: resin and hardener. The components are metered, mixed and injected as fluids. An exothermal reaction starts during the mixing. This leads to a three dimensional, interlocked network. Occasionally further components, so called additives are added to the resin system. They either support the processing (e.g. lower demolding forces or reaction acceleration) or they support the performance (e.g. for flame protection or higher impact resistance).

Epoxy resin systems are utilized within the group of thermosets, due to their comparably high mechanical performance. These resin systems are identified by their epoxy group. For curing, a homopolymerisation initiated by a catalytic curing agent or a polyaddition/copolymerization reaction with a multifunctional curing agent is executed [60]. The choice of hardener is dependent on the target properties of the cured resin system [60, 61]. The hardeners are commonly based on primary, secondary and tertiary amines. One, two or three hydrogen (H) atoms are replaced by an alkyl group respectively. Since the resin systems investigated in this thesis are epoxy resins with amine based hardener, the interlocking with a primary amine is described in the following (see Fig. 2-4).

Fig. 2-4 Structural formula of the epoxy group (left) and primary amine hardener (right)

Fig. 2-5 indicates the reaction of a diepoxid and a diamine. Hereby each amine active hydrogen connects with an epoxy group. These molecules interlock and build the final structure.

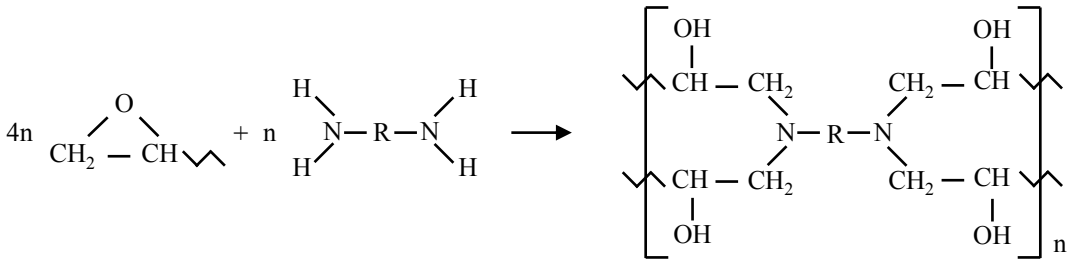

Fig. 2-5 Growth of a polymer chain at the reaction of a diepoxy and a diamine

If the alkoxide ion (RO-) is stabilized by adding an accessory agent the reaction will be accelerated. For this, hydroxyl groups are used. They either develop during curing or

as additional component. The more acid the group has, the more effective. At the beginning of the reaction, resin and hardener reactive groups interlock. During cure, larger molecules are formed. However the average molecular size is still small when half of the reactive groups are interlocked. The molecular size increases as cure progresses and some highly branched molecules are formed. A highly branched structure is developed. Gelation occurs when the branched structures extends throughout the whole sample. The gel point describes the existence of both a fluid and gel fraction in the sample. To produce a structural material, the curing is continued until most of the resin system is connected to a three dimensional network. [60]

Because of its transition from a fluid to a solid, the curing process has a major influence on the properties of the polymer. An important parameter of the cured polymer is the glass transition temperature T_g. It describes the range where the cured polymer changes from a solid state into a viscous or rubbery state. Gillham [62] introduced the Time Temperature Transition (TTT) diagram in 1986. A simplified version thereof is pictured in Fig. 2-6. If the curing temperature is below the zero glass transition temperature T_{g0}, the reaction will be inhibited. If the curing temperature T_{cure} is higher, a vitrification will occur before gelation. Generally spoken, higher curing temperatures correlate with a higher glass transition temperature due to a higher crosslinking of the network. At lower curing temperatures ($T_{curing} < T_g$), the curing reaction is controlled by diffusion and becomes slower until it stops. At higher curing temperatures ($T_{curing} > T_g$), the rate of reaction is chemically and kinetically controlled. For this, resin systems which are processed at lower temperatures are often post-cured at elevated temperatures [60]. Target is, that the final glass transition temperature $T_{g\,final}$ of the resin system reaches its maximum glass transition temperature $T_{g\,max}$. A further increase of the curing temperature leads to a thermal degradation, which in turn leads to a reduction of the resin system performance. [62]

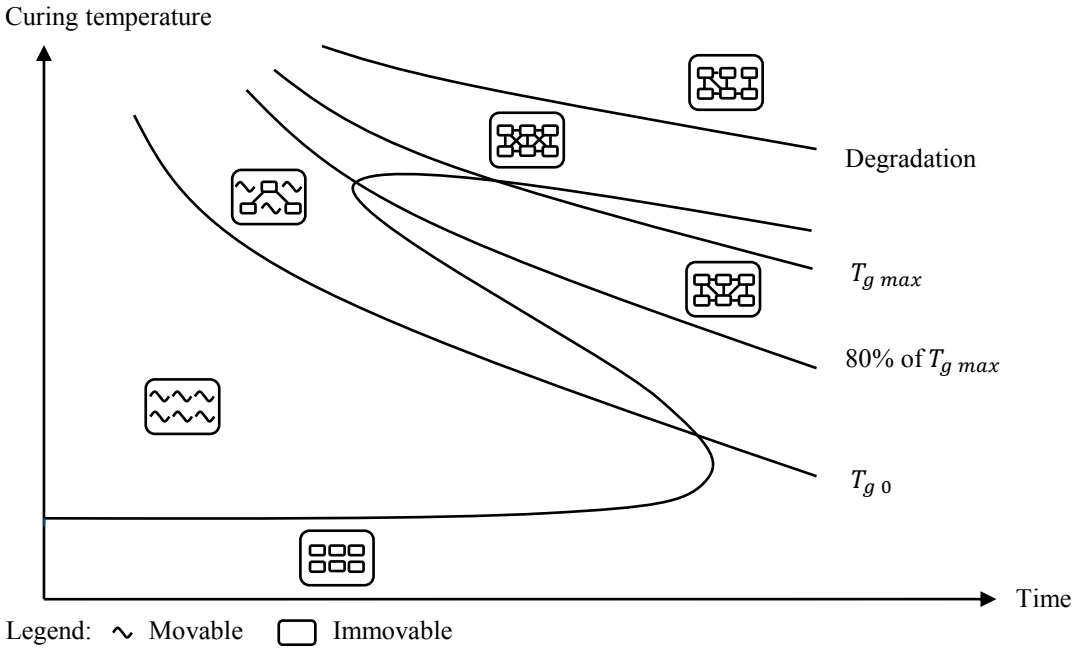

Fig. 2-6 Simplified Time Temperature Transition diagram (TTT) (similar to [62])

In general both the mixing and the tempering during the processing of a resin system determines its property homogeneity and network density.

2.2.3 Resin system flow through a preform

The flow of the resin system during the impregnation of the dry preform is described by Darcy's law. He claims a direct proportional correlation between the volume flow $\dot{V}$ and the occurring pressure gradient dp/dx [63]. The constant of proportionality is the quotient of the preform permeability K and the dynamic fluid viscosity η. The superficial flow velocity u results from the volume flow $\dot{V}$ and the drained area A_{cross}. Eq. 2-2 shows Darcy's law for the one dimensional flow in x-direction:

$$u = \frac{\dot{V}}{A_{cross}} = -\frac{K_x}{\eta}\frac{dp}{dx} \qquad \text{Eq. 2-2}$$

Darcy's law is derived from the Navier-Stokes equation for fluid mechanics. The mathematical operations are outlined in the literature [64–66]. Fig. 2-7 shows the parameters of the equation in the context of the injection setup:

- Volume flow $\dot{V}$ is the amount of resin system continuously metered by the metering device (see chapter 2.3.2).
- Area A_{cross} is the cross sectional area of the mold
- Permeability K_x in x-direction represents the resistance of the preform against the impregnation in x-direction.

- Dynamic viscosity η describes the liquidity of the resin system (see chapter 2.4.1).
- Pressure gradient dp/dx describes the gradient between the pressures in the fluid before it enters the preform and the pressure at the flow front position. At saturated flow conditions, the flow front position is equal to the outlet.

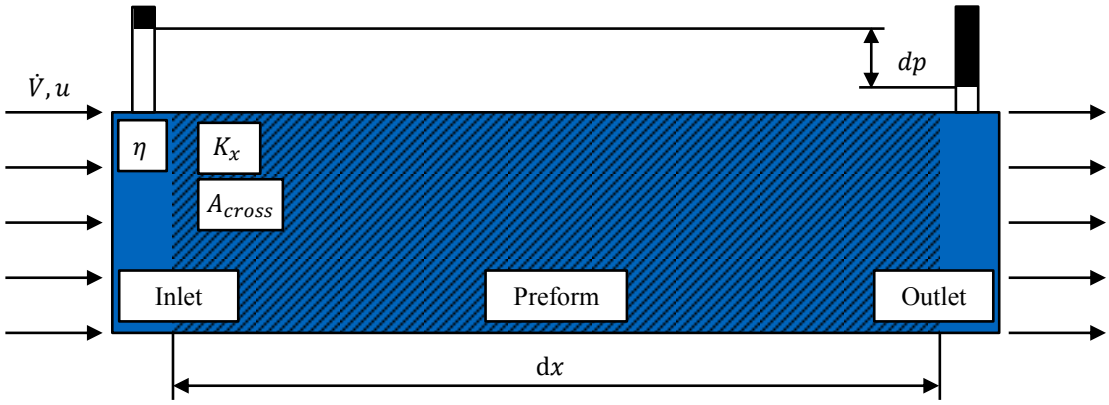

Fig. 2-7 One dimensional flow of a fluid through a preform at a saturated state

Even though Darcy's law is extensively used for calculations of the injection process parameters, it has to be taken into account that a number of assumptions are estimated. Some of these are critical for its practical application [66]:

- Newtonian fluid: the viscosity of some resin systems shows a dependency on the shear rate and viscoelastic behavior [66].
- Chemical inert fluid: after the mixing of the resin system, reactive partners within the resin system interlock (see chapter 2.2.2).
- Homogeneous porous, inelastic medium: The porosity of the preform is inhomogeneous as it consists of stacked layers. Further, the compaction changes throughout the injection due to the lubrication of the fibers [67, 68].
- Saturated flow conditions: A saturated flow is reached when a porous medium is fully impregnated and a continuous fluid occurs. Most processes are stopped directly after the preform is fully impregnated. Walther et al. [69] identified unsaturated and saturated flow conditions during the impregnation.

2.2.4 Resin Transfer Molding variants

Liquid composite molding (LCM) processes define the manufacturing of composite parts by impregnating a dry reinforcement with a liquid resin system. The dry preform is draped to the final part contour before injection. Parts produced with these processes commonly achieve a fiber volume fraction (FVF) of 50 to 60 %. The Resin Transfer Molding (RTM) describes a subgroup of LCM. This is characterized by the use of two

rigid mold halves. Its main advantages are the good surface quality and the small dimensional tolerances. [70]

The RTM cycle is outlined in Fig. 2-8. At first, the preform is inserted in the rigid mold. Then, the mold is closed. The height of the cavity and the architecture of the preform define the FVF of the final part. A resin system consisting of either single or multi components is injected in the cavity. Various strategies for the resin system processing are revealed in chapter 2.2.5. After the cavity is filled, the resin system is cured: either isothermal or at elevated temperatures. After curing, the part is demolded and the mold is prepared for the insertion of the next preform.

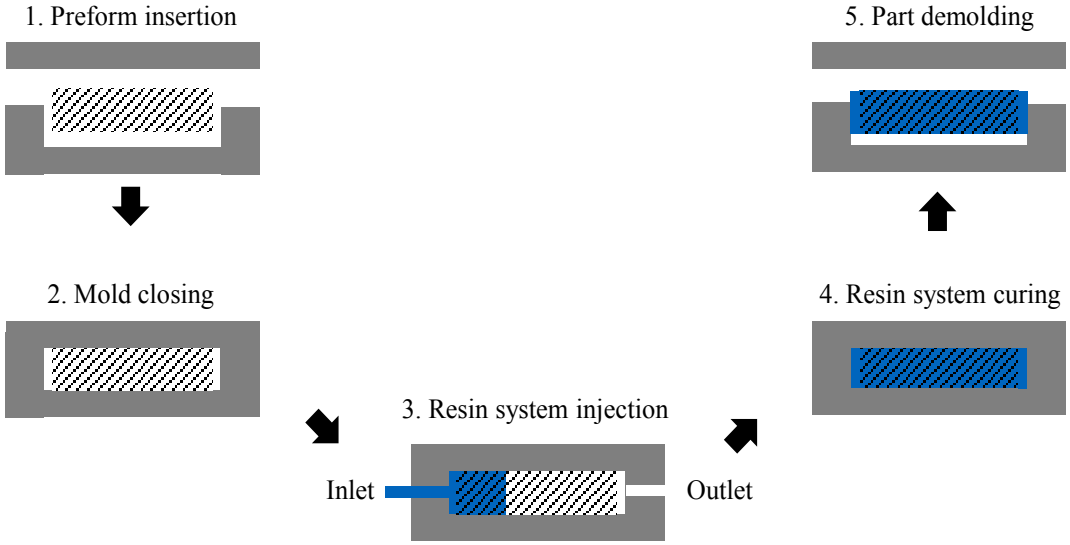

Fig. 2-8 Principle of the Resin Transfer Molding (RTM) cycle

The number and size of air inclusions, namely porosity, should be minimized to increase the final part quality. For this, two additional steps can be applied. They vary the pressure conditions in the cavity [71–73]: First, vacuum is applied after closing the mold and/or during the injection at the cavity outlet. This process is called Vacuum assisted Resin Transfer Molding (VaRTM). Second, after the filling of the cavity, the injection pressure is raised. This is called a post-pressure step.

To shorten the injection time two strategies are distinguished to raise the permeability of the preform and therefore lower its resistance during the impregnation [70, 74]: Gap impregnation RTM denotes a unilateral closing of the mold during injection. Compression RTM describes an injection of the complete amount of resin system before the mold is closed entirely. Thus, the resin system is dispersed at high permeable conditions and the final impregnating takes predominantly place in the thickness direction of the part [17].

2.2.5 Resin system processing for Resin Transfer Molding

For the processing of the matrix materials (see chapter 2.2.2) in RTM, different equipment is utilized. They provide the resin systems in certain conditions with reference to the application. In the following the layouts of the most common devices are explained: the pressure pot, the low and the high pressure mixing devices.

2.2.5.1 Pressure pot

The pressure pot (see Fig. 2-9) is the simplest method for processing single component resin systems. In these systems, the components are already premixed in a batch chamber. The resin system is filled in the pressure pot. Mostly electrical heating devices are integrated to heat the resin system. The resin system can also be degassed before the injection by vacuum application. For the injection, excess air pressure is applied to the pot.

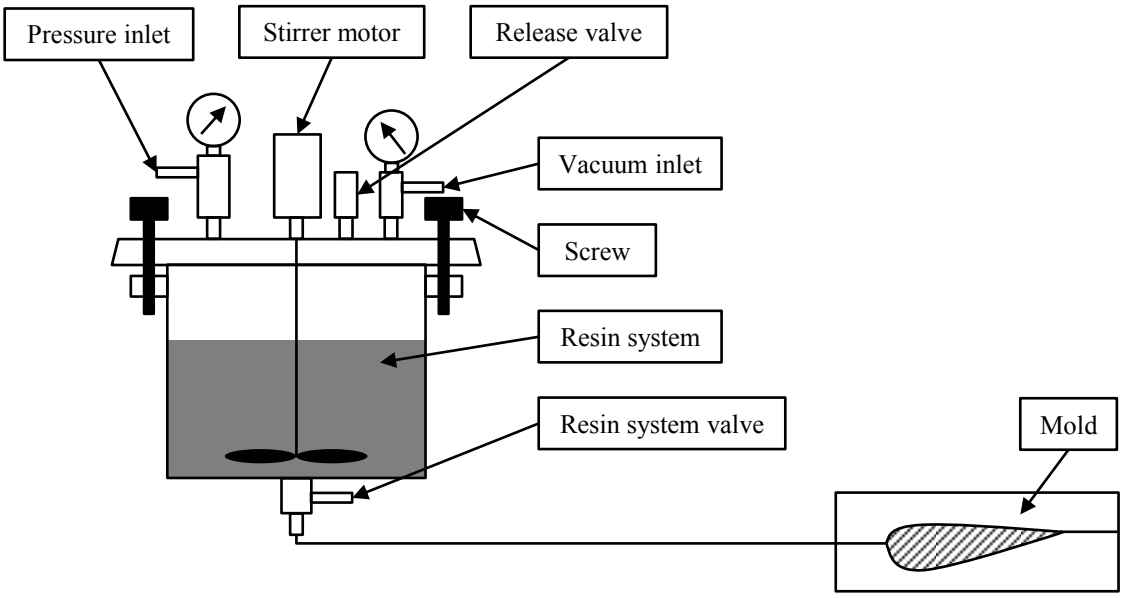

Fig. 2-9 Pressure pot injection machine (similar to [75])

The main advantages of this device are its easy handling and the comparable low investment costs. Two major drawbacks are identified: First, the resin system is handled manually before the injection. For this, resin systems with slow reactions are processed exclusively leading to a time and cost intensive procedure. Second, the control of the volume flow and therefore a constant flow is hardly achievable. Since the pressure gradient dp/dx decreases with the propagating flow front. For this, the superficial flow velocity decreases during the filling of the cavity, too (see Eq. 2-2). This leads to constantly varying impregnation conditions. Raising the pressure as counteracting effect is insufficient since the volume flow is not solely dependent on this parameter [75, 76].

2.2.5.2 Low pressure Resin Transfer Molding

For processing two or more component resin systems, mixing heads with low mixing pressure can be utilized. The components are stored in separate reservoirs at the metering device. A connection to a vacuum pump can enable the degassing of the components in the reservoirs [77]. Dependent on the layout of the device, mostly electrical heating systems are attached to the reservoir, tubes, pumps and the mixing head. Alternatively, circulating air heating is implemented into the cabinet of the metering device. The volume flow can be created by single or double acting pneumatic piston pumps. These pumps enable precise metering. They are restricted to discontinuous processes due to the necessary stop for refilling. To overcome this issue, gear pumps are utilized to continuously meter the resin components (see Fig. 2-10). Although the internal geometry of these pumps is precise, it is possible for the resin components to flow back between the outer casting of the pumps and the gears. However, volume control systems (VC) in each tube recognize the volume flow and adjust the pump movement. Thus, the stoichiometric ratio of the resin system is ensured [76]. This enables an accurate and a constant volume flow even at varying injection pressure during the preform impregnation [78]. A solvent flushes the sections of the injection machine contaminated with a reactive resin system after each injection. Later in this chapter this cleaning process is discussed in detail (see Fig. 2-12). Even though these devices are more expensive compared to the pressure pot (see chapter 2.2.5.1), major advantages are achieved for the high volume production. Due to the storage of the resin components in separate reservoirs, no freezer storage or mixing of the resin system before each injection is necessary. Highly reactive resin systems with a pot life between 30 s and 5 min are processible due to the online mixing of the components during the injection. The cycle time is drastically reduced compared to the pressure pot. Further, less resin system is wasted since the metering can accurately be adjusted to the required volume.

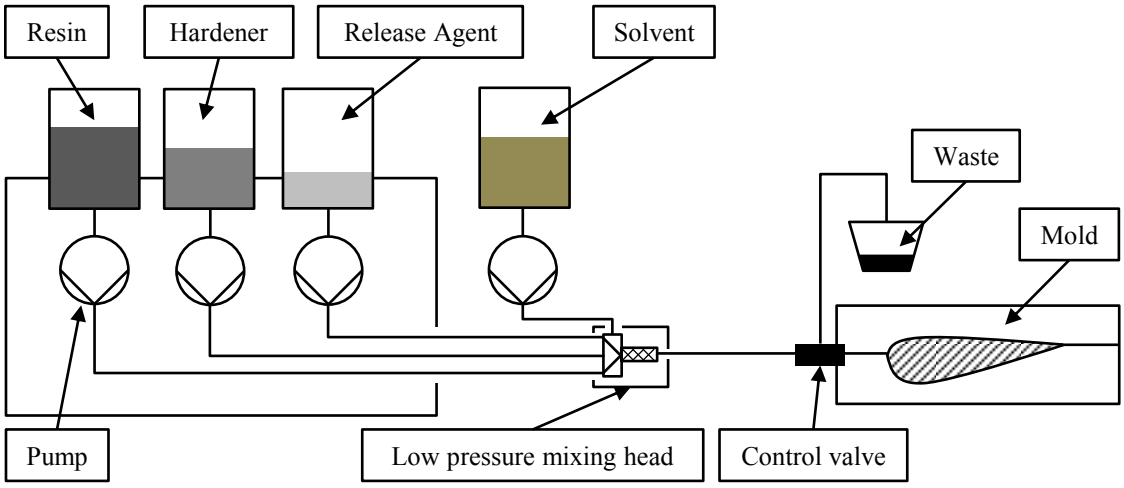

Fig. 2-10 Low pressure RTM injection machine

Low pressure mixing heads use shear elements to divide and merge the resin components [79, 80]. Dependent on the streaming conditions, laminar streaming or laminar streaming superimposed by tubular cross streaming swirls occurs. At each shear element within the mixing chamber the laminar flow is divided into sub streams. Latter are radial distributed and combined in a reordered sequence. This process is repeated at each shear element. Two layers are separated into four layers at the first shear element, into eight layers at the second shear element and so on (see Fig. 2-11).

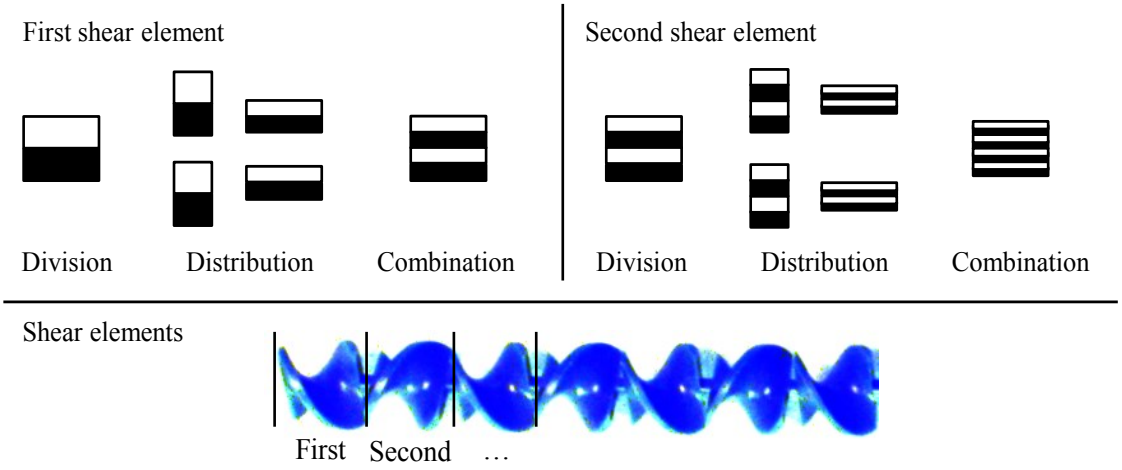

Fig. 2-11 Mixing process in a static mixing device; division, distribution and recombination of the first and second shear element (upper part similar to [79])

The reorientation of the resin system by shear elements causes a friction between the elements and the resin system. This results in a pressure gradient within the mixing chamber. The height of the delta depends on resin system properties like the viscosity [81, 82], on process parameters like the volume flow [81], on mixing chamber properties like the geometry [83], on the shear element type [82, 83] and on the shear element number [81–83]. The pressure drop ranges from less than 1 bar to 30 bar. An overview of the various types of static mixers is given in the literature [14, 15].

Fig. 2-12 shows the injection and cleaning principle of a low pressure mixing head. During the injection, the components are continuously feed throughout the mixing chamber. After the injection, the mixing chamber and the tubing system between mixing head and mold inlet are filled with reactive resin system which would lead to a blockade of the process after curing [17]. To prevent this from happening, the mixing chamber and the tubing system are flushed by an appropriate solvent or a resin component before the gelation of the resin system occurs.

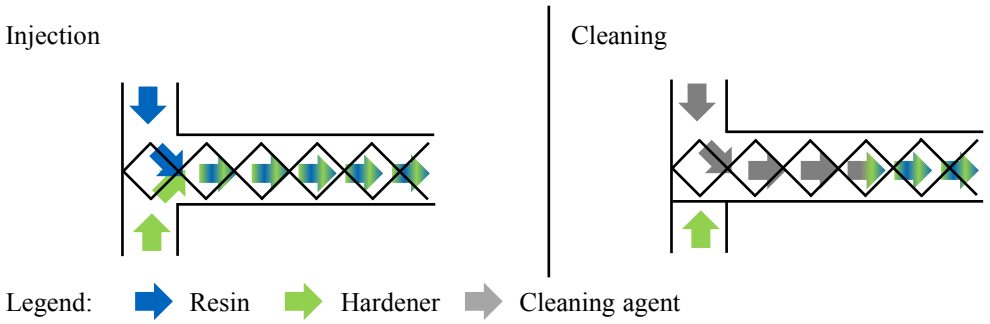

Fig. 2-12 Low pressure mixing head; injection process (left) and cleaning process (right)

The cleaning process is therefore the major drawback of this technique for the high volume production. The cleaning of the mixing chamber and tubing system results in a special waste of mixed, reactive resin system and solvent after each injection. The alternative is to replace the respective mixing chamber, tubes and connectors. This however is labor intensive and waste productive.

2.2.5.3 High pressure Resin Transfer Molding

The high pressure Resin Transfer Molding process is based on a high pressure mixing head, which uses impingement mixing. It is particularly used for high volume production and targets cycle times <5 min. [84]. In the literature this technique is termed Structural Reaction Injection Molding (SRIM) or high pressure RTM whereas the equipment for both processes is identical [17]. The high pressure RTM is drafted in Fig. 2-13. The liquid resin components are stored, heated and optionally degassed in separate reservoirs. In the given case gear pumps are used to feed the components to the mixing head. The resin system components circulate between mixing head and reservoir until the mandatory mixing pressure is reached. To produce the necessary pressure, needle plug valves are used at the openings of the resin system components in the mixing chamber. Hereby, pressures between 50 to 230 bar are set to the resin and hardener section between the dosing pumps and the mixing head [17]. The mixing chamber is directly attached to the mold inlet.

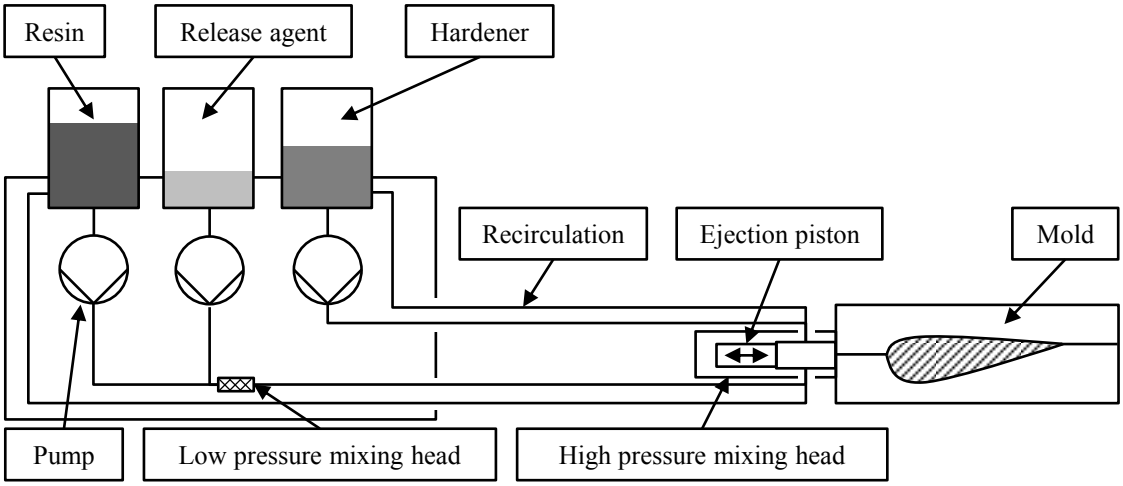

Fig. 2-13 High pressure RTM injection machine

Fig. 2-14 shows the injection and cleaning process of the high pressure mixing head. The components are mixed by impingement in the mixing chamber and guided into the cavity during the injection process. The mixing chamber is cleaned by a piston movement after the injection. Hereby, the resin system is pushed into the cavity before it cures. This movement is possible due to the absence of elements within the mixing chamber.

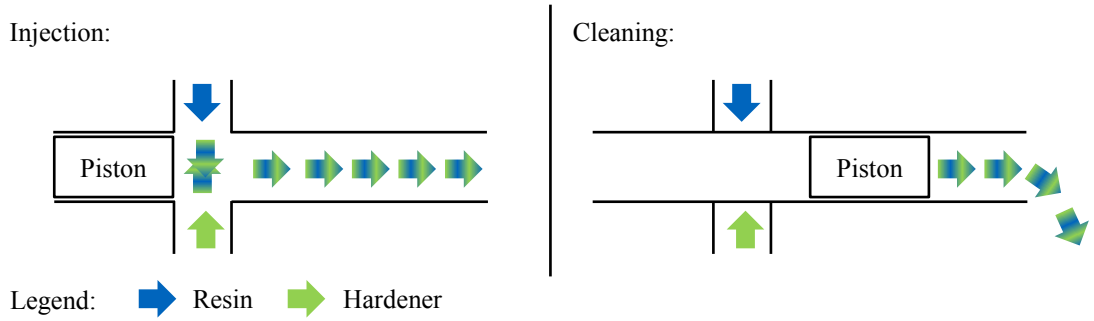

Fig. 2-14 High pressure mixing head; injection (left) and cleaning process (right)

The major advantage of high pressure mixing heads compared to low pressure mixing heads is the so called 'self-cleaning' [20, 85] process that terms the ejection of the resin system. Thus, the solvent flushing process is not required. The major drawback is the high mixing pressure in addition to the injection pressure. Due to the volumetric filling at the end of the injection, not only the metering device, but also the mold and press equipment have to withstand up to 150 bar solely to realize the mixing by impingement. Hence, the investment costs for high pressure RTM are roughly ten times the investment costs for low pressure RTM.

2.3 Material specifications

The equipment used for the investigations in this thesis (see chapter 3, chapter 5, chapter 6 and chapter 7) is specified and set in context to the state of the art technology.

Therefore, the ultrasonic device (see chapter 2.3.1), the metering device (see chapter 2.3.2) and the epoxy resins (see chapter 2.3.3) are discussed in detail.

2.3.1 Ultrasonic device

A Hielscher UIP1000hdt ultrasonic device (see Fig. 3-1) is utilized for the sonication. This equipment consists of a generator which creates a high frequency alternating electrical current and a transducer which converts the alternating current into a mechanical oscillation by a piezo ceramic. The device handles a maximum power of 1000 W at a frequency of approximately 20 kHz. This frequency at the lower end of the ultrasonic spectrum is selected due to its supportive character of transient cavitation creation (see chapter 2.1.6). The precise frequency is adjusted by a scanning process at the beginning of the sonication. Hereby, the generator starts stimulating the sonotrode at a frequency of 21 kHz. The frequency is continuously reduced until a natural frequency of the sonotrode is reached. Thereby, sonotrodes with frequencies between 19 kHz and 21 kHz are applicable. During the actual sonication, two ultrasound parameters are distinguished: First, the amplitude A, which denotes the end-to-end movement of the sonotrode. Second, the power Pw, which describes the entire effort of the ultrasonic device to execute the ultrasonic movement of the sonotrode. Two control modes can be selected to operate the ultrasonic device:

- Amplitude control: In here, the amplitude is kept constant and the power is adjusted according to the process conditions.
- Power control: Hereby, the power value is preset and the amplitude value is adjusted. If the selected power consumption cannot be achieved, the amplitude is set to its maximum value.

Two titan sonotrodes are utilized to transfer the sonication to the fluids: a cylindrical sonotrode from Hielscher (HS) with a tip diameter of 34 mm and a self-designed sonotrode (UMHS) with a tip diameter of 15 mm construed for the UMH. The amplitudes and resonance frequencies of the sonotrodes are listed in Tab. A-1 and Tab. A-2. They are measured by a Laser Doppler Vibrometer (see chapter 2.1.5) at idealized conditions. The actual amplitudes can vary up to 5 % dependent on the sonication conditions like the fluid pressure, the fluid temperature or the sonotrode temperature.

In the literature, either the power of the ultrasonic device [22, 86, 87] or the quotient of the power and the area of the sonotrode front plane [29, 30] is inspected to describe the intensity of the cavitation zone. In this thesis, a continuous volume flow of the resin system through the cavitation zone occurs (see chapter 4). For this, an additional parameter is introduced. It is named energy density (see Eq. 2-3).

$$\rho_E = \frac{E}{V} = \frac{Pw * t_{exp}}{V} \qquad \text{Eq. 2-3}$$

This parameter is defined as the quotient of the energy E and the volume V of the cavitation zone. Hereby, the energy E consists of the power Pw and the exposure time t_{exp}.

2.3.2 Metering devices

Two low pressure RTM metering devices from Dekumed are utilized. The devices only differ by the number of processible resin components: two and three. The resin components are degassed in batch chambers before they are carefully filled into the reservoir at the metering device. The heating of the components is done electrically in the reservoir, the tubes and the utilized mixing head. The cabin of the metering device is heated by a circulating air heating system. To meter the components, gear pumps combined with VC are utilized. During an injection, a constant volume flow is provided by the metering device.

2.3.3 Resin systems

Three epoxy resin systems are utilized in this thesis:

- RIM (see Fig. A-1) is a two component epoxy resin system of Hexion. It consists of the resin component, EPIKOTE™ Resin MGS® RIM 135 and the diamine based hardener component, EPIKURE™ Curing Agent MGS® RIMH 1366. The resin system is mixed by a ratio of 100:36 per unit volume and is mainly applied in infusion and injection processes. Pot life reaches from 10 min at elevated to 4 h at room temperature. Meier [66] provides a detailed description of its rheological behavior. In the thesis at hand RIM is used for the laboratory investigation (see chapter 3), the process characteristics (see chapter 5) and the RTM characteristics (see chapter 6).
- XB (see Fig. A-2) is a fast curing two component epoxy resin system of Huntsman. The resin component XB 3585 is mixed with the amine based hardener XB 3458 in a mixing ratio of 100:23 per unit volume. Pot live reaches from 30 s at elevated temperature to 18 min at room temperature. It is formulated for high volume productions and targets short cycle times. Keller et al. [88] revealed extensive investigations on the rheological and thermal behavior of this resin system. In this thesis, it is used for the RTM characteristics (see chapter 6).
- TRAC (see Fig. A-3) is a fast curing three component epoxy resin system of Hexion. The resin component EPIKOTE™ Resin TRAC 06170, the hardener component EPIKURE™ Curing Agent TRAC 06170 and the third component HELOXY™ Additive TRAC 06805 are mixed 100:16:3 by weight. The third component is an internal release agent to lower the demolding stresses. The pot life is 2 min at elevated and 42 min at room temperature. In

this thesis, the resin system is utilized for the automated injection process (see chapter 7).

The resin components are degassed before usage to minimize the damping of the sonication by entrapped air and the occurrence of stable cavitation (see chapter 2.1.2).

2.4 Measurement methods

Danckwerts [89] already identified the need to quantify the 'goodness of mixing' in 1952. Since then, numerous indicating numbers are revealed. However, all these key figures are hypothetical values or require a calibration process. Therefore, in this thesis, the focus is on performance parameters. Hence rheological, thermal and mechanical properties of sonicated resin systems are investigated. The number of samples n represents an excerpt of the main unit of all possible investigations. The standard deviation s based on a sample (SD) is used to indicate the distribution of the measured values x in reference to their arithmetic mean (AM) value $\bar{x}$ (see Eq. 2-4):

$$s = \sqrt{\frac{\Sigma(x - \bar{x})^2}{(n-1)}} \qquad \text{Eq. 2-4}$$

The error bars in figures show the SD of all samples at a parameter setting. The description is given before, the explanation is given after each figure.

2.4.1 Rheometry

Rheology describes the qualitative and quantitative relation of deformations and stresses respective their derivatives. Vadhar and Kyu [90] investigated the influence of mixing strategies of ultrahigh molecular weight polyethylene and low density polyethylene. Differences in the development of the viscosity are traced back to different mixing strategies, which lead to different polymer structures. Emmerson et al. [91] claim that the rheology of a filled resin system changes subject to ultrasound cavitation. Therefore this measurement method is selected to quantify the development of the viscosity and the transition from a viscous to a solid structure. Various techniques and equipment are outlined in the literature [66, 92–95]. In the following, the principles thereof are extracted to specify the measurement method used in this thesis.

In Fig. 2-15 a shear streaming between two parallel plates is pictured. If the axial force F is applied to the upper plate, shear stress τ will occur due to the contact area A between the fluid and the plates. A laminar velocity profile $v(y)$ takes place for a Newtonian fluid. The resulting speed of the upper plate is dependent on the dynamic viscosity η of the fluid.

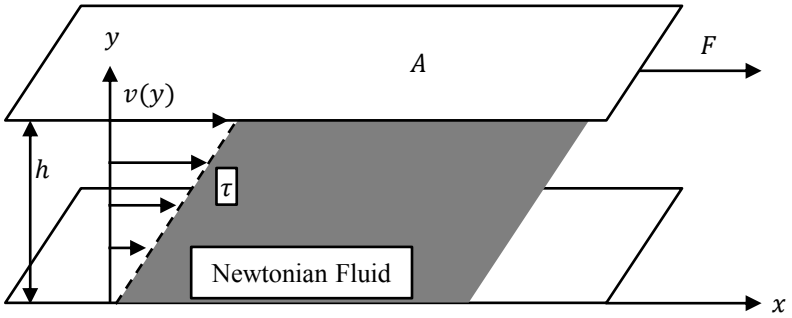

Fig. 2-15 Velocity profile of a one dimensional streaming of a Newtonian fluid between two plates

Eq. 2-5, Eq. 2-6 and Eq. 2-7 show the correlations of the respective parameters. If the velocity profile is linear due to a Newtonian fluid, the shear rate $\dot{\gamma}$ is constant throughout the height h of the profile. This behavior is called ideal viscos, because of the deformation energy, which dissipates. The fluid remains in the current form when the load is released. Eq. 2-6 is Newton's law.

$$\tau = \frac{F}{A} \qquad \text{Eq. 2-5}$$

$$\eta = \frac{\tau}{\dot{\gamma}} \qquad \text{Eq. 2-6}$$

$$\dot{\gamma} = \frac{dv}{dh} \qquad \text{Eq. 2-7}$$

If the deformation energy is stored due to an elastic behavior of the material, it will deform back to the initial shape after the load is released. This correlation is described by Hooke's law, which includes the shear modulus G (see Eq. 2-8).

$$\eta = \frac{\tau}{G} \qquad \text{Eq. 2-8}$$

Most of the fluids show both a viscos and an elastic behavior. The Maxwell model describes this behavior by a series circuit of a spring damper system. Hereby, the spring represents the elastic behavior (Hooke's law) whereas the damper represents the viscos model (Newton's law). To describe this context mathematically, the complex shear modulus G^* is introduced. It consists of the storage modulus G' and the loss modulus G'' (see Eq. 2-9).

$$G^* = G' + iG'' \qquad \text{Eq. 2-9}$$

Analogous to the shear modulus G the viscosity is divided into a viscose η' and an elastic η'' component. Their sum defines the complex viscosity η^* (see Eq. 2-10).

$$\eta^* = \eta' + i\eta'' \qquad \text{Eq. 2-10}$$

Rheometry describes the experimental methods to determine these rheological properties of a material. In this thesis three parameter of this measurement method are considered:

- The initial dynamic viscosity $\eta_{initial}$ represents the initial flow behavior after mixing. It gives a feedback on the processability of the resin system.
- The development of the dynamic viscosity η respective the complex viscosity η^* describes the buildup of the polymer network (see chapter 2.2.2) throughout the reaction.
- Gel time t_{gel} defines the duration until the storage modulus exceeds the loss modulus and therefore the transition from a liquid to a solid. The resin system is insoluble in a solvent after this transition according to Ehrenstein [58].

The recommended procedures are executed according to the standard DIN 1342 [96]. The main correlations are described in the following. Fig. 2-16 shows the machine parameters at the plate-plate measurement system.

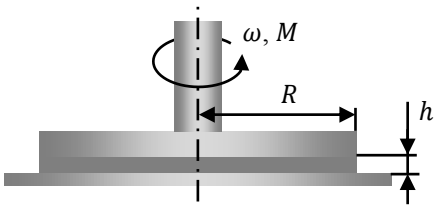

Fig. 2-16 Plate-plate measurement system of the rheometer

The shear rate is not consistent above the radius of the plate at this setup. Therefore, the shear stress (see Eq. 2-11) and the shear rate (see Eq. 2-12) occurring at the outer rim are selected for the calculation.

$$\tau(R) = \frac{2\,M}{R^3\pi} \qquad \text{Eq. 2-11}$$

$$\dot{\gamma}(R) = \frac{r\omega}{h} \qquad \text{Eq. 2-12}$$

The dynamic viscosity is calculated by a rotatory measurement. For this, Eq. 2-11 and Eq. 2-12 is inserted in Eq. 2-6. An oscillatory measurement is executed to detect the complex viscosity (see Eq. 2-10) and the gel time. Each of the moduli is hereby calculated out of the quotient of the shear stress amplitude τ_0 and the shear deformation amplitude γ_0, and the phase shift angle δ between the shear stress and the shear defor-

mation (see Eq. 2-13, Eq. 2-14). The loss factor $tan\delta$ is defined as quotient of the loss modulus and the storage modulus (see Eq. 2-15). If this parameter undercuts a value of one, the storage modulus will exceed the loss modulus. The duration from the end of mixing to this transition is defined as gel time.

$$G' = \frac{\tau_0}{\gamma_0} cos\delta \quad \text{Eq. 2-13}$$

$$G'' = \frac{\tau_0}{\gamma_0} sin\delta \quad \text{Eq. 2-14}$$

$$tan\delta = \frac{G''}{G'} \quad \text{Eq. 2-15}$$

For the investigations in this thesis, a Modular Compact Rheometer MCR302 of Anton Paar is used. The temperature is controlled by the tribology measurement cell H-PTD 200d of Anton Paar. The specifications of the test setups are revealed in the materials and methods chapter of the respective investigation: chapter 3.1.1 refers to the laboratory investigation and chapter 5.1.3.2 refers to the process characteristics.

2.4.2 Differential Scanning Calorimetry

Differential Scanning Calorimetry (DSC) is a thermal characteristics method to reveal the behavior of a material during the application of a thermal load. Ritzenthaler et al. [97] used various thermal techniques to investigate the polymer structure of thermoplastically modified epoxy resin systems before and after cure. Vadhar and Kyu [90] measured different glass transition temperatures of thermoplastic blends with different metering ratio. Vanlandingham et al. [98] investigated changes in the microstructure dependent on the epoxy to amine stoichiometry. Differences in the glass transition temperature are correlated with the crosslink density of the polymer network. For this, the DSC is capable of detecting variations in the network buildup and the performance of the cured resin system.

Dependent on the investigated material and target parameters, different techniques and equipment are utilized. Detailed descriptions are given in the literature [99–101]. In the following chapters, the principles of this literature are taken to specify the measurement method used in this thesis.

The T_{zero} temperature method is used (see Fig. 2-17). Hereby, a sample pan with resin system and an empty reference pan is exposed to a temperature load. The measurement temperature T_{set} is preset by the device. During the measurement, the heat flow to the sample pan $\dot{Q}_{sample}$ and to the reference pan $\dot{Q}_{ref}$ is measured. Further, the sample temperature T_{sample} and the reference temperature T_{ref} is detected. By separating the pans by the T_{zero} method, the interaction between sample pan and reference pan is minimized. [100]

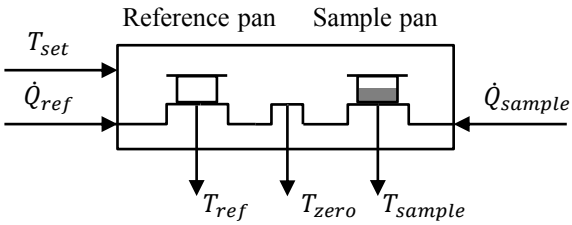

Fig. 2-17 Heat flow within the DSC chamber (similar [100])

The corresponding equations describe the temperature difference ΔT (see Eq. 2-16) and the heat flow difference $\Delta \dot{Q}$ (see Eq. 2-17).

$$\Delta T = \left(T_{ref} - T_{zero}\right)\left(T_{sample} - T_{zero}\right) \quad \text{Eq. 2-16}$$

$$\Delta \dot{Q} = \dot{Q}_{ref} - \dot{Q}_{sample} \quad \text{Eq. 2-17}$$

In this thesis, three responses are evaluated by this measurement method:

- The initial glass transition temperature $T_{g\ initial}$ gives a feedback on the network that is already built at the start of the measurement.
- The residual enthalpy ΔH_{res} describes the residual energy of the exothermal reaction in the sample. After the mixing of the resin systems, a storing process is required due to transportation matters. Therefore, the measured enthalpy is not the entire enthalpy of the sample and termed as residual.
- The final glass transition temperature $T_{g\ final}$ describes the transition of the cured sample from a solid to a gel state. This value indicates the homogeneity and density of the built network in the cured part.

The recommended measurements are executed according to the standard DIN EN ISO 11357 [102]. Therefore two dynamic temperature cycles are performed. Even though both cycles are similar, the sample properties measured at each cycle differ (see Fig. 2-18):

- The first cycle provides two parameters: the initial glass transition temperature and the residual enthalpy. The initial glass transition temperature is measured at the turning point during the first drop of the heat flow. The residual enthalpy is the change of heat flow because of the exothermal reaction. For this, the area limited by the heat flow curve and a straight line is measured.
- The second cycle is used to detect the final glass transition temperature. Its value is detected at the turning point of the heat flow during the second

ramp. No residual enthalpy is left in the sample. It represents the final material property of the fully cured resin system.

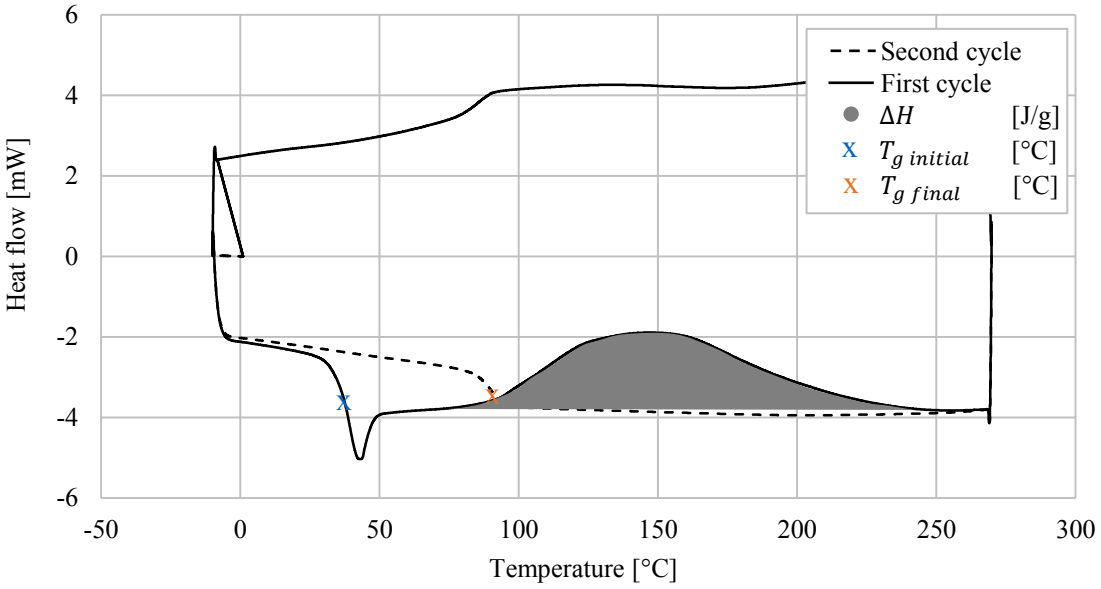

Fig. 2-18 Exemplary heat flow to temperature correlation during the program of the Differential Scanning Calorimetry

For the thermal analysis, a TA Q 2000 of TA Instruments is used. The sample preparation and the test procedures parameter are revealed in the materials and methods chapter of the respective investigation: chapter 3.1.1 refers to the laboratory investigation and chapter 5.1.3.2 refers to the process characteristics.

2.4.3 Mechanical test

Mechanical tests of specimens produced with ultrasonic mixing are carried out to compare their mechanical performance to the state of the art mixing technology. Almeida and Monteiro [103] investigated the mechanical performance of an epoxy resin system at different resin to hardener ratios. The resin rich systems showed a brittle behavior. This is associated with the buildup of a rigid macromolecular structure. On the contrary, the hardener rich systems displayed a fracture behavior characteristics of materials with a larger deformation capacity. Further, they investigated the influence of changing metering ratios of the resin system on the mechanical performance of glass fiber composites [104]. A change of the ratio is identified as a parameter to change the matrix properties of the composite. Analogously to their neat resin experiments, the hardener rich samples showed a higher deformation rate. Bakar et al. [105] investigated the influence of the amplitude and exposure time on the mechanical performance of epoxy resin systems with nanoclay. Saleh et al. [106] investigated the influence of a hardener content variation on the mechanical performance of the epoxy

resin. Hereby the tensile strength and the Young's modulus were depended on the metering ratio of the resin system components.

Two types of tests are conducted in this thesis. The mixing quality is hereby considered as local metering quality. Tensile tests (see chapter 2.4.3.1) are executed with specimens of neat resin plates (NRP) and in plane shear tests (see chapter 2.4.3.2) are executed with specimens of fiber reinforced plates (FRP).

2.4.3.1 Tensile test

The tensile test of neat resin system samples are preformed according to the standard DIN EN ISO 527-2 [107]. Hereby the stress axial strain curve is measured as an indicator for the mixing quality. The stress σ is defined as the quotient of the axial force F which is applied to the specimen and its initial cross sectional area A_{cross} (see Eq. 2-18). The engineering strain ε is calculated for each specimen, too.

$$\sigma = \frac{F}{A_{cross}} \qquad \text{Eq. 2-18}$$

Based on these formulas, two responses are depicted:

- Tensile strength σ_{max} describes the ultimate stress of the specimen.
- Young's modulus E (see Eq. 2-19) describes the secant of the stress axial strain curve in the linear elastic section between $\varepsilon_1 = 0.00050$ and $\varepsilon_2 = 0.0025$ and σ_1 and σ_2 denotes as the stresses at ε_1 and ε_2, respectively.

$$E = \frac{\sigma_2 - \sigma_1}{\varepsilon_2 - \varepsilon_1} \qquad \text{Eq. 2-19}$$

An electromechanical testing machine (Hegewald & Peschke Inspect Table 100), equipped with a 100 kN load cell, is used. The sample preparation, the test procedure and the digital image correlation to calculate the responses are revealed in the materials and methods chapter (see chapter 6.1.5.2).

2.4.3.2 In plane shear test

In plane shear tests are performed according to the standard DIN EN ISO 14129 [108]. Hereby the fibers within the preform are oriented in +45°/-45° direction relative to the tensile direction. This load case is selected since the results are influenced by the fiber and the resin system characteristics. The shear stress τ_{12} is derived from the axial force F and the cross sectional area A_{cross} of the sample (see Eq. 2-20). The engineering shear strain γ_{12} (see Eq. 2-21) is the difference between the longitudinal strain ε_x and the transversal strain ε_y.

$$\tau_{12} = \frac{F}{2A_{cross}} \quad \text{Eq. 2-20}$$

$$\gamma_{12} = \varepsilon_x - \varepsilon_y \quad \text{Eq. 2-21}$$

Based on these formulas two responses are depicted:

- The shear strength τ_{12M} (see Eq. 2-22) is calculated at the maximum tensile force F_m of a samples failure. If the sample does not fail before a shear deformation of 0.05, the tensile force at a shear deformation of 0.05 is used for the calculation.
- The shear modulus G_{12} (see Eq. 2-23) is defined as the quotient of the shear stress and the shear deformation at $\gamma''_{12} = 0.005$ and $\gamma'_{12} = 0.001$.

$$\tau_{12M} = \frac{F_m}{2A_{cross}} \quad \text{Eq. 2-22}$$

$$G_{12} = \frac{\tau''_{12} - \tau'_{12}}{\gamma''_{12} - \gamma'_{12}} \quad \text{Eq. 2-23}$$

Analogously to the tensile test a 100 kN load cell of a Hegewald & Peschke tensile test machine is used. The sample preparation and the test procedure are revealed in the materials and methods chapter (see chapter 6.1.5.2).

3 Laboratory investigation

To enable the development of an Ultrasonic Mixing Head (UMH) (see chapter 4), the response of an epoxy resin system on ultrasound excitation is investigated in the controlled environment of the laboratory. Hereby, three aspects are taken into account as regards the cavitation effect on an epoxy resin system: First, the areal extension of the cavitation zone is detected by a high speed camera observation (see chapter 3.1). Hereby, the scale of the effect is investigated. Second, the viscosity development of the ultrasonically mixed resin system by a rheometer inspection (see chapter 3.2) to examine the processability after mixing. Third, the thermal properties of the cured resin system are measured by a Differential Scanning Calorimetry. The impact of ultrasonically treatment on the curing behavior is investigated (see chapter 3.3).

The experimental setup for the creation of the samples is identical for these investigation (see Fig. 3-1). The Hielscher UIP1000hdt ultrasonic device (see chapter 2.3.1) is utilized. Hereby, the transducer is clamped in a stand. The sonotrode is dipped into the mixing vessel to sonicate the fluid. The volume of the mixing vessel varies according to the purpose of the respective investigation.

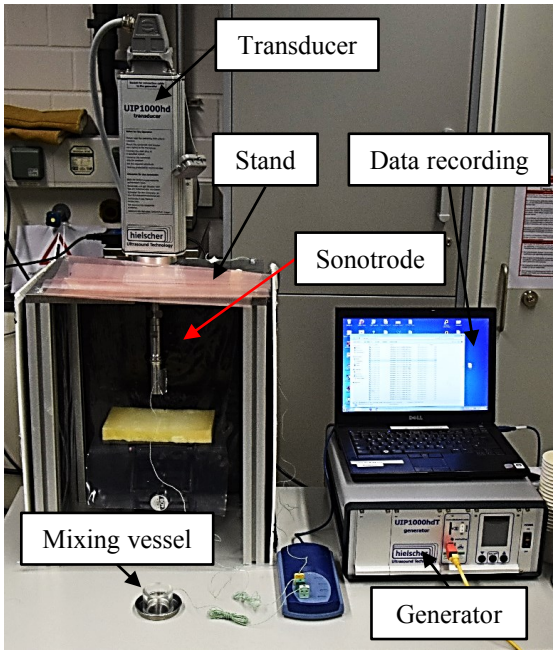

Fig. 3-1 Experimental setup for the sonication of a resin system in the laboratory

Two sonotrodes are utilized: a cylindrical sonotrode from Hielscher (HS) and a self-designed sonotrode (UMHS) construed for the Ultrasonic Mixing Head (UMH). The UMHS is manufactured after the UMH development (see chapter 4). However, the results of both sonotrodes are revealed in parallel.

3.1 Cavitation zone measurement

In the literature, different techniques are described to observe cavitation in liquids. Hereby, mostly water is used. Burdin et al. [109] and Tsochatzidis et al. [110] utilized various laser techniques to measure the size, volumetric concentration and velocity of acoustic in bi-distilled water on a microscopic scale. Luther et al. [111] used a high speed camera and data image correlation to reconstruct the trajectory of cavitation bubbles in water. Guo et al. [112] recorded cavitation bubbles with a high speed camera. The micromixing and mesomixing effects of the cavitation (see chapter 2.1.2) led to the dispersion of agglomerated crystals suspended in ethanol. Tzanakis et al. [113] recorded the cavitation effect in different liquids with a digital camera. Their results show a range from a conical shape in water to symmetrical vortexes in glycerin. In Ethanol a single bubble occurred instead of a stream.

No literature respective the response of epoxy resin on ultrasonic treatment is available. In this thesis an observation by a high speed camera is selected. Hereby the extension of the cavitation zone is detected.

3.1.1 Materials and methods for the cavitation zone measurement

The setup of the ultrasonic device is pictured in Fig. 3-1. In addition, Fig. 3-2 shows the arrangement of the high speed camera. Hereby, the ultrasonic device (see chapter 2.3.1) is equipped with the HS (see Tab. A-1). The sonotrode is dipped into a mixing vessel filled with 500 cm³ of the fluid. The diameter of the glass mixing vessel is distinctly larger than the sonotrode diameter to ensure no interaction between the ultrasound cavitation and the vessel walls. The high speed camera is placed horizontally in front of the glass vessel to detect the areal extension of the cavitation zone. Hereby a Photron SA 5 VKT high speed camera set to 50 frames/s and a resolution of 1024 x 1024 pixels is operated. The Photron FASTCAM Viewer picture analysis software is utilized for its evaluation.

The resin component RIM 135 of the resin system RIM (see chapter 2.3.3) is utilized as fluid. Thus, an influence of the resin system reaction on the results is prevented. Monnier et al. [114] found that a higher viscosity provokes a higher damping of the sonication. For this, the sonication of the resin component is a worst case scenario for the extension of the cavitation zone. Prior to each experiment the resin temperature is adjusted to 25 °C.

The amplitude is identified as a crucial factor for the various developments of the cavitation zone [22, 105, 113]. Sonications at four amplitudes A are applied for an exposure time t_{exp} of 5 s each: 12.90 µm, 19.55 µm, 26.40 µm and 44.05 µm. The cavitation zone geometry, the extension in z-direction l_z and the power Pw of the generator are analyzed.

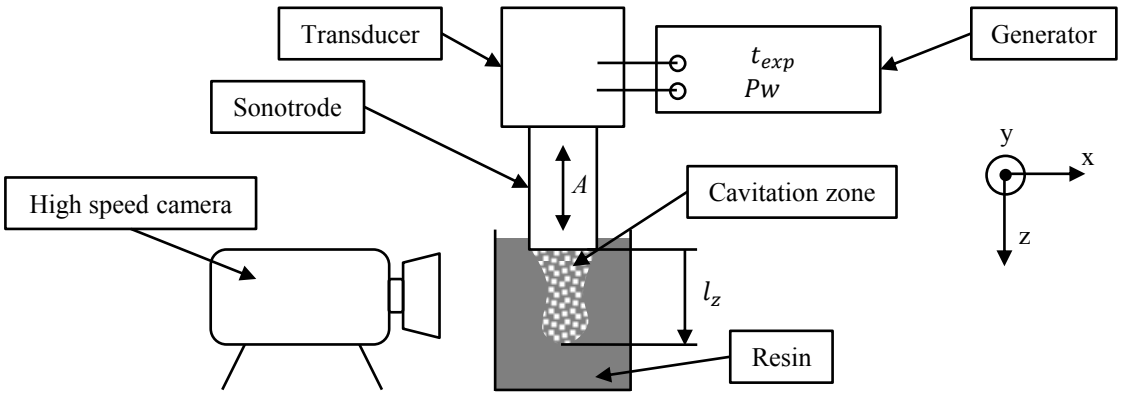

Fig. 3-2 Cavitation zone measurement by a high speed camera

3.1.2 Results of the cavitation zone measurement

Fig. 3-3 shows the dilatation of the cavitation zone during the first 3 s of exposure at an amplitude of 44.05 µm. A white and fuzzy cone structure occurs below the sonotrode end plane. The shape of the fungoid structure is already built after 1 s of exposure. During further exposure, the cavitation zone grows. Hereby, a macroscopic streaming in z-direction occurs apart from the cavitation bubbles. It elongates longitudinally in z-direction and contracts in x- and y-direction in the middle section of the fungoid structure. After 3 s of exposure the cavitation zone growth is supplied by a self-feeding effect. This occurs at the sonotrode front end plane and is achieved by cavitation bubbles which fly back in the macroscopic streaming. These mechanisms are continued until the end of the experiment.

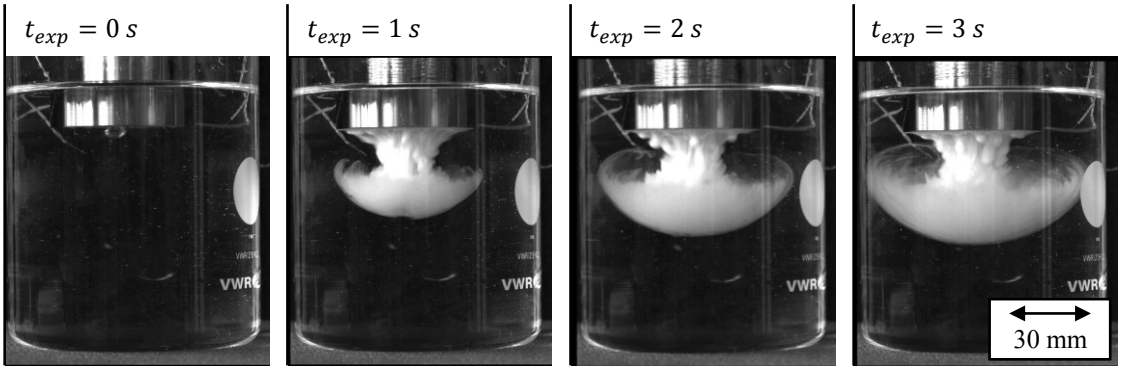

Fig. 3-3 Dilatation of the cavitation zone at an amplitude of 44.05 µm in the resin component RIM 135 during 3 s exposure time

Fig. 3-4 shows the dilatation of the cavitation zone after 5 s of exposure at various amplitudes. At an amplitude of 12.90 µm, a few thready cords appear at the sonotrode end plane. The cords do not bundle below the sonotrode end plane, but they lead to the cylinder shell of the sonotrode. At 19.55 µm, more thready structures appear at the sonotrode end plane. They stay below the sonotrode end plane and only few threads, end up at the cylinder shell. At 26.40 µm a fungoid structure is visible. It comes from locally summarized knots which cover the whole sonotrode end plane. At 44.05 µm, more and more knots occur at smaller areal sizes. A fully developed fungoid structure is visible. By increasing the amplitude, a concentrated cavitation zone shaped as a cone is developed out of separated single cords. Further, the cavitation zone is larger at higher amplitudes.

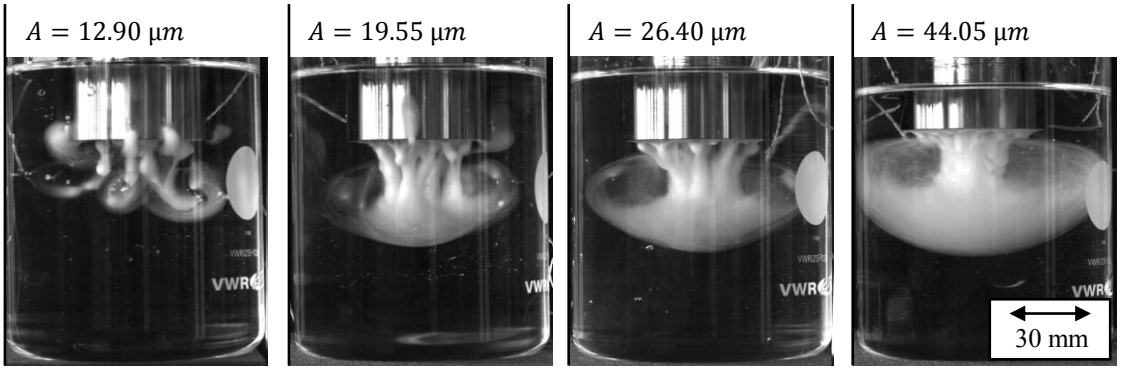

Fig. 3-4 Dilatation of the cavitation zone at various amplitudes in the resin component RIM 135 at 5 s exposure time

Cumulating the results visible in Fig. 3-3 and Fig. 3-4 similarities to the sonication of glycerin by Tzanakis et al. [113] are detected. They describe a cavitation zone consisting of summarized knots at an amplitude of 17 µm.

In Fig. 3-5 a), the extension in z-direction l_z is outlined. It goes from the sonotrode end plane to the tip of the cavitation zone. The lowest amplitude setting 12.90 µm, is excluded since no measurable cavitation zone occurs (see Fig. 3-4). The extension increases mostly within the first second of exposure and continues to grow at a smaller

gradient afterwards. The cavitation zone extension is fastest at an amplitude of 44.05 µm within the first three seconds. In the interval of three to five seconds, a similar gradient occurs at all amplitudes. Fig. 3-5 b) reveals the power of the ultrasonic device during the experiment. After the buildup of the oscillation, the power value is at a constant level for each amplitude. The power corresponds to the amplitude: higher amplitudes require more power. Hereby, an increase of the amplitude from 19.55 µm to 26.40 µm shows a small increase of the power. A further amplitude increase to 44.05 µm results in a significant increase of the power.

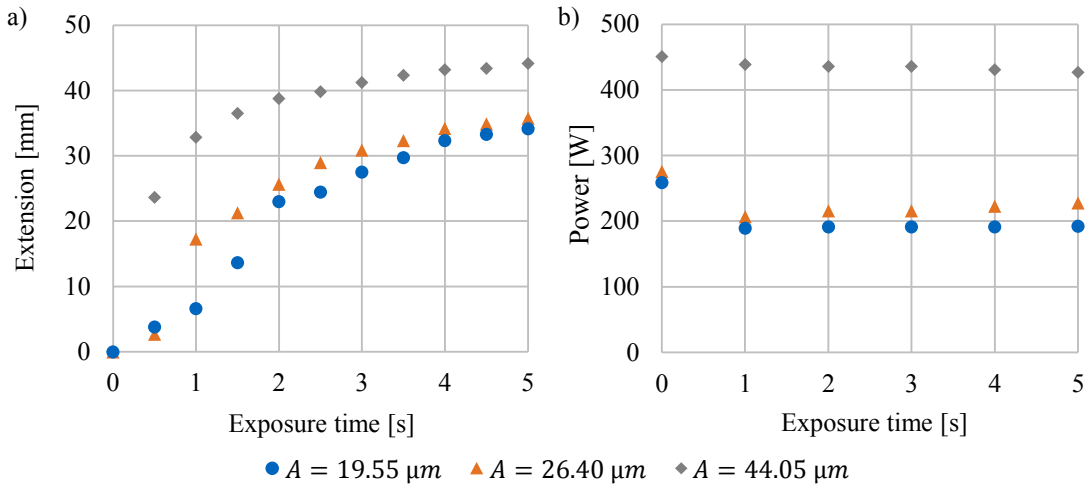

Fig. 3-5 **Extension of the cavitation zone in z-direction a) and power of the ultrasonic device b) during sonication at different amplitudes**

Generally spoken, the cavitation zone develops mostly within one second. During this time, a sonotrode with an end plane diameter of 34 mm can build a cavitation zone, which extends more than 30 mm. Afterwards, the cavitation zone continuously grows.

3.1.3 Interpretation of the cavitation zone measurement

The following conclusions are drawn from the inspection of the cavitation zone in a resin component exposed to ultrasonic cavitation and put in a mixing vessel:

- The cavitation zone development depends on the amplitude. Higher amplitudes lead to a more homogeneous, volumetrically larger, fungoid cavitation zone. The emerging geometry is similar at amplitudes above 19.55 µm.
- The cavitation zone builds up mostly within one second after the start of sonication.
- The cross sectional area of the sonotrode is entirely covered by cavitation only until a few millimeters beneath.
- The power correlates with the amplitude during the sonication.

3.2 Rheology analysis of an ultrasonically mixed resin system

Target of this investigation is to measure the rheology of a resin system thoroughly mixed by ultrasound cavitation. The results are compared to manual mixing. Herby, not the mixing quality itself (see chapter 5), but the effect of cavitation on the resin system is examined. Thus, conclusions can be drawn as regards the processability of resin systems mixed by sonication. For this, two parameters (responses) are detected: First, the dynamic viscosity (see Eq. 2-6) development after mixing, to examine the viscosity raise during processing. Second, the gel time is taken into account. It denotes the transition of the resin system from a fluid to a gel state (see Eq. 2-13). The physical basics of the measurement method and the specification of the rheology equipment used in this thesis are given in chapter 2.4.1.

3.2.1 Materials and methods for the rheology analysis

Fig. 3-1 shows the experimental setup. The mixing vessel is a 7 mm thick glass tube bonded to a metal sheet. The glass cylinder is slightly wider than the sonotrode to ensure mixing primarily below the sonotrode and to avoid an interaction between the sonotrode shell and the mixing vessel. The mixing vessel is placed on a foamed underlay to uncouple the mixing vessel from the environment. A labor lifting ramp is used to adjust the immersion depth of the sonotrode to a few millimeters in the mixing vessel. Thus, cavitation is enabled in almost the complete mixing vessel.

For this investigation, the resin system RIM (see chapter 2.3.3) is utilized due to its comparably long pot life (see Fig. A-1). For this, it can be handled manually. The cavitation zone only develops at the sonotrode front end plane (see chapter 3.1). For this, two sizes of mixing vessels, which are slightly wider than the sonotrode front end plane, are used:

- Large mixing vessel (LMV): The resin system mass is set to 23.10 g and the hardener component mass to 6.90 g. This results in a resin system mass of 30.00 g and a volume of 28.04 cm³, respectively. The LMV is used with the HS.
- Small mixing vessel (SMV): The resin system mass is set to 1.15 g and the hardener component mass to 0.35 g. This results in a resin system mass of 1.50 g and a volume of 1.40 cm³, respectively. The SMV is used with the UMHS.

The masses of the resin components are weighted by a XS205 precision balance of Mettler Toledo at a precision of 0.01 mg. The resin component RIM 135 is heated to 25 °C to ensure the equal viscosity before each experiment. The hardener component RIMH 1366 is left at room temperature (RT) due to its low viscosity. Latter is nearly independent of the temperature. Further, the components are degassed for 15 min by a

vacuum pump to promote the occurrence of transient cavitation (see chapter 2.1.2). The test procedure is visible in Fig. 3-6. The content of each step is described in the following.

			Manual mixing			
Process	Metering	Folding	Sonication	Dwell	Positioning	Measurement
Δt	30 s	30 s	10 s	30 s	30 s	Various

Fig. 3-6 Sample preparation procedure for the rheology investigation

The resin and hardener are metered into the mixing vessel. Hereby, the hardener tends to wander to the surface because of its lower density. For this, a folding step (see Fig. 3-7) is required. A wooden spatula is used to perform ten folding movements. Afterwards, the resin system components are not thoroughly mixed, but the phase separation is randomized in the mixing vessel. This enables a sonication of both resin system components.

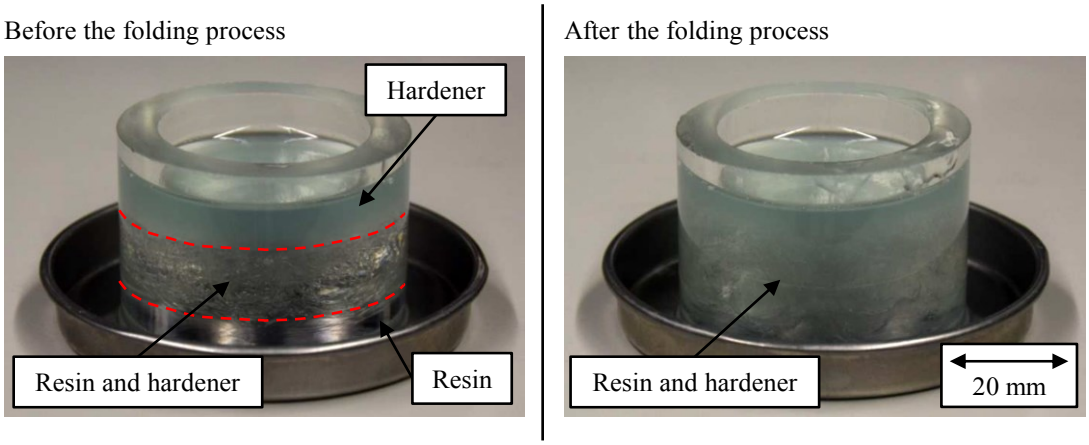

Fig. 3-7 Metered sample in mixing vessel before (left) and after (right) the folding process

Pre trails showed that sonication without the folding step leads to the splashing of the hardener without cavitation at the phase separated state (see Fig. 3-7, left). Since in this investigation the target is to analyze differences in the rheology of the thoroughly mixed resin system, the folding step is permitted.

Fig. 3-8 shows the resin system inside of a mixing vessel before, during and after the mixing by sonication. The treatment lasts 10 s. Since the thorough manual mixing takes 40 s with a wooden spatula, a dwell time of 30 s is added to the procedure of the sonicated samples to continue simultaneously (see Fig. 3-6).

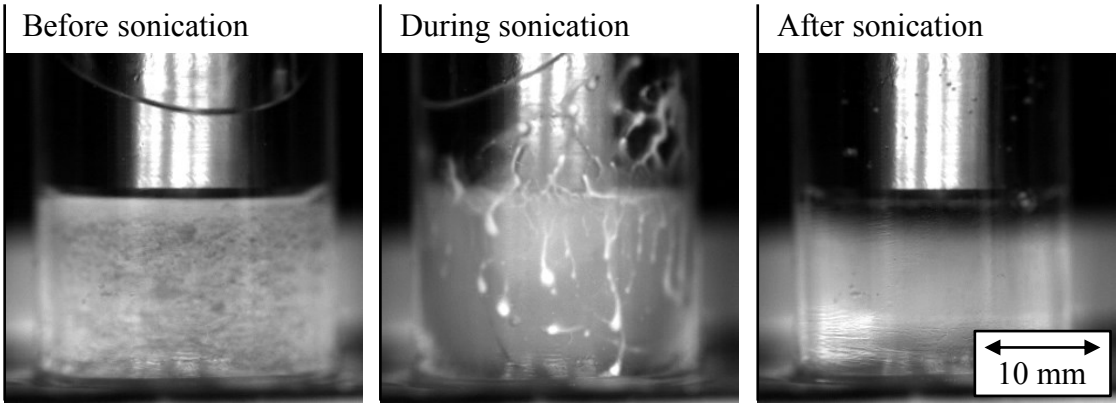

Fig. 3-8 **Before (left), during (middle) and after (right) mixing a two component resin system by sonication with a 15 mm diameter sonotrode dipped into the SMV**

Afterwards, a pipette is used to extract a sample of 0.5 cm³ off the mixing vessel and to position the sample in the rheometer (see Fig. 2-16). A plate-plate setup is used with a plate diameter of 25 mm and a gap size of one millimeter. The examination is conducted according to the standard DIN 1342-2 [96]. Two procedures are distinguished:

- Test procedure for the LMV samples:
  - A rotatory measurement is executed, until a dynamic viscosity of 2.50 Pa s is reached. The plates are heated to a temperature of 60 °C and rotate at a shear rate of 500 1/s. At this section the dynamic viscosity development of the sample is recorded. Meier [66] revealed a shear thinning behavior of RIM at shear rates below 100 1/s. To exclude an impact on the results by shear rate variations due to measurement inaccuracies a comparably high shear rate is selected.
  - An oscillatory measurement is performed subsequent, until the gelation of the resin system occurs. The measurement is performed at a temperature of 90 °C, a frequency of 10 Hz and a deformation rate of 1 %. The gel time is detected by this measurement.
- Test procedure for the SMV samples:
  - An oscillatory measurement is executed, until the gelation of the resin system occurs. The measurement is performed at a temperature of 60 °C, a frequency of 10 Hz and a deformation of 1 % to detect the gel time.

The parameter variation is revealed in Tab. 3-1. Hereby, two factors are varied: First, the amplitude is differed. For this, the resin system is placed in the LMV and sonicated with the HS. Second, the exposure time is changed. Hereby, the SMV and the UMHS are used.

Tab. 3-1 Parameter variation for the rheometer batch investigation

Mixing vessel	Mixing technique	A [µm]	t_{exp} [s]	Repetition [-]
LMV	HS	12.90	10	3
LMV	HS	25.86	10	3
LMV	HS	38.84	10	3
LMV	Manual	-	-	3
SMV	UMHS	53.71	10	3
SMV	UMHS	53.71	30	3
SMV	UMHS	53.71	50	4
SMV	Manual	-	-	3

Because of controlling procedures in the ultrasonic device, the values of sonication are not recorded by the device for the last second of sonication. Therefore, they are not available in the protocol. Due to the constant level of the parameter values before this lack of information, equal values are assumed for the last second.

3.2.2 Results of the rheology analysis

Fig. 3-9 shows the ultrasound power in the LMV sample at various amplitudes. After a sonication of three seconds the power shows steady values. The three times repetition at each amplitude show a sufficient repeatability of the trends.

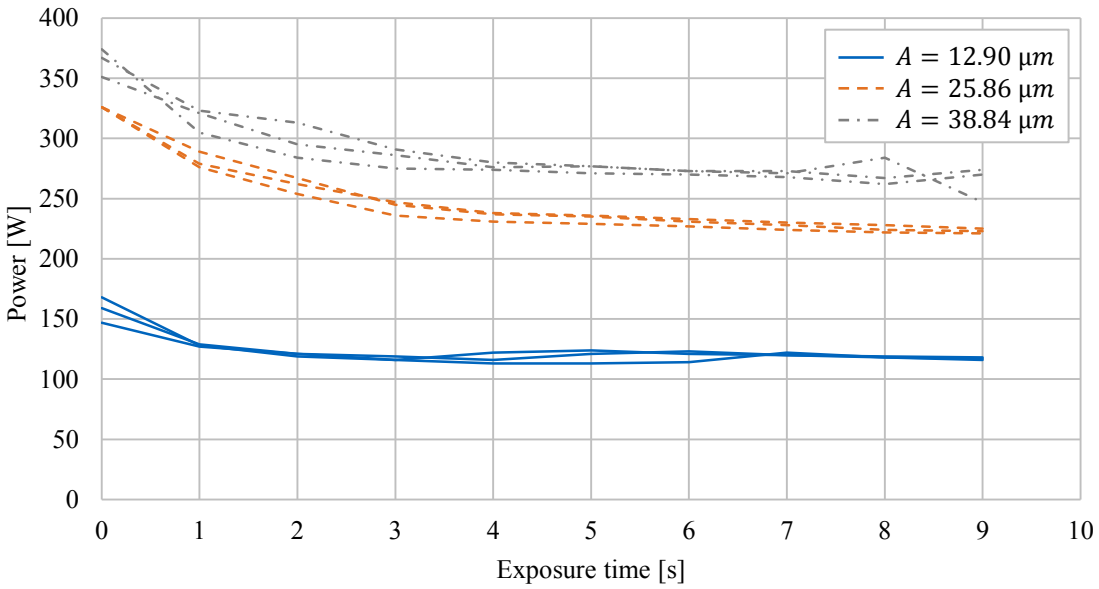

Fig. 3-9 **Power to exposure time plot at amplitudes of 12.90 µm, 25.86 µm and 38.84 µm in the LMV, three samples per setting**

The power values are similar to the power values of the cavitation zone measurement (see Fig. 3-5). However, the cavitation zone fills the entire mixing vessel (see Fig. 3-8). All SMV samples are sonicated at an amplitude of 53.71 µm and show steady power values of approximately 140 W to 150 W.

In Fig. 3-10, the dynamic viscosity developments of the LMV samples are plotted. Hereby, the slowest and the fastest viscosity increases are detected at the manually mixed samples.

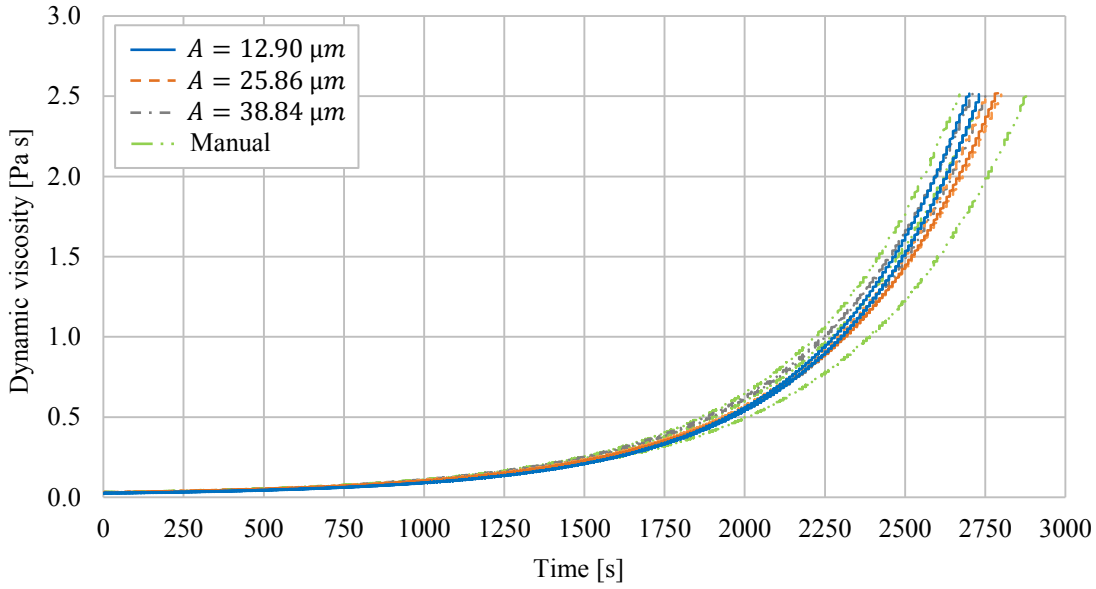

Fig. 3-10 Dynamic viscosity to time plot at amplitudes of 12.90 µm, 25.86 µm and 38.84 µm in the LMV, three samples per setting

Fontanier et al. [115] claim the upper dynamic viscosity limit of 1 Pa s for an injection. However the inject ability of a resin system depends on further parameters, like part geometry, filling concept, fiber volume fraction or fiber architecture. For this, no differences between the varying amplitudes and mixing techniques are significant as regards to the scattering of the repetitions.

Fig. 3-11 shows the gel time of both mixing techniques at different energy densities (see Eq. 2-3) and the standard deviation (see Eq. 2-4). Fig. 3-11 a) reveals the gel times of the samples produced in the LMV. Even though a significant variation between the energy densities 44.05 W s/cm³, 90.39 W s/cm³ and 103.10 W s/cm³ occurs, the difference of the AM is less than 2.60 %. Fig. 3-11 b) shows the gel times of the SMV samples. The energy densities achieved in this setup are more than ten times higher compared to those of the LMV. At an energy density of 3239.01 W s/cm³, a gel time reduction of 6.29 % is measured. At an energy density of 4924.50 W s/cm³, a gel time reduction of 24.50 % is measured referred to the AM at 1256.18 W s/cm³. The SD (see Eq. 2-4) of the samples is larger at higher energy densities.

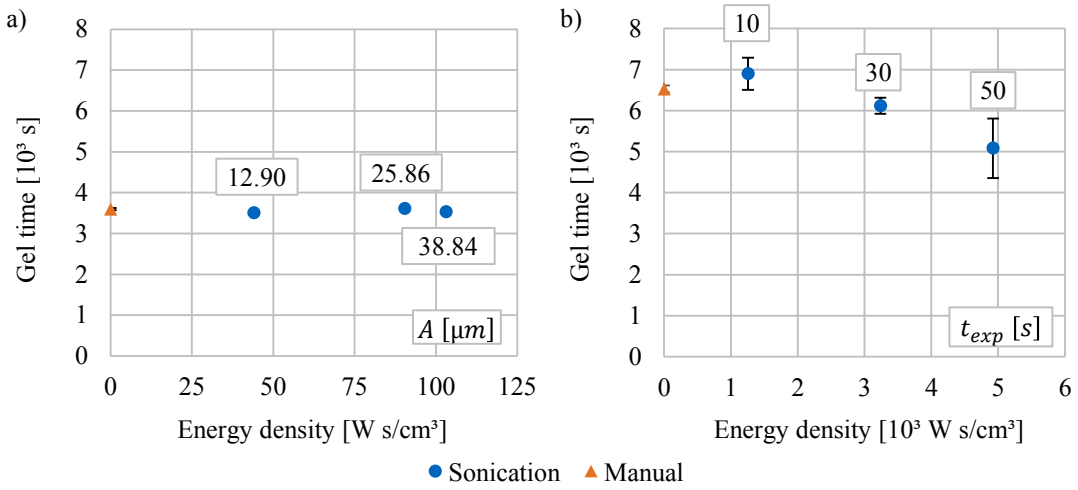

Fig. 3-11 **Gel time at various energy densities; results of amplitude variation in LMV (a) and exposure time variation in SMV (b) compared to manual mixing (HM)**

The sonication of the resin system comprises its heating. The increase of the temperature is not tracked due to the time sensitive handling after mixing. For this it is obvious but not quantified, that the acceleration of the reaction at energy densities of 3239.01 W s/cm³ and 4924.50 W s/cm³, is traced back to the temperature increase of the resin system during exposure. Quantitative correlations of amplitude, power and resin system temperature values are given in the results chapter of the process characteristics (see chapter 5.2) and the RTM characteristics (see chapter 6.2).

3.2.3 Interpretation of the rheology analysis

For the processing of a resin system mixed by sonication, the following conclusions are drawn from the rheology measurements in the laboratory investigation:

- Due to the low deviation at the dynamic viscosity inspections up to 2.50 Pa s, no difference in the filling behavior is expected during the injection of ultrasonically mixed resin systems compared to manually mixed resin systems.
- The gel times at a broad spectrum of energy densities from 44.05 W s/cm³ to 1256.18 W s/cm³ are similar to the manually mixed samples. This is independent of the adjusted parameter, amplitudes or exposure times.
- The gel time at an energy density of 3239.01 W s/cm³ and above is reduced. This is traced back to the sonochemical effect of the ultrasound cavitation, which leads to a heating of the resin system.

3.3 Thermal analysis of an ultrasonically mixed resin system

As third laboratory investigation the influence of ultrasonic waves on the thermal properties is examined during and after cure of a resin system. The target is to detect if the sonochemical effect of the cavitation influences the buildup of the network and/or the performance of the resin systems. Since the parameters detected by a DSC analysis are sensitive to the network structure (see chapter 2.4.2), this measurement technique is selected. In particular, three parameters are investigated: the initial glass transition temperature, the residual enthalpy and the final glass transition temperature (see Fig. 2-18). The physical basics of the measurement method and a specification of the DSC equipment are given in chapter 2.4.2.

3.3.1 Materials and methods for the thermal analysis

The sample fabrication, consisting of the metering, folding and mixing step is analogous to the LMV sample fabrication of the rheology inspection (see chapter 3.2). Thus, solely the variation after mixing is described in the following.

			Manual mixing			
Process	Metering	Folding	Sonication	Dwell	Storing	Measurement
Δt	30 s	30 s	10 s	30 s	50 days	98 min

Fig. 3-12 Sample preparation procedure of the thermal investigation

After mixing, the sample is directly stored in a freezer at -5 °C to prohibit a further reaction of the resin system and to enable a randomization of the experiment run order. The water uptake of the samples during freezing and unfreezing is prohibited by using hermetical closing bags.

Then a sample is defreezed and a mass of approximately 10 mg is placed in an aluminum pan. Afterwards, the pan is positioned in the DSC.

The examination is conducted according to the standard DIN EN ISO 11357 [102]. The program consists of two cycles. It starts isothermal at a temperature of -10 °C for 5 min followed by a 10 °C/min ramp to a temperature of 270 °C. This temperature is held for 2 min. After a 10 °C/min descent down to a temperature of -10 °C, the second cycle is equally performed. The procedure to calculate the initial glass transition temperature $T_{g\ initial}$, the residual enthalpy ΔH_{res} and the final glass transition temperature $T_{g\ final}$ are described in chapter 2.4.2. An exemplary heat flow which is detected during this program is shown in Fig. 2-18.

Menczel and Prime [116] detected degradation effects at samples cured above the final glass transition temperature. Further, Carbas et al. [117] correlated high curing temper-

atures and low final glass transition temperatures. Thus, the peak temperature of 270 °C is applied for 2 min only to exclude a degradation of the resin system during the first cycle. Preliminary tests are performed. Thereby, a five time repetition of the procedure shows no reduction of the final glass transition temperature throughout the test.

The parameter variation for the thermal investigation is listed in Tab. 3-2. Hereby, the amplitude is altered. To detect the maximum enthalpy in a sample, an additional sample is directly tested after the manual mixing.

Tab. 3-2 Parameter variation for the DSC batch investigation

Mixing vessel	Mixing technique	Repetition [-]	Storage at -5 °C	A [µm]	t_{exp} [s]	ρ_E [W s/cm³]
LMV	HS	3	Yes	12.90	10	43.32
LMV	HS	3	Yes	19.55	10	65.34
LMV	HS	3	Yes	25.86	10	86.09
LMV	HS	3	Yes	32.58	10	87.00
LMV	HS	3	Yes	38.84	10	104.21
LMV	Manual	3	Yes	-	-	-
LMV	Manual	1	No	-	-	-

It should be noted that, due to the variation of the exposure time and the coupling of amplitude and power value, different amplitudes go along with different energy densities (see Tab. 3-2). The given energy density values are the AM of the repetitions.

3.3.2 Results of the thermal analysis

In Fig. 3-13 the residual enthalpies of the ultrasonically and manually mixed samples are plotted. The values of the ultrasonically mixed samples are at a similar level as the manually mixed samples at amplitudes of 12.91 µm, 25.86 µm and 32.58 µm. However, the residual enthalpies of the ultrasonically mixed samples are elevated at amplitudes of 19.55 µm and 38.84 µm.

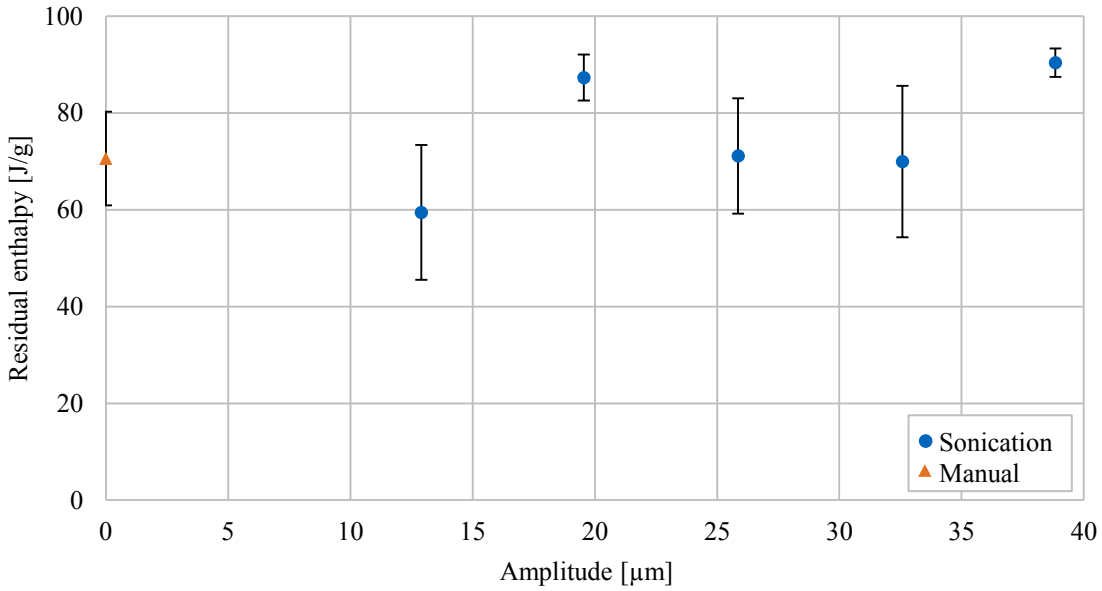

Fig. 3-13 Residual enthalpy of samples mixed at various amplitudes in the LMV compared to manually mixed samples

The manually mixed and directly measured sample showed an enthalpy of 466 J/g. This means that the storage in the refrigerator leads to a residual enthalpy of less than 21 % of the overall enthalpy in the resin system. The comparably elevated AM at amplitudes of 19.55 µm and 38.84 µm are traced back to inaccuracies during the freezing and unfreezing of the samples.

Fig. 3-14 shows both the initial glass transition temperature after storing and the final glass transition temperature after curing. The initial glass transition temperature slightly decreases with increasing amplitudes compared to the manually mixed samples. On the contrary the final glass transition temperature is higher for the ultrasonically mixed samples compared to the manually mixed reference. At the highest amplitude, an AM final glass transition temperature of 91 °C occurs.

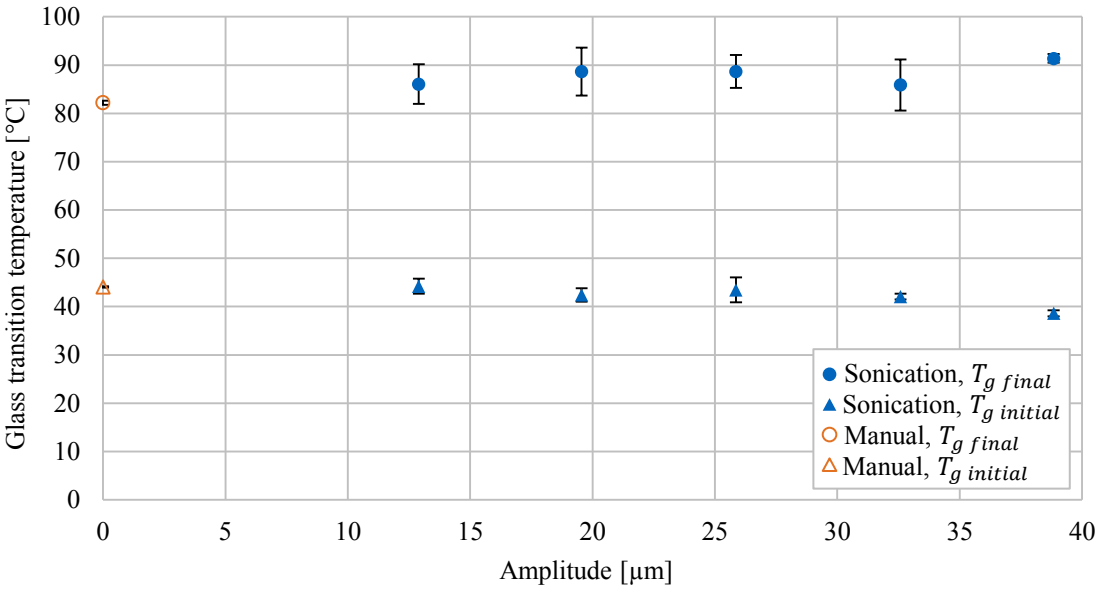

Fig. 3-14 **Initial and final glass transition temperatures of samples mixed at various amplitudes in the LMV**

According to the data sheet, a maximum final glass transition temperature of approximately 82 °C is reached after curing the resin system at 60 °C for 25 hours. Even though a measurement deviation of approximately 1 °C has to be taken into account, the increase of the final glass transition temperatures at the highest amplitude is distinctive. The higher temperature until the glass transition is traced back to a more homogeneous, tightly interconnected polymer network. This efficient interlocking could occur due to a more accurate positioning of the reactive partners at high amplitudes. Thereby the diffusion distance of the molecules is shorted and the creation of a homogeneous, tightly interconnected polymer network is enabled. The initial glass transition temperatures are not elevated. This indicates, that no notable earlier interlocking takes place. This finding is consistent with Ellis [60]. He claims, that the molecular size, representing the number of interlocks, is still small after half of the reaction.

3.3.3 Interpretation of the thermal analysis

The following conclusions are drawn from the thermal analysis of a resin system exposed to sonication in a mixing vessel:

- No influence of the sonication on the residual enthalpy is measured. The residual enthalpy is mainly reduced of all samples due to their storage in the freezer before the measurement.
- The final glass transition temperature is not reduced by the sonication of a resin system. A slightly increased final glass transition temperature is measured at high amplitudes.

4 Development of an Ultrasonic Mixing Head for injection processes

The development of an Ultrasonic Mixing Head (UMH) is based on concepts derived from the 'theory of inventive problem solving' (TRIZ) by Altschuller. The creation process (see chapter 4.1) is revealed and a function analysis is executed (see chapter 4.1.1). Further, the implementation of the concept into structural features of the UMH is described. Hereby, the sonotrode design is deduced from a finite element method (FEM) analysis (see chapter 4.2.2).

4.1 Concept development

G. Altschuller developed the 'theory of inventive problem solving'. This is as the Russian acronym TRIZ. Hua et al. [118] described it as "a problem-solving, analysis and forecasting tool derived from the study of patterns of invention in the global patent literature". Between 1946 and 1985, Altschuller and colleagues analyzed more than three million patents according to patterns and predicted the breakthrough solutions to problems. The research proceeded over the last sixty years and its three primary findings are as follows [119]:

- Problems and solutions are repeated across industries and sciences. The classification of the contradictions in each problem predicts the creative solutions to that problem.
- Patterns of technical evolution are repeated across industries and sciences.
- Creative innovations use scientific effects outside the field where they were developed.

Altschuller published his theories in several books [120–122]. The TRIZ journal further published numerous investigations on his theories in the fields of business, architecture, food, quality management or software. An overview of the basic tools of TRIZ is given by Mann [123]. Hereby, a problem is abstracted to a generic problem solving framework. The task is to put the specific problems and solutions to and away from the generic framework according the creativity of the user (see Fig. 4-1).

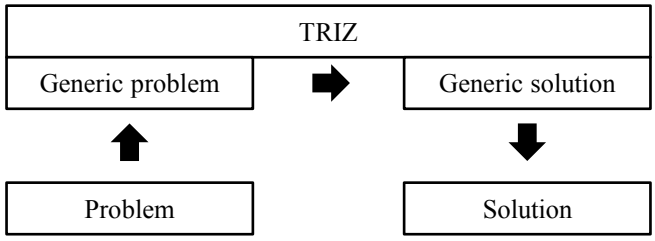

Fig. 4-1 Problem analogous to solving a problem with TRIZ (similar [47])

As revealed in the motivation (see chapter 1.3) and outline (see chapter 1.4) of this thesis, its target is the establishment of the physical phenomenon of ultrasound cavitation as mixing principle in RTM. Thus, the deficits of currently applied mixing technologies can be compensated. For this, the use of TRIZ is assumed as appropriate.

4.1.1 Function analysis of the injection process

One of the TRIZ tools is the function analysis, which targets a function map of an engineering system. The function map is used to understand the system and to highlight problem areas and issues. Thus, it gives an overview of how to prioritize and solve problems. Hereby, the function map consists of components, functions and contradictions of a system. In this thesis, the analyzed system is a state of the art Static Mixing Head (SMH) which is utilized for low pressure RTM (see chapter 2.2.4). This system is selected, because of the aim to utilize the UMH for low pressure RTM, too. The procedure to execute the function analysis follows Lindemann's theory [124]. To map, analyze and improve a system, the following steps are necessary:

- Component analysis: the relevant elements within the technical system (target) and super system (environment) are determined.
- Interaction analysis: the interaction between elements are analyzed
- Function modelling: the function performed by the elements are modelled and emphasized.

4.1.1.1 Component analysis

In this chapter, the components of the technical system are identified. Further the elements of the super system which interacts with the elements of the technical system are described. Fig. 4-2 shows an overview of the component analysis. Hereby the mixing head (technical system) mixes (changes) the resin system (target).

The injection machine (super system) is divided into four elements:

- Metering device (see chapter 2.3.2) describes the part of the injection machine where the components of the resin system are stored in separate reservoirs. Further, the components are tempered and metered by this device.
- Mold (see chapter 2.2.4) designates a rigid, heated tool equipped with a preform. The cavity is filled with resin system during the injection.

- Impurity is the hypernym to describe the environmental contamination of the mixing head and the injection machine.
- Inspection describes the examination of the part quality to verify the metering and mixing processes.

The mixing head (technical system) is divided in six elements:

- Mixing device is the volume which comprises shear elements to mix the resin components.
- Feeder defines the start and the end of an injection by being open during the injection and closed otherwise.
- Heating describes the electrical heating device at the mixing head, which tempers the resin components and mixed resin.
- Inlet and outlet are used to guide the resin components into and the resin system out of the mixing chamber.
- Sealing is the hypernym to describe the features which prevent the SMH from leaking.
- Cleaning describes the process of flushing the SMH with a solvent after each injection (see chapter 2.2.5.2).

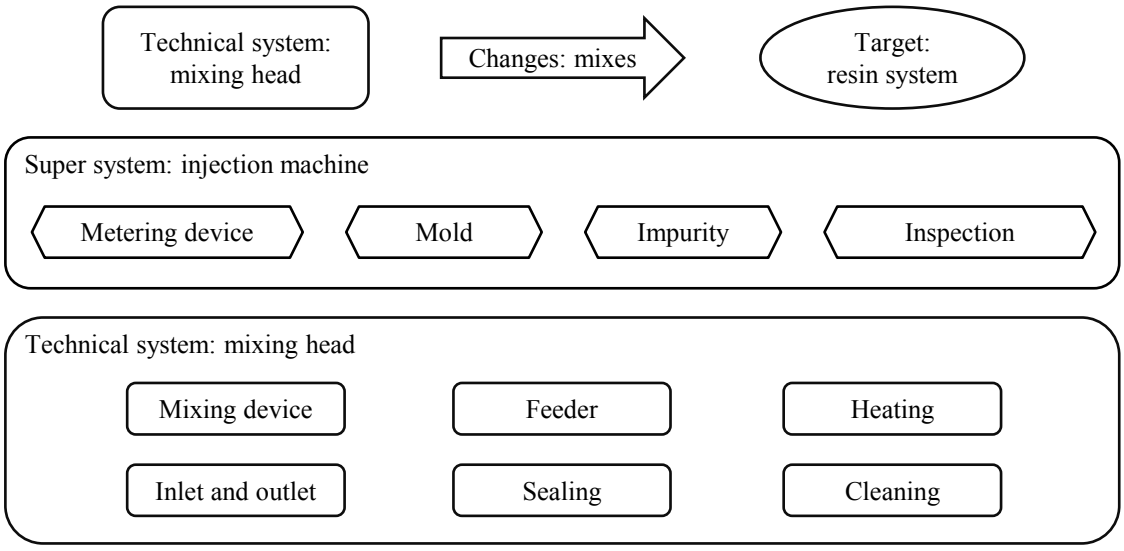

Fig. 4-2 Component analysis of the low pressure injection machine

4.1.1.2 Interaction analysis

In this chapter of the function analysis, the interaction between the elements of the technical system, the elements of the super system and the target is identified. In Tab. 4-1, the interactions are listed. The result is a square, symmetric table. The interactions are based on the injection technology (see chapter 2.2) and the low pressure RTM technology (see chapter 2.2.5.2). The mixing device features most interactions of the technical system elements.

Tab. 4-1 Element interaction of the technical system, super system and target; + interaction, - no interaction

	Technical system						Super system				Target
	Mixing device	Inlet and outlet	Feeder	Sealing	Heating	Cleaning	Metering device	Mold	Impurity	Inspection	Resin system
Mixing device	0	-	-	+	+	+	+	-	+	+	+
Inlet and outlet	-	0	-	-	+	-	-	-	+	-	-
Feeder	-	-	0	-	+	-	+	-	+	-	-
Sealing	+	-	-	0	+	+	-	-	+	-	+
Heating	+	+	+	+	0	-	-	-	-	-	+
Cleaning	+	-	-	+	-	0	-	-	-	-	+
Metering device	+	-	+	-	-	-	0	+	+	+	+
Mold	-	-	-	-	-	-	+	0	-	-	+
Impurity	+	+	+	+	-	-	+	-	0	-	+
Inspection	+	-	-	-	-	-	+	-	-	0	+
Resin system	+	-	-	+	+	+	+	+	+	+	0
Interactions	7	2	3	5	5	3	6	2	6	3	8

4.1.1.3 Function modelling

In this step, the function model is drafted. Interactions identified in chapter 4.1.1.2 are transferred to a function consisting of three parts [125] (see Fig. 4-3): First, the subject element is the initiator of an action or influence within a system. It represents the provider of the function. Second, the object element is the passive receiver of an action or influence within a system changed by the former action. The action or influence describes the effect of the subject on the object in a particular field, e.g. mechanical, thermal, electrical or magnetic. Third, the Harvard simple approach further specifies the effect on the object by distinguishing between a useful, useful but insufficient and harmful action.

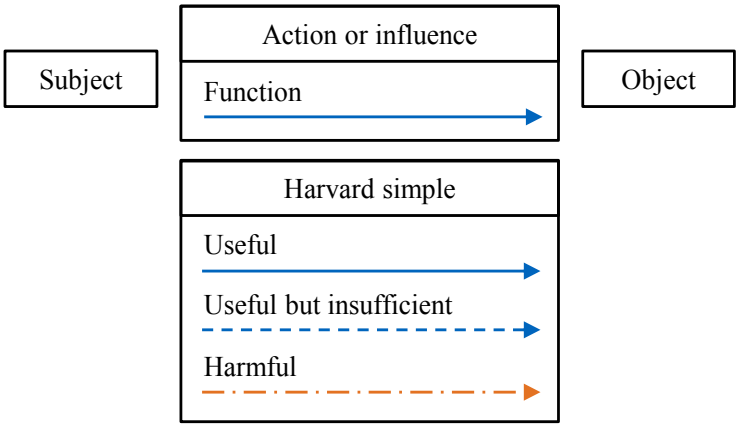

Fig. 4-3 Function definition according to TRIZ

The resulting function model of the SMH is revealed in Fig. 4-4.

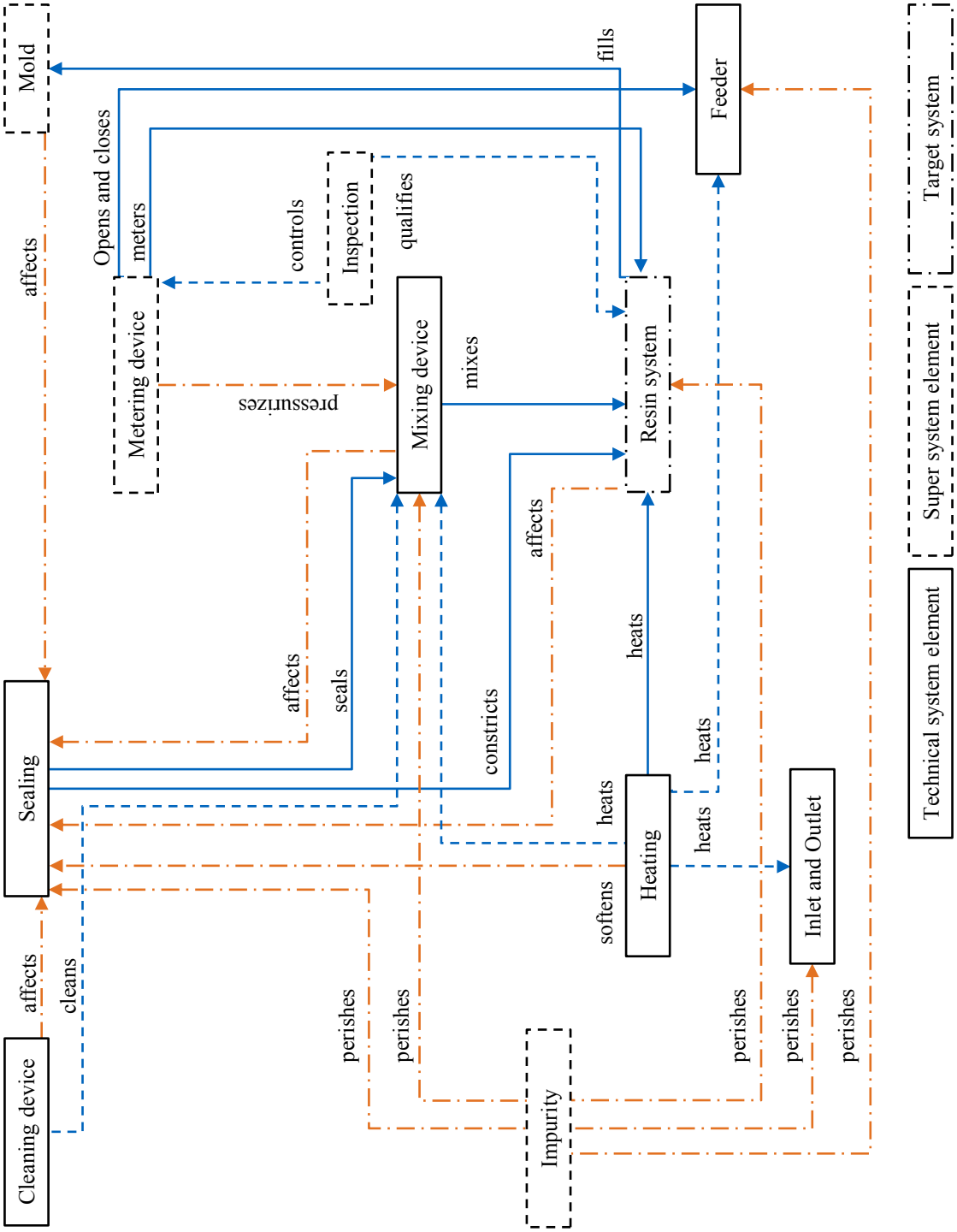

Fig. 4-4 Function model of the state of the art Static Mixing Head (SMH)

Hereby, each element interaction (see Tab. 4-1) is transferred to a function. Based on this model, four functions are identified which can be performed by the ultrasound technology (see chapter 2.1). The realization of these functions with reference to the state of the art is pointed out in the following (see Fig. 4-5):

- Mixing:
  - Low pressure mixing heads use shear elements to divide and merge the resin components.
  - High pressure mixing heads inject the resin components at a high pressure into the mixing head. Hereby, tubular streaming is used.
- Cleaning:
  - Low pressure mixing heads use a solvent to flush the mixing device or replace the chamber instead.
  - High pressure mixing heads use a piston movement to clean the mixing chamber.
- Heating:
  - Currently both, low pressure RTM and high pressure RTM use electrical heating systems. Hereby, either the resin component line alone or all component lines are heated from the reservoir until the mixing head.
- Inspection:
  - Both low pressure RTM and high pressure RTM use an inspection of the cured resin system to evaluate the quality of the metering and mixing process.

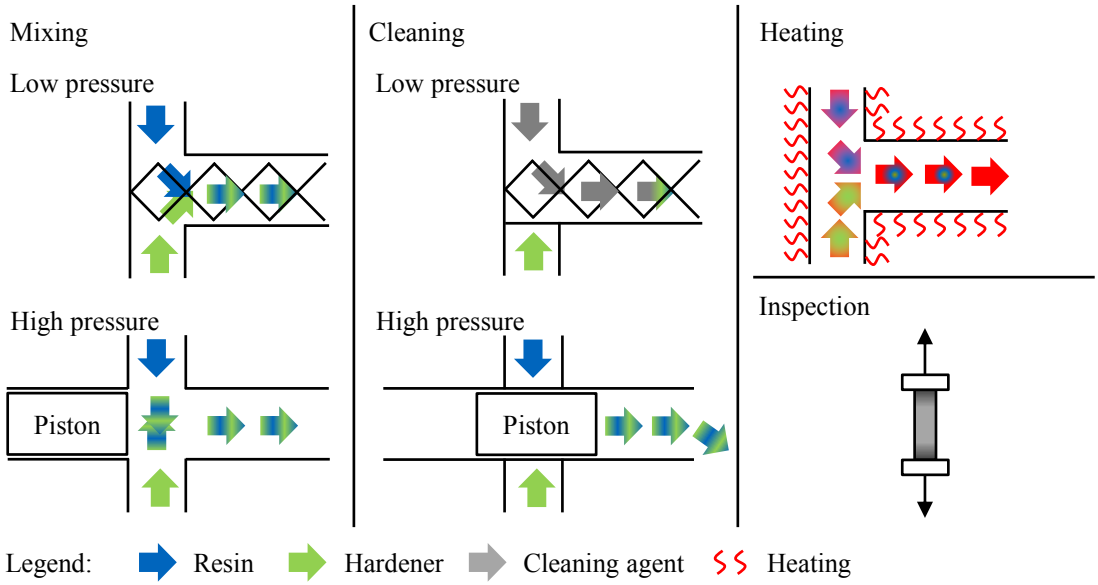

Fig. 4-5 State of the art solutions for the functions of mixing heads for RTM

To optimize the state of the art SMH, the trimming method is utilized. Hereby, the function of an element is performed by another technical system element or super system element. As described in chapter 2.1 the ultrasound technology activates the resin system.

The following elements are trimmed or enhanced:

- The cleaning device is trimmed since the mixing effect occurs without the attendance of shear elements. Therefore, a self-cleaning process similar to the cleaning of high pressure mixing heads is performed. This is done by the mixing device itself.
- The heating device is trimmed since the sonochemical effect of ultrasound cavitation leads to a temperature increase of the resin system during the occurrence of transient cavitation. This heat effect is utilized to trim the heating device. Further the heating of the periphery of the technical system: the feeder, the mixing device and the inlet and outlet could be replaced.
- The inspection method is enhanced. The solely inspection of the final part is ineffective to evaluate the resin system mixing and metering processes since hereby, the properties of the fiber and the composite system overlie the resin system properties. When utilizing the ultrasound technology, two new mixing parameter are available: amplitude and power. An online measurement of these parameters should be used to determine the resin system quality after metering and mixing.

Fig. 4-6 shows the function model of the UMH. Hereby the cleaning device, the heating device and an additional inspection method are integrated as functions of the mixing device.

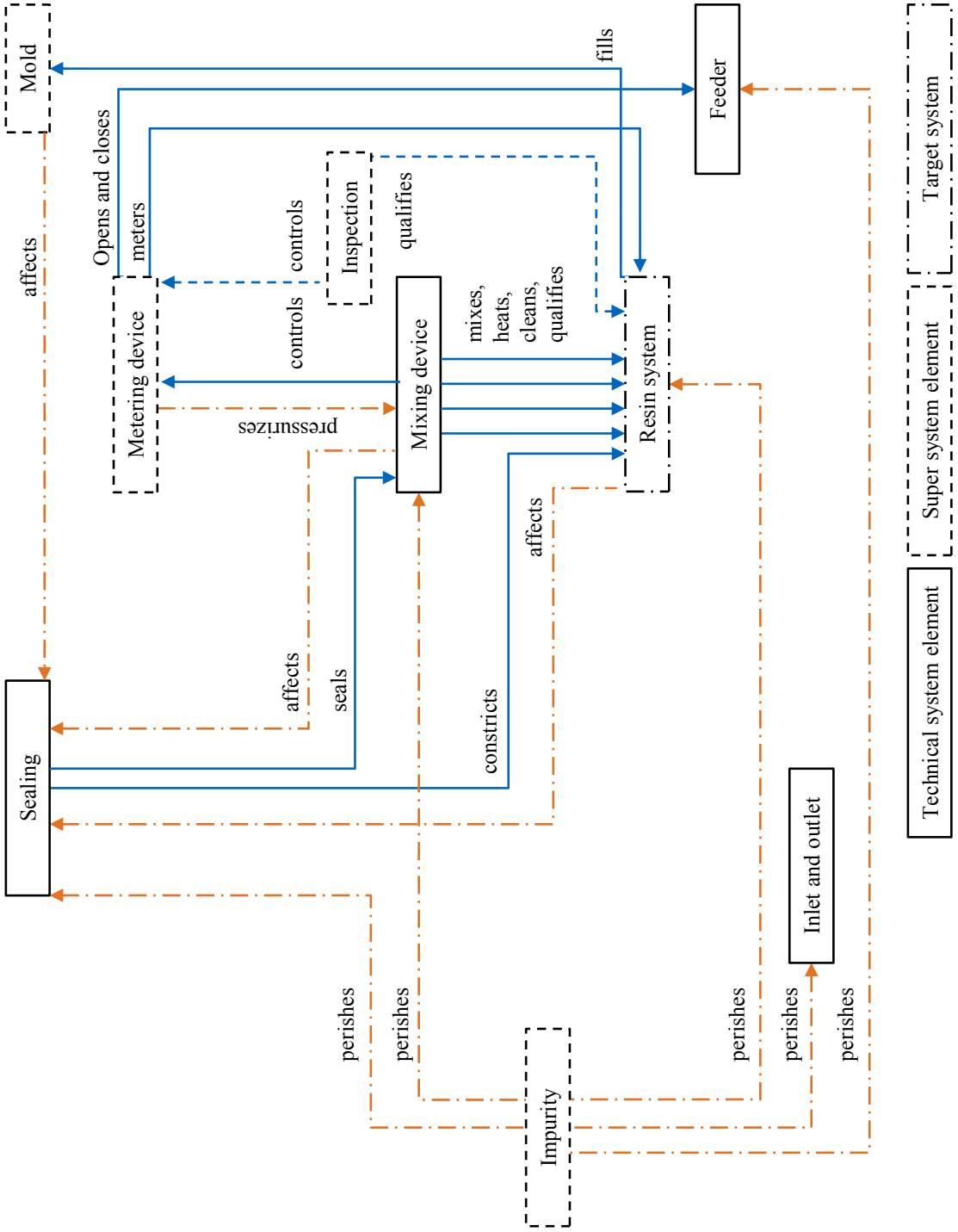

Fig. 4-6 **Trimmed function model of the Ultrasonic Mixing Head (UMH) including the incremental improvement approach; it replaces the state of the art Static Mixing Head (SMH)**

4.1.2 Integration into an Ultrasonic Mixing Head

Three aspects are examined to implement the concept based on the function analysis in a mixing head: First, the method to transfer the ultrasonic movement of the sonotrode to the flowing resin system is investigated (see chapter 4.1.2.1). Second, the sealing concept to ensure fluid and vacuum tightness of the UMH is inspected (see chapter 4.1.2.2). Third, the integration of the concept into the RTM injection cycle is accomplished (see chapter 4.1.2.3).

4.1.2.1 Ultrasound coupling

The transfer of the ultrasonic movement from the sonotrode to the resin system can be distinguished by the propagation direction of the ultrasonic waves in relation to the flow direction (see Fig. 4-7):

- First, a sonication from the back side of the chamber is taken into account. The wave propagation direction is in parallel to the resin system flow direction in this case. The sonotrode is in direct contact with the resin system. The cavitation zone development is expected to be similar to the one that is analyzed in the laboratory investigation (see chapter 3.1). The sealing between the sonotrode and the chamber case of the mixing head is highly loaded, since it has to withstand a pressure load during the injection. Hereby, the friction caused by the ultrasonic movement of the sonotrode is added to the pressure of the resin system.
- Second, a coupling from the side wall occurs and waves are released. Their propagation direction runs perpendicular to the resin system flow direction. Since the movement provided by the ultrasonic device goes back and forth instead of concentrically, the amplitudes are not equal with the cross section. Due to the results of the cavitation zone measurements (see chapter 3.1), it is assumed that this inconsistency would lead to a varying distribution of cavitation bubbles at the cross section. The sonotrode is fixed on the outer side wall. For this, the welding seam between the sonotrode and the outer side wall is critical. Since this area of the side wall transfers the ultrasonic waves to the resin system, not solely the sonotrode, but the sonotrode in conjunction with the side wall has to be stimulated at a specific frequency of the ultrasonic device. A sealing between sonotrode and side wall is not practicable due to the circular cross section. A rectangular sonotrode front end in conjunction with a flat mixing chamber could be utilized to overcome this issue. In this case, the sonotrode front end itself would lead to inhomogeneous amplitudes due to its non concentric design.

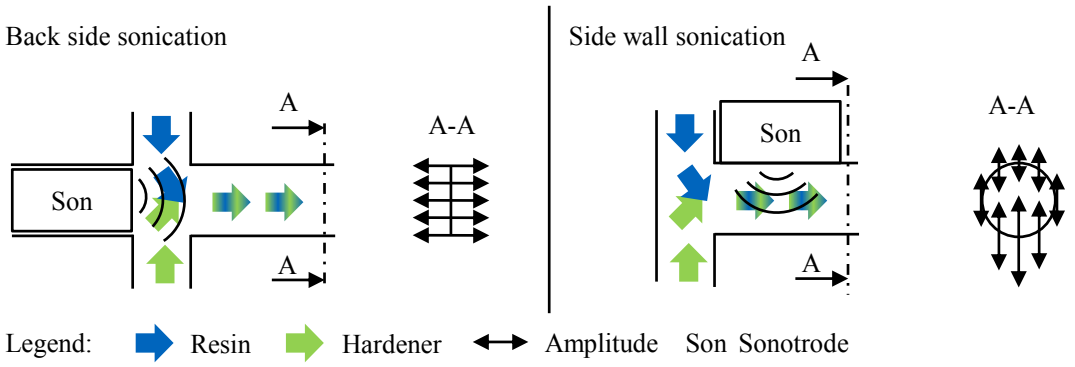

Fig. 4-7 **Back side sonication (left) and side wall sonication (right) of the ultrasonic device for the coupling of the ultrasonic wave in the resin components**

Because the occurrence of the cavitation bubbles depends on the amplitude the back side stimulation is selected. This method leads to equal amplitudes in the entire cross sectional area. Further, it is assumed that a direct coupling of the sonotrode and the resin system is more efficient since the stimulation of the side wall in addition to the sonotrode is eliminated.

4.1.2.2 Sealing concept

The sealing is identified as a critical aspect of the back side coupling method (see chapter 4.1.2.1). The friction caused by the ultrasound movement in addition to the pressure of the resin system load the sealing. To withstand the pressure load, a concept with two O-rings is applied (see Fig. 4-8). Hereby, their positioning in relation to the oscillating sonotrode is crucial. The sonotrode moves longitudinally in the shape of halve a sinus wave. The sonotrode end planes execute the maximum movement. This means that a knot of oscillation appears between the end planes. The first sealing P_1 is positioned at this particular point since no relative movement between sonotrode and chamber wall occurs. The second sealing P_2 is positioned at the front end plane of the sonotrode. This sealing serves as a barrier for the resin system. If the resin system cures at the shell surface of the sonotrode, the sonotrode movement would be inhibited afterwards.

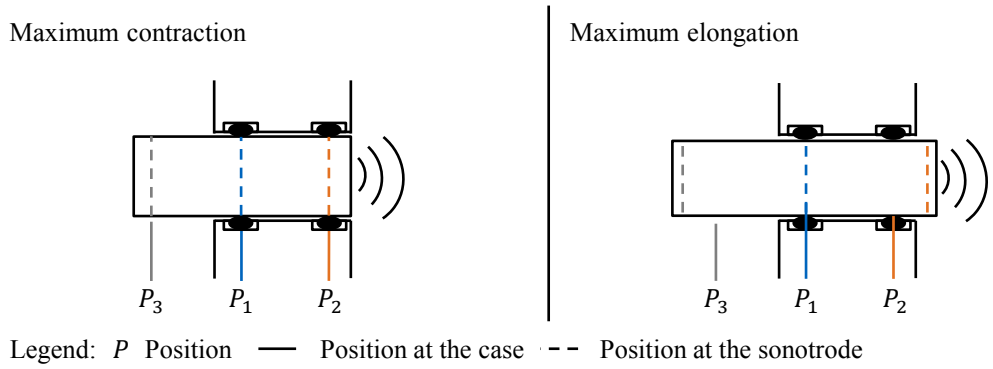

Fig. 4-8 **Sealing position P_1 and P_2 at the chamber and sonotrode during maximum contraction (left) and elongation (right)**

In Fig. 4-8, an idealized knot position is visible. This cuts a cylindrical sonotrode into halves. The real location of the oscillation knot is revealed in the modal analysis of the sonotrode described in chapter 4.2.2.

4.1.2.3 Implementation of the Ultrasonic Mixing Head concept into the RTM procedure

Fig. 4-9 shows the final concept of the UMH, which has its foundation in the function analysis (see chapter 4.1.1). Further the back side stimulation (see chapter 4.1.2.1) as well as the sealing concept (see chapter 4.1.2.2) is integrated. Dependent on the respective process step of the RTM cycle, two positions of the sonotrode are distinguished (see Fig. 4-9):

- Injection: During the injection process, the resin system components are continuously fed in the chamber by the metering device. The sonotrode at the back side of the chamber couples ultrasonic waves in the resin system, which leads to cavitation. After the components are mixed and heated, the resin system flows into the cavity of the mold.
- Ejection: The resin system within the mixing chamber is either demolded as a neat resin area attached to the cured part or the resin system is ejected into the cavity before curing. For this, the sonotrode is used as an ejection piston and moves along the mixing chamber and no neat resin spot remains.

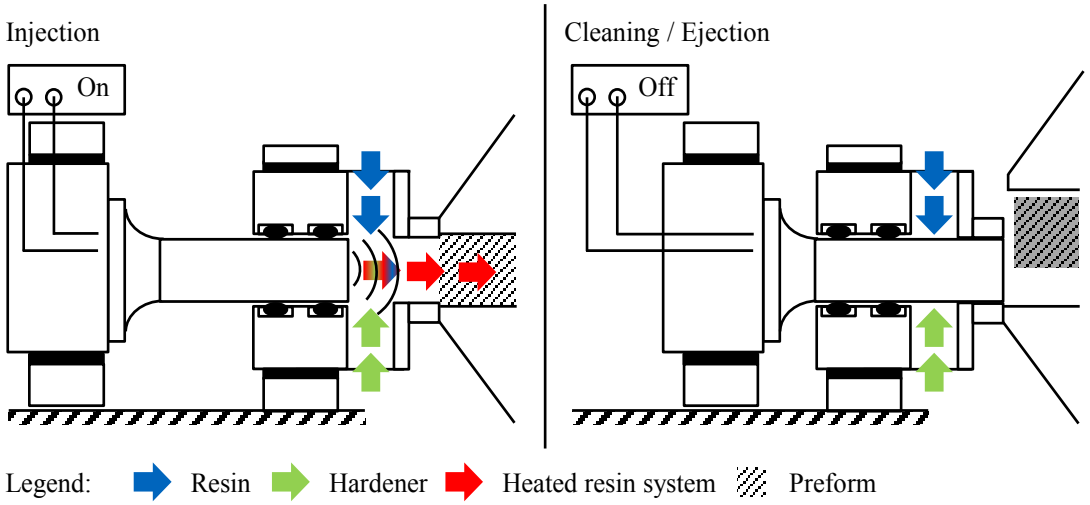

Fig. 4-9 **Concept of the UMH: Integrating the mixing, heating and control device in an element**

4.2 Construction of the Ultrasonic Mixing Head

As main considerations for the process specifications of the UMH, the feasibility, the results of the laboratory investigations with the HS (see chapter 3) and the RTM injection requirements (see chapter 2.2) are taken into account. The following process parameters are specified for the UMH thereof:

- Volume flow from 50 cm³/min to 150 cm³/min
- Maximum injection pressure of 20 bar
- Maximum resin component temperature of 80 °C

The sonotrode is identified as main item of the UMH. For this, two aspects of its construction are examined: First, the sonotrode diameter influencing the chamber volume is considered. Second, a FEM modal analysis is executed, to realize the punctual sealing concept (see chapter 4.1.2.2)

4.2.1 Definition of the sonotrode diameter

The diameter of the sonotrode is derived from the resulting exposure time within the UMH. This parameter indicates the time of the resin system being exposed to ultrasound during the flow through the mixing chamber. Based on the results in chapter 3.1, a minimum exposure time of one second is assumed as sufficient to build a stable cavitation zone. Fig. 4-10 shows the exposure time at various sonotrode diameters and lengths of the cavitation zone at a volume flow of 50 cm³/min and 150 cm³/min. Hereby, a diameter of 15 mm is identified as suitable for the UMH. To ensure an exposure time of one second at a volume flow of 50 cm³/min, a cavitation zone length of 5 mm (see Fig. 4-10 a)) is mandatory. If the resin system should be in the cavitation zone for one second at a volume flow of 150 cm³/min, a cavitation length of 15 mm (see

Fig. 4-10 b)) is required. Based on the cavitation zone developments measured in chapter 3.1, it is assumed that this lengthwise extension of the cavitation zone is creatable during the injection.

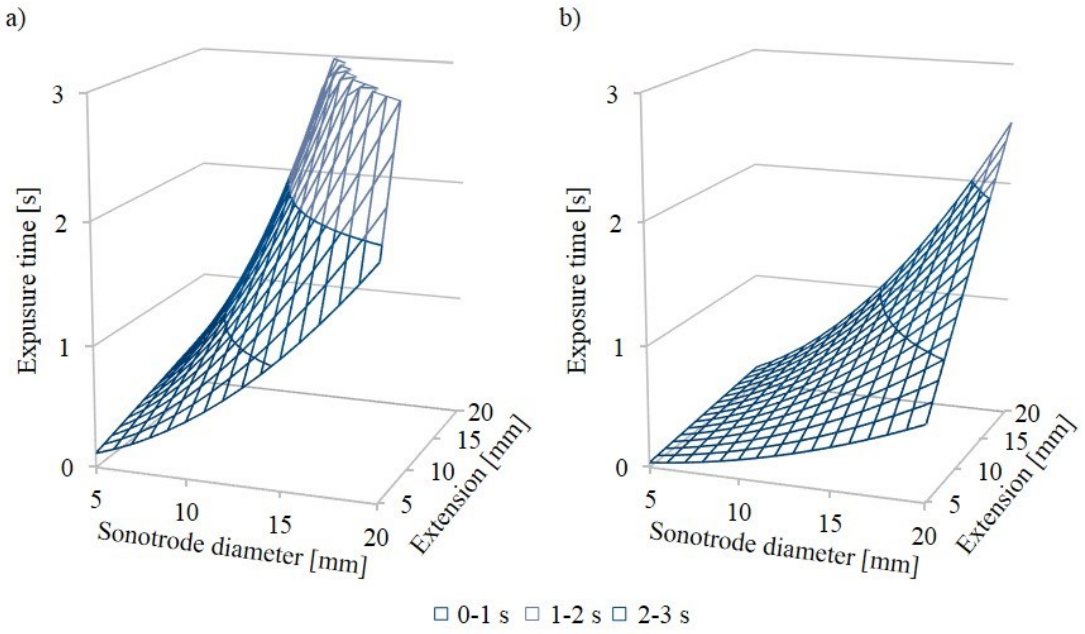

Fig. 4-10 Correlations between sonotrode diameter, chamber length and exposure time at a volume flow of 50 cm³/min a) and 150 cm³/min b)

The selection of a smaller sonotrode diameter would lead to an exposure time of less than one second at a high volume flow and therefore, to potentially insufficient mixing. A larger sonotrode diameter comes along with a higher effort (power) of the ultrasonic device to realize the movement. In particular, the increase of the power caused by an increase of the pressure within the sonicated fluid is unknown in the literature. Since in this thesis, injection pressure of 20 bar are conceivable, a rather small sonotrode diameter is preferred. As a compromise, a sonotrode diameter of 15 mm is selected.

4.2.2 Modal analysis of the Ultrasonic Mixing Head sonotrode

In this chapter, the Finite Element Method (FEM) to design the sonotrode, which is then implemented in the UMH, is carried out. A modal analysis determines the natural frequencies as well as the corresponding modes of a structure [53, 126] . Hereby, two sonotrodes are evaluated: The analysis of the Hielscher sonotrode (HS) serves as a reference for the simulation procedure. The design of the Ultrasonic Mixing Head sonotrode (UMHS) is based on the identical simulation procedure.

The modal analysis of the sonotrodes are described simultaneously, even though the geometry of the HS existed beforehand. The geometry of the UMHS is finalized by an

iterative calculation loop. The UMH concept (see chapter 4.1) and the ultrasound technology (see chapter 2.1) lead to restrictions for the design of the sonotrode:

- The sonotrode must own a natural frequency mode of approximately 20 kHz. This frequency is detected as most efficient for the formation of transient cavitation [55, 114]. In addition, ultrasound generator and transducer (see chapter 2.3.1) are designed for the sonication at a frequency of 20 kHz and can stimulate a sonotrode exclusively in a spectrum from 19 to 21 kHz.
- The mode of the sonotrode at 20 kHz has to execute a longitudinal oscillation. Torsional or flexural sonotrode movements could damage the ultrasonic device.
- A node of oscillation has to exist at the cylindrical part of the sonotrode. This enables to position the sealing at a point without a relative movement between the sonotrode and the UMH (see chapter 4.1.2.2).
- An ejection of the mixed resin system has to be enabled after its injection by a sonotrode movement (see Fig. 4-9). Therefore, the length of the cylindrical section is critical between P_1 and P_3 (see Fig. 4-8).
- The front end plane must oscillate at amplitudes of more than 30 µm similar to the amplitude range of the HS (see Tab. A-1).

Since, for the HS sonotrode, the composition of the titan material is not known, the modal analysis for both sonotrodes is performed with titan grade 2 ($Ti2$) [127] (see Tab. A-9) as well as titan grade 5 ($Ti5$) [128] (see Tab. A-10).

4.2.2.1 Preprocessing of the modal analysis

The geometries of the sonotrodes are designed with the computer-aided design (CAD) software CATIA V5R21. The simulation is carried out with the modal analysis tool of Ansys workbench 14.5.7.

Al-Budairi [32] designed and analyzed an ultrasonic sonotrode for longitudinal and torsional vibrations. He recommends tetrahedral elements for the complex geometries of the sonotrode. Therefore, area-related, tetrahedral elements are selected for the mesh in this thesis. A structural solid element, SOLID187 consisting of ten nodes, is picked. This element type fits particularly for the modeling of irregular meshes built in CAD systems [126].

Fig. 4-11 shows the meshed geometry of both sonotrodes. In either case it is structured according to organized plains and is automatically created. The HS mesh (see Fig. 4-11 a)) consists of 14815 elements covering the cylindrical parts at both sides, the flange in the middle and the connection to the transducer. The UMHS mesh (see Fig. 4-11 b)) consists of 28464 elements and three sections: the cylindrical part at the front, a larger diameter section including a plane area to locate an open-end spanner, and a thread at the back for the connection to the transducer.

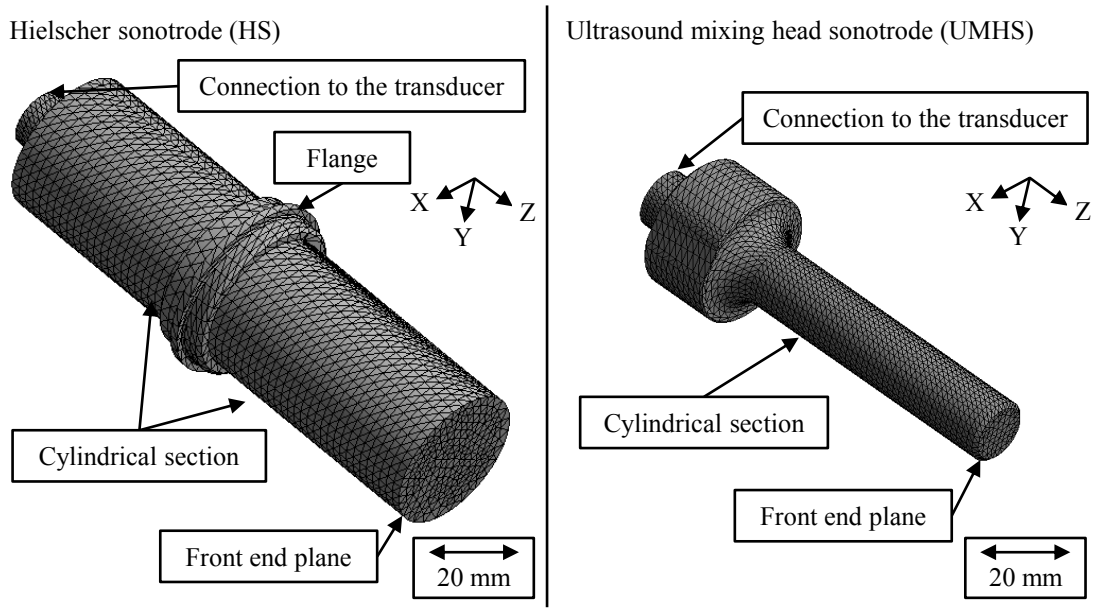

Fig. 4-11 Tetrahedral mesh of the Hielscher sonotrode (HS) and Ultrasonic Mixing Head sonotrode (UMHS)

A dense mesh typically results in a more accurate solution. Here, the computation time increases, too. Since the computation time is not critical for the simulation of the sonotrodes, a fine mesh is selected for the simulation.

4.2.2.2 Solver of the modal analysis

The simulations are processed by a Windows 7, 64 Bit system with 6 GB main memory and an Intel® Core™ i5-2467M CPU processor at 2.54 GHz.

For the modal analysis, the frequency domain is limited from 10 kHz to 30 kHz and to a maximum of 8 modes. The PCG Lanczos Eigensolver is used to compute the eigenvalues and eigenvectors since this solver is designed for the detection of less than 100 modes [126].

4.2.2.3 Postprocessing of the modal analysis

Fig. 4-12 reveals the natural frequencies and mode types of both titan grades for the HS. Hereby the natural frequencies of the titan grade 5 sonotrode are above the ones of titan grade 2. The mode types are identical at each mode. It is visible, that only mode 4 fulfills the requirements of the ultrasonic device. This mode is in the sonication spectrum of the ultrasonic device (19 kHz to 21 kHz) as well as the proceeding of a longitudinal oscillation for both titan grades.

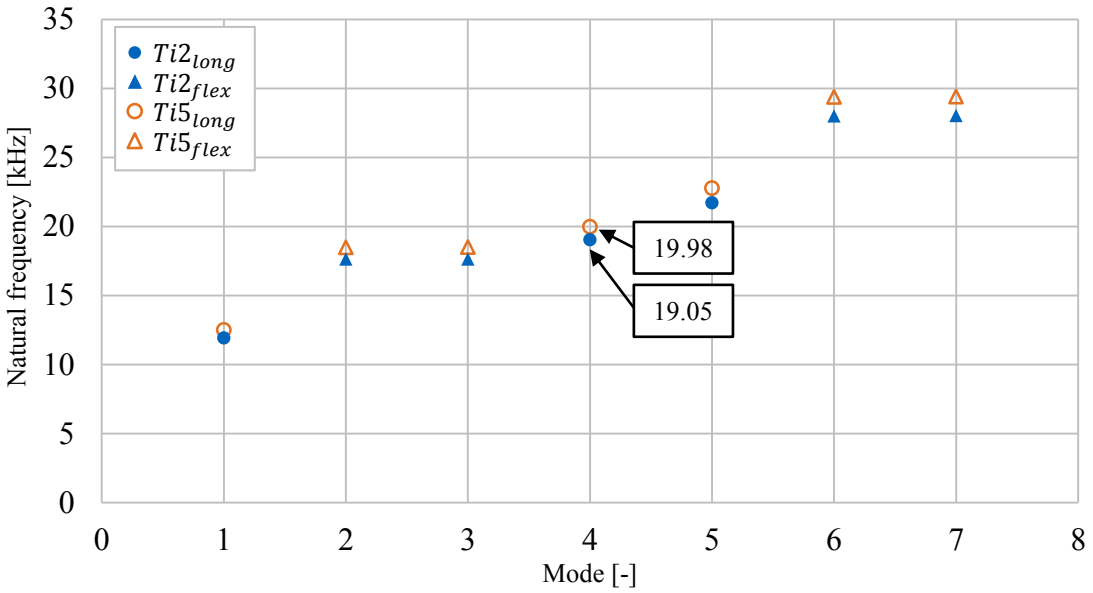

Fig. 4-12 **Comparison of the natural frequency at different modes of the HS sonotrode out of titan grade 2 and titan grade 5**

In Fig. 4-13, the overall deformation of the mode 4 out of titan grade 5 and mode 5 out of titan grade 2 are shown. Latter is the nearest natural frequency (21.72 kHz) to the sonication spectrum of the ultrasonic device (19 kHz to 21 kHz). Whereas mode 4 at the titan grade 5 sonotrode shows a single oscillation knot at the flange of the sonotrode, the mode 5 at the titan grad 2 possess two knots at the cylindrical part of the sonotrode.

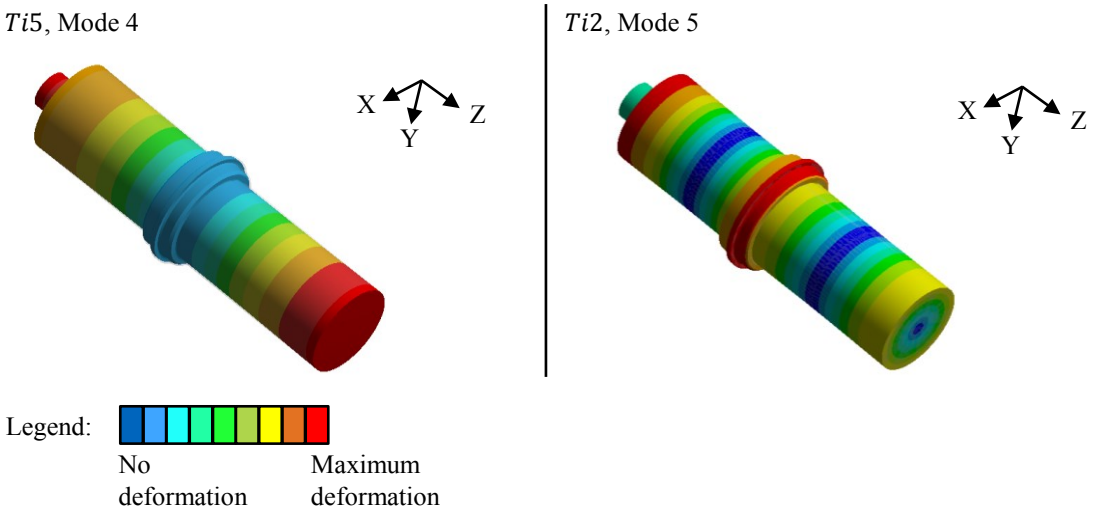

Fig. 4-13 **Overall deformation of the Hielscher sonotrode; titan grade 5 mode 4 (left) and titan grade 2 mode 5 (right)**

The flange in the center is designed by Hielscher to enable the decoupling of the sonotrode movement from the surrounding at closed installations, e.g. a chamber (see chapter 2.1.5). Since the frequencies at mode 4 of both titan grades are within the soni-

cation spectrum, a statement to the titan grade of the HS is not possible. The occurring natural frequency of the real sonotrode is measured 19.59 kHz. Therefore, the simulation method is valid for the modal analysis and thus, to design the UMHS.

Fig. 4-14 reveals the natural frequency and the mode type of the UMHS built of titan grade 2 or titan grade 5. Analogous to the simulation of the HS, the natural frequencies of the titan grade 5 are above the natural frequencies of titan grade 2. The mode types are equal for both materials. At mode 4, both titan grades show a longitudinal oscillation within the allowed stimulation spectrum. Both titan grades can be used for building the UMHS and thus Titan grade 5 is selected due to its higher corrosion resistance.

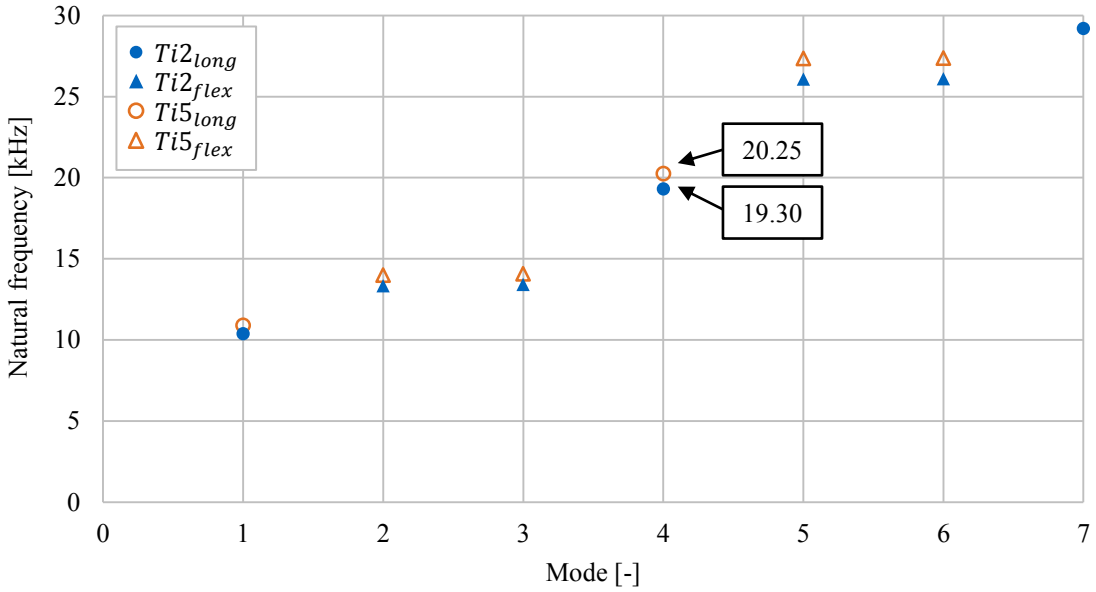

Fig. 4-14 Natural frequencies at different modes of the UMHS sonotrode built of titan grade 2 and titan grade 5

In Fig. 4-15, the total deformation of the mode 3 to mode 5 made of titan grade 5 are pictured. Mode 3 and mode 5 show a flexural deformation of the cylindrical section. The natural frequencies of these modes occur more than 5 kHz apart from the stimulation frequency spectrum of the ultrasonic device, which is between 19 kHz and 21 kHz. Therefore, these frequencies are not stimulated during the scanning of the ultrasonic device (see chapter 2.3.1). Mode 4 exhibits a longitudinal movement including a knot of oscillation at the cylindrical section. Further, this mode possesses a natural frequency of 20.25 kHz and thus, is in the operational range of the ultrasonic device.

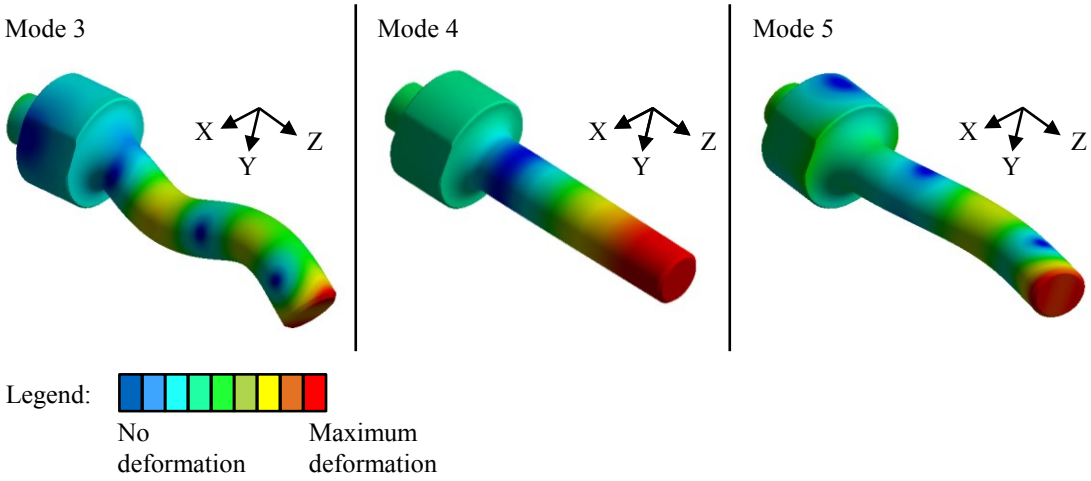

Fig. 4-15 Overall deformation of the Ultrasonic Mixing Head sonotrode (UMHS) made of titan grade 5; mode 3 to 5

However, it has to be taken into account that the modal analysis only allows the detection of natural frequencies and mode types. An infinite deformation at the maximum, here, the sonotrode end planes, is assumed. The absolute amplitude cannot be determined by the modal analysis. Mason and Peters [27] derive the amplitude at the front end plane of a sonotrode from the transition between the back end plane connected to the transducer and the front end plane (see chapter 2.1.5). Since the back end plane diameter of the sonotrode is 32 mm and the front end plane diameter is 15 mm, an enhancement of the factor 2.13 can be assumed. Supposed that the amplitudes of the HS are not changed due to the pure cylindrical shape, the amplitudes of the UMHS must cover a range from 10.65 µm to 57.56 µm. The actual amplitudes of both sonotrodes are listed in Tab. A-1. An overview of the current research on the simulation of the cavitation effect, created by sonication is given by Znidarcic et al. [129].

5 Process characteristics of the Ultrasonic Mixing Head

The process characteristics of the Ultrasonic Mixing Head (UMH) are investigated, since the response of a resin system to sonication is unknown for online mixing and tempering. For this, the UMH is connected to a metering device. The following objectives are pursued as regards the use of the UMH:

- The dominating process factors are identified
- The quantitative effects and their interactions of the process parameters are determined.
- The rheological and thermal properties of the sonicated resin system are detected.

Hereby, injection and infusion process conditions are simulated. The results of the UMH are compared to the performance of an SMH. Further information on the definition of these processes can be found in chapter 2.2. Parts of this chapter are published in [130].

5.1 Materials and methods for the process characteristics

At first, the Design of Experiment (DoE) approach (see chapter 5.1.1) is revealed, followed by the experimental setup and procedure (see chapter 5.1.2). Further, the data collection (see chapter 5.1.3) from the metering device data log is outlined, and the rheology and the thermal analysis are described.

5.1.1 Concept of the Design of Experiment

The investigation of the process parameter is carried out by using a Design of Experiment (DoE) approach. Latter comprises a Central Composite Face Centered (CCF) design. This method enables the investigation of several parameters at a reasonable number of experiments. Box and Draper [131] describe the basic principles of this method. Hereby, every input parameter, called factor has two levels (values). At each experiment, the levels of several parameters are simultaneously changed. Then, the influence of each parameter on the result value is stochastically calculated. Further, runs at the center point, which consist of experiments with the factors at the mean values of the levels, are executed. At axial points of the experimental space, one factor is set to a level value and the remaining factors are set the mean values. These factor sets

describe the face areas of the experimental space and are therefore, characteristics of the CCF design. The precision of the experiment is derived from a four time repetition of the center point and a randomized execution order. The CCF is selected since this design is appropriate for an experimental space where all level combinations can be reached [132]. This is fulfilled, because the UMH is developed to target these factor levels (see chapter 4.2). Weissman and Anderson [133] reviewed the use of the central composite face design in process development.

For the DoE approach, factors, responses and influencing variables, which consist of disturbance variables and control variables, are distinguished. The parameters are specified in the following.

The factors for an experiment are the input parameter set to the levels and the mean value respectively. Three factors are selected based on their importance for processing and are therefore, examined at both mixing heads:

- The volume flow ($\dot{V}$) is controlled by the metering device and defines the cavity fill time and thus, the injection time. Further, the variation of the volume flow leads to varying exposure times of the resin system in the mixing chamber.
- The temperature of the resin component (T_{resin}) determines the resin viscosity. A variation thereof determines the processability of a resin system by the respective mixing head.
- The counter pressure (p) affects the pressure condition during mixing. It is adjusted by pressurizing a pressure pot connected to the mixing chamber outlet. The pressure level represents a stationary preform flow resistance or a particular unsaturated preform impregnation state during injection.

For the UMH, two additional factors are added to be able to investigate the influence of the cavitation:

- The amplitude (A) is identified as crucial parameter in ultrasound processing (see chapter 3). Describing the sonotrode oscillation height, it influences the number, size, density and characteristics of the cavitation bubbles. For this a variation of the amplitudes determines the influence of the cavitation on the processing.
- The volume of the mixing chamber ($V_{chamber}$) is varied by changing its length. The parameter varies the volume where cavitation can occur.

These factors, their abbreviations (ABB) and quantitative factor steps are listed in Tab. 5-1. The accuracy of each factor is limited by the utilized sensor (see chapter 5.1.2).

Tab. 5-1 Factor steps for the process characteristics of the UMH and SMH

Factor	ABB	Factor steps	Accuracy	Unit	UMH	SMH
Volume flow	$\dot{V}$	50.0 / 100.0 / 150.0	+/-0.5	cm³/min	Yes	Yes
Resin temperature	T_{resin}	25.0 / 42.5 / 60.0	+/-1.0	°C	Yes	Yes
Counter pressure	p	0.0 / 1.5 / 3.0	+/-0.5	10^5 Pa	Yes	Yes
Amplitude	A	25.0 / 37.5 / 50.0	+/-0.5	µm	Yes	No
Chamber volume	V	2.5 / 3.75 / 5.0	+/-0.0	cm³	Yes	No

Further responses representing the results of the investigations are defined. The values of these parameters are measured by different systems:

- Three responses are recorded by the injection machine software:
  - The Power (Pw) is measured by the ultrasonic device and represents the effort of the ultrasonic device to execute an oscillation at a certain amplitude. This value is only available for the UMH.
  - The Pressure delta (Δp) is calculated as the pressure difference between the mixing chamber outlet and the resin component inlet ($p_{mix} - p_{resin}$). This value is collected to verify if the UMH operates at a low mixing pressure.
  - The Temperature delta (ΔT) is calculated as the temperature difference between the mixing head outlet and the resin component inlet ($T_{mix} - T_{resin}$). It identifies the temperature change during mixing.
- Two responses are recorded by a rheological measurement. The rheometer and the definition of the parameters are described in chapter 2.4.1.
  - The initial complex viscosity ($\eta_{initial\ com}$) is calculated as the average value of the first three seconds of the measurement. Target is the comparison of the initial viscosities after mixing.
  - The gel time (t_{gel}) describes the duration until the first polymer chain lasts throughout the whole sample. At this point, the storage modulus value transcends the loss modulus value and remains above it until full cure.
- Three responses are detected by a Differential Scanning Calorimeter (DSC) measurement. The definitions of the parameters are given in chapter 2.4.2.
  - The residual enthalpy (ΔH_{res}) is the energy that is set free during the curing of the sample and is therefore, a feedback parameter on the interlocking process during cure.

- The initial glass transition temperature ($T_{g\ initial}$) determines the network which is built up before the measurement.
- The final glass transition temperature ($T_{g\ final}$) is the temperature the cured part needs to transit from a glassy to a rubbery state. Thus, it is a parameter determining the homogeneity of the polymer network.

Apart from these factors (input parameters) and responses (output parameters), disturbance and control variables must be identified and analyzed. These variables are analogous to the factors potentially influencing the responses. Control variables are parameters that can be set to a decisive value and kept during the experiment. Disturbance variables are parameters that cannot be controlled. In the following, the control variables and disturbance variables are identified and actions to control respective prevent them are outlined.

Four control variables are identified:

- The ambient temperature influences the temperature of the metering device and of the measurement device. Therefore, the reservoirs, tubes and systems which are in contact with the resin system components or the resin system itself are separately heated to certain temperatures. Further, the ambient temperature is kept constant at approximately 25 °C.
- The state of the degassing process influences the character of the cavitation: stable or transient (see chapter 2.1.2). The target is to achieve primarily transient cavitation. For this, the resin system components are degassed before they are filled in the respective reservoirs at the metering device.
- The length of the tubing system before and after the UMH influences the heating of the resin system and the pressure state in the tubes. Therefore, the length of the tubes is kept constant at all experiments.
- The quality of the resin system components is kept equal by using the material of one batch throughout the investigation.

Further three disturbance variables are taken into account:

- The ramp up process of the metering device including gear pumps, volume control devices and pneumatic systems influences the volume flow and resin temperature. Samples only at a stationary flow state are taken.
- The accuracy of the metering device is limited since the gear pumps of the metering device show a leakage flow dependent on the volume flow, resin component temperature and pressure state [134, 135]. The flow of the resin system components is continuously controlled by volume control devices which contend finer gears, even though these devices are also not entirely free of leakage. For this, a calibration of the volume control devices is executed at their extreme conditions within the experimental space. The lowest volume flow (50 cm³/min) is combined with the highest resin temperature (60 °C) at ambient pressure. Volumes of 200 cm³ resin component and

72 cm³ hardener component are metered into standard cylinders (DIN EN ISO 4788 [136]) by the metering device. After calibration, a maximum metering deviation of +/-1.00 % occurs at a three times repetition. Therefore, the accuracy of the metering device is within the permitted deviation of +/-3.00 % given in the resin system data sheet (see Fig. A-1).

- A contamination of the measurement equipment as well as the components in contact with the mixed resin system have to be taken into account. To ensure a constantly clean initial experimental setup, the measurement device, which consists of sensors to detect the resin system temperature T_{mix} and the resin system pressure p_{mix} as well as the mixing chamber of the UMH are cleaned. For this, these sections are disassembled, chemically and mechanically cleaned, and reassembled after each experiment. The mixing chamber of the SMH is also replaced, each time.

In Fig. 5-1 the factors, control variables, disturbance variables and responses of the DoE approach are listed.

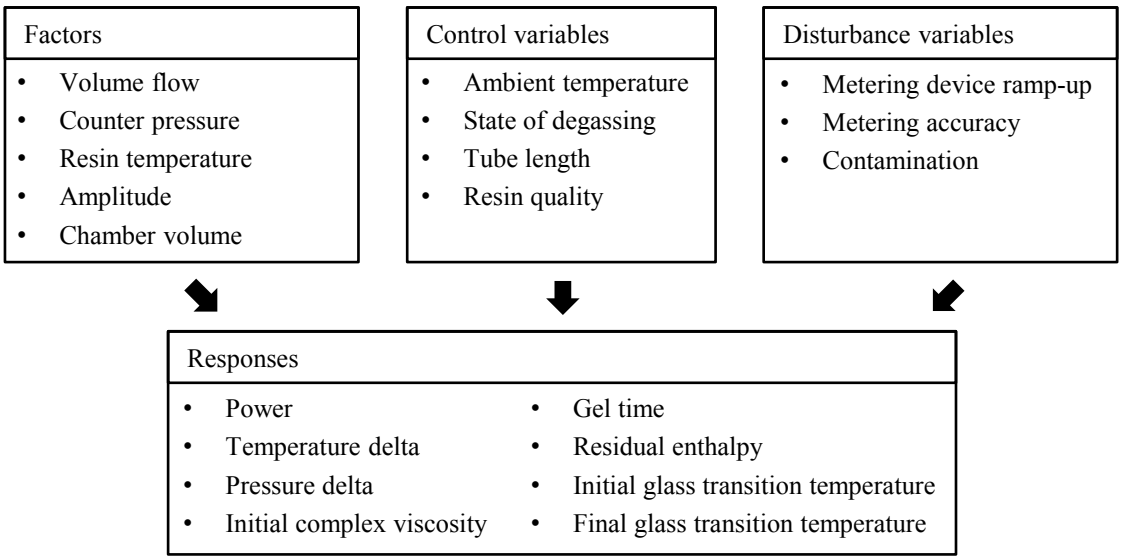

Fig. 5-1 Factors, control variables, disturbance variables and responses of the Design of Experiment (DoE) approach

For further evaluation, only the factors are varied and their impact on the response values is measured whereas the control variables are kept constant and the disturbance variables are minimized.

5.1.2 Setup and procedure of the process characteristics

For this investigation, the two component resin system RIM (see chapter 2.3.3) is used. This resin system enables a broad variation of process parameter values due to its comparably long pot life. Further, the basic process performance and the material characteristics of this resin system is known from the laboratory investigations (see chapter 3). The UMH contains the self-developed UMHS (see chapter 4.2.2). As reference, a two component Static Mixing Head (SMH) of Dekumed operated with a Statomix static mixing device of Sulzer Chemtech is used. The Statomix contains 32 shear elements in a 234 mm long, 6.4 mm inner diameter tube.

The test setup with the UMH as mixing head is pictured in Fig. 5-2. Each component is heated and stirred in the respective reservoir of the metering device.

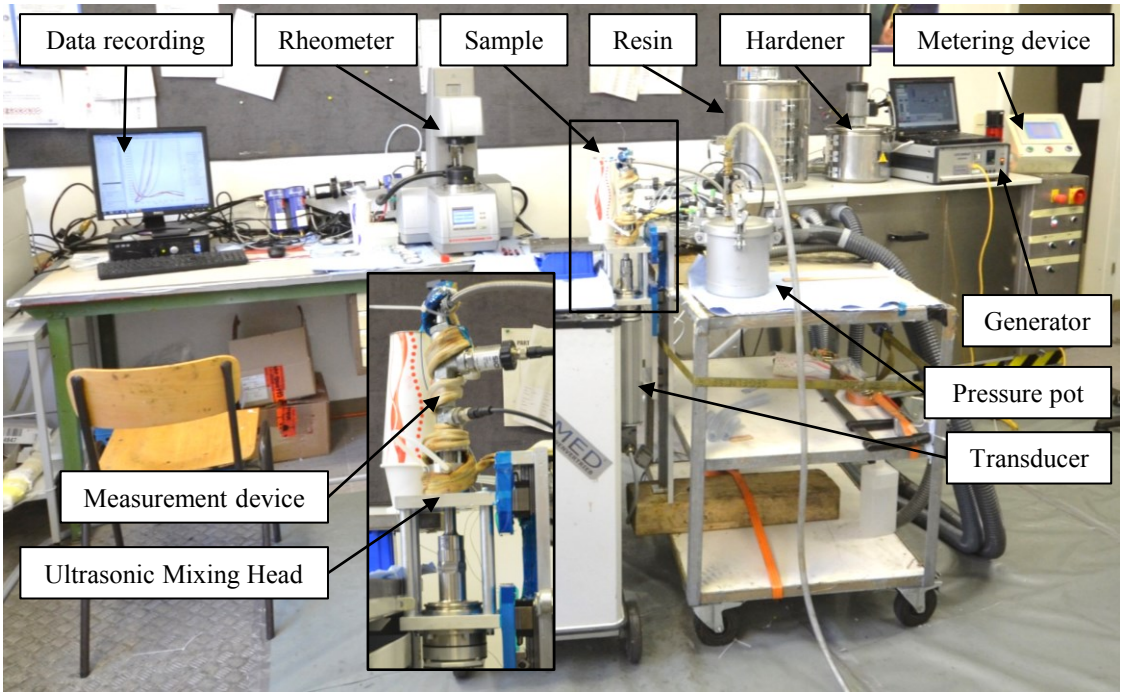

Fig. 5-2 Experimental setup of the process characteristics

For the experimental procedure (see Fig. 5-3), the resin system components are fed through heated tubes into the UMH or SMH. After being mixed in the chamber, the resin system flows through a measurement device, which consists of temperature and pressure sensors. Since the resin system temperature is more sensitive to environmental influences than its pressure, the temperature sensors are placed next to the mixing head. To measure the parameters in the resin component and in the measurement device, PT100 temperature sensors with the trade number 6042538 and 0-100 bar pressure sensors with the trade number 6038815 produced by SICK are utilized. After flowing through the measurement device, the resin system is guided to the pressure pot by a three way ball valve (Va, equal to position 1-2 in Fig. 5-5). When a resin system

volume of 150 cm³ is metered, the three way ball valve is switched from the pressure pot position to the sample position (equal to position 1-3 in Fig. 5-5). A sample of 20 cm³ is extracted. Thereof, 0.5 cm³ are taken from the tube by a pipette and put in the rheometer for the rheology inspection (see chapter 5.1.3.2). The procedure to extract the resin system till the start of the rheological measurement takes 10 s. The rest of the resin system within the sample is stored in a refrigerator at -10 °C and used for the DSC measurement (see chapter 5.1.3.3). The freezing prevents the curing reaction when they are transported. The DSC equipment is not located at the site of the experimental setup and therefore, no direct testing is possible.

Process	Pre injection	Sample taking
V	150 cm³	20 cm³

Rheometer	Positioning	Measurement
Δt	10 s	Various

Thermal analysis	Freezing	Measurement
Δt	~ 21 days	Various

Fig. 5-3 Sample preparation and test procedure of the UMH process characteristics

5.1.3 Data collection for the process characteristics

In this chapter, the methods to control the factor values and detect the response values are described. The factor positions at both mixing heads are pictured in Fig. 5-4.

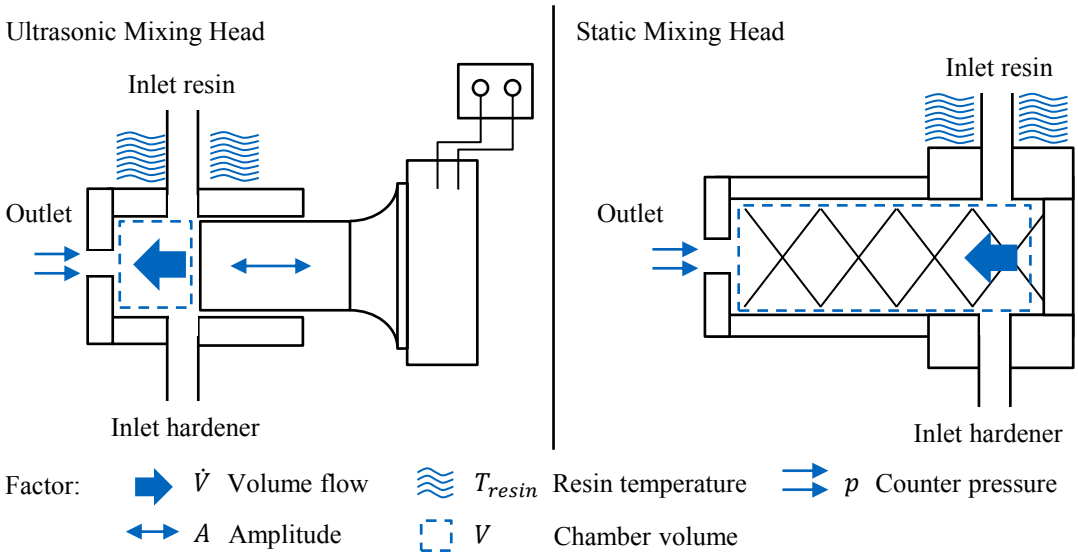

Fig. 5-4 Factor positions for the investigations of the process characteristics of the UMH and SMH

The influence of factor variations and their interactions are detected by various response values. Fig. 5-5 shows the corresponding response positions within the experimental setup. The source of the data collection is highlighted. Details on the responses

are given in chapter 5.1.1 and on the measurement methods in chapter 2.4.1 and in chapter 2.4.2.

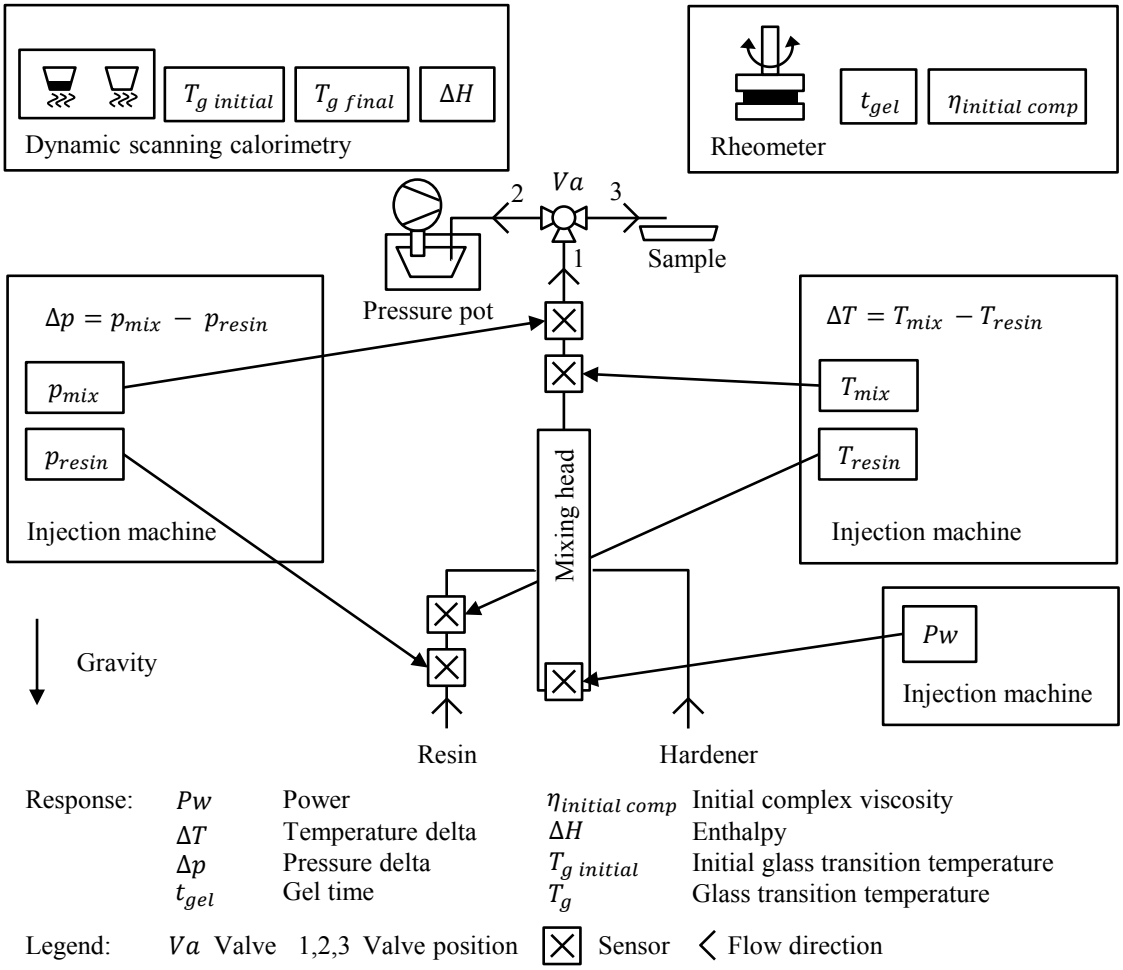

Fig. 5-5 Response positions for the investigation of the process characteristics of the UMH

In the following, the parameters are distinguished by their sources: the data log of the injection machine (see chapter 5.1.3.1), the rheology inspection (see chapter 5.1.3.2) and the thermal analysis (see chapter 5.1.3.3).

5.1.3.1 Data log of the injection machine

The data log of the injection machine, which consists of the data log of the metering device and the ultrasonic device, is used to control all factors and the responses power, temperature delta and pressure delta. The resin system within the sample passes the sensors to detect the factors and responses at various times throughout the experiment. Therefore, the selected section in the data log has to match with the volume between the respective positions within the setup.

The following sensor positions are defined (see Fig. 5-6):

- P_1 describes the data collection position of the temperature T_{resin} and the pressure p_{resin} of the resin component. This simplification is made as the volume between these sensor positions can be neglected.
- P_2 is located at the mixing chamber inlet. For the UMH, it defines the start of sonication.
- P_3 describes the outlet position which varies with the chamber volumes.
- P_4 is located within the measurement device at the temperature sensor T_{mix}.
- P_5 is located within the measurement device at the pressure sensor p_{mix}.
- P_6 defines the location of the sample taking.

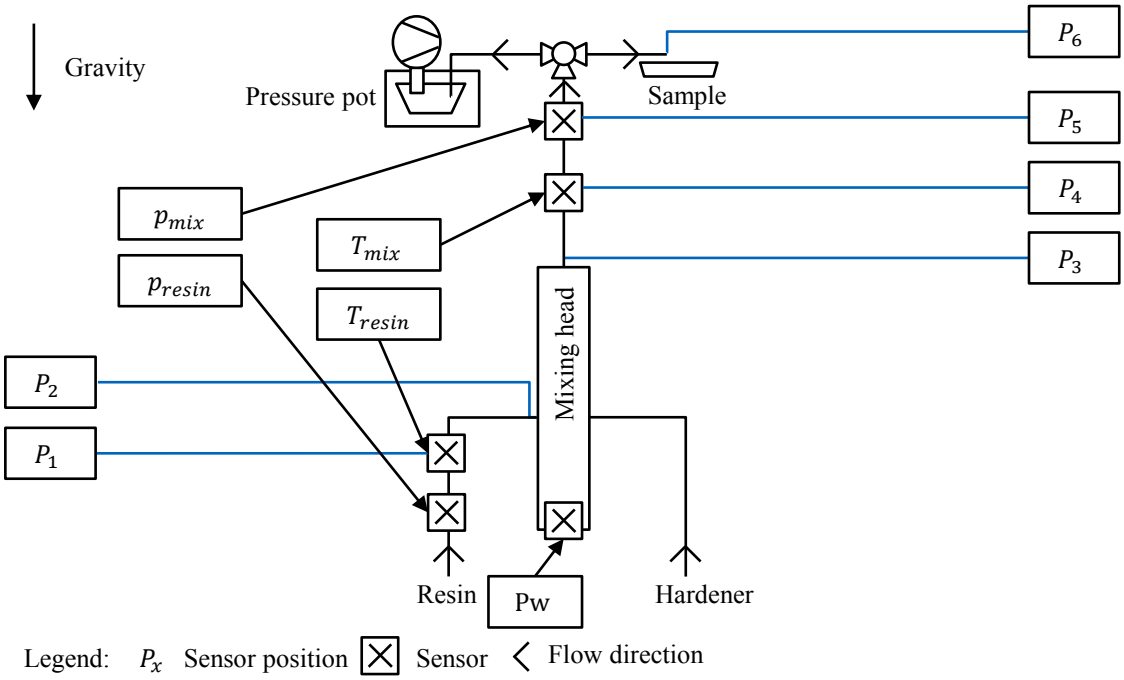

Fig. 5-6 Positions of the sensors to extract the process parameters of the data log

The volumes between the positions are measured by a metering cylinder (DIN EN ISO 4788 [136]). For this, the temperatures at the hardener reservoirs, tubes, mixing heads and measurement device are set to 25 °C. The corresponding volumes are listed in Tab. A-3. A Visual Basic for Applications (VBA) code is used to extract the data from the injection machine data log. A detailed description is included in the comments of the VBA code.

5.1.3.2 Rheology data for the process characteristics

For the rheology measurement, a resin system sample is taken out of the flow and fed into the plate-plate configuration of an Anton Paar Rheometer MCR-302. The plates with a diameter of 25 mm are closed to a gap of 1 mm height. The measurement starts 10 s after sample taking. The data is recorded at a 5 s interval. Hereby, an oscillatory

measurement, at a frequency of 10 Hz and a deformation of 1 % is performed until the gel point is reached. The temperature is set to 80 °C instead of the 60 °C used in the test procedure for the SMV of the rheology laboratory investigation (see chapter 3.2). The temperature is raised to imitate common RTM injection conditions. Hereby the mold temperatures are higher than the resin component temperature. During the measurement, the initial complex viscosity and the gel time are detected. Basic formulas with regard to the rheology inspection are given in chapter 2.4.1.

5.1.3.3 Thermal analysis data for the process characteristics

A Q2000 Differential Scanning Calorimetry (DSC) by TA Instruments (see chapter 2.4.2) is used for the thermal analysis of the resin system. After extraction, the samples are stored in a freezer at T = -10 °C to prohibit further curing of the material (see chapter 5.1.2). To ensure the freezing and unfreezing of the resin system without an absorption of water, the samples are encapsulated in hermetical closing bags. After transportation, a bag is taken out of the freezer and a sample of approximately 10 mg is placed in an aluminum pan. Two dynamic temperature cycles are executed: Starting at -80 °C the sample is heated at 5 °C/min to 260 °C. After a dwell time of 1 min, it is cooled down to -10 °C at 20 °C/min. A second ramp from 5 °C/min to 260 °C takes place. The procedures to calculate the responses, the residual enthalpy and the glass transition temperatures are equal to those of the laboratory investigations (see chapter 3.3) and are described in chapter 2.4.2.

5.2 Results of the process characteristics

Two plot types are used to compare the results of the process characteristics of the UMH to those of the SMH. The factor effect plot pictures the influence of a single factor on a response. The interaction plot highlights the effect of two interacting factors on a response. The remaining factors are respectively set to their mean values. The results of each response are discussed for the UMH and the SMH simultaneously.

5.2.1 Experimental design approach

The adjusted factor values of each experiment are listed in Tab. A-4 for the UMH and in Tab. A-5 for the SMH. The corresponding response values are listed in Tab. A-6 for the UMH and in Tab. A-7 for the SMH. The model validity for each response of the CCF approach is monitored by examining the respective R^2 and Q^2 values for each response. Hereby, the value R^2 describes the fraction of the variation of each response. The value Q^2 is an indicator for the variation of the response value which is predicted by the model according to the cross validation. These indicators range from 0 to 1 with 1 indicating a perfect fit between reality and model. The R^2 and Q^2 of each response are listed in Tab. 5-2. At both mixing heads, the R^2 and Q^2 values for the responses of the power, the temperature delta and the pressure delta are high. This points to an ex-

cellent model validity and prediction accuracy. The indicators for the rheological responses, initial viscosity and gel time, show satisfactory values. The thermal analysis shows the lowest values of these indicators. The Q^2 value of the final glass transition temperature is small of both mixing heads because of a high reproducibility of the response value. The results for the SMH concerning the initial glass transition temperature as well as the residual enthalpy are excluded from the investigation because of their poor predictability.

Tab. 5-2 R^2 and Q^2 values indicating the model validity and prediction accuracy of the experimental design approach

Response	ABB	UMH		SMH	
		R^2	Q^2	R^2	Q^2
Power	Pw	0.99	0.99	-	-
Temperature delta	ΔT	0.99	0.78	0.99	0.97
Pressure delta	Δp	0.96	0.90	0.96	0.91
Initial complex viscosity	$\eta_{initial\ com}$	0.40	0.12	0.64	0.10
Gel time	t_{ges}	0.51	0.16	0.76	0.41
Enthalpy	ΔH_{res}	0.81	0.63	0.51	- 0.2
Initial glass transition temperature	$T_{g\ initial}$	0.75	0.41	0.34	- 0.2
Final glass transition temperature	$T_{g\ final}$	0.73	0.03	0.44	0.03

The high accuracy of the responses collected from the injection data log is obvious. These responses are recorded by sensors within the injection machine during the experimental procedure. The rheology measurement is performed subsequent to the experiment with the minor disruption of extracting the sample and placing it to the rheometer. The comparably poor prediction of the enthalpy and the initial glass transition temperature of the SMH are traced back to two effects: First, the relatively few experiments of the SMH to detect these high sensitive responses and second, the necessary freezing and unfreezing processes needed to transport the samples.

5.2.2 Power response

This response value is based on the data log of the ultrasonic device and therefore only generated in UMH experiments. The results show, that the power is influenced by four factors: volume flow, resin temperature, amplitude and counter pressure. Fig. 5-7 shows the linear increase of the power dependent on a varying counter pressure at low and high amplitudes. By varying the counter pressure and amplitude, a range between 77.42 W and 274.76 W is covered.

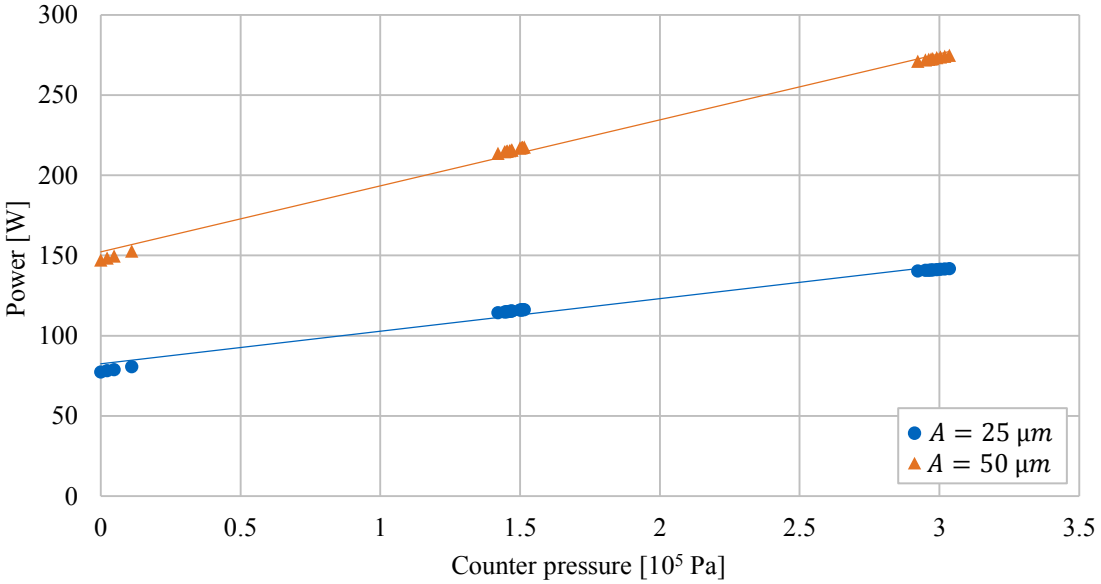

Fig. 5-7 UMH, influence of the interaction plot between counter pressure and amplitude on the power, remaining factors are set to their mean values

The power represents the effort of the ultrasonic device to execute an oscillation. Both a longer distance due to a higher amplitude and a higher resin system resistance due to a higher counter pressure increase this effort and therefore, the power.

A lower resin temperature (see Fig. 5-8 a)) or a higher volume flow (see Fig. 5-8 b)) lead to a higher power, too. The power changes approximately 12 W with the variation of the resin temperature and approximately 9 W with the variation of the volume flow. Therefore, the influence of both factors on the power is less compared to the influence of the amplitude and counter pressure.

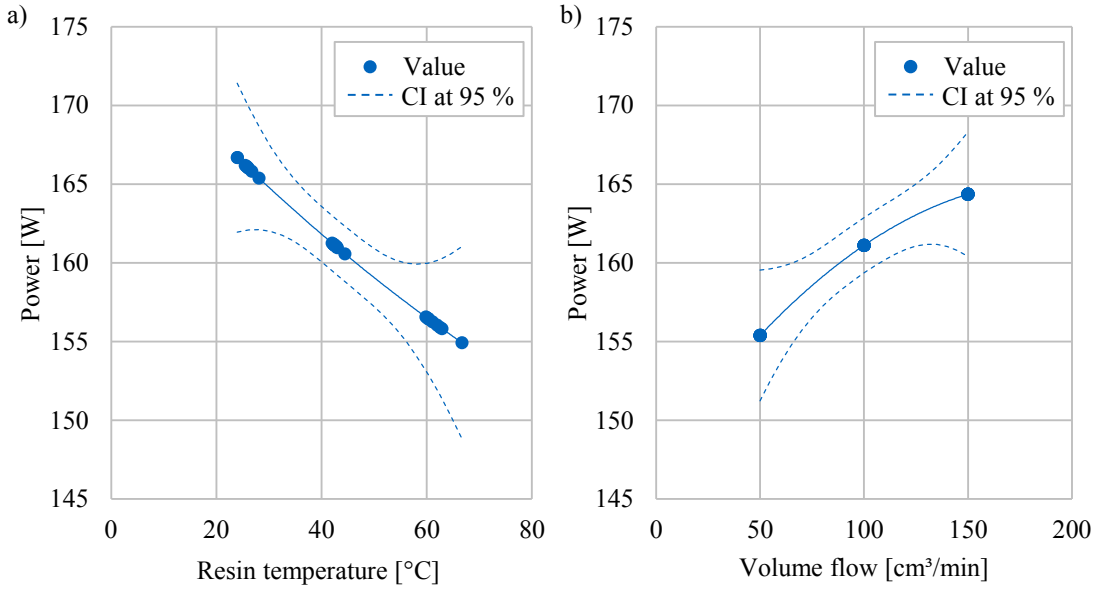

Fig. 5-8 UMH, factor effect plot of the resin temperature on the power

The decrease of the power alongside the increase of the resin temperature is traced back to the corresponding viscosity of the resin system. Since a low resin temperature is accompanied by a higher viscosity, the resistance of the resin system to the movement of the sonotrode and therefore, the power increases. In their study, Monnier et al. [114] describe the influence of ultrasound on mixing of viscous liquids on a molecular scale. Hereby, the increase of the power also correlates with the increase of the viscosity. The slight dependency of the power on the volume flow is not fully understood until now. It is assumed that this effect mainly occurs because higher volume flow leads to higher friction at the inner wall of the mixing chamber. Therefore, the occurring higher power at higher volume flow is a superposition of a locally slightly higher pressure near the sonotrode in the mixing chamber.

5.2.3 Temperature delta response

The temperature delta at the UMH is influenced by four factors: volume flow, resin temperature, amplitude and counter pressure. Fig. 5-9 pictures the variation of the counter pressure, the volume flow and the resin temperature on the temperature delta at low and high amplitudes.

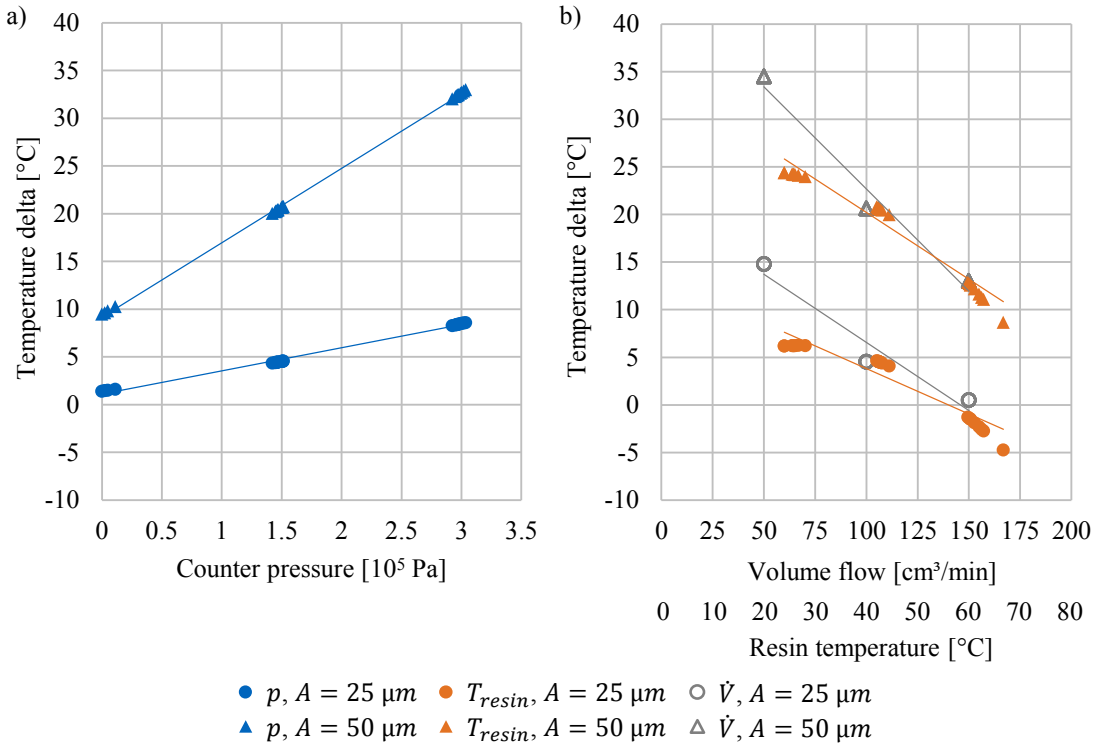

Fig. 5-9 **Interaction plot of counter pressure (a), volume flow (b) and resin temperature (b) at low and high amplitudes on the temperature delta, remaining factors are set to their mean values**

The temperature delta in the UMH clearly depends on the height of the amplitude (see Fig. 5-9 a)). At high amplitudes, the ultrasonically treated area that enables bubble creation is larger. For batch investigations, this correlation is already mentioned at the cavitation zone measurement (see Fig. 3-4, chapter 3.1). More implosions of collapsing bubbles imply more heat dissipation in the resin system and thus, the temperature rises. Further, higher counter pressures accompanied by higher power values lead to more violent collapses of the bubbles and therefore, the resin system heats up faster. The raising of the counter pressure (see Fig. 5-9 b)) leads to the linear increase of the temperature delta. Further, a higher counter pressure correlates with a higher power (see Fig. 5-8). The increase of the volume flow from 50 cm³/min to 150 cm³/min (see Fig. 5-9 b)) more than halves the temperature delta. The volume flow is indirectly proportional to the exposure time of the resin system in the mixing chamber. A longer exposure time correlates with more cavitation bubbles per treated volume and therefore, with a heating of the resin system. The decrease of the temperature delta at increasing resin temperatures is reasonable due to the lower heating effect by sonication if the resin system is already heated before and therefore shows a lower viscosity.

In Fig. 5-10 the raw data of the responses temperature delta and power are correlated without the modeling approach of the DoE. These responses do not show a sufficient correlation. If the energy density built by the quotient of the power and the volume

flow (see Eq. 2-3) is plotted, a correlation between the energy density and the temperature delta is visible.

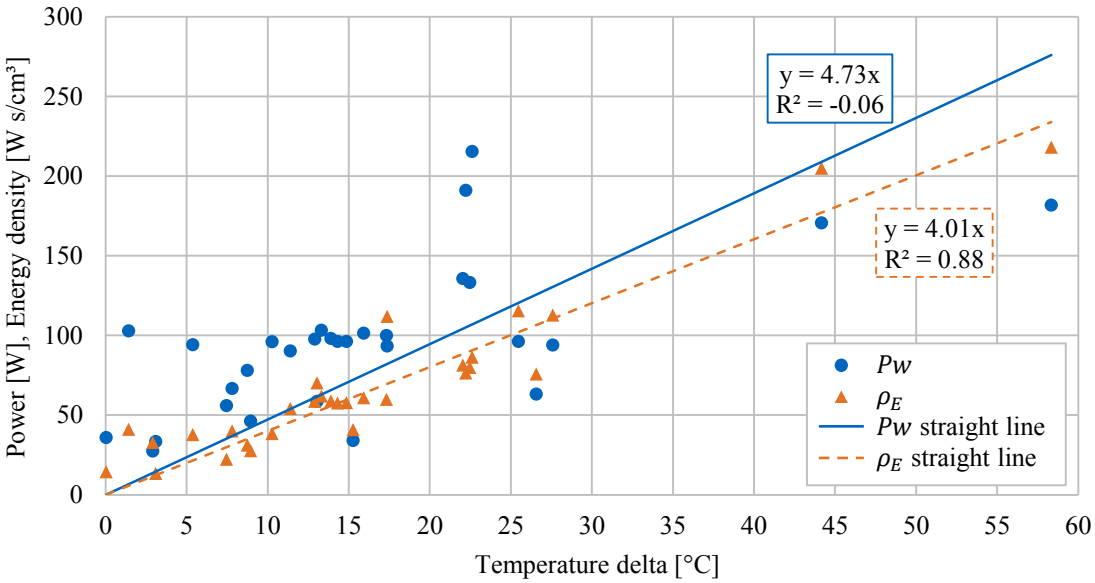

Fig. 5-10 Power and energy densities at different temperature deltas

By neglecting the remaining factors, the quotient of the responses power and volume flow enables a prediction of the temperature delta response. The increase of the energy density is approximately four times the one of the temperature delta.

The temperature delta in the SMH depends on two factors: volume flow and resin temperature. Fig. 5-11 displays the temperature delta dependent on the resin temperature at low and high volume flows. For both mixing heads, lower volume flows and higher resin temperatures increase the heat dissipation.

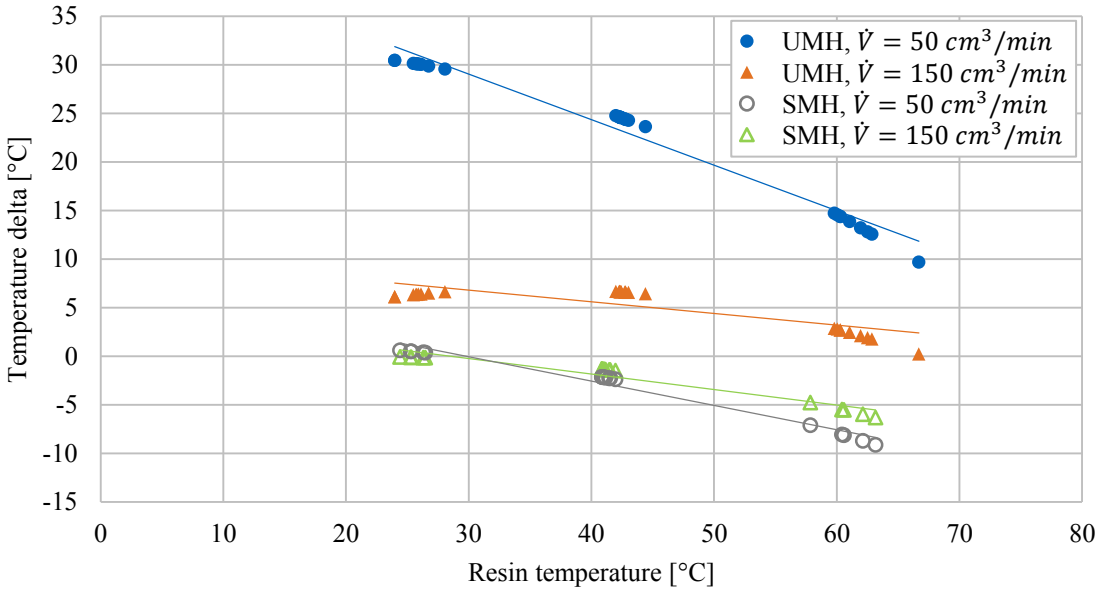

Fig. 5-11 **UMH and SMH, interaction plot of resin temperature and volume flow on the temperature delta, remaining factors are set to their mean values**

This effect is traced back to the room temperature of the experimental environment, which cools the resin system during processing. However, as described above, for the UMH, the cooling effect of the ambient temperature of the environment is counteracted by heating it up via transient cavitation.

5.2.4 Pressure delta response

The pressure delta in both mixing heads is influenced by two factors: volume flow and resin temperature (see Fig. 5-12). A minor influence on the pressure delta is detected at elevated resin temperatures. At a low resin temperature coupled with a high volume flow, a pressure drop of approximately $1.5*10^5$ Pa is detected in both mixing heads.

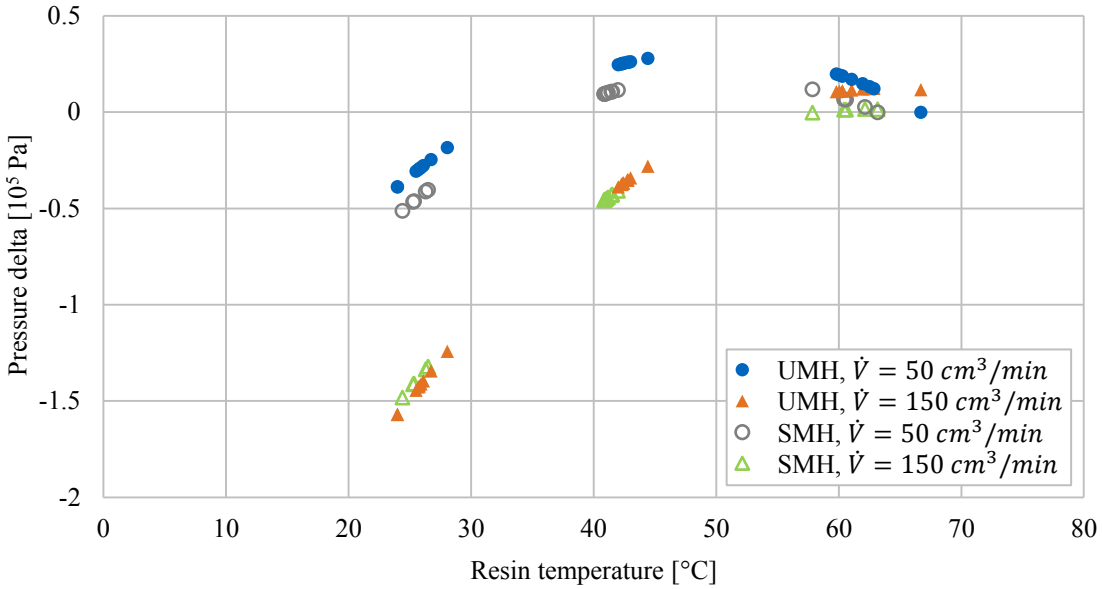

Fig. 5-12 UMH and SMH, interaction plot of resin temperature and volume flow on the pressure delta, remaining factors are set to their mean values

The positive pressure delta at high resin temperatures of both mixing heads is physically not justifiable and is traced back to the accuracy of the sensor. It is considered that the pressure delta occurring at low resin temperatures is caused by the flow resistance of the walls inside of the mixing heads. At the SMH a pressure drop of several bars caused by the friction between the shear elements and the resin system in the mixing chamber, as documented in the literature [16, 137], is not detected.

5.2.5 Rheology response

For both mixing heads, no factor and factor interaction shows an effect on the initial viscosity. This independency can exist due to the temperature of the rheometer. To imitate a mold surface the plate-plate setup is heated to 80 °C, which is 20 °C above the highest resin temperature value in this investigation. For this, the heating effect of the cavitation (see chapter 5.2.3) is equalized before the rheology measurement. The initial viscosities at the beginning of each test are balanced.

The gel time of the resin system processed with the UMH is influenced by two factors: amplitude and counter pressure. On the contrary, the SMH samples show a minor effect as regards the variation of the counter pressure (see Fig. 5-13). Both mixing heads produce resin systems of a similar gel time at a low counter pressure. At a counter pressure of $1.5*10^5$ Pa, resin systems processed with UMH show the lowest gel time. The gel time of UMH samples is further reduced by an increasing amplitude.

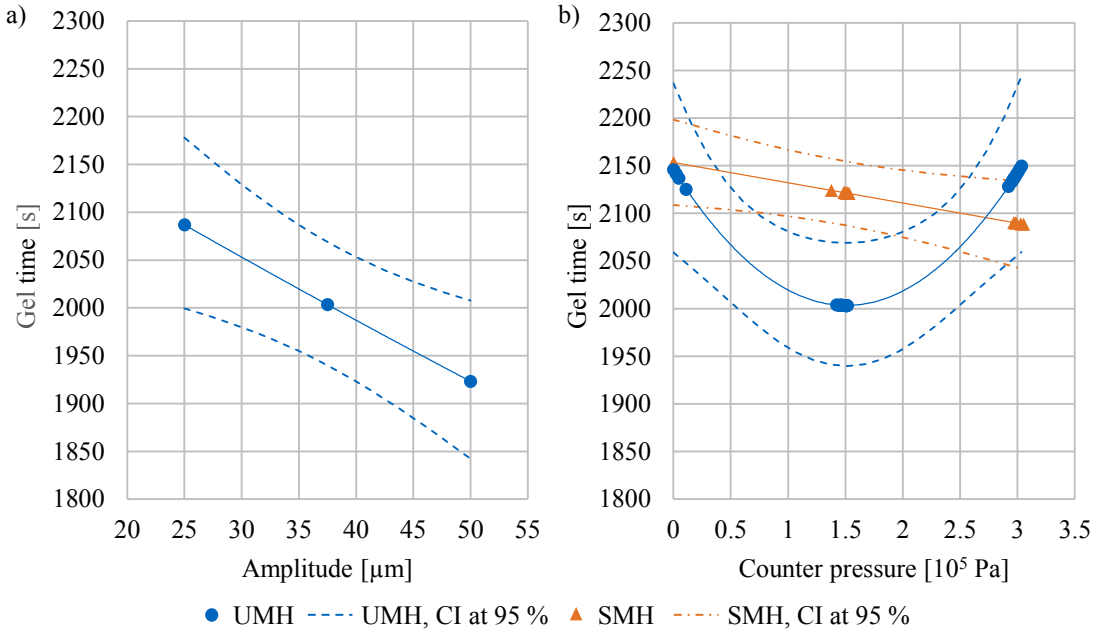

Fig. 5-13 UMH and SMH, factor effect plot of amplitude (a) and counter pressure (b) on the gel time, remaining factors are set to their mean values

The differences in the gel time could exist due to the influence of the counter pressure and amplitude on the bubble creation. Peuker et al. [22] found that a high counter pressure can lead to less and smaller bubbles with more energy. Furthermore, they state that a high power can support the creation of stable, larger bubbles. This also leads to fewer implosions. Tzanakis et al. [138] describe an optimum power for transient cavitation for liquid aluminum. Further, the power is mainly affected by the amplitude and counter pressure (see chapter 5.2.2). Taking this into account, both Peuker et al. [22] and Tzanakis et al. [138] claim an influence on the cavitation based on the amplitude and counter pressure. This is analogous to the investigation at hand. Hereby, a minimum gel time is reached at 50.0 µm amplitude and $1.5*10^5$ Pa counter pressure.

The energy densities (see Fig. 5-10) of this investigation are similar to the energy densities of the laboratory investigation, with no gel time reduction (see Tab. 3-1, Tab. 3-2). A reduction of the gel time, detected at higher energy densities in the laboratory (see Fig. 3-11) does not occur.

5.2.6 Thermal response

The initial glass transition temperatures of the samples processed with the UMH and detected during the first ramp (see chapter 2.4.2) are mostly between -10 °C and 0 °C. No clear trend is found for this parameter. This is traced back to the storage of the samples in a freezer for approximately 21 days. As described in the experimental design approach (see chapter 5.2.1) for the SMH samples, no significant model is detected for the residual enthalpy. The residual enthalpies of the samples processed with the UMH show a dependency on two factors: counter pressure and amplitude (see

Fig. 5-14). The enthalpy value is similar at low and mid amplitudes and increases at high amplitudes. The enthalpy decreases with increasing counter pressure.

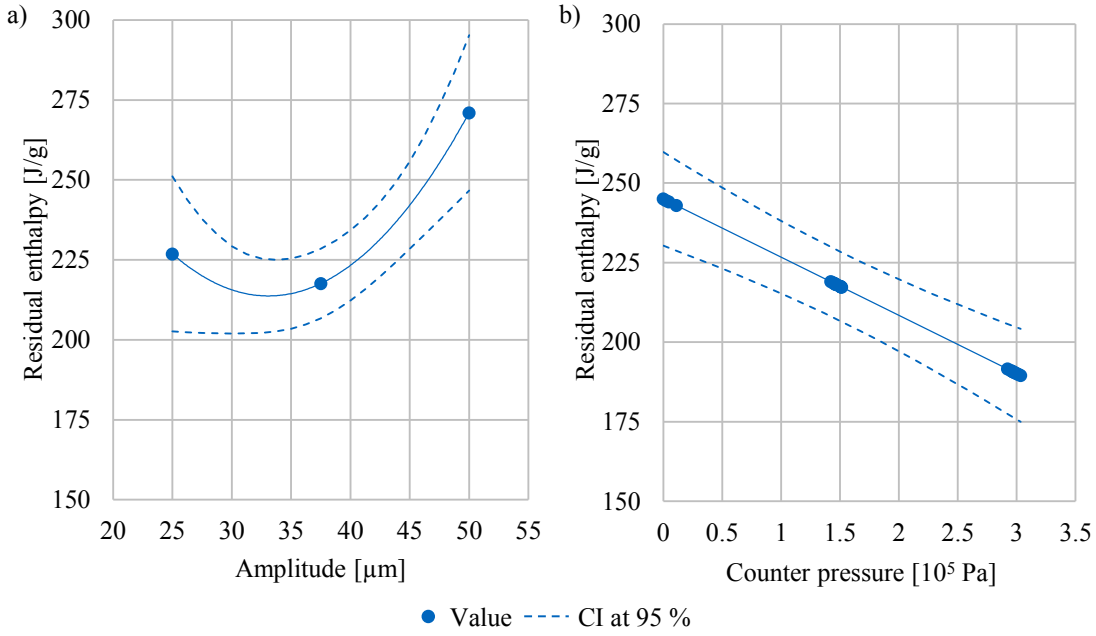

Fig. 5-14 Factor effect plot of amplitude (a) and counter pressure (b) on the residual enthalpy, remaining factors are set to their mean values

Analogous to the gel time, amplitude and counter pressure are the dominant factors (see chapter 5.2.5). Further, the opposing trend of these factors indicates that a compromise thereof leads to the ideal condition for the bubble formation. The higher enthalpy values compared to those of the thermal analysis in the laboratory investigation (see chapter 3.3) are traced back to the lower heating rate of 5 °C/min and the shorter (21 days) and cooler (-10 °C) storage in the freezer before measuring. On the contrary, hand mixed and directly measured samples show an enthalpy of 470 J/g. The enthalpy is equally reduced for all samples.

The final glass transition temperature of the UMH samples shows a dependency on the counter pressure. Whereas the final glass transition is high at low pressures it decreases and high counter pressure values. The SMH results show an effect of two factors on the final glass transition temperature: counter pressure and volume flow (see Fig. 5-15).

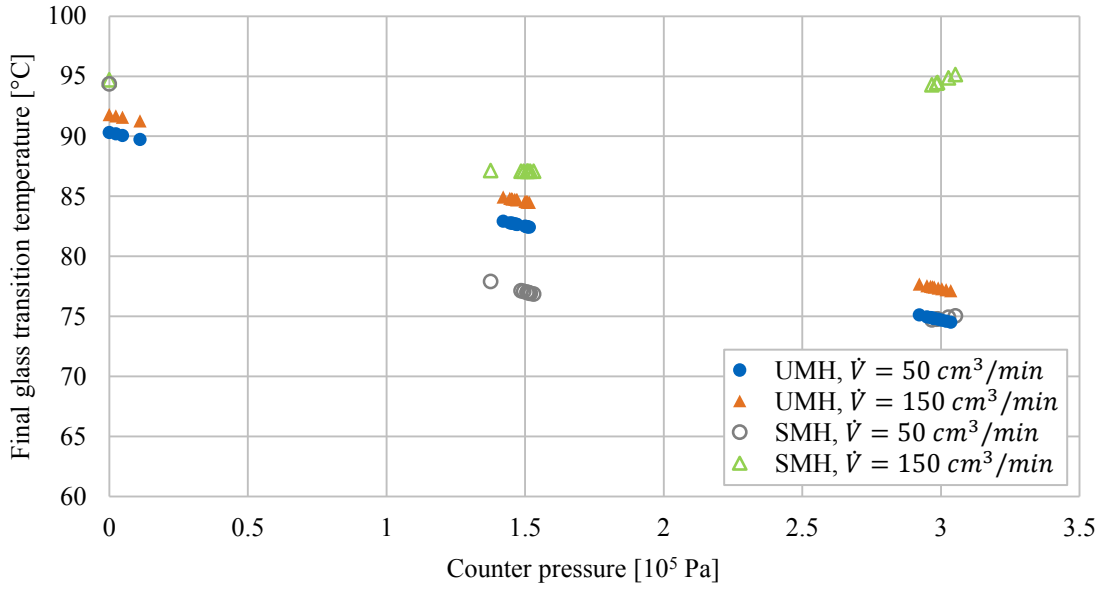

Fig. 5-15 Influence of the counter pressure on the final glass transition temperature, remaining factors are set to their mean values

The decrease of enthalpy and final glass transition temperature in the UMH samples at higher counter pressure could be explained by the threshold reachability. At a high counter pressure, the bubble formation is hindered. The pressure variation induced by sonication and needed to undercut the cavitation threshold (see chapter 2.1.2) covers a smaller volume. This leads to a poor mixing and results in a lower reactivity (residual enthalpy) and poorer network homogeneity (final glass transition temperature). By increasing the amplitude the pressure variation is increasing and this benefits the undercut of the threshold value for bubble creation and mixing. Thus, the residual enthalpy is higher at high amplitudes even though no dependency of the final glass transition temperature on varying amplitudes is detected. The samples of the SMH show a high final glass transition temperature at a high volume flow independent of the counter pressure. At low volume flow coupled with high counter pressure, the final glass transition temperature is reduced. It is assumed that this case represents the lower end of the mixer's operation spectrum and therefore, leads to an imperfect mixing.

5.3 Interpretation of the process characteristics

Cumulating the generated data from a statistical point of view, amplitude and counter pressure are identified as the dominating factors for the process parameter: power, temperature delta and pressure delta as well as the rheological and thermal material properties. The factors resin temperature and volume flow only show a restricted impact.

It this study, a variation of the chamber volume between 2.5 cm³ and 5 cm³ does not show an effect on the responses. Monnier describes a higher mixing quality by changing the chamber volume from 100 cm³ [114] to 50 cm³ [29] in his investigations on

micro mixing. Pohl et al. [51] detected no effect on a precipitation results by changing the chamber volume between 0.67 cm³ and 0.82 cm³. Scaling the cavitation zone volume detected in the laboratory investigation with the HS (see chapter 3.1), the cavitation zone provided by the UMHS does not fill the entire mixing chamber during sonication. Therefore, the cavitation zone development is assumed to be undisturbed from the chamber volume.

The response power is identified as a sensitive feedback parameter as regards the heating and mixing processes inside the UMH. The power is sensitive to both dominating process factors: amplitude and counter pressure.

Since the pressure delta analysis displays a small pressure drop in the mixing head, the feasibility of the mixing head to run RTM at low mixing pressure (see chapter 2.2.4) is proven. The glass transition temperature decreases with an increase of the counter pressure. Therefore, the amplitude spectrum is extended to higher values for the RTM characteristics (see chapter 6).

6 Resin Transfer Molding characteristics of the Ultrasonic Mixing Head

After the batch investigation in the laboratory (see chapter 3) and the process characteristics of the UMH connected to a metering device (see chapter 5), the UMH and metering device is now linked to a RTM mold. The target is to discover the behavior and the influence of the ultrasound parameters amplitude and power on the injection and derive a process window for the UMH. For this, it must be clarified which of these two parameters is the controlling one (factor) and which is the one to be regulated (response) (see chapter 2.3.1). A comparison between the results gained from the process and RTM characteristics should investigate the reliability of the findings of the process characteristics under RTM conditions (see chapter 6.2.3). Further, the mechanical performance of the parts produced with the UMH is evaluated (see chapter 6.2.4). Parts of this chapter are published in [139, 140].

6.1 Materials and Methods for the Resin Transfer Molding characteristics

At first, the concept of the RTM characteristics (see chapter 6.1.1) is described, followed by the experimental setup (see chapter 6.1.2), the preforming procedure (see chapter 6.1.3) and injection process (see chapter 6.1.4). Further, the data collection by the injection machine data log as well as the mechanical test is outlined (see chapter 6.1.4).

6.1.1 Concept of the Resin Transfer Molding characteristics

To evaluate the UMH performance in RTM, two types of plates are manufactured: neat resin plates (NRP) and fiber reinforced plates (FRP). Further, two resin systems are processed. The slow reactive resin system RIM is compared to the high reactive resin system XB (see chapter 2.3.3). Thereby, a variety of process conditions is achieved.

Amplitude and counter pressure are identified as the dominating process parameters in chapter 5. Amplitudes between 25.0 µm and 62.5 µm are used for the RTM injections. The adjustment of the counter pressure, now injection pressure, is more difficult. This parameter is not a factor, but a response in RTM injections for controlled volume flow rates. The resistance of the fiber material leads to an increasing injection pressure during cavity filling (unsaturated flow) and to a constant injection pressure during cavity

flushing (saturated flow) at a constant volume flow (see Eq. 2-2). The injection pressure is modified by means of the volume flow. Latter is varied between 50 cm³/min and 200 cm³/min.

6.1.2 Setup of the Resin Transfer Molding characteristics

In Fig. 6-1, the experimental setup of the RTM characteristics is shown. The resin system components are metered by the metering device of Dekumed 2K (see chapter 2.3.2). The layout of the metering device and the mixing heads are identical to the setup of the process characteristics (see Fig. 5-2). Since the investigation of the process characteristics (see chapter 5.3) shows that the chamber size does not have a significant influence on the processability, the midsize mixing chamber volume is utilized for this investigation. The three way ball valve placed behind the measurement device is connected to the mold inlet with a 6 mm inner diameter tube made out of polytetrafluoroethylene (PTFE). The mold is made of aluminum and creates a 500 x 300 x 2 mm³ cavity. It also has round edges with a 25 mm radius each. The upper cavity comprises the mold inlet and mold outlet. The lower cavity comprises a 10 mm broad, 1.5 mm high excess pressing area to hold the preform in position. The surfaces of both mold halves are grounded. The closing and the opening of the mold are performed by a Joos HP-S30 press closing with a force of approximately 200 kN. The outlet is connected to the resin trap with a PTFE tube. A vacuum pump can vacuum the resin trap and the cavity. A solvent based cleaning device is attached to release the mixing head, the measurement device and the tubes from the resin system after the injection.

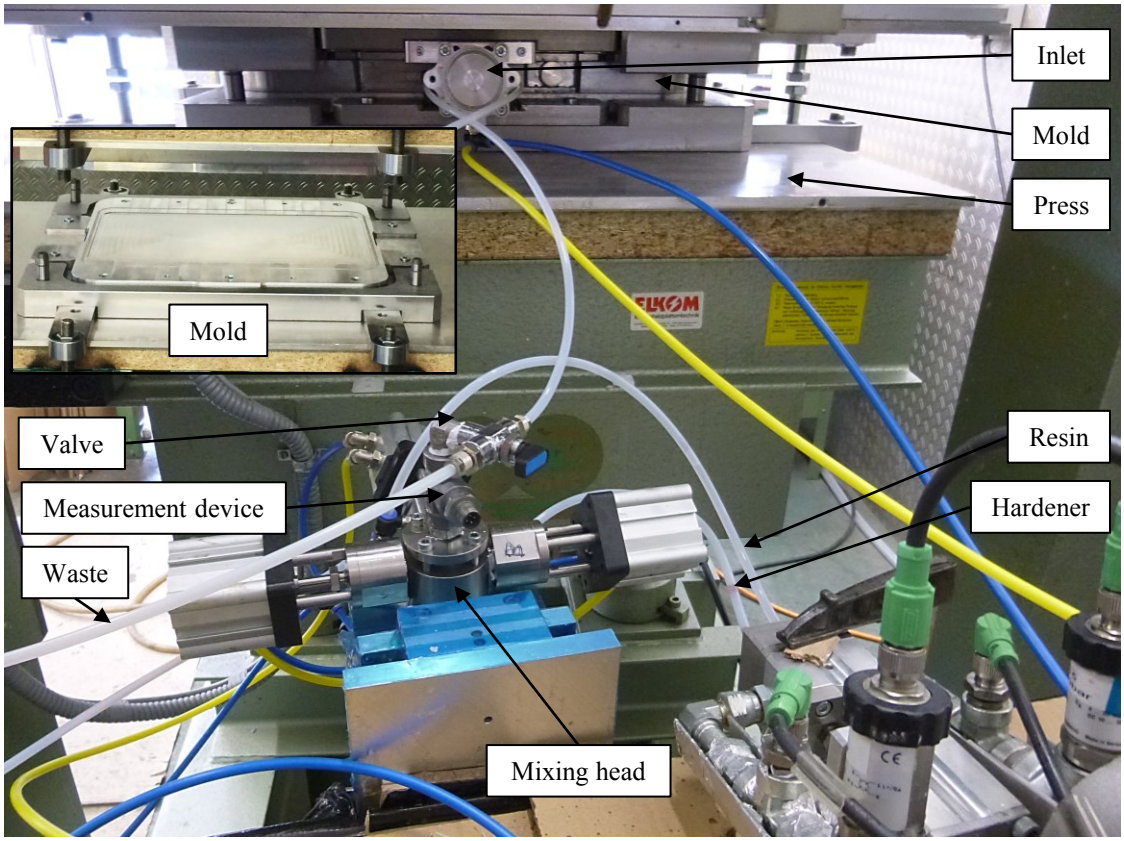

Fig. 6-1 Experimental setup of the RTM characteristics

A sketch of the test setup and the sensor positions is drawn in Fig. 6-2. The sensor types and the position at the metering device, mixing head and measurement device are identical to the setup of the process characteristics (see Fig. 5-5). Sensors are added in the mold. In the upper mold half, pressure sensors of the type FP5245-3-100BG manufactured by Measurement Specialties are integrated. One sensor is located near the inlet (p_{inlet}) and one sensor is located near the outlet (p_{outlet}) at a distance of 390 mm to each other. Six temperature sensors W-GYK PT100 of Heraeus Sensor Technology, three sensors per mold half, are positioned diagonally across the cavity to monitor the mold temperature T_{cavity}.

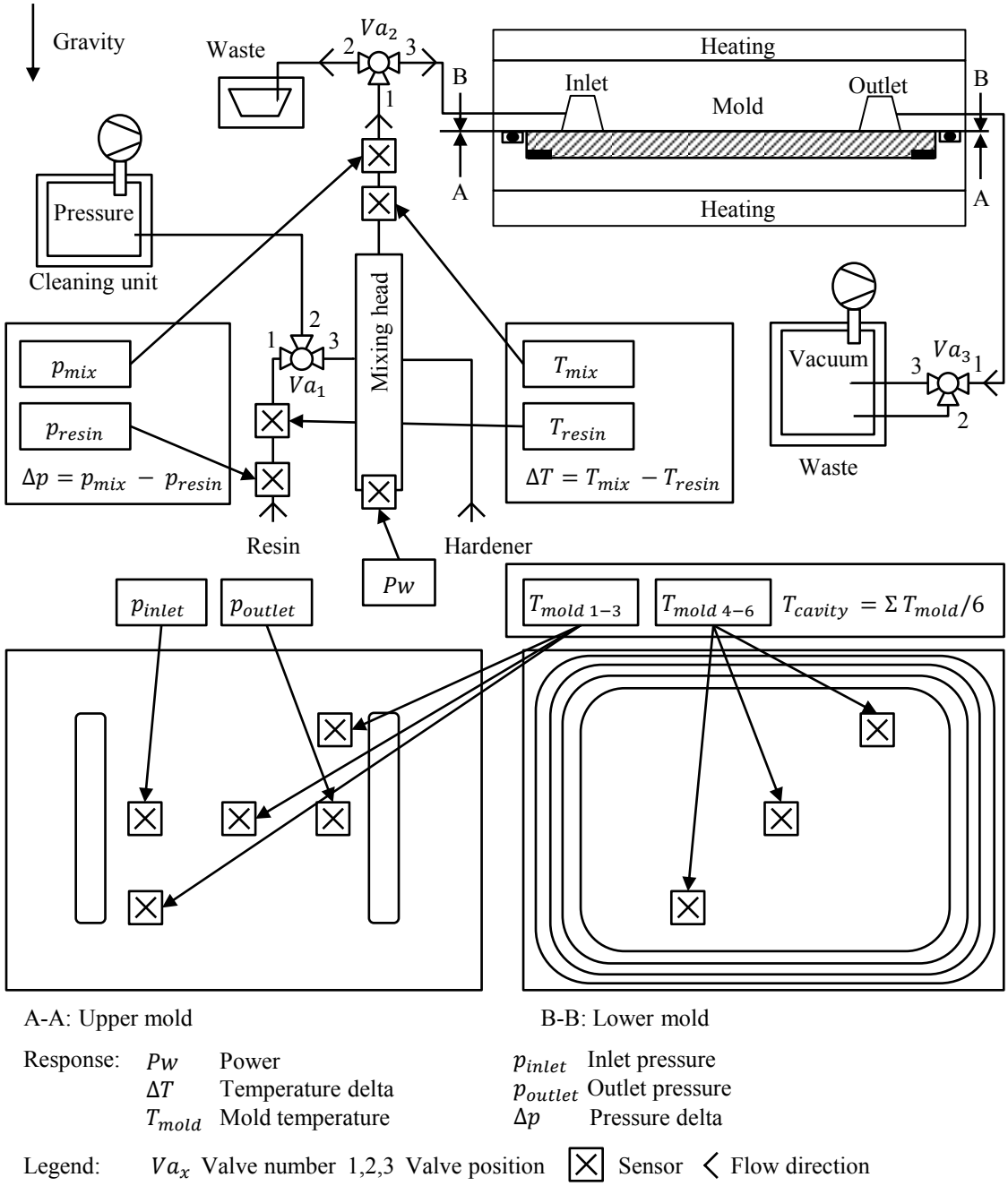

Fig. 6-2 Sensors and parameters of the RTM characteristics

Two resin systems are utilized as matrix material. The resin system RIM (see Fig. A-1) is a comparably slow curing resin system. It allows a broad variety of process parameter settings due to its relatively long pot life. The resin system RIM is used for the laboratory investigation (see chapter 3) and the process characteristics (see chapter 5), too. In addition, the snap cure resin system XB (see Fig. A-2) is chosen. Latter possesses a comparably short pot life and therefore, a high sensitivity towards process parameter settings. More information and their current fields of application are given

in chapter 2.3.3. The external release agent Loctite Frekote 770 NC by Henkel [141] is applied to the mold surface to lower the demolding stresses.

As fiber material, a non-crimp fabric E-glass with an areal weight of 610 g/m² produced by Saertex [142] is processed. The raw material consists of a +/- 45° oriented stack. The layers are stitched together by a yarn in warp direction. No binder is used to exclude an effect thereof on the resin system performance.

As reference mixing head the SMH is utilized. Analogous to the process characteristics (see chapter 5), the SMH is operated with a Statomix static mixing device of Sulzer Chemtech. It contains 32 shear elements in a 234 mm long, 6.4 mm inner diameter tube.

6.1.3 Preforming procedure of the Resin Transfer Molding characteristics

Four unidirectional layers of the glass fiber material are stacked to a (-45°/+45°/- 45°/+45°//+45°/-45°/+45°/-45°) preform. A theoretical fiber volume fraction (FVF) of 47.22 % is achieved assuming a glass fiber density of 2.55 g/cm³ [143]. This FVF is within the range from of a standard high volume RTM cycle. Here, the FVF ranges from 45 % to 50 % [20]. The final contour of the preform is produced by die cutting. The stacked layers are placed in the Joos HP-S30 press upon a PTFE plate. A welded cutting tool possessing the mold cavity contour, which is circularly reduced by 1 mm, is placed on top of the stacked layers. The press is closed at a force of 50 kN and the layers are cut to the final shape.

6.1.4 Injection procedure of the Resin Transfer Molding characteristics

The press is set to a closing force of 200 kN and its electrical heating system is used to heat the mold to 80 °C. The temperature of the resin component is adjusted according to Tab. 6-1 whereas the temperature of the hardener component is set to 25 °C for all injections. In the following, the specification of each injection procedure step is described. Details on their purposes are given in chapter 2.2.4 and chapter 2.2.5:

- Evacuation (see Fig. 6-2, open valves: Va_1 1-3, Va_2 1-2, Va_3 1-3): This step is performed for the production of the FRP. Hereby, a vacuum pump is connected to the outlet of the mold. It vacuums the cavity and the resin trap. Hereby, an absolute pressure <5 mbar is achieved. The vacuum is applied during the injection step, too.
- Injection:
  - Pre injection (see Fig. 6-2, open valves: Va_1 1-3, Va_2 1-2, Va_3 1-3): This step is performed to exclude the metering inaccuracies during the ramp-up of the metering device from the resin system inside the plates.

It also ensures a constant resin temperature and a constant injection pressure before the cavity filling.

- Cavity filling (see Fig. 6-2, open valves: Va_1 1-3, Va_2 1-3, Va_3 1-3): During this step, the cavity of the mold is filled with resin system. Whereas the filling of the empty mold for the NRP production is performed at a constant injection pressure, the resistance of the fiber material in the mold for the production of the FRP leads to an increase of the injection pressure throughout the cavity filling.
- Cavity flushing (see Fig. 6-2, open valves: Va_1 1-3, Va_2 1-3, Va_3 1-3): This section describes the state, when the cavity is fully filled by the resin system and a saturated volume flow occurs at a constant injection pressure. For this, the valve configuration is equal to the cavity filling step.
- Post pressure (see Fig. 6-2, open valves: Va_1 1-3, Va_2 1-3, Va_3 2-3): This process step describes the metering and the mixing of the resin system while the outlet is closed. Hereby, the pressure rises inside the cavity.

- Curing (see Fig. 6-2, open valves: Va_1 2-3, Va_2 1-2, Va_3 2-3): After the injection, the resin system is isothermally cured in the cavity. Here, the cycles suggested in the respective data sheets at a mold temperature of 80°C are performed (see Tab. 6-1, Fig. A-1, Fig. A-2).
- Cleaning (see Fig. 6-2, open valves: Va_1 2-3, Va_2 1-2, Va_3 2-3): Since the mixing head as well as the measurement device are filled with reactive resin system after the injection, the equipment has to be cleaned before the resin system is cured therein. Thus, acetone and compressed air are alternately flushed through the devices.
- Post curing: The plates are post cured in an oven according to the data sheets (see Tab. 6-1, Fig. A-1, Fig. A-2) after three weeks of storage at room temperature.

The process parameters of both plate types and resin systems for the RTM characteristics are given in Tab. 6-1.

Tab. 6-1 Overview of the process settings for the RTM characteristics

Resin system, plate type	RIM, NRP	RIM, FRP	XB, NRP	XB, FRP
Preforming	NN	Die cutting	NN	Die cutting
Resin temperature	42.5 °C	42.5 °C	60.0 °C	42.5 °C, 60.0 °C, 80.0 °C
Evacuation	NN	30 s	NN	30 s
Pre injection	100 cm³	100 cm³	50 cm³	50 cm³
Cavity filling	300 cm³	150 cm³	300 cm³	150 cm³
Cavity flushing	250 cm³	150 cm³	Various	Various
Post pressure	NN	~7*10^5 Pa	NN	> 8*10^5 Pa
Curing	30 min at 80 °C		20 min at 80 °C	
Post curing	24 h at 25 °C and 15 h at 80°C		2 h at 120 °C	

6.1.5 Data collection for the Resin Transfer Molding characteristics

The process parameter are distinguished by their source of detection: the data log of the injection machine (see chapter 6.1.5.1) or the mechanical testing (see chapter 6.1.5.2).

6.1.5.1 Data log of the injection machine

In this investigation, the mixing head is connected to a RTM tool for the injection. Therefore two factors of chapter 5 are renamed: the counter pressure p_{mix} is named injection pressure p_{inject} and the resin system temperature after the mixing head T_{mix} is named injection temperature T_{inject} (see Fig. 5-4). The data log of the injection machine, which consists of the data log of the metering device and of the ultrasonic device is used to control the factors volume flow, resin temperature, amplitude and injection pressure. Further it is used to record the development of the responses power, temperature of the resin system after mixing and the injection pressure. At the XB resin system injection, the injection pressure is not measured by the pressure sensor next to the mixing chamber p_{inject} since the neat resin area below the pressure sensor leads

to an acceleration of the exothermal reaction in this area before the resin system reaches the mold. For this, the pressure sensor at the inlet is utilized p_{inlet} (see Fig. 6-1). This sensor is tarred after the mold closes. Its measurement is influenced by the change of the preform compaction during impregnation [67, 68, 144]. Therefore the measurement is not as confident as the injection pressure sensor to evaluate the pressure state in the mixing chamber but is still usable for an estimation.

The data log is separated according to the steps of the injection (see Tab. 6-1). A data extraction at different positions, as in the process characteristics (see chapter 5.1.3.1), is not necessary. Here, the focus is on the development of the parameters during the whole injection and not on the characteristics of a resin system sample.

6.1.5.2 Mechanical testing

For the mechanical investigation, two test methods are selected: Samples of the NRP are tested in a tensile test according to the standard DIN EN ISO 527-2 [107]. As described in chapter 2.4.3, this method enables to draw a conclusion on the network homogeneity of the mixed resin system. Samples of the FRP are exposed to a in plane shear (IPS) load according to the standard DIN EN ISO 14129 [108]. This load case is selected due to its higher sensitivity towards the matrix properties compared to other load cases, for example a tensile load in fiber direction. Two restrictions are made compared to the guidelines of the IPS standard [108]. Due to the high areal weight of the selected fiber material, 8 instead of the required 16 layers are stacked. Further, not all parameter combinations allow a preparation of five samples because of locally insufficient hardening of the part.

Sample preparation

For the production of the NRP samples, water jet cutting is performed. The samples are shaped according to the series 1BA, because of the sample thickness restriction to the cavity height of 2 mm. The critical effects of water jet cutting, namely the temperature input [145] as well as the striation by the drift of the water jet while cutting [146], are minimized by the low sample thickness. Further, the alternative, i.e. casting, would imply another mold geometry accompanied by the loss of comparability with the FRP injection conditions. Even though some of the produced samples are excluded from the mechanical testing, due to notches at the edges of the sample. These defects occur because of a non controlled deflection of the water jet at the cutting table. The FRP samples are cut by a diamond saw.

The samples are cut perpendicularly to the inlet-outlet axis at both plate types. Six samples are cut out of each plate. Putative property variations caused by different fill states of the cavity can be recognized in these samples. After cutting the samples, their surfaces are cleaned by a solvent. Then, an acryl based white paint is sprayed on one flat side by an airbrush. Latter is repeated three times with a 15 min break in between.

After that, a black dot pattern is applied. A dot size of approximately six pixel and a randomized distribution are targeted.

Testing

A picture of the test setup can be seen in Fig. 6-3. The sample is placed in between the clamping jaws, which are attached to a 100 kN load cell of Hegewald & Peschke. After the sample is oriented vertically, an abrasive paper is added to reinforce the friction between the clamping jaws and the sample. A force of 5 N is applied to the NRP samples and a force of 10 N is applied to the FRP samples to gain a preload in the samples. The tests are conducted under displacement control and a cross head displacement rate of 2 mm/min at the testing of the NRP samples and a cross head displacement rate of 4 mm/min at the testing of the FRP samples are imposed. The test is finished after a force drop of 60 %, which indicates the final failure of the sample.

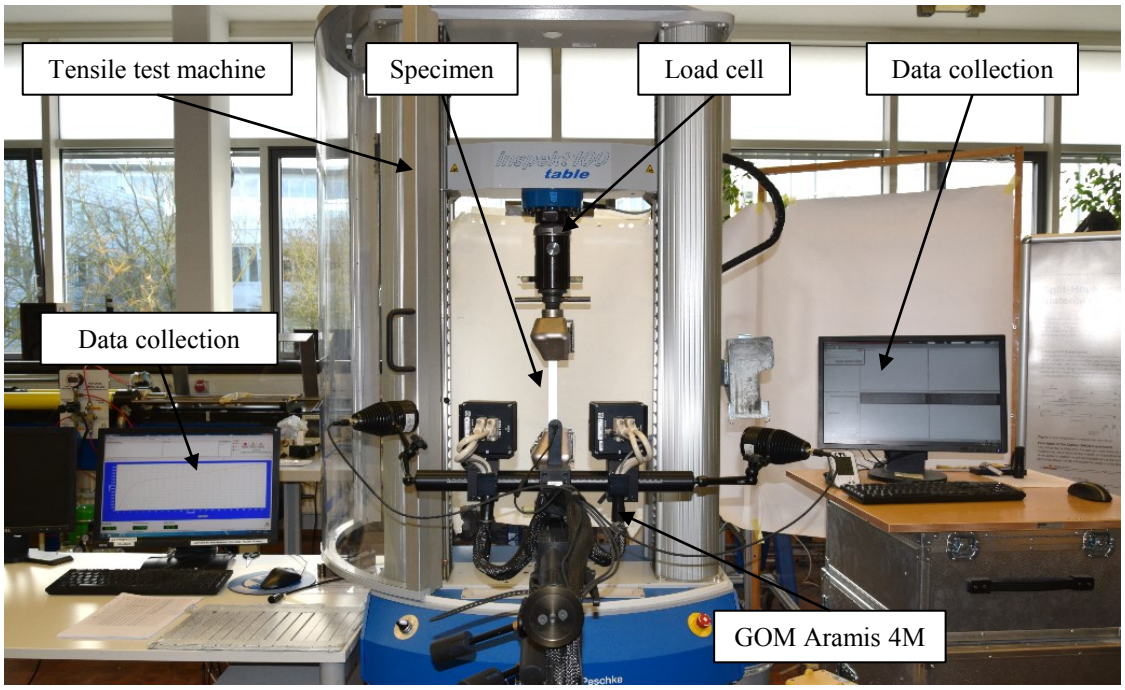

Fig. 6-3 Tensile test machine with a 100 kN load cell and a in plane shear (IPS) sample

Analysis

The digital image correlation system GOM Aramis 4M combined with the Aramis software 6.3.1 of GOM is used to detect the strain of the samples. The frame rate is set to 2 Hz and the facet size to 20x20 pixel. The facet step is 15x15 pixel and the computation size is 3x3 pixel. A virtual strain gage is applied to the sample to measure the strain. The virtual strain gauge at the NRP covers an area of 30x5 mm², the virtual strain gage at the FRP an area of 40x10 mm². These sizes are selected to achieve a stable strain field without the influence of the clamping area. Hereby the mean value of the strain detected in the respective area of the virtual strain gage is calculated. Fig. 6-4

shows the images of a neat resin sample and a fiber reinforced sample within the Aramis software during the test and the broken samples after the test.

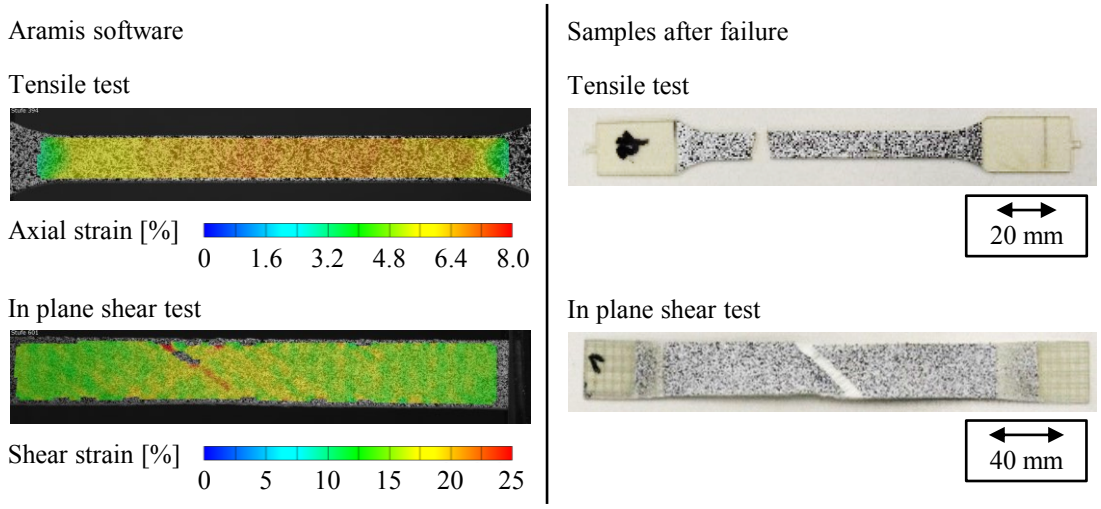

Fig. 6-4 Tensile and in plane shear (IPS) sample after the test: Aramis system (left) and real sample (right), the images are rotated 90° counterclockwise

The measurement noise of the punctual strain signal of Aramis is 0.02 % and averaged 0.0002 %. Since strains of 1 % to 2 % are expected, the measurement method is valid. For the processing of the results, a Matlab code is used.

6.2 Results

The results of the RTM characteristics are divided into three aspects: First, the optical inspection of the plates is carried out (see chapter 6.2.1). Hereby, the focus is on a qualitative evaluation of the injected plates produced at various process settings (see Tab. 6-1). Second, the quantitative analysis of the process parameters during the injection process is performed. This includes a comparison of these results to the process characteristics results (see chapter 6.2.2). Third, the results of the mechanical tests are revealed and discussed (see chapter 6.2.4).

6.2.1 Optical inspection of the plates

Not all combinations of process parameter lead to a sufficiently injected plate. To determine the overall quality, the injected plates are distinguished by the occurrence of wet spots or dry spots (see Fig. 6-5). Plates without defects describe a completely filled and cured, rigid plate. Wet spots imply an insufficient mixing of the resin components, which led to no or partly curing of the resin system. These wet areas are gluey and possess a glossy surface. Dry spots specify an area without resin system after curing. For the occurrence of these spots, three reasons are distinguished: First, the curing reaction starts before the plate is fully filled. Second, an inhomogeneous permeability of the preform leads to race tracking [147]. This denotes the flushing of the resin system

in areas of high permeability. Areas with low permeability stay dry. Third, the vacuum level in the cavity is insufficient and the dry spot results from the inclusion of air.

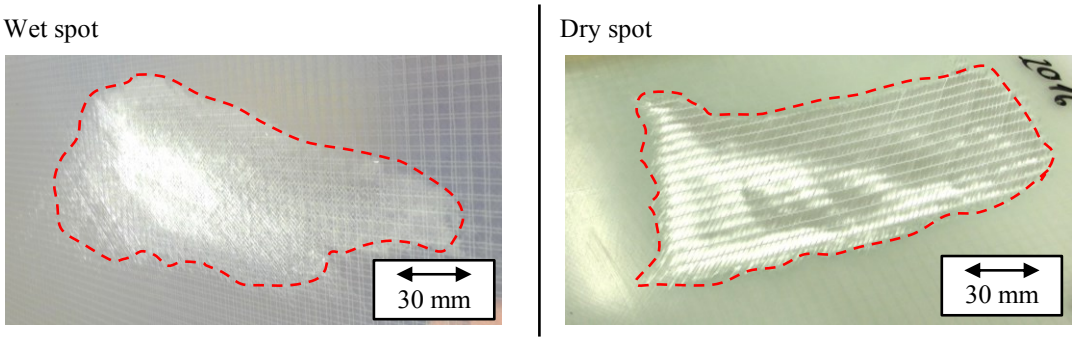

Fig. 6-5 Defects at the FRP plates, optical inspection; wet spot (left) and dry spot (right)

In Tab. 6-2 the quality of the injected plates of both resin systems and plate types is shown. The results are fielded by the amplitude and the volume flow variation. The production of plates out of RIM without defects is possible with the UMH at an amplitude of 50.0 µm and 62.5 µm as well as the SMH. At lower amplitudes, the results of the UMH are diverse. Plates without defects are built at a volume flow of 50 cm³/min independent of the amplitude. Plates with a wet spot occur at a volume flow of 150 cm³/min for NRP and at a volume flow of 100 cm³/min and of 150 cm³/min for FRP. The parameter combinations leading to a plate without defects are reduced by using XB instead of RIM as resin system. The short pot life of XB needs a shift of the inspected volume flow steps from 50 – 100 – 150 cm³/min to 100 – 150 – 200 cm³/min. By this, a complete filling of the cavity before curing is theoretically enabled. Analogous to the NRP results with RIM, the NRP produced with XB show an amplitude threshold for the production of plates without defects. Hereby, the threshold value is dependent on the volume flow: at a volume flow of 100 cm³/min, an amplitude of 50.0 µm is sufficient whereas at a volume flow of 150 cm³/min only the injection at an amplitude of 62.5 µm results in a plate without defects. If this threshold is undercut, a wet spot occurs. The injection of the FRP with XB shows the highest sensitivity to a parameter variation. The process window is reduced to an operation point. Thereby, an amplitude of 50.0 µm is combined with a volume flow of 150 cm³/min. The reduction of the amplitude leads to a wet spot. The increase of the amplitude to 62.5 µm or the reduction of the volume flow to 100 cm³/min results in a dry spot. The FRP produced with the SMH result in a plate with a dry spot at a volume flow of 100 cm³/min. At a volume flow of 150 cm³/min and of 200 cm³/min, plates without defects are manufactured.

Tab. 6-2 Overview of the injected plates for the RTM characteristics: variation of the resin system (RIM, XB) and the plate type (neat resin plate (NRP), fiber reinforced plate (FRP))

Resin system, plate type	RIM, NRP			RIM, FRP			XB, NRP			XB, FRP		
$\dot{V}$ [*10 cm³/min]	5	10	15	5	10	15	10	15	20	10	15	20
UMH, A, Pw												
25.0 µm	1			1								
37.5 µm	1	1	1	1	1	2	1				1	
50.0 µm	1	4	1	1	3	1	3	1	1	1	3	
62.5 µm	1	1	1	1	1	1	1	1	1	1	1	1
500 W											1	
SMH												
	1	3	1	3	3	1	1	3	1	1	3	1

Legend:

Plate without defects | Plate with wet spot | Plate with dry spot | x Quantity of plates

The processing of the UMH in RTM shows a lower amplitude threshold for both resin systems and plate types to produce parts without a wet spot. Hereby, the threshold value depends on the volume flow. Since the amplitude of the sonotrode defines the pressure variation in the sonicated fluid, this value defines the volume as well as the density of the cavitation zone (see Fig. 3-4). Guo et al. [112] have detected a higher density of the cavitation zone at higher amplitudes during the sonication of agglomerated crystals in ethanol. Tzanakis et al. described a larger cavitation zone at higher amplitudes in ethanol [113]. Based on these results and the findings in this thesis, it is claimed that a lower amplitude threshold value exists for the sufficient mixing of resin components in RTM. Further the FRP produced with XB show an upper limit. The exceedance of this limit leads to plates with dry spots. This limit is not detected for the NRP with XB as well as for both plate types produced with RIM. During the production of the FRP with XB a high injection pressure occurs compared to those of the other setups. The high injection pressure is accompanied by a high injection temperature in the UMH (Fig. 6-13) which leads to an acceleration of the exothermal reaction of the resin system. This, in turn, results in a dry spot in the plate. It is assumed that the temperature delta in the UMH and therefore, the limit of this process, can be controlled by adjusting the power (see Eq. 2-3, Fig. 5-10). This claim is examined by an injection trial at a constant power (see chapter 6.2.3).

6.2.2 Injection parameters

Target of the process parameter inspection is to quantify the effect of these process parameters and to detect their interaction during the injection. Further, the liability of the process characteristics (see chapter 5.2) for predictions on the behavior of the process parameter is investigated. The results are split according to the saturation state (see chapter 2.2.3) of the resin system flow during the injection:

- First, the parameters at a saturated flow are inspected. For the FRP, this condition is reached when the preform is fully impregnated and a continuous volume flow through the cavity occurs. This process step is called cavity flushing (see Tab. 6-1). The injections of FRP with XB do not show stationary conditions at the flush through step due to the fast curing reaction. For this XB is excluded from the saturated flow inspection. Due to the constant injection pressure during the saturated flow, these results are used to verify the model of the process characteristics (see chapter 5.2).
- Second, the parameters at an unsaturated flow during the FRP production with both resin systems are examined. This condition exclusively occurs during the cavity filling of the FRP. Hereby, a constantly increasing injection pressure appears (see Tab. 6-1). Due to the absence of a preform for the NRP injections, the conditions are assumed to be stationary during cavity filling.

At each flow condition, the results are separated by the process parameters. First, the injection pressure is analyzed, followed by the power and the resin system temperature. For the saturated flow condition, the comparison to the results of the process characteristics of the UMH is added. Since the occurrence of wet spots is traced back to the mixing process parameters, plates exhibiting these defects are integrated into this analysis. Plates with dry spots show an insufficient injection. Latter is not dependent on a sole altering of the mixing process parameters. These plates are excluded.

6.2.2.1 Saturated flow during injection

Saturated flow conditions occur during the cavity flushing. Stationary flow is assumed from a metered resin system volume from 100 cm³ to 125 cm³ of the cavity flushing step (see Tab. 6-1).

Injection pressure at saturated flow conditions

In Fig. 6-6, the injection pressure development of the FRP injection is shown. Hereby, the results at different volume flows are revealed for both resin systems and both mixing heads. At the injection with RIM (Fig. 6-6 a)), the injection pressure is slightly lower for the UMH at the highest volume flow while no difference between the mixing heads is visible at middle and low volume flow values. The amplitude variation does not show an effect on the injection pressure. The injection with XB (Fig. 6-6 a)) shows more than three times higher inlet pressures compared to the resulting injection pres-

sure with RIM. Further, the inlet pressure at the UMH is slightly higher than the inlet pressure at the SMH.

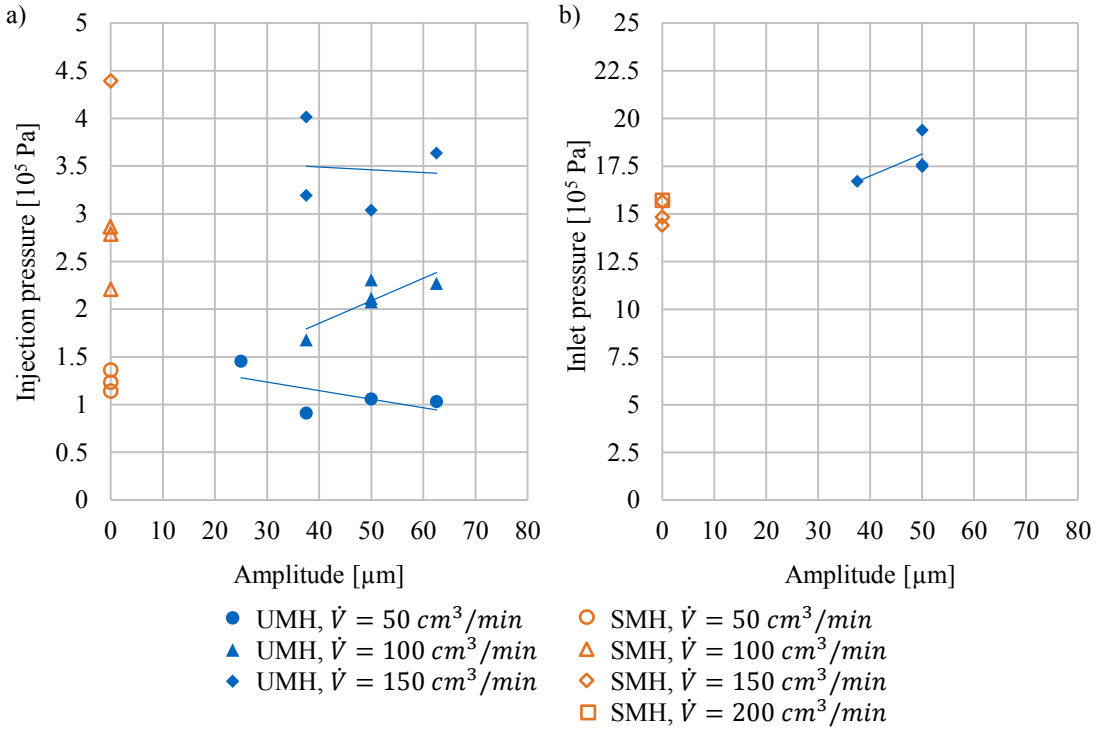

Fig. 6-6 Injection pressure at varying amplitudes during saturated flow through the FRP preform injected with RIM (a) and XB (b) using the UMH and the SMH

The accuracy of the pressure sensors is specified with $0.1*10^5$ Pa. At a volume flow of 150 cm³/min differences between the mixing heads are visible: injections with RIM show a lower injection pressure at the UMH compared to the SMH. These small deviations are traced back to the reduced viscosity and therefore, friction of the resin system in the tube between the UMH and the mold. In contrast, a higher inlet pressure occurs at the UMH injections than at the SMH injections with XB. Steady inlet pressure values are detected before the preform is volumetrically filled for the XB resin system (see chapter 6.2.2.2). It is assumed that race tracking disturbs the increase of the pressure by the preform resistance and therefore, the saturated inlet pressure values are inconsistently reduced by this effect.

Power and resin system temperature at saturated flow conditions

In Fig. 6-7, the responses power and injection temperature of the NRP are shown of both mixing heads. They are injected with RIM (see Fig. 6-7 a)) and XB (see Fig. 6-7 b)). Hereby, the amplitude variation at different volume flows is displayed. For the UMH, the resin component is heated to 42.5 °C for RIM and to 60.0 °C for XB before mixing. The injection of both resin systems with the UMH shows a higher power and higher injection temperature at higher amplitudes. This trend is detected at all volume flow settings. A higher volume flow correlates with a lower injection tempera-

ture. Further, the slope of the power to the amplitude and the slope of the injection temperature to the amplitude decrease with a higher volume flow. The RIM injection temperatures are smaller than the respective XB injection temperatures. The injection temperature of the trials with SMH is not affected by the mixing technique. The resin component is heated to 42.5 °C for RIM and to 60.0 °C for XB while the hardener components are set to 25.0 °C (see Tab. 6-1).

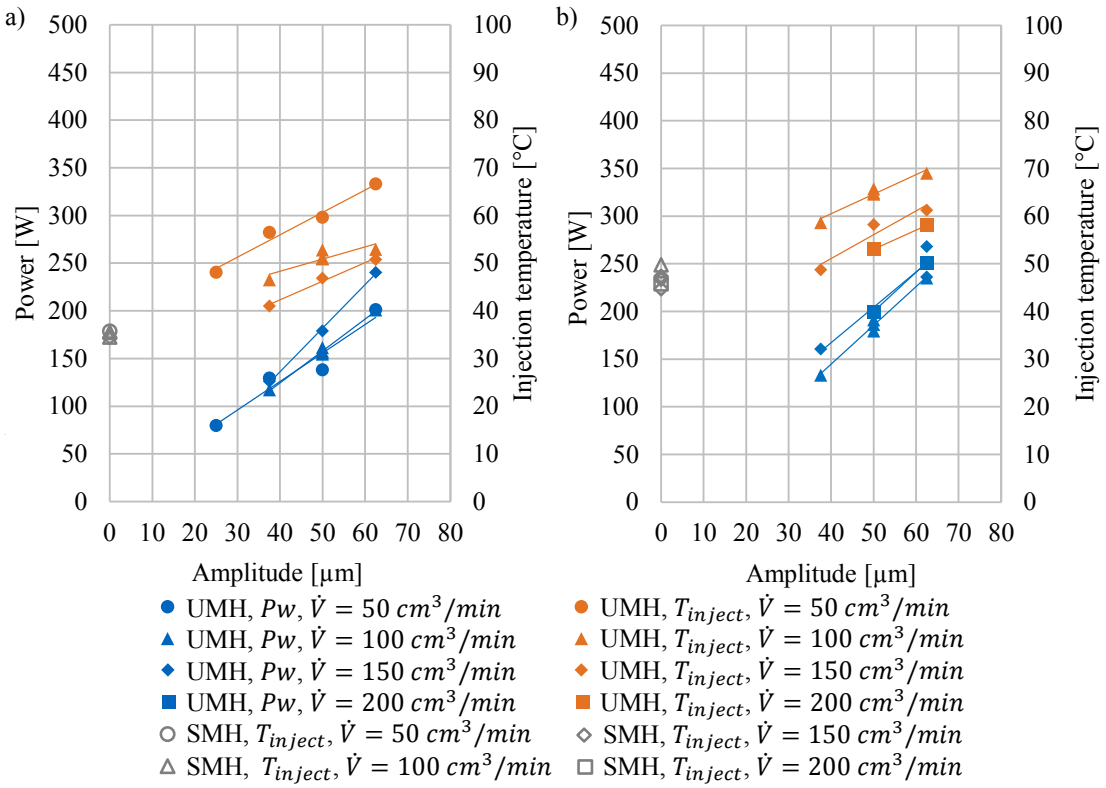

Fig. 6-7 **Power and injection temperature at varying amplitudes during saturated flow through the NRP preform injected with RIM (a) and XB (b) using the UMH and the SMH**

The higher injection temperature at a higher amplitude is explained by reaching the cavitation threshold (see chapter 2.1.2) for the bubble creation. At a high amplitude, more bubbles occur. This leads to a higher number of implosions and therefore, a higher temperature in the resin system. Since the exposure time shortens if the volume flow is increased, the heating effect is reduced at a higher volume flow. The power is higher for XB compared to RIM at the NRP injections. The viscosity of the XB resin system inside the tube between the UMH and the mold is higher due to its shorter pot life. This leads to a higher injection pressure and therefore power.

The power and injection temperature are pictured in Fig. 6-8 for the FRP injections. For both resin systems namely RIM (see Fig. 6-8 a)) and XB (see Fig. 6-8 b)), the trends are analogous to the NRP production (see Fig. 6-8). For the UMH, a high amplitude results in higher values for power and injection temperature. A lower temperature

increase at higher volume flow is detected, too. However, both responses are at higher values compared to the NRP injection and are more sensitive to an amplitude variation. The injection temperature of the SMH for the FRP injections are similar to the NRP injections.

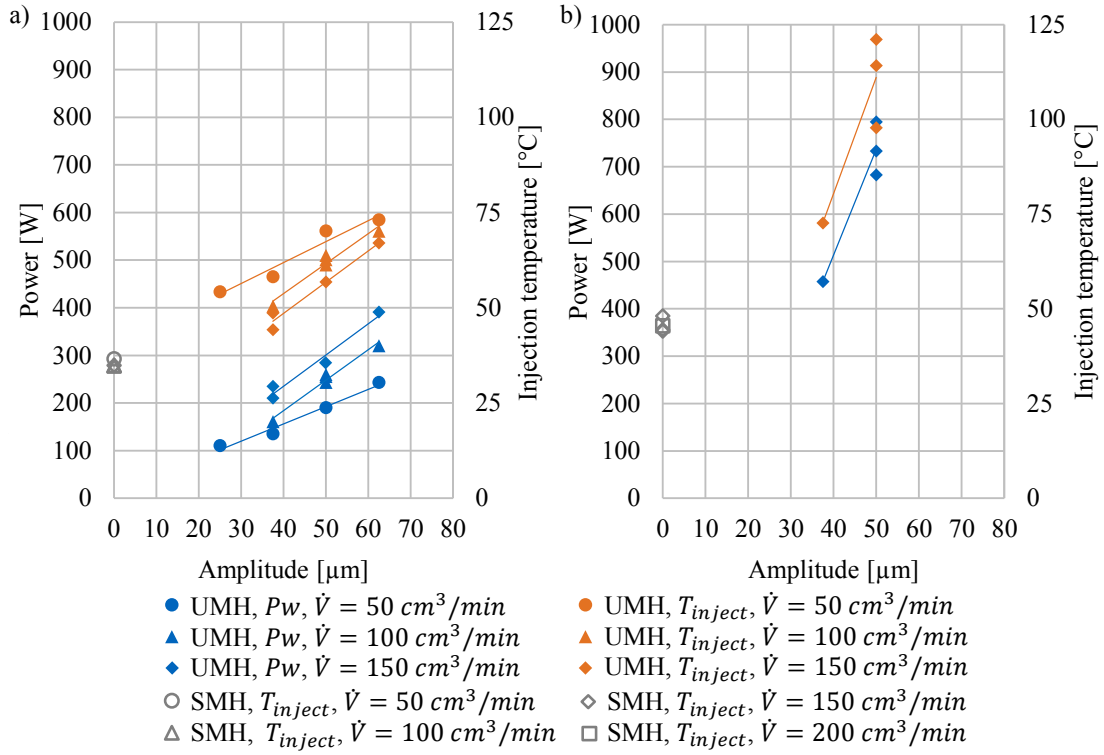

Fig. 6-8 **Power and injection temperature at varying amplitudes during saturated flow through the FRP preform with RIM (a) and XB (b) using the UMH and the SMH**

The increase of the power and injection temperature values within the FRP injection is explained by the increase of the injection pressure. The preform acts as a flow resistance (see Fig. 6-6). This leads to higher injection pressures and therefore power and injection temperatures (see Fig. 6-6). Within the XB injection, the comparably fast viscosity rise further increases the injection pressure. The injection temperature is even higher and more sensitive to an amplitude variation. The resin temperature of the SMH is not affected by producing FRP instead of NRP.

Verification of the process characteristics model by implementing the parameters of the RTM characteristics

The trends and findings at saturated flow conditions are analogous to the results of the process characteristics (see chapter 5). Apart from the process parameters, the setup of the process characteristics is used for the analysis of the rheology and the thermal analysis of the resin system. For this, the preform resistance is imitated by a pressure pot (see Fig. 5-2, Fig. 5-5). Thus, the injection pressure counts as an adjustable factor instead of a response, which is the case in the RTM characteristics. The ultrasound

parameters in both investigations are compared to prove if this replacement is valid. By this, the transferability of the rheology response and the thermal response to a RTM injection is evaluated. The following is assumed: If both ultrasound parameters amplitude and power show similar values the mixing mechanism is equal at both investigations. The amplitude is a factor, the power is a response in both cases. For this, the occurring parameter of the RTM injections volume flow, resin temperature, injection pressure, chamber volume and amplitude are inserted as factors into the DoE model of the process characteristics. The factor values of each injection are listed in the appendix (see Tab. A-8). In Fig. 6-9, the power values of the RTM characteristics and the prediction based on the process characteristics model are revealed. The injections of the NRP (see Fig. 6-9 a)) and the injections of FRP injections (see Fig. 6-9 b)) show a good agreement of the predicted values with the observed values. The trends between the power values of the injections are displayed. A tendency concerning an over prediction or under prediction of the real values is not detected.

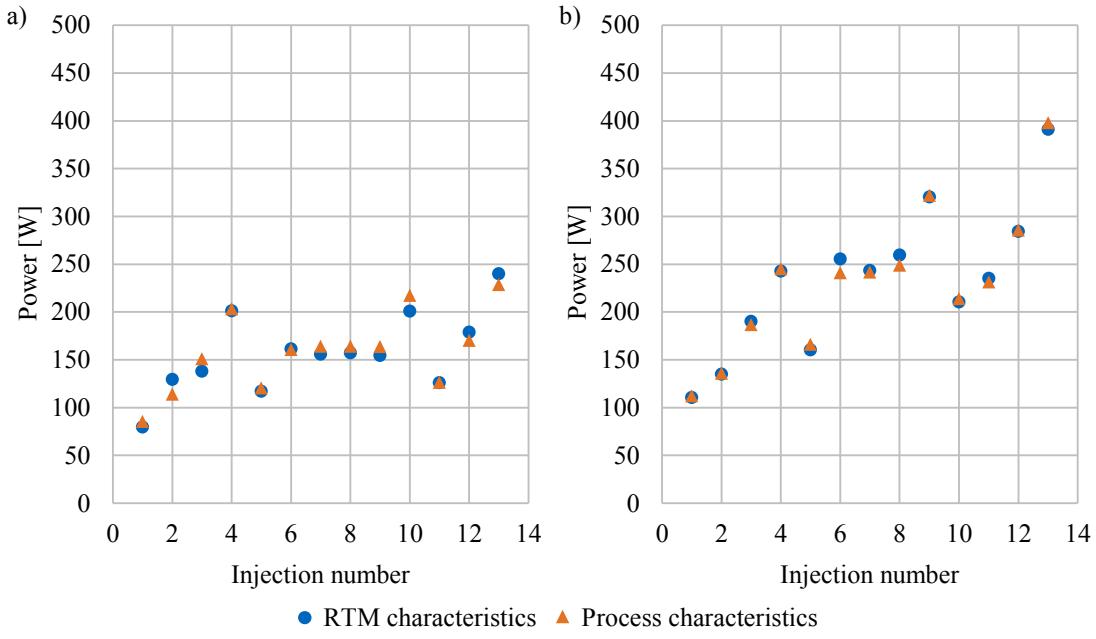

Fig. 6-9 **Power values predicted by the process characteristics model and occurred once within the RTM characteristics for the NRP a) and FRP b)**

It has to be taken into account that the RTM values are detected during a plate production. Hereby, additional inaccuracies caused by control variables, e.g. handling, fiber orientation or positioning of the preform in the mold, could influence the consistency of the power response. An overall good agreement between the occurring and predicted power values is detected. The experimental results of the process characteristics are valid. The rheological and the thermal properties of the resin system can be derived for RTM thereof. Further, the process characteristics model can be utilized for the prediction of the ultrasound parameters in RTM. Even though, a prediction of the mixing quality can only be achieved by a consideration of the process parameter, namely vol-

ume flow, counter pressure, resin temperature and the ultrasound parameter, namely amplitude and power.

6.2.2.2 Unsaturated flow during injection

In this chapter, the process parameters at unsaturated flow conditions are inspected, which occur during the filling of the cavity (see chapter 2.2). This condition solely occurs during the impregnation of the preforms in the context of FRP injections. The repetitions of the injection at a volume flow of 100 cm³/min and an amplitude of 50.0 µm is occasionally not shown in the following figures. This is done for a higher clarity of the figures. Nevertheless, the scattering of the repetitions is taken into account for the discussion of the results. The injection time starts parallel to the cavity filling step (see chapter 6.1.4).

Injection pressure at unsaturated flow conditions

In Fig. 6-10 the injection pressure at various volume flows is pictured for the production of FRP with RIM. Thereby, both mixing heads are considered. In general three phases are distinguished: First, the cavity filling takes place. It is characterized by the rise of the pressure. This represents the unsaturated flow condition. Second, the cavity flushing takes place. It is characterized by a constant injection pressure. Third, the post pressure section takes place. It is characterized by a high pressure gradient. It is visible that a higher volume flow corresponds with a higher gradient of the injection pressure during cavity filling. This is true for both mixing heads. At the UMH the gradient of the injection pressure varies with changing amplitudes. Even though no distinct dependency between amplitude and gradient of the injection pressure is detected. The three times repetition at a volume flow of 100 cm³/min at the SMH and an 50 µm amplitude at the UMH shows a similar scattering as the amplitude variations at the same volume flow with the UMH.

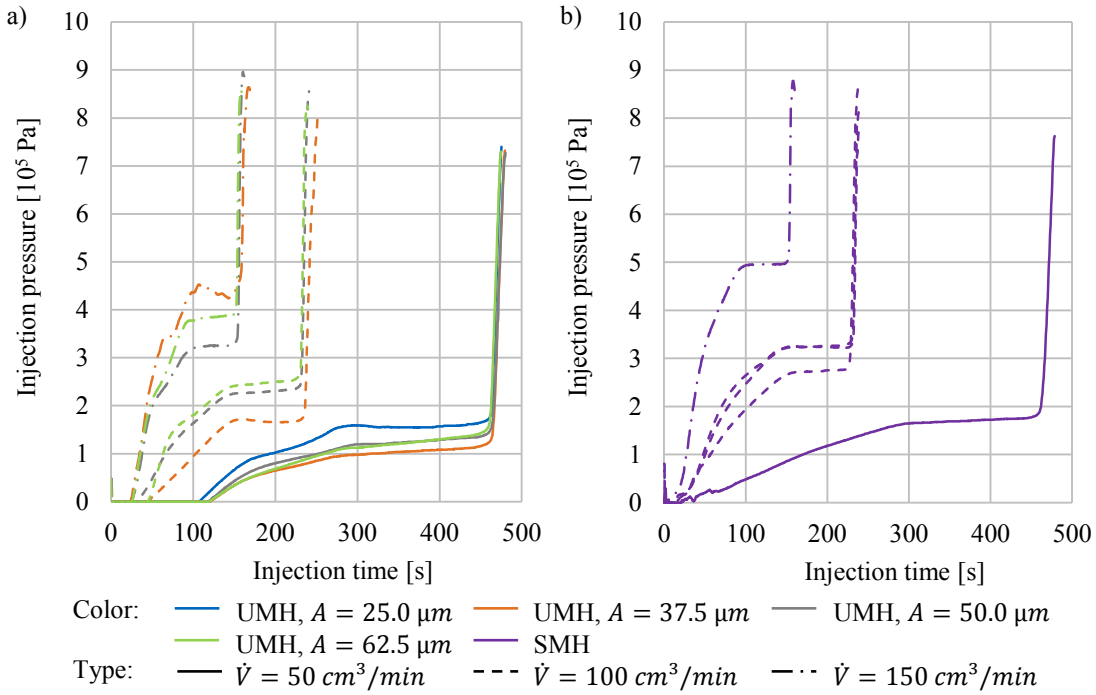

Fig. 6-10 Injection pressure at varying volume flows through the FRP preform injected with RIM using the UMH (a) and the SMH (b)

The injection pressure curves correlate with findings of W. Raffelt [19]. In his investigations he claims, that the mold temperature dominates the resin system temperature and therefore its viscosity during filling. For this the influence of the amplitude on the injection temperature and thus, the resin system viscosity before entering the cavity has a minor impact on its conditions in the mold. The injection pressures are slightly reduced for the injections with the UMH compared to the SMH.

The inlet pressure during the FRP injection with XB is revealed in Fig. 6-11. For the UMH injection (Fig. 6-11 a)), the pressure rises to approximately $20*10^5$ Pa within 60 s. For the SMH (Fig. 6-11 b)), a similar gradient is detected at both volume flows.

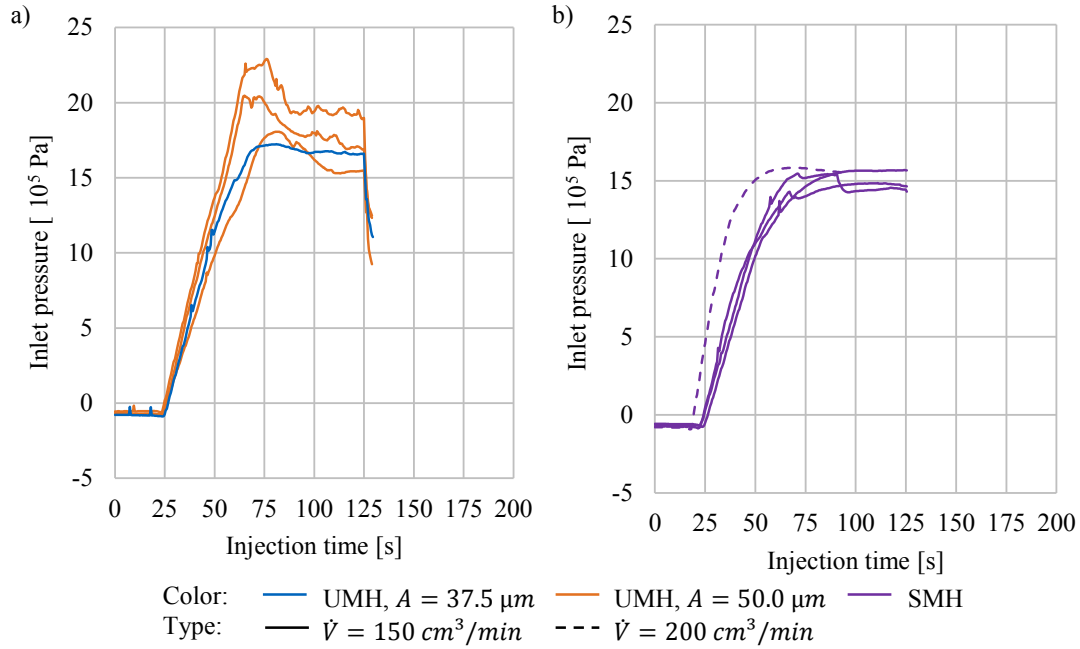

Fig. 6-11 Injection pressure at varying volume flows through the FRP preform injected with XB using the UMH (a) and the SMH (b)

Even though the inlet pressure is detected for XB and the injection pressure for RIM, the difference in the pressure gradient throughout the cavity filling is distinct. As already mentioned in the discussion of the injection pressure under saturated flow conditions (see chapter 6.2.2.1), an optical inspection of the resin system shows a gelatinous consistency of the first amount of XB reaching the outlet. The higher pressure gradient is traced back to the faster curing reaction of XB. This leads to a viscosity rise of the resin system throughout the cavity filling. The independency of the inlet pressure from the volume flow variation is retraced to the cavity filling behavior. The saturated state of the preforms impregnated with XB is reached approximately 60 s after the start of the injection. In comparison, it takes 100 s to impregnate the preform completely at the injections with RIM. It is assumed that due to the high injection pressure at the XB injections, a bypass stream between preform and mold side wall occurs. This effect is called race tracking. For this, a constant pressure similar to a saturated state occurs even before the preform is completely impregnated.

Power at unsaturated flow conditions

The power at different amplitudes throughout the injections with both resin systems is revealed in Fig. 6-12. For both resin systems, the power follows the trend of the injection pressure (see Fig. 6-10). For the RIM injections (see Fig. 6-12 a)), an effect of the amplitude variation superimposes the influence of the injection pressure. At higher amplitudes, the sensitivity of the power is higher. Higher gradients during the cavity filling appear. The results of XB (see Fig. 6-12 b)) show the power during the injection at a volume flow of 100 cm³/min and the repetitions at a volume flow of 150 cm³/min.

Analogous to the pressure curve, the power value increases faster and to an more than two times higher value compared to the respective one at the RIM injection. Further, the power fluctuation is clearly higher, too.

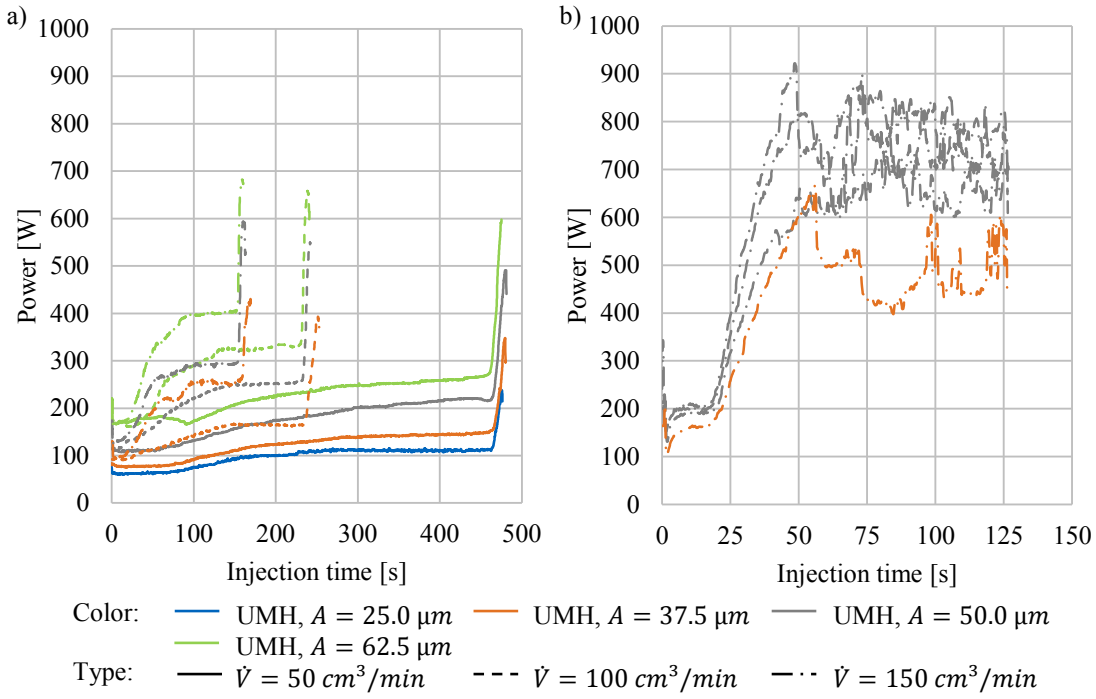

Fig. 6-12 Power at varying volume flows through the FRP preform injected with RIM (a) and XB (b) using the UMH

The development of the power is analog to the findings of the process characteristics (see chapter 5.3). There, amplitude and the injection pressure, namely counter pressure, are identified as the main influencing parameters on the power. Therefore, a distinctive influence on the power by these parameters is visible during the cavity filling under unsaturated flow conditions, too.

Resin temperature at unsaturated flow conditions

In Fig. 6-13, the injection temperature development during the injection of both resin systems processed with the UMH for the production of the FRP is revealed. For the injection with RIM, the injection temperature (see Fig. 6-13 a)) in contrast to the power (see Fig. 6-12), does not follow the injection pressure curve (see Fig. 6-10). Instead, a continuous rise of the injection temperature is visible. It lacks a clear distinction between unsaturated and saturated flow. Further, no sensitivity to the volume flow is shown. A dependency of the injection temperature on the amplitude is detected. The injection temperature at the XB injections (see Fig. 6-13 b) rapidly raises at the beginning of the cavity filling and continues to increase at a lower gradient afterwards. A difference in the heating of the resin system dependent on the amplitude is visible.

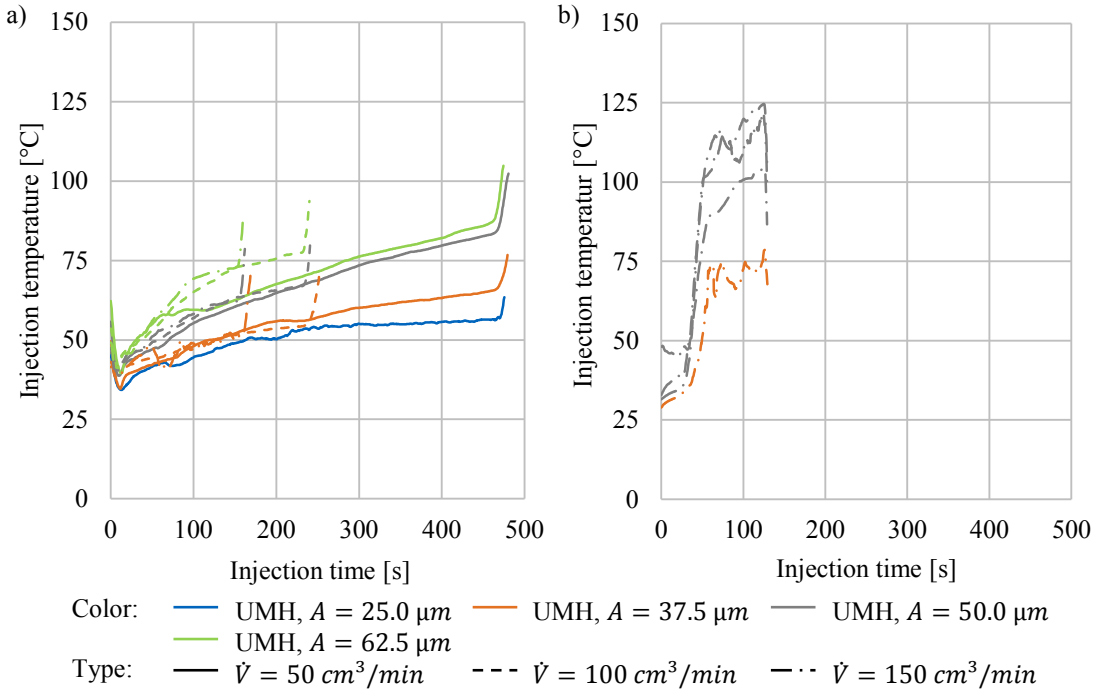

Fig. 6-13 Resin temperature at varying volume flows through the FRP preform injected with RIM (a) and XB (b) using the UMH

The missing kink at the RIM injection temperature curve between the cavity filling and the cavity flushing process step is explained with the heat transfer of the resin system to the UMH as well as to the measurement device. It is assumed that the heating of these components influences the heating of the resin system. The rapid rise of the injection temperature in the XB injections occurs within 10 s. The heat transfer of the resin system to the UMH and to the measurement device plays a subordinated role in this short interval. The fast heating of the resin system temperature above 110 °C shortens the gel time to 1 - 2 min. (see Fig. A-2). The production of plates with dry spots at the highest amplitude of 62.5 µm (see Tab. 6-2) is therefore traced back to a gelation of the resin system in the tube before it enters the cavity.

6.2.3 Injection guidance of the ultrasound parameters

Another target of the RTM characteristics is to select an ultrasound parameter amplitude or power for the guidance of the sonication during an RTM injection. As discussed in chapter 2.3.1 one of these parameter is the factor and the other one is the response during sonication. In the labor investigation (see chapter 3) and the process characteristics (see chapter 5), the amplitude value is selected as the factor and the power as the response parameter. This strategy is chosen due to the influence of the amplitude on the occurrence of cavitation bubbles (see Eq. 2-1). The investigation in this chapter reveals two thresholds, which restrict the process window of injections with the UMH. On the one side, the amplitude entails a lower limit regarding the mixing quality. An undercut of this limit leads to a poor mixing of the resin system. The

result is a plate with a wet spot (see Tab. 6-2). On the other side, the power entails an upper limit regarding the processing of a resin system by heating the resin system during mixing. The heating of the resin system to temperatures above 110 °C in the mixing chamber combined with its flow through a tube before entering the mold leads to a viscosity rise. Latter occurs before the resin system enters the mold and thus, the preform impregnation is hindered. If this upper limit is exceeded, a dry spot occurs within the plate.

An injection of an FRP with XB at a constant power of 500 W is performed (see Tab. 6-1) to compare the development of the ultrasound parameters as well as of the resin temperature during the injection with the respective injection at a constant amplitude guidance. Fig. 6-14 shows the power, the amplitude and the injection temperature of an injection guided by the amplitude (see Fig. 6-14 a)) and the power (see Fig. 6-14 b)). The constant amplitude of 50.00 µm leads to a maximum power of approximately 700 W to 800 W. The injection temperature rises at the end of the saturated flow to a peak value of 120 °C. Thus, for the power guidance the parameter is restricted to a maximum of 500 W. Since the power value would exceed this value, the amplitude is automatically reduced to 38.60 µm and a peak injection temperature of 83 °C at the end of the saturated flow occurs.

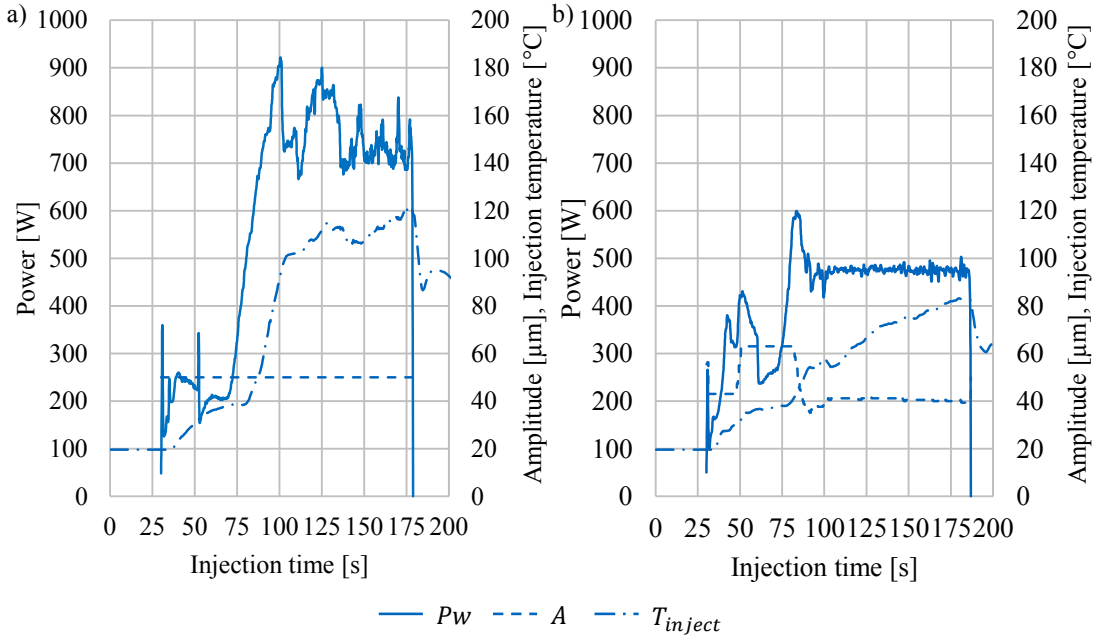

Fig. 6-14 Power, amplitude and injection temperature at an amplitude (a) and a power controlled (b) injection

The comparison of amplitude and power guidance shows that a process guidance by a power control enables the restriction of the resin system temperature increase caused by cavitation. For this, a power guidance allowing the maximum heat input is preferred for the processing of heat sensitive snap cure resin systems, like XB and TRAC (see chapter 2.3.3). This means that the amplitude is set to the maximum allowable value

throughout the injection. It is reduced if the power would exceed the maximum allowable value. It has to be taken into account that the amplitude can only be reduced so far as to the lower amplitude threshold value (see Tab. 6-2) to ensure a sufficient mixing of the resin system.

6.2.4 Mechanical parameters

The mechanical properties of the plates produced at various process parameter sets are determined. The target is to compare the performance of both mixing heads as regards the mechanical properties of the resin system. This investigation focuses on the inspection of plates without defects (see Tab. 6-2). Results with reference to plates with defects are added occasionally for the discussion. For this, the tensile test results of the NRP samples are revealed (see chapter 6.2.4.1), followed by the in plane shear test (IPS) results of the FRP (see chapter 6.2.4.2).

6.2.4.1 Tensile test

The results of the NRP tensile tests are an indicator for the performance of the neat resin system. They define the capacity of the material to withstand loads during axial strain. Hereby, two responses are considered: the tensile strength σ_{max} and the Young's modulus E. Basic formulas with regard to these properties are given in chapter 2.4.3.1.

Tensile strength

Tensile strength describes the maximum stress the material withstands before final failure. Exemplary, the stress axial strain curve of the RIM samples produced at a volume flow of 150 cm³/min and an amplitude of 50.0 µm respective 62.5 µm are shown in Fig. 6-15.

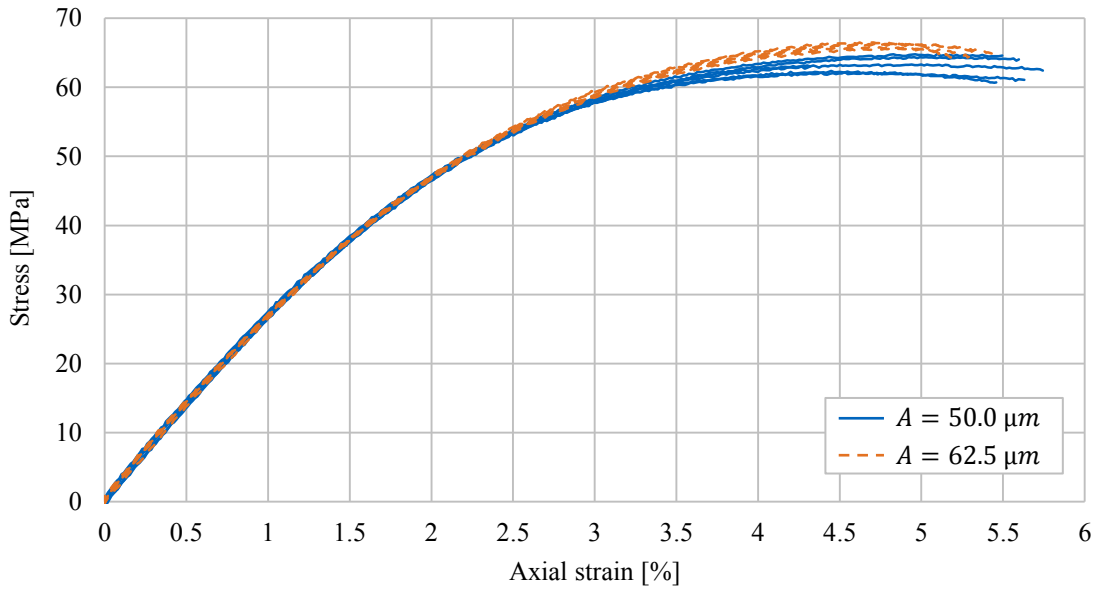

Fig. 6-15 **Stress axial strain curve of the RIM samples produced at a volume flow of 150 cm³/min and an amplitude of 50.0 µm respective 62.5 µm, six samples per setting**

In Fig. 6-16, the tensile strength of the RIM samples produced with both mixing heads are pictured. The highest deviation occurs at the repeated process settings: for the UMH this is the case at a volume flow of 100 cm³/min and an amplitude of 50.0 µm and for the SMH, at a volume flow of 100 cm³/min. At both mixing heads neither parameter variation shows a significant influence on the tensile strength.

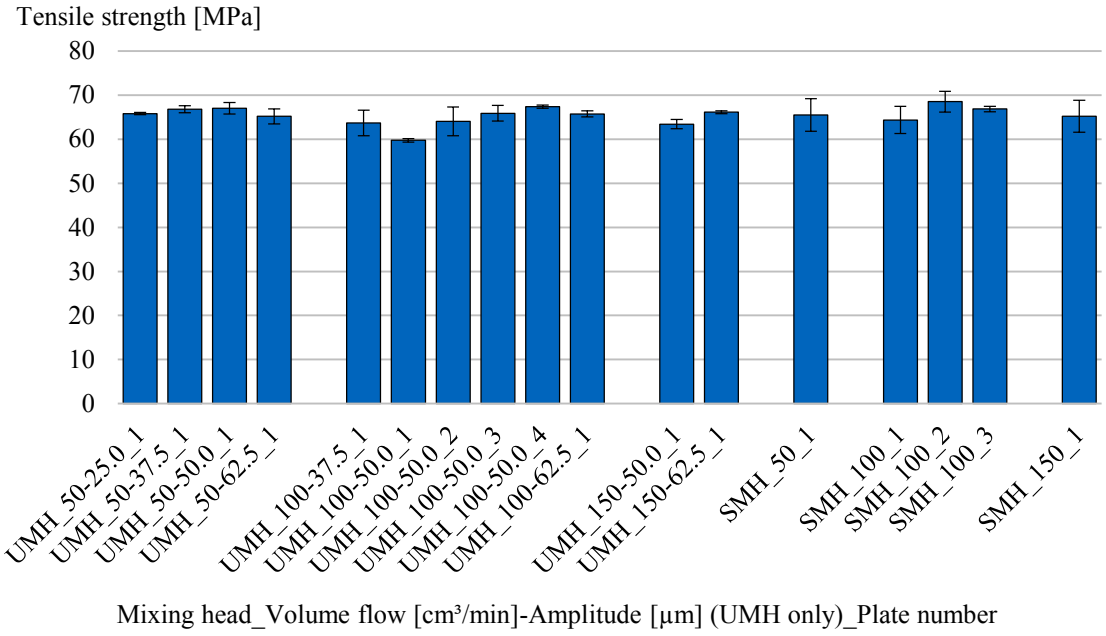

Fig. 6-16 **Tensile strength of the NRP samples out of RIM at varying amplitudes and volume flows using the UMH and the SMH**

All specimens of this investigation are within a tensile strength range from 60 MPa to 75 MPa as revealed in the data sheet (see Fig. A-1). To confirm the sensitivity of the tensile strength of a resin system to mixing inaccuracies, samples are cut out of the rigid area of a plate with a wet spot (volume flow: 150 cm³/min, amplitude: 37.5 µm) caused by insufficient mixing. The tensile strength of these samples is 46.0 MPa (8.22% SD) and therefore significantly below the values of the plates without defects (see Fig. 6-16). The minor tensile strength variation of the samples cut out of the plates without defects is therefore traced back to preparation and measurement inaccuracies, not insufficient mixing.

Fig. 6-17 reveals the tensile strength of samples out of plates produced with XB as resin system. The SD of the XB samples within a plate is higher compared to the SD of the RIM samples within a plate. Most of the samples show similar values for the tensile strength. The UMH sample produced at a volume flow of 150 cm³/min and an amplitude of 50.0 µm as well as the SMH sample produced at a volume flow of 200 cm³/min show a reduced tensile strength.

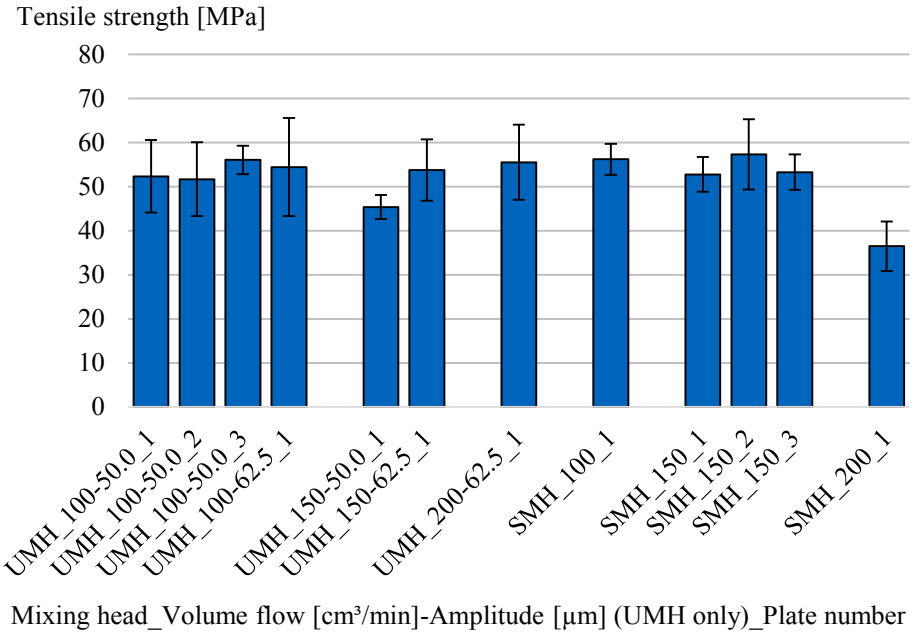

Fig. 6-17 Tensile strength of the NRP samples out of XB at varying amplitudes and volume flows using the UMH and the SMH

According to the XB data sheet (see Fig. A-2), a tensile strength of 60 MPa to 80 MPa might be achievable with this resin system by curing 10 min at 80 °C and 2 h at 120 °C. The mean values of the tensile strength are slightly below this range for most of the plates independent of the selected mixing head. The reason for this overall strength reduction could be due to two aspects: First, the waterjet cutting procedure is critical due to the sand particles roughening the edges and planes of each sample. Micro cracks can locally concentrate stresses and therefore act as initiator for the final failure of the sample even before the material failure. Second, the performed curing

process included to store the plates at room temperature for approximately three weeks before the curing for 2 h at 120°C. This room temperature storing could lead to a reduced mobility of the reactive partners while interlocking and thus a lower network density. Further, the resin system could take up moisture during that storage and therefore show a reduced tensile strength. However, the equal cutting procedure and simultaneous curing of all plates at an identical temperature cycle ensures an equally reduction of the tensile strength within all plates. For this, a comparability is still valid even though the data sheet level is not achieved. The clearly reduced tensile strength at a volume flow of 150 cm^3/min and an amplitude of 50.0 µm with the UMH might be traced back to a reduced mixing quality by undercutting the amplitude threshold value. For the SMH sample, the volume flow of 200 cm^3/min is assumed to be too high for the selected mixing chamber. This also leads to poor mixing. However, both plates do not show a wet spot at the optical inspection (see chapter 6.2.1).

Young's modulus

The Young's modulus represents the resistance of the material against deformation. According to DIN EN ISO 527-2 [107], the Young's modulus is calculated in the range of axial strain between 0.05 % and 0.25 % (see chapter 2.4.3.1). However, in this thesis, the range from 0.10 % to 0.30 % is used. This adaption is made due to a slight bending of the initial clamped specimens (see Fig. 6-18). Therefore, it is straightened before stretched at the beginning of the measurement for the Young's modulus calculation. For this, the axial strain range to detect the Young's modulus is shifted from the lower to the higher axial strain range. By this, the effects of the initial clamping are reduced and a more robust measurement is achieved.

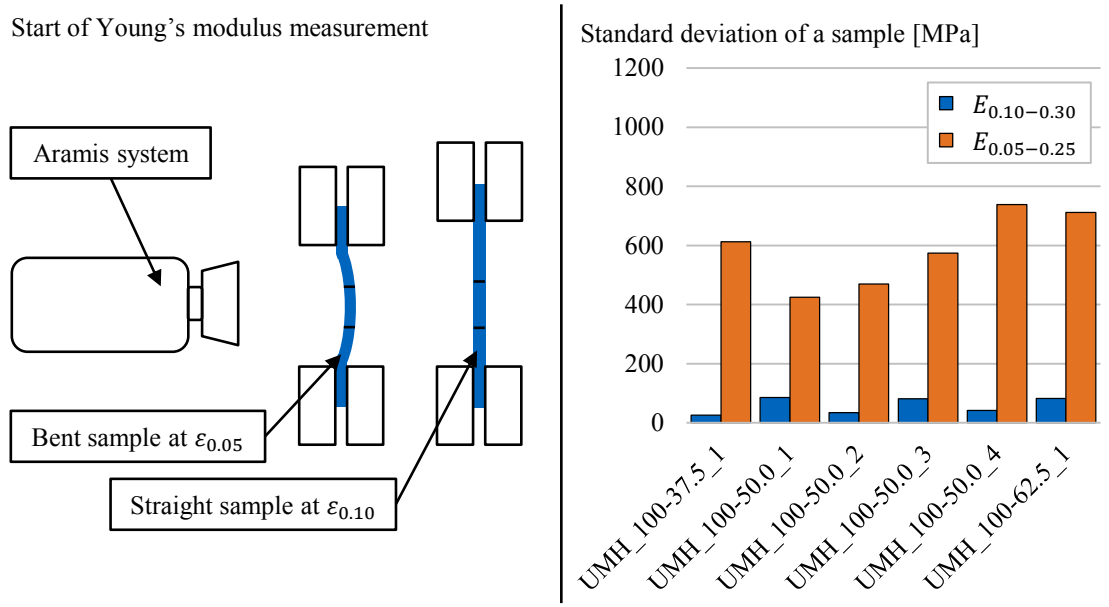

Fig. 6-18 Standard deviation of the stress axial strain curve indicates the straightening effect of the samples before their stretching of RIM samples

Fig. 6-19 shows the Young's modulus of the NRP samples for both mixing heads produced with RIM. All samples show similar values for the Young's modulus. This means that neither the amplitude nor the volume flow variation influences the Young's modulus of the rigid plates.

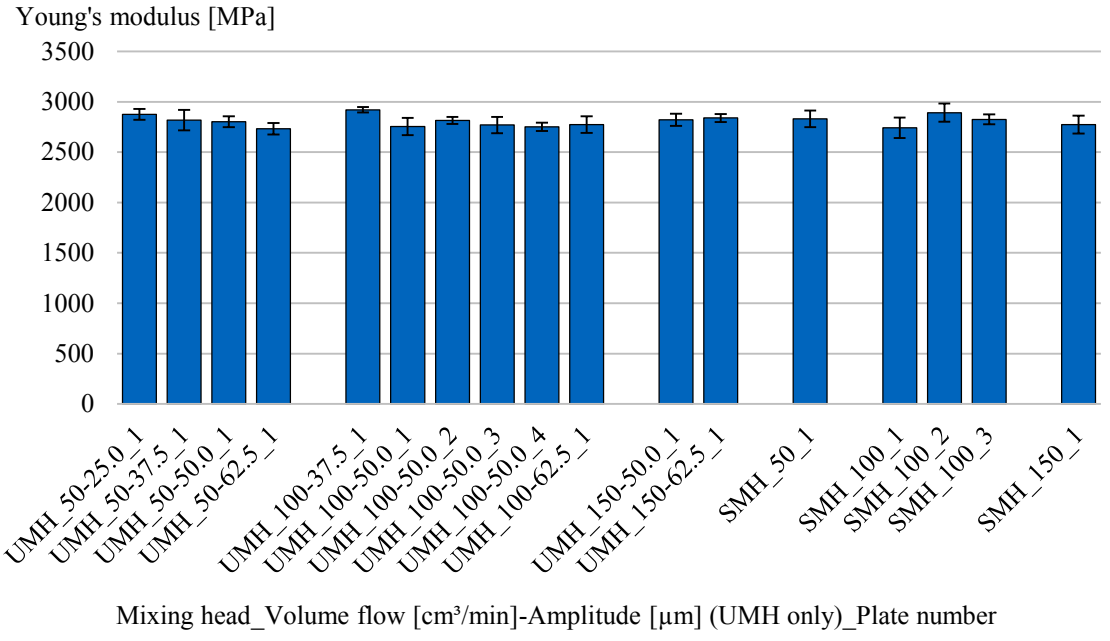

Fig. 6-19 Young's modulus of the NRP samples out of RIM at varying amplitudes and volume flows using the UMH and the SMH

The Young's modulus of RIM is stated from 2700 to 3200 MPa in the datasheet (see Fig. A-1). The mixing quality of these samples is assumed to be sufficient since analogous to the tensile strength, the values of the samples are within this specification.

The Young's modulus of the XB samples of both mixing heads is revealed in Fig. 6-20. Most of the samples show similar values. The injection processed with the UMH at a volume flow of 150 cm³/min and an amplitude of 50.0 µm, possesses a reduced tensile strength (see Fig. 6-17). It also shows a Young's modulus comparable to the other UMH samples. The Young's modulus of the injection processed with the SMH at 200 cm³/min is reduced analogous to the tensile strength.

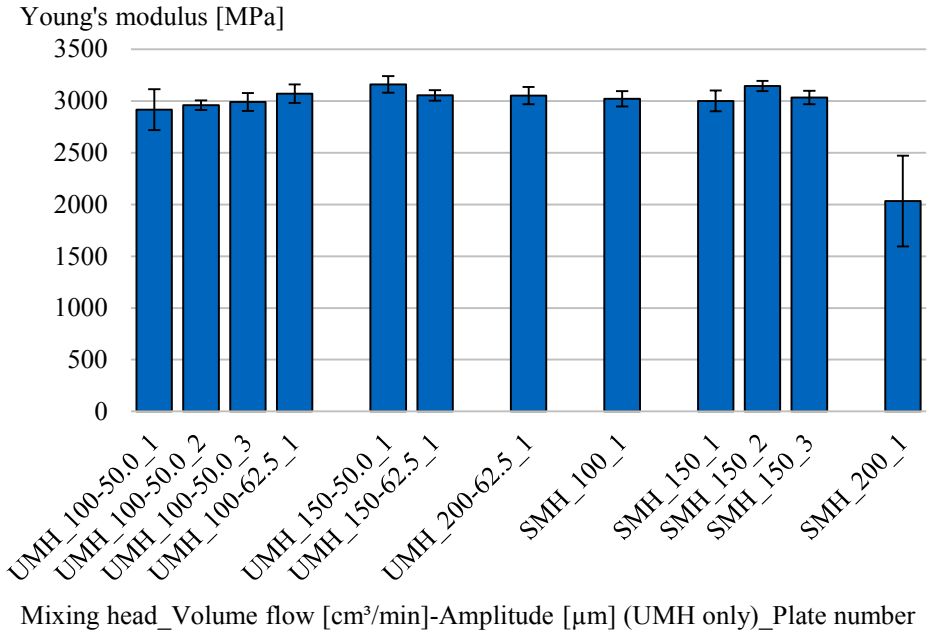

Fig. 6-20 Young's modulus of the NRP samples out of XB at varying amplitudes and volume flows using the UMH and the SMH

The XB data sheet reveals a Young's modulus of 3100 MPa to 3400 MPa. Similar to the tensile strength, the Young's modulus is overall reduced. Even though some samples meet the requirement. This minor reduction is traced back to the curing interruption by the storage of the samples at room temperature for three weeks maybe combined with moisture uptake before the post curing (see chapter 6.1.4). The additional reduction because of the surface roughening by water jet cutting mentioned at the tensile strength results has only a minor effect. The Young's modulus is detected in an axial strain range from 0.10 % to 0.30 % and therefore comparable low stresses occur. The comparably high Young's modulus of the UMH sample at a volume flow of 150 cm³/min and an amplitude of 50.0 µm could indicate that the polymer network is mostly developed. This leads to ordinary reverse elastic properties and solely a loss of strength at the ultimate load occurs. The reduction of the Young's modulus in the context of the injection processed with the SMH at 200 cm³/min is traced back to a poor

mixing. Therefore, an inhomogeneous network is built up. This is also indicated by the comparably high SD.

6.2.4.2 In plane shear test

The results of the in plane shear tests are an indicator for the performance of the cured fiber composite plates. They define the capacity of the composite to withstand shear load during shear strain. For this two responses are examined: the shear strength and the shear modulus.

Shear strength

At first, the shear strength of the FRP produced with RIM is analyzed. Fig. 6-21 shows the shear stress shear strain curve of the RIM samples produced at a volume flow of 150 cm³/min and an amplitude of 50.0 µm respective 62.5 µm. The failure of all samples occurred at shear deformations higher than 0.05. For this, the shear strength is calculated at a shear deformation of 0.05 for all samples as suggested in the standard DIN EN ISO 14129 [108]. Basic formulas with regard to these properties are given in chapter 2.4.3.2.

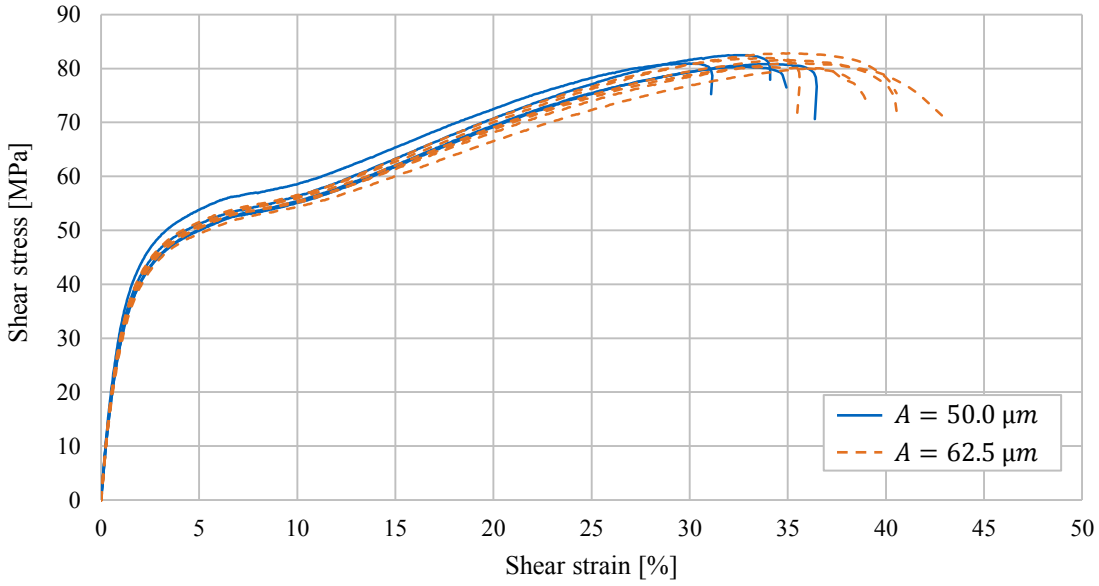

Fig. 6-21 Shear stress shear strain curve of the RIM samples produced at a volume flow of 150 cm³/min and an amplitude of 50.0 µm respective 62.5 µm, four samples per setting

Fig. 6-22 shows, that no influence of the parameter variation occurs apart from the samples produced at a volume flow of 50 cm³/min with the UMH. Hereby, the samples produced at an amplitude of 25.0 µm show a 6.6 MPa higher shear strength compared to the samples produced at an amplitude of 37.5 µm.

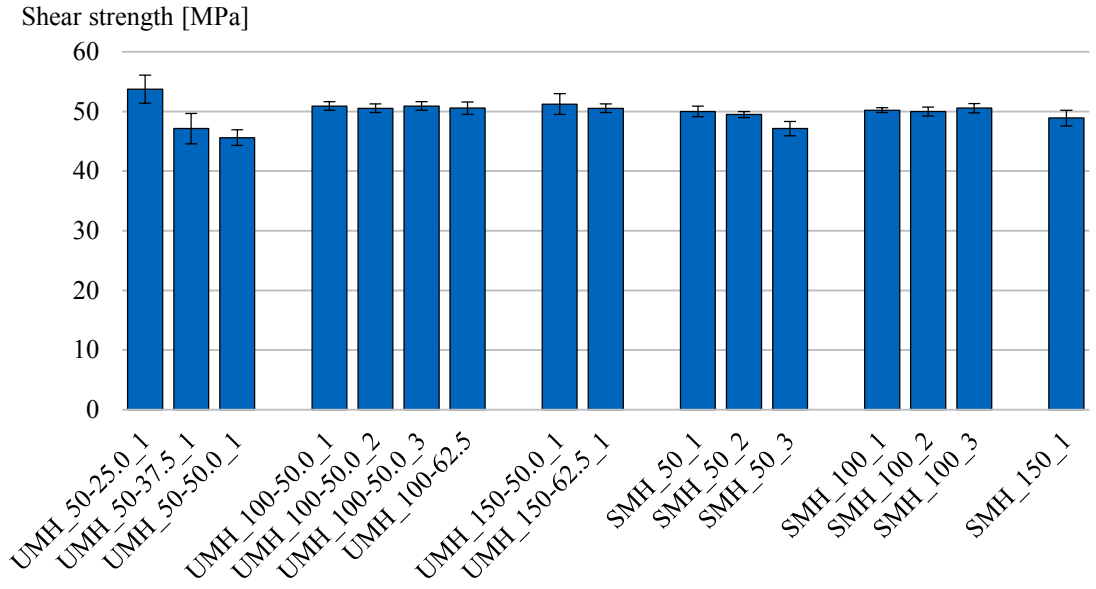

Fig. 6-22 Shear strength of the FRP samples out of RIM at varying amplitudes and volume flows using the UMH and the SMH

A higher shear strength indicates that the material withstands more load at the same shear strain. The detected increase at the lowest amplitude is contrarious to the findings of the NRP investigation (see chapter 6.2.4.1). It is assumed that the higher shear strength is traced back to a deviation of the initial fiber orientation due to the manual stacking of the preforms in the +45°/-45° orientation. This could explain, that this effect is not detected at other volume flows.

The shear strength of XB is revealed in Fig. 6-23. The largest differences of these values occur at the samples of the three plates manufactured at a volume flow of 150 cm³/min and at an amplitude of 50.0 µm. The shear strength is similar at both mixing heads. The highest shear strength of 55.4 MPa is achieved by samples of the plate produced with a power guidance limited at 500 W.

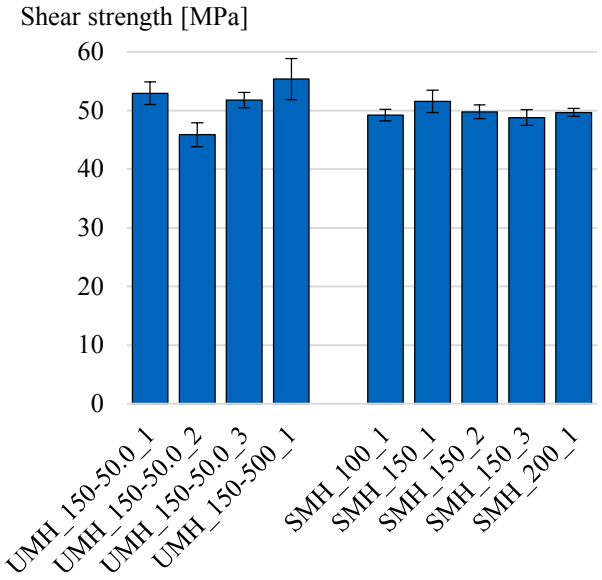

Mixing head_Volume flow [cm³/min]- Amplitude or power: 50 µm or 500 W (UMH only)_ Plate number

Fig. 6-23 Shear strength of the FRP samples out of XB at varying amplitudes and volume flows using the UMH and the SMH

The higher process parameter sensitivity and the reduced processability of XB compared to RIM is already discussed in chapter 6.2.1. It is assumed that the deviation in the shear strength at the repeated factor settings is a result of the overall process parameter sensitivity. The fiber orientation can be deviated due to the manual stacking inaccuracies during the preforming or local fiber wash during the mold filling caused by the gelation of the fast curing resin system.

Shear modulus

Shear modulus describes the material stiffness and therefore, the resistance of the material against shear deformation. Fig. 6-24 reveals the shear modulus of the FRP. Analogous to the shear strength (see Fig. 6-22), the shear modulus at a volume flow of 50 cm³/min and at an amplitude of 25.0 µm shows the highest shear modulus 3697.2 MPa. The rest of the samples are at a similar level.

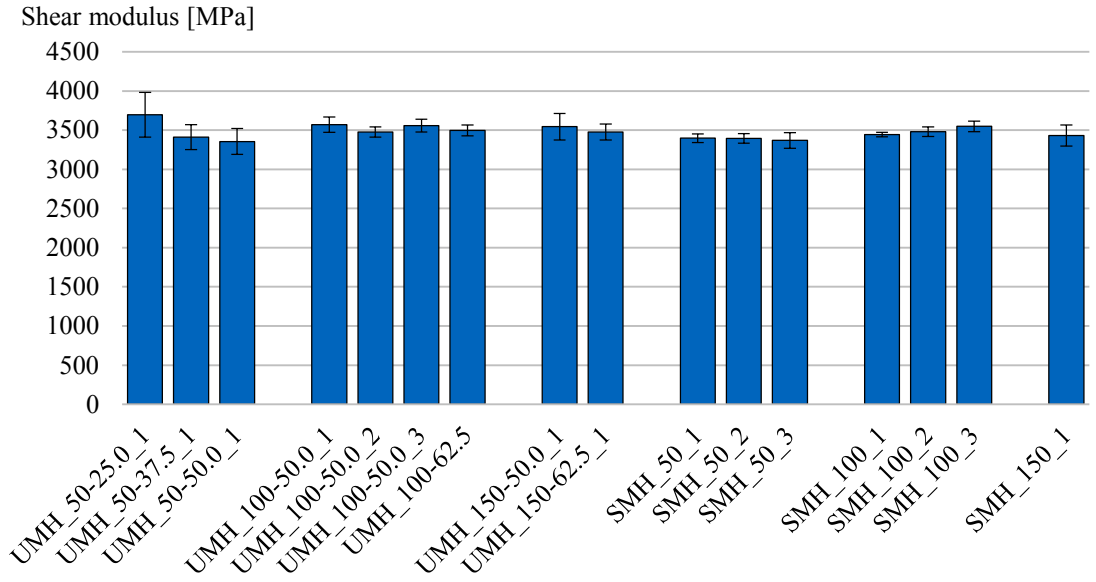

Fig. 6-24 Shear modulus of the FRP samples out of RIM at varying amplitudes and volume flow using the UMH and the SMH

Analogous to the shear strength analysis, the higher shear modulus at a volume flow of 50 cm³/min and an amplitude of 25 µm is traced back to a deviation of the initial fiber orientation within the preform.

In Fig. 6-25, the shear modulus of the FRP produced with both mixing heads are shown. Analogous to the shear stress investigation, the results with reference to XB show a higher scattering than the results with reference to RIM. The highest deviation is measured at the repeated setting with a volume flow of 150 cm³/min.

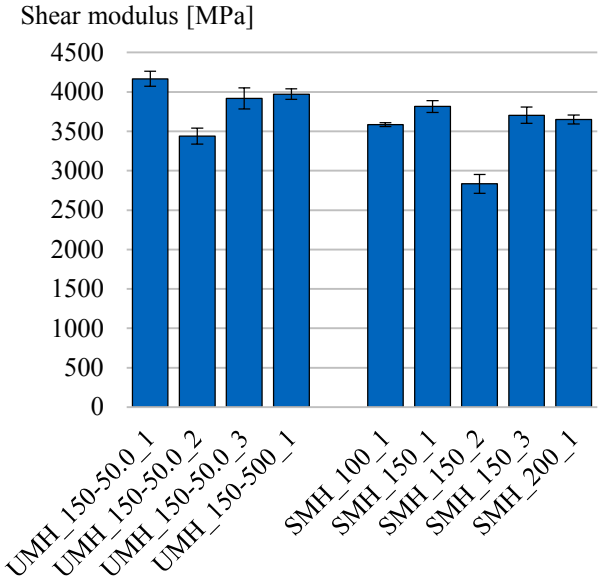

Fig. 6-25 Shear modulus of the FRP samples out of XB at varying amplitudes and volume flows using the UMH and the SMH

Analogously to the results of the shear strength, the higher scattering at XB is traced back to its higher reactivity and therefore, process variation sensitivity. The variation is similar at both mixing heads. The deviation of the shear modulus is traced back to a deviation of the fiber orientation within the preform. The fiber orientation can be deviated due to the manual stacking inaccuracies during the preforming or local fiber wash during the mold filling caused by the gelation of the fast curing resin system. It further indicates, that the processing of this resin system is hardly achievable with the used injection setup.

6.3 Interpretation of the Resin Transfer Molding characteristics

The performances of RTM injections processed with the UMH are compared to the ones processed with the SMH. The UMH is capable of producing NRP and FRP with two resin systems, namely RIM and XB. Hereby, the development of the process parameters during the unsaturated and saturated flow conditions are consistent with the findings of the process characteristics (see chapter 5). The DoE model set up in the process characteristics is identified as sufficient for the prediction of the ultrasound parameters development during RTM injections.

The guidance and the control of the ultrasound parameters amplitude and power are crucial for the RTM injection. A lower threshold for the amplitude is detected. At an amplitude of 50 µm both plate types with both resin systems are producible without

defects. Even though the value of the lower threshold for the amplitude is dependent on the volume flow and the injection pressure. The mixing is insufficient if this threshold is undercut. This leads to a reduced mechanical performance of the cured resin system or even wet spots within the plates. An upper threshold for the power is detected. This parameter correlates with the temperature increase of the resin system during mixing. When the power threshold is exceeded, a notable acceleration of the resin system is detected. Injections of the fast curing resin system XB showed that at this injection setup a power threshold at approximately 700 W occurs. This prohibits the complete impregnation of the preform. The power threshold is dependent on the selected volume flow since the quantity of the temperature increase is proportional to the energy density (see Eq. 2-3, Fig. 5-10). For this, a power guidance is suggested for temperature critical injections. It limits the injection temperature and simultaneously entails the largest amplitude, at the current injection pressure. This guidance is feasible, as a variation of the amplitude above the threshold leads to a consistent mechanical performance equal to plates produced with the SMH.

7 Automation of the Ultrasonic Mixing Head for Resin Transfer Molding

The process capability of the ultrasound in an RTM injection is revealed. A fully automated RTM injection with the UMH is realized to meet the requirements of the concept development (see chapter 4.1), an implementation of the heating, the cleaning and the inspection function in the UMH. The integration of the UMH in the automated RTM cycle is described in chapter 7.1, followed by the resulting injection procedure in chapter 7.2 and the interpretation of the results in chapter 7.3.

7.1 Integration of the Ultrasonic Mixing Head into an automated Resin Transfer Molding process

The equipment used for the automated RTM injection is described in the following (see Fig. 7-1):

- Metering device: To meter the TRAC resin system (see chapter 2.3.3), a three component metering device of Dekumed is used (see chapter 2.3.2). This device is analogous equipped as the two component metering device used for the process (see chapter 5) and RTM characteristics (see chapter 6).
- RTM mold: A composite tool developed by P. Kammerhofer of the Technical University of Munich (TUM) and manufactured by Qpoint Composite GmbH is utilized. The resistive heating device, which warms carbon fibers within the mold and the low heat capacity of the mold enable a fast heating for curing after the injection. The mold is restricted to a maximum injection pressure of $4*10^5$ Pa.
- RTM software: A program based on a SIMATIC STEP 7 control of Siemens is developed to guide the metering device, the mold heating device and the ultrasonic device during the injection and the curing. The power guidance is realized as proposed in chapter 6.2.3. Hereby, the program adjusts the amplitude based on the comparison of power response and power target value.

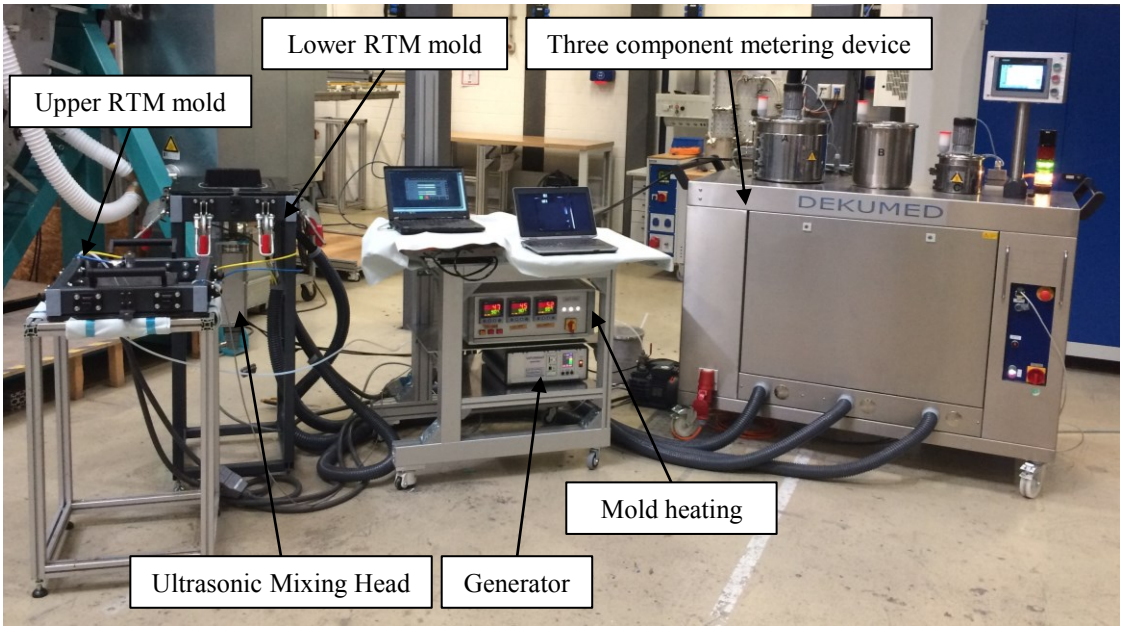

Fig. 7-1 Experimental setup for the automated RTM injection

The UMH is attached to the inlet of the mold. The design of the mixing chamber is identical to those of the previous investigations (see chapter 5, chapter 6), where the sonotrode is attached to the backside of the mixing chamber. The ejection movement longwise the mixing chamber is accomplished by an electrical linear guidance RSDG202B-C1-P-5-200 of Misumi. The resin system TRAC (see chapter 2.3.3), which consists of a resin component, a hardener component and an internal release agent, is utilized. This resin system targets, short cycle times, similar to XB and reduced demolding stresses by use of an internal release agents. The mixing ratio is 100:16:3 % by weight. Investigations on the function of internal release agents are given in the literature [148–151].

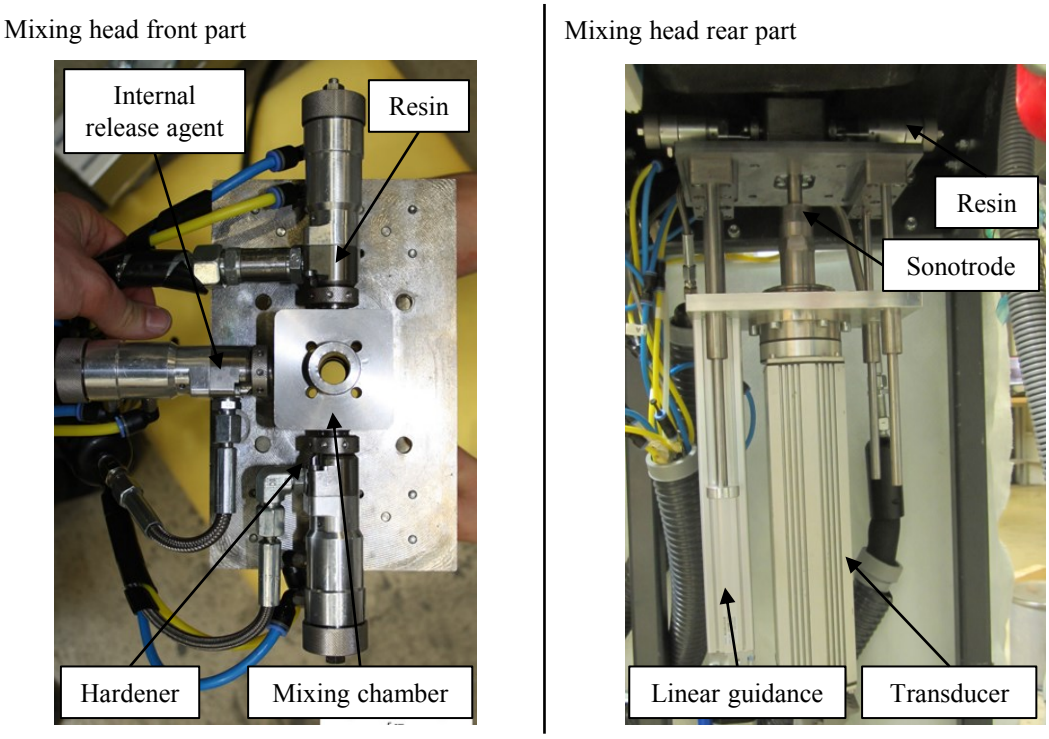

Fig. 7-2 Feeders of the resin system components into the mixing chamber (left) and integration of the UMH into the tool inlet (right)

The preforms for the tablet holders are developed and produced by A. Mierzwa, F. Sommer and C. Ebel of the TUM. As raw material, a unidirectional carbon fiber layer stacked to 0°/90° [152] and +45°/-45° [153] is used. It is produced by SGL as HPT 310. A binder (B) EPIKOTE Resin 05390 [154] by Momentive is added between each layer to reinforce the stack for handling. The layer are stacked according to the following fiber orientation (+45°/-45°/B/0°/90°/B/-45°/+45°/B/+45°/-45°/B/90°/0°/B/-45°/+45°). Then a diaphragm forming process is performed to drape the stack and activate the binder. The preform is trimmed by ultrasonic cutting and positioned onto the lower half of the mold (see Fig. 7-3).

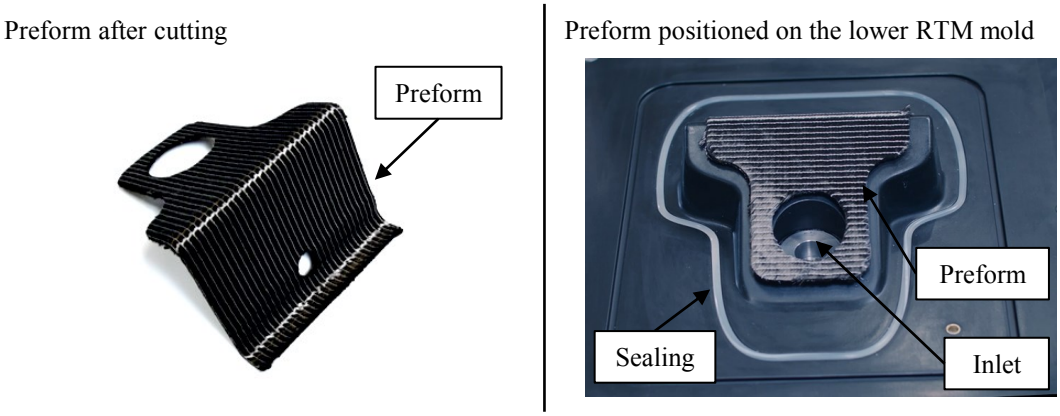

Fig. 7-3 Draped and cut preform (left) and preform positioned onto the lower mold (right)

The upper mold half is placed on top and the mold is closed by toggle joints. The preform is compacted to the cavity height of 2 mm. By this, the FVF is approximately 50 % in the tablet holder.

7.2 Injection procedure of the Resin Transfer Molding automation

The parameter settings for the automated injection are defined based on an iterative process development. The following temperatures are identified as most suitable: a mold temperature of 80 °C, a resin component temperature of 70 °C, a hardener component temperature of 25 °C and an internal release agent temperature of 35 °C.

The following injection procedure is guided by the RTM software:

- 00:00 Start of process and sonication
- 00:02 Start of injection
  at a volume flow of 57.14 cm³/min (equal to 60 g/min)
- 00:22 Opening of the Outlet, leading to a vacuum support
  at a metered volume of 19.05 cm³ (equal to 20 g)
- 01:02 Closing the Outlet, leading to a vacuum disconnection
  at a metered volume of 57.14 cm³ (equal to 60 g)
- 02:20 End of filling the cavity
  at a metered volume of 131.43 cm³ (equal to 138 g)
- 02:21 Start of metering the internal release agent
  at a volume flow of 285.71 cm³/min (equal to 300 g/min)
- 02:30 End of injection, sonication and internal release agent metering
  at a metered volume of 2.43 cm³ (equal to 2.5 g)
- 02:50 Start of curing at 120 °C
- 07:50 End of curing at 120 °C
- 08:30 Demolding of the part (see Fig. 7-4)
- 09:00 End of process

The internal release agent is added solely at the end of the injection to the resin system, which cures next to the inlet. Its function to lower the demolding stress is only applicable at a metal surfaces like the inlet (see Fig. 7-3). Therefore a metering of the internal release agent during the filling of the composite mold is not applied. In an injection series, 15 tablet holders (see Fig. 7-4) are produced in a row to show the durability of the injection machine.

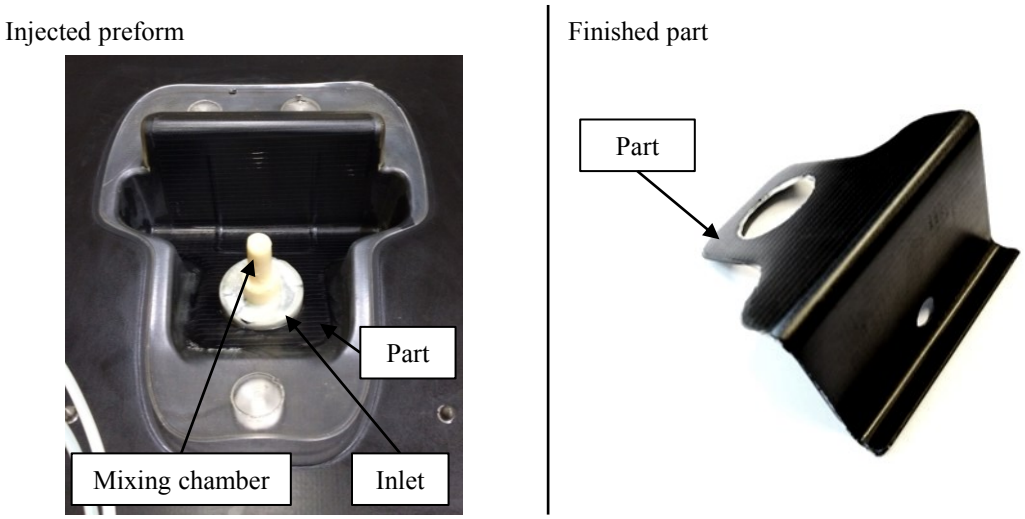

Fig. 7-4 Injected part with neat resin at the inlet (left) and the final part (right)

Fig. 7-5 shows the amplitude and power development during the injection. Hereby the amplitude is at its maximum value of 63.09 µm as long as the power threshold value of 240 W is not reached. The power would exceed its threshold at an injection time of approximately 115 s because of the increasing injection pressure during the impregnation of the preform. For this, the amplitude is lowered and thereby the power value.

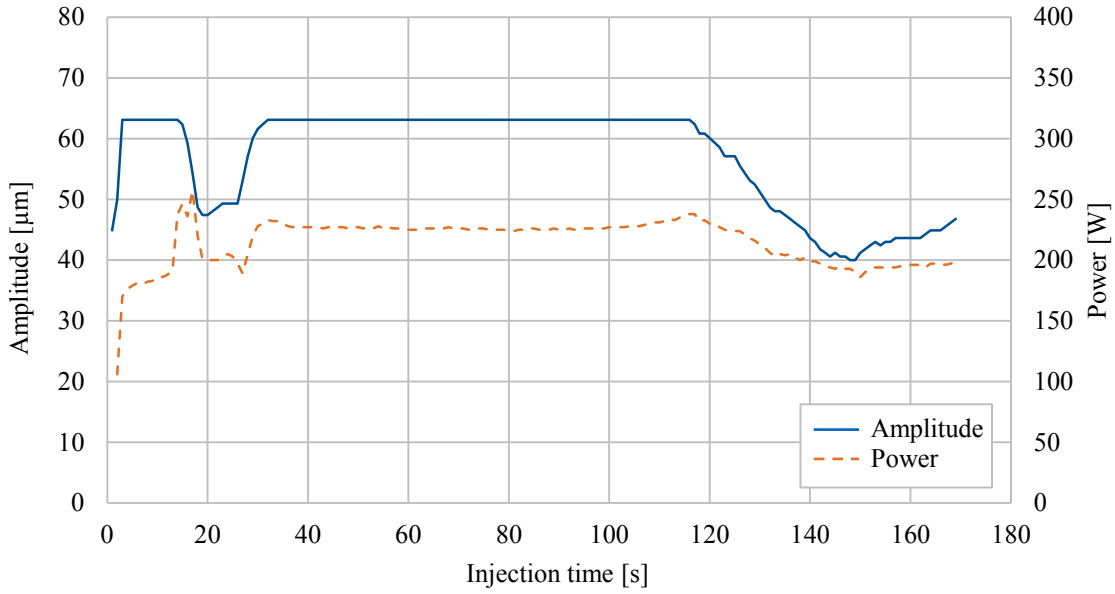

Fig. 7-5 Power and amplitude development during the injection, the power guidance is set to a threshold value of 240 W

The outlet is opened at an injection time of 20 s. This leads to the evacuation of the mold and therefore a variation of both ultrasound parameter at that time.

During the injection series, two aspects are identified to further improve the robustness of the UMH:

- Sealing material: The sealing concept (see chapter 4.1.2) is proved a success, whereas the material of the sealing is a weak point. The utilized viton rubber is stable to temperatures of approximately 120 °C. Even though these temperatures do not seem to occur during the injection of the tablet holder, it is conceivable that the temperature in the mixing chamber could exceed this temperature. For this, a more thermally stable material should be considered for the sealing.
- Ejection process: The ejection of the resin system material before curing is not performed. Pretrials showed that (see Fig. 4-9) an interlocking between mixing chamber wall and sonotrode occurs in the ejection position. This is caused by the thermal expansion of the resin system during curing. For the tablet holder injection, the cured resin system within the mixing chamber is released as attachment to the cured tablet holder (see Fig. 7-4). The ejection movement could be mandatory for other mold geometries. Latter are characterized by a demolding direction which differs from the longside direction of the mixing chamber. For this, an integration of a hydraulic system, instead of an electric system, should be considered to enforce the sonotrode movement.

7.3 Interpretation of the automation

The TRIZ function analysis (see chapter 4.1) proposes, that the addition of the cleaning, heating and controlling function in parallel to the mixing is achievable by using the UMH instead of a SMH. The injection of 15 tablet holder in a row indicate, that this function integration is partly achieved. The cleaning function is successfully integrated. A solvent flushing is not mandatory, since the resin system within the mixing chamber is removed as neat resin area after curing. A heating of the resin component before the sonication is still mandatory since the heating effect by sonication depends on the mixing effect and is not solely adjustable. The process guidance by power control qualifies the amplitude response to be a sensitive indicator for the online mixing quality control. Hereby, an amplitude above the amplitude threshold value is a necessary but not sufficient criterion. Therefore, the inspection method used for parts built with RTM is enhanced.

8 Conclusion

The thesis at hand deals with the usage of ultrasonic cavitation, which has actually been established in the sonochemistry and green chemistry, to process resin systems in Resin Transfer Molding (RTM). Fundamentals on the behavior of epoxy resin systems towards their exposure to sonication are therefore investigated in the laboratory for the first time. These results are utilized to develop an Ultrasonic Mixing Head (UMH) for RTM. To investigate the performance of the UMH, three steps are performed, whereby each step increases the complexity: First, the process characteristics of the UMH are examined at saturated flow conditions. For this, the UMH is connected to a metering device. Second, the characteristics of the UMH within the RTM injection are scrutinized at unsaturated and saturated flow conditions. For this, the UMH and the metering device are connected to a RTM mold. Third, the UMH is integrated into a fully automated RTM injection. For this, an ultrasound power guidance based on the findings of the previous chapters is implemented.

The effect of acoustic cavitation on a resin system is investigated by a sonication of the epoxy resin system RIMR135/RIMH1366 of Hexion in the laboratory. The results of this investigation show a dependency of the cavitation effect on the amplitude: the higher the amplitude, the larger and the denser the cavitation zone. At 44.05 µm, a closed, fungoid structure is observed in the epoxy resin component RIMR135. To evaluate the impact of the sonication, the parameter energy density is introduced. Thereby, the sonication power, the exposure time and the sonicated volume are taken into account. The rheological inspection of the resin system shows a gel time reduction of 6.29 % at an energy density of 3240 W s/cm³ and a gel time reduction of 24.50 % at an energy density of 4924 W s/cm³. The thermal analysis reveals a slight increase of the glass transition temperature at the highest tested energy density of 104.21 W s/cm³ compared to a manually mixed resin system.

The TRIZ function analysis of a static mixing head shows that the functions to clean the mixing chamber, to heat the resin system and to control the mixing process can simultaneously take place with the mixing by a change of the mixing principle to sonication. For this, the sonotrode, which transfers the ultrasonic movement to the resin system, is located at the backside of the mixing chamber. It enables the mixing during the injection and the release of the cured resin system within the mixing chamber. The heating is an effect of the collapsing bubbles. To control the mixing process, the amplitude, which describes the height of the sonotrode movement, and the power of the ultrasonic device, which describes the effort to execute the movement, are investigated.

The process analysis is based on a center composite face approach to create a model according to the process behavior of the UMH. The amplitude (25-50 µm), the volume flow (50-150 cm³/min), and the pressure inside the mixing chamber (0-3*10^5 Pa) have the highest influence on the process, the rheological and the thermal properties of the resin system. The resin temperature (25-60 °C) shows a minor effect whereas a variation of the chamber volume (2.5-5.0 cm³) does not show any effect on the resin system characteristics. The temperature increase during the mixing by cavitation is proportional to the energy density applied to the resin system. By sonicating a resin system, an optimum parameter set is discovered for shortening its gel time as well as for maximizing its final glass transition temperature.

The injection of neat resin plates and of glass fiber reinforced plates with a slow curing (RIMR135/RIMH1366 by Hexion) and a fast curing resin system (XB 3585/XB3458 by Huntsman) show the limits of the UMH processability for RTM. A lower threshold of the amplitude is detected when no sufficient mixing occurs and thus, no homogeneous network is built during curing. Further, an upper threshold of the power is detected. Analogous to the process characteristics, a correlation of the temperature increase during the mixing by cavitation and the power respective the energy density of the sonication is found. By exceeding the power limit, a curing of the resin system occurs before the cavity of the mold is completely filled. For this, a power guidance is proposed for the use of the UMH in RTM. Hereby, the amplitude is at the highest possible value to not exceed the power limit. If the limit is exceeded due to process conditions, like a high injection pressure or a high resin system viscosity, the amplitude will be reduced and thereby the power. This allows the usage of the entire spectrum of amplitudes above the lower amplitude threshold, which ensure a sufficient mixing. A comparison between the power values predicted by the model based on the process characteristics and the detected values of the RTM characteristics is made. It proves the validity of the model for the prediction of the ultrasonic response values as regards the process parameters volume flow, injection pressure and resin temperature. Tensile tests of neat resin samples and in plane shear tests of glass fiber reinforced samples produced within the amplitude and power limits show a similar performance to a standard low pressure static mixing head.

The implementation of the UMH into a fully automated RTM injection to produce a generic part proved the durability of the mixing head. The addition of the cleaning, heating and controlling function in parallel to the mixing, as proposed by the TRIZ function analysis, by using the cavitation effect is partly achieved. A solvent free, low pressure RTM injection is successfully executed. A heating of the resin component before the sonication is still mandatory since the heating effect by sonication depends on the mixing effect and is not solely adjustable. The process guidance by power control qualifies the amplitude response to be the indicator for the online mixing quality. Hereby, an amplitude above the amplitude threshold value is a necessary but not sufficient criterion.

9 Outlook

The work described within this thesis offers multiple opportunities for further research. Since ultrasonic cavitation is introduced to the processing of resin systems, two possibilities for the further use of cavitation in liquid composite molding processes are discussed in the following chapter.

9.1 Infusion processes

Infusion processes are used in various industries like aerospace, sports or leisure. All these processes have in common that the resin system is metered and mixed in a batch chamber before the fibers are impregnated by applying under pressure at the outlet. Current mixing devices are not capable of processing volume flows below 20 cm^3/min. However they are necessary for these processes. Nowadays, infusion processes are restricted to slow curing resin systems, long cycle times and a manual handling of reactive resin systems. Since the Ultrasonic Mixing Head has already proven its durability at a volume flow of 50 cm^3/min, it is assumed that a resizing of the mixing chamber is feasible. For the infusion process, amplitudes above the lower amplitude threshold should be chosen. The upper power threshold could be more critical for processing since the exposure time and therefore, the temperature increase of the resin system is higher at a lower volume flow. Graham et al. [155] pointed out that the consolidation and the curing of graphite-epoxy composites plates benefits from sonication. Between others, he mentions that curing accelerates due to the temperature effect of cavitation. Transferred to infusion processes, its lower mold temperature compared to injection processes could enhance this effect. By choosing an appropriate resin temperature the sonication could enable a controlled acceleration of the curing by heating. Latter depends on the impregnation progress conditions. For this, an investigation of the ultrasonic treatment during infusion processes is recommended.

9.2 Nano composites

The field of nanocomposites is a fast growing section in the composite industry. Their main benefit is the capability to modify the resin system properties and hereby add more functionality to the composite parts [156, 157]. These nanoparticle in liquid dispersions are called nanofluids [158]. Kabir et al. [159] identified the dispersion of nanoparticles as most critical step for the production of nanofluids respective nanocomposites. Haddad et al. [160] reviewed methods to disperse nanoparticles in fluids. They concluded that sonication is among the most frequently used techniques. Even though

sonication is already used to produce nanofluids, the sonication is still done in batch chambers. Even if a small amount within the scale of cubic centimeters is sonicated, an exposure time between minutes and hours is mandatory. Therefore, investigations on the cavitation effect in nanofluids are obligatory to increase the production volume of nanofluids and therefore extend their field of application. Keck [87] et al. analyzed the influence of particles on sonochemical reactions in aqueous solutions. There, the particles disturb the creation of cavitation bubbles. The damping effect of the nanoparticles on the ultrasonic wave propagation is identified as crucial for the dispersion time. It is assumed, that the cavitation zone will be smaller compared to the cavitation zones discussed in this thesis. For this, investigations on the shape and density of the cavitation zone dependent on the mixing chamber geometry in particular the inflow and near-field of the sonotrode, should be undertaken.

Bibliography

[1] R. Heuss, N. Müller, Wolff van Sintern, A. Starke, A. Tschiesner, *Lightweight, heavy impact*: McKinsey and Company, 2012.

[2] F. C. Campbell, *Structural composite materials*: ASM International, 2010.

[3] M. Frondel, C. M. Schmidt, and C. Vance, "A regression on climate policy: The European Commission's legislation to reduce CO_2 emissions from automobiles," *Procedia - Social and Behavioral Sciences*, vol. 45, no. 10, pp. 1043–1051, 2011.

[4] R. Lässig, M. Eisenhut, A. Mathias, R. T. Schulte, F. Peters, T. Kühmann, T. Waldmann, W. Begemann, *Serienproduktion von hochfesten Faserverbundbauteilen: Perspektiven für den deutschen Maschinen- und Anlagenbau*: VDMA, 2012.

[5] G. Gardiner, "Cannon solutions for mass production of composite parts," *Reinforced Plastics*, vol. 60, no. 5, pp. 316–323, 2016.

[6] G. Gardiner, "Turnkey manufacturing systems Automated RTM for aerospace," *CompositesWorld*, 2016.

[7] Z. Wang *et al.,* "Intrinsic Hybrid Composites for Lightweight Structures: Tooling Technologies," *AMR*, vol. 1140, pp. 247–254, 2016.

[8] C. Hopmann, P. N. Wagner, R. Bastian, K. Fischer, and A. Böttcher, "Mold technology for mass production of continuous fiber-reinforced sandwich parts," *Journal of Polymer Engineering*, vol. 36, no. 6, 2016.

[9] D. A. Lakho, D. Yao, K. Cho, M. Ishaq, and Y. Wang, "Study of the Curing Kinetics toward Development of Fast-Curing Epoxy Resins," *Polymer-Plastics Technology and Engineering*, vol. 56, no. 2, pp. 161–170, 2016.

[10] M. Villanueva, I. Fraga, J. A. Rodríguez-Añón, and J. Proupín-Castiñeiras, "Study of the influence of a reactive diluent on the rheological properties of an epoxy-diamine system," *Journal of Thermal Analysis and Calorimetry*, vol. 98, no. 2, pp. 521–525, 2009.

[11] G. Cicala, G. Recca, S. Carciotto, and C. L. Restuccia, "Development of epoxy/hyperbranched blends for resin transfer molding and vacuum assisted resin transfer molding applications: Effect of a reactive diluent," *Polymer Engineering & Science*, vol. 49, no. 3, pp. 577–584, 2009.

[12] X. D. Liu, A. Sudo, and T. Endo, "Efficient accelerating effect of carbonyldiimidazole on epoxy-dicyandiamide curing system," *Journal of Polymer Science Part A: Polymer Chemistry*, vol. 49, no. 1, pp. 250–256, 2011.

[13] X. D. Liu, M. Kimura, A. Sudo, and T. Endo, “Accelerating effects of N-aryl-N',N'-dialkyl ureas on epoxy-dicyandiamide curing system,” *Journal of Polymer Science Part A: Polymer Chemistry*, vol. 48, no. 23, pp. 5298–5305, 2010.

[14] R. K. Thakur, C. Vial, K. Nigam, E. B. Nauman, and G. Djelveh, “Static Mixers in the Process Industries - A Review,” *Chemical Engineering Research and Design*, vol. 81, no. 7, pp. 787–826, 2003.

[15] A. Ghanem, T. Lemenand, D. Della Valle, and H. Peerhossaini, “Static mixers: Mechanisms, applications, and characterization methods - A review,” *Chemical Engineering Research and Design*, vol. 92, no. 2, pp. 205–228, 2014.

[16] H.-S. Song and S. P. Han, “A general correlation for pressure drop in a Kenics static mixer,” *Chemical Engineering Science*, vol. 60, no. 21, pp. 5696–5704, 2005.

[17] R. Chaudhari, *Characterization of high-pressure resin transfer molding process variants for manufacturing high-performance composites*. Ph.D. Thesis. Karlsruhe, Germany: Karlsruhe Institute of Technology, 2014.

[18] R. Chaudhari, M. Karcher, P. Elsner, F. Henning, “Characterization of high pressure RTM processes for manufacturing of high performance composites,” Venice, Italy, 2012.

[19] W. Raffelt, *Beitrag zur Hochdruck-RTM-Prozessentwicklung für die automobile Großserie*. Munich, Germany: Ph.D. Thesis, Technical University of Munich, 2017.

[20] R. Chaudhari, P. Rosenberg, M. Karcher, S. Schmidhuber, P. Elsner, F. Henning, *High-Pressure RTM Process Variants for Manufacturing of Carbon Fiber Reinforced Composites*. Paris, France: Proceedings of the 19th International Conference on Composite Materials, 2013.

[21] G. Chatel, “How sonochemistry contributes to green chemistry?,” (eng), *Ultrasonics Sonochemistry*, 2017.

[22] U. Peuker, U. Hoffmann, U. Wietelmann, S. Bandelin, R. Jung, *Ullmann's encyclopedia of industrial chemistry: Sonochemistry,* 6th ed. Weinheim, Germany: Wiley-VCH, 2003.

[23] S. Asgharzadehahmadi, A. A. Abdul Raman, R. Parthasarathy, and B. Sajjadi, “Sonochemical reactors: Review on features, advantages and limitations,” *Renewable and Sustainable Energy Reviews*, vol. 63, pp. 302–314, 2016.

[24] V. Hessel, H. Löwe, and F. Schönfeld, “Micromixers - a review on passive and active mixing principles,” *Chemical Engineering Science*, vol. 60, no. 8-9, pp. 2479–2501, 2005.

[25] J. P. Joule, “On the effects of magnetism upon the dimensions of iron and steel bars,” *Philosophical Magazine Series 3*, vol. 30, no. 199, pp. 76–87, 2009.

[26] K. Kreher, *Festkörperphysik*. Wiesbaden, Germany: Vieweg+Teubner Verlag, 1976.

[27] T. J. Mason and D. Peters, *Practical sonochemistry: Uses and applications of ultrasound,* 2nd ed. Chichester, England: Horwood, 2002.

[28] J. Krüger, *Untersuchungen zum Einfluss von Leistungsultraschall auf Mischungsvorgänge und Fällungsreaktionen*. Clausthal-Zellerfeld, Germany: Ph. D. Thesis, Clausthal University of Technology, 2002.

[29] A. M. W. H. D. H. Monnier, “Effects of ultrasound on micromixing in flow cell,” *Chemical Engineering Science*, vol. 55, pp. 4009–4020, 2000.

[30] Kenneth S. Suslick, Ed., *Organometallic Sonochemistry*. vol 25, pp. 73-119: Elsevier, 1986.

[31] G. Eskin, “Cavitation mechanism of ultrasonic melt degassing,” *Ultrasonics Sonochemistry*, vol. 2, no. 2, pp. S137-S141, 1995.

[32] Hassan Dakhil Al-Budairi, *Design and Analysis of Ultrasonic Horns Operating in Longitudinal and Torsional Vibration*. PhD Thesis. Glasgow: University of Glasgow, 2012.

[33] M. Ashokkumar *et al.,* “The detection and control of stable and transient acoustic cavitation bubbles,” (eng), *Physical chemistry chemical physics*, vol. 11, no. 43, pp. 10118–10121, 2009.

[34] K. S. Suslick, Y. Didenko, M. M. Fang, T. Hyeon, K. J. Kolbeck, W. B. McNamara III, M. M. Mdleleni, M. Wong, *Acoustic cavitation and its chemical consequences*. University of Illinois at Urbana-Champaign, Illinois, USA: The Royla Society.

[35] E. A. Neppiras, “Acoustic cavitation,” *Physics Reports*, vol. 61, no. 3, pp. 159–251, 1980.

[36] M. S. Plesset, R. B. Chapman, “Collapse of an initially spherical vapour cavity in the neighbourhood of a solid boundary,” *Journal of Fluid Mechanics*, vol. 47, no. 2, pp. 283–290, 1971.

[37] A. A. Aganin, M. A. Ilgamov, L. A. Kosolapova, and V. G. Malakhov, “Dynamics of a cavitation bubble near a solid wall,” *Thermophys. Aeromech.*, vol. 23, no. 2, pp. 211–220, 2016.

[38] L. Crum, *Collapsing cavitation bubble*. University of Washington, Washington, USA. [Online] Available: http://tcspasa.org/gallery-of-acoustics. Accessed on: Jul. 05 2017.

[39] S. Sochard, A. M. Wilhelm, and H. Delmas, “Modelling of free radicals production in a collapsing gas-vapour bubble,” *Ultrasonics Sonochemistry*, vol. 4, no. 2, pp. 77–84, 1997.

[40] A. Prosperetti, “Bubble phenomena in sound fields: Part one,” *Ultrasonics*, vol. 22, no. 2, pp. 69–77, 1984.

[41] R. I. Nigmatulin and N. S. Khabeev, “Dynamics of vapor-gas bubbles,” *Fluid Dynamics*, vol. 11, no. 6, pp. 867–871, 1977.

[42] S. Vajnhandl and A. Le Majcen Marechal, “Ultrasound in textile dyeing and the decolouration/mineralization of textile dyes,” *Dyes and Pigments*, vol. 65, no. 2, pp. 89–101, 2005.

[43] J. Bałdyga and J. R. Bourne, *Turbulent mixing and chemical reactions*. Chichester, Great Britain: Wiley, 1999.

[44] K. S. Suslick, “Ultrasound Its Chemical, Physical, and Biological Effects,” *Z. Chem.*, vol. 29, no. 4, p. 156, 1989.

[45] M. E. Fitzgerald, V. Griffing, and J. Sullivan, “Chemical Effects of Ultrasonics - Hot Spot Chemistry,” *The Journal of Chemical Physics*, vol. 25, no. 5, pp. 926–933, 1956.

[46] M. A. Margulis, “Sonoluminescence and sonochemical reactions in cavitation fields. A review,” *Ultrasonics*, vol. 23, no. 4, pp. 157–169, 1985.

[47] T. J. Mason, “Ultrasonic cleaning: An historical perspective,” (eng), *Ultrasonics Sonochemistry*, vol. 29, pp. 519–523, 2016.

[48] Y.-S. Chen, *Zur Frage des Einsatzes von Hoch-Intensitaets-Ultraschall in mehrphasigen Systemen*. Ph.D. Thesis. Clausthal-Zellerfeld, Germany: Clausthal University of Technology, 1997.

[49] K. A. Kusters, S. E. Pratsinis, S. G. Thoma, and D. M. Smith, “Ultrasonic fragmentation of agglomerate powders,” *Chemical Engineering Science*, vol. 48, no. 24, pp. 4119–4127, 1993.

[50] R. J. Wood, J. Lee, and M. J. Bussemaker, “A parametric review of sonochemistry: Control and augmentation of sonochemical activity in aqueous solutions,” *Ultrasonics Sonochemistry*, vol. 38, pp. 351–370, 2017.

[51] B. Pohl, R. Jamshidi, G. Brenner, and U. A. Peuker, “Charakterisierung der Mischung und Fällung bei sonochemischen Reaktoren unter besonderer Berücksichtigung der Reaktorform,” *Chemie Ingenieur Technik*, vol. 84, no. 1-2, pp. 70–80, 2012.

[52] S. Machunsky and U. A. Peuker, “Designstudie eines kontinuierlichen Ultraschall-Fällungsreaktors,” *Chemie Ingenieur Technik*, vol. 79, no. 3, pp. 251–256, 2007.

[53] A. Cardoni and M. Lucas, “Enhanced vibration performance of ultrasonic block horns,” *Ultrasonics*, vol. 40, no. 1-8, pp. 365–369, 2002.

[54] Y. Daud, M. Lucas, and Z. Huang, “Modelling the effects of superimposed ultrasonic vibrations on tension and compression tests of aluminium,” *Journal of Materials Processing Technology*, vol. 186, no. 1-3, pp. 179–190, 2007.

[55] T. J. Mason, A. J. Cobley, J. E. Graves, and D. Morgan, “New evidence for the inverse dependence of mechanical and chemical effects on the frequency of ultrasound,” (eng), *Ultrasonics Sonochemistry*, vol. 18, no. 1, pp. 226–230, 2011.

[56] M. Neitzel, P. Mitschang, U. Breuer, Ed., *Handbuch Verbundwerkstoffe: Werkstoffe, Verarbeitung, Anwendung*. Munich, Germany: Hanser Fachbuchverlag, 2014.

[57] M. Flemming, G. Ziegmann, and S. Roth, *Faserverbundbauweisen: Halbzeuge und Bauweisen*. Berlin, Germany: Springer, 1996.

[58] G. W. Ehrenstein, *Faserverbund-Kunststoffe: Werkstoffe, Verarbeitung, Eigenschaften,* 2nd ed. Munich, Germany: Hanser, 2006.

[59] E. Witten, T. Kraus, M. Kühnel, *Composites Market Report 2016: Marktentwicklungen, Herausforderungen und Chancen*: AVK and CCeV, 2016.

[60] B. Ellis, *Chemistry and Technology of Epoxy Resins*. Dordrecht, Netherlands: Springer, 1993.

[61] H. Lee and K. Neville, *Handbook of epoxy resins*. New York, USA: McGraw-Hill, 1982.

[62] J. K. Gillham, “Formation and properties of thermosetting and high tg polymeric materials,” *Makromolekulare Chemie. Macromolecular Symposia*, vol. 7, no. 1, pp. 67–74, 1987.

[63] H. Darcy, *Les Fontaines publiques de la ville de Dijon: Exposition et application des principes à suivre et des formules à employer dans les questions de distribution d'eau…* Paris, France: V. Dalmont, 1856.

[64] S. Whitaker, “Flow in porous media I: A theoretical derivation of Darcy's law,” *Transport in Porous Media*, vol. 1, no. 1, pp. 3–25, 1986.

[65] B. R. Gebart, “Permeability of Unidirectional Reinforcements for RTM,” *Journal of Composite Materials*, vol. 26, no. 8, pp. 1100–1133, 1992.

[66] R. Meier, *Über das Fließverhalten von Epoxidharzsystemen und vibrationsunterstützte Harzinfiltrationsprozesse*. Munich, Germany: PhD Thesis, Technical University of Munich, 2017.

[67] W. A. Walbran, H. Körber, *Fast and efficient permeability and compaction characterisation of dry textiles: Considerations for a proposed technique*. Se-

ville, Spain: Proceedings of the 16th European Conference on Composite Materials, 2014.

[68] W. A. Walbran, S. Bickerton, and P. A. Kelly, “Measurements of normal stress distributions experienced by rigid liquid composite moulding tools,” *Composites Part A: Applied Science and Manufacturing*, vol. 40, no. 8, pp. 1119–1133, 2009.

[69] J. Walther, P. Simacek, and S. G. Advani, “The effect of fabric and fiber tow shear on dual scale flow and fiber bundle saturation during liquid molding of textile composites,” *International Journal of Material Forming*, vol. 5, no. 1, pp. 83–97, 2012.

[70] P. Simacek, S. G. Advani, and S. A. Iobst, “Modeling Flow in Compression Resin Transfer Molding for Manufacturing of Complex Lightweight High-Performance Automotive Parts,” *Journal of Composite Materials*, vol. 42, no. 23, pp. 2523–2545, 2008.

[71] T. S. Lundström and B. R. Gebart, “Influence from process parameters on void formation in resin transfer molding,” *Polymer Composites*, vol. 15, no. 1, pp. 25–33, 1994.

[72] T. S. Lundstrom, B. R. Gebart, and C. Y. Lundemo, “Void Formation in RTM,” *Journal of Reinforced Plastics and Composites*, vol. 12, no. 12, pp. 1339–1349, 1993.

[73] J. S. Hayward and B. Harris, “The effect of vacuum assistance in resin transfer moulding,” *Composites Manufacturing*, vol. 1, no. 3, pp. 161–166, 1990.

[74] K. Potter, *Resin transfer moulding*. Netherlands: Springer, 1997.

[75] C. D. Rudd, *Liquid moulding technologies: Resin transfer moulding, structural reaction injection moulding and related processing techniques,* 1st ed. Warrendale, USA: SAE International [et al.], 1997.

[76] L. Broadbent, R. Bland, S. Leonard-Williams, S. Sharma, J. Summerscales, *An advanced Resin Transfer Molding system for the production of advanced composite structures*. Edinburgh, Great Britain, 2009.

[77] T. M. Kruckenberg, R. Paton, *Resin transfer moulding for aerospace structures*. Dordrecht, Netherlands: Springer, 2013.

[78] R. Kötte, *Verfahrensanalyse des Resin-Transfer-Molding-Prozesses (RTM)*. Cologne, Germany: Verlag TÜV Rheinland, 1991.

[79] E. L. Paul and V. A. Atiemo-Obeng, S. M. Kresta, *Handbook of industrial mixing: Science and practice*. Hoboken, USA: Wiley-Interscience, 2004.

[80] S. Liu, A. N. Hrymak, and P. E. Wood, “Laminar mixing of shear thinning fluids in a SMX static mixer,” *Chemical Engineering Science*, vol. 61, no. 6, pp. 1753–1759, 2006.

[81] H. Z. Li, C. Fasol, and L. Choplin, “Pressure Drop of Newtonian and Non-Newtonian Fluids Across a Sulzer SMX Static Mixer,” *Chemical Engineering Research and Design*, vol. 75, no. 8, pp. 792–796, 1997.

[82] D. Rauline, J.-M. Le Blévec, J. Bousquet, and P. A. Tanguy, “A Comparative Assessment of the Performance of the Kenics and SMX Static Mixers,” *Chemical Engineering Research and Design*, vol. 78, no. 3, pp. 389–396, 2000.

[83] D. M. Hobbs and F. J. Muzzio, “Optimization of a static mixer using dynamical systems techniques,” *Chemical Engineering Science*, vol. 53, no. 18, pp. 3199–3213, 1998.

[84] P. Rosenberg, R. Chaudhari, P. Albrecht, M. Karcher, F. Henning, *Effect of Process Parameters on Cavity Pressure and Component Performance in High Pressure RTM Process Variants*. Detroit, USA: Proceedings of the SPE ACCE 2014, 2014.

[85] C. Fais, “Lightweight automotive design with HP-RTM,” *Reinforced Plastics*, vol. 55, no. 5, pp. 29–31, 2011.

[86] F. Contamine, F. Faid, A. M. Wilhelm, J. Berlan, and H. Delmas, “Chemical reactions under ultrasound: discrimination of chemical and physical effects,” *Chemical Engineering Science*, vol. 49, no. 24, pp. 5865–5873, 1994.

[87] A. Keck, E. Gilbert, and R. Köster, “Influence of particles on sonochemical reactions in aqueous solutions,” *Ultrasonics*, vol. 40, no. 1-8, pp. 661–665, 2002.

[88] A. Keller, K. Masania, A. C. Taylor, and C. Dransfeld, “Fast-curing epoxy polymers with silica nanoparticles: Properties and rheo-kinetic modelling,” *Journal of Materials Science*, vol. 51, no. 1, pp. 236–251, 2016.

[89] P. V. Danckwerts, “The definition and measurement of some characteristics of mixtures,” *Applied Scientific Research, Section A*, vol. 3, no. 4, pp. 279–296, Jul. 1952.

[90] P. Vadhar and T. Kyu, “Effects of mixing on morphology, rheology, and mechanical properties of blends of ultra-high molecular weight polyethylene with linear low-density polyethylene,” *Polymer Engineering and Science*, vol. 27, no. 3, pp. 202–210, 1987.

[91] G. T. Emmerson, D. M. Shenfield, P. Saxton, I. Farid, C.-M. Cheng, D. J. Duffy, “Method of changing rheology in filled resin systems using cavitation,” WO 2008/066995 A2 PCT/US2007/077734, Jun 5, 2008.

[92] A. I. Malkin and A. I. Isayev, *Rheology:: Concepts, methods and applications,* 2nd ed. Toronto, USA: ChemTec Publishing, 2012.

[93] T. A. Osswald and N. Rudolph, *Polymer Rheology: Fundamentals and Applications*. Munich, Germany: Hanser Gardner Publications, 2014.

[94] R. P. Chhabra and J. F. Richardson, *Non-Newtonian Flow and Applied Rheology: Engineering Applications,* 2nd ed.: Elsevier Science, 2011.

[95] T. Mezger, *The Rheology Handbook: For users of rotational and oscillatory rheimeters,* 3rd ed. Hannover, Germany: Vincentz Network, 2013.

[96] *Viscosität DIN 1342-2*, 2003.

[97] S. Ritzenthaler, E. Girard-Reydet, and J. P. Pascault, "Influence of epoxy hardener on miscibility of blends of poly(methyl methacrylate) and epoxy networks," *Polymer*, vol. 41, no. 16, pp. 6375–6386, 2000.

[98] M. R. Vanlandingham, R. F. Eduljee, and J. W. Gillespie Jr., "Relationships between stoichiometry, microstructure, and properties for amine-cured epoxies," *Journal of Applied Polymer Science*, vol. 71, no. 5, pp. 699–712, 1999.

[99] John M. Barton, Ed., *Epoxy Resins and Composites I; The Application of Differential Scanning Calorimetry (DSC) to the Study of Epoxy Resin Curing Reactions*. Berlin, Heidelberg, Germany: Springer, 1985.

[100] G. W. Ehrenstein, G. Riedel, and P. Trawiel, *Praxis der thermischen Analyse von Kunststoffen,* 2nd ed. Munich, Germany: Hanser, 2003.

[101] D. Dykeman, *Minimizing Untercertainty in Cure Modeling for Composites Manufacturing*. PhD Thesis. Vancouver, Canada: The University of British Columbia, 2008.

[102] *Kunststoffe - Dynamische Differenz-Thermoanalyse, DIN EN ISO 11357*, 2010.

[103] J. d'Almeida and S. N. Monteiro, "The effect of the resin/hardener ratio on the compressive behavior of an epoxy system," *Polymer Testing*, vol. 15, no. 4, pp. 329–339, 1996.

[104] J. d'Almeida and S. N. Monteiro, "The Role of the Resin Matrix/Hardener Ratio on the Mechanical Properties of Low Volume Fraction Epoxy Composites," *Advanced Performance Materials*, vol. 4, no. 3, pp. 285–295, 1997.

[105] M. Bakar, M. Kostrzewa, A. Białkowska, and Z. Pawelec, "Effect of mixing parameters on the mechanical and thermal properties of a nanoclay-modified epoxy resin," *High Performance Polymers*, vol. 26, no. 3, pp. 298–306, 2014.

[106] Najat j Saleh, A. a. a. Razak, M. A. Tooma, M. E. Aziz, "A Study Mechanical Properties of Epoxy Resin Cured at Constant Curing Time and Temperature with Different Hardeners," *Engineer & Technical Journal*, vol. 29, no. 9, 2011.

[107] *Kunststoffe - Bestimmung der Zugeigenschaften, DIN EN ISO 527-2*, 2012.

[108] *Fibre-reinforced plastic composites - Determination of the in-plane shear stress/strain response, including the in-plane shear modulus and strength, by the +/- 45° tension test, DIN EN ISO 14129*, 1998.

[109] F. Burdin, N. A. Tsochatzidis, P. Guiraud, A. M. Wilhelm, and H. Delmas, "Characterisation of the acoustic cavitation cloud by two laser techniques," *Ultrasonics Sonochemistry*, vol. 6, no. 1-2, pp. 43–51, 1999.

[110] N. A. Tsochatzidis, P. Guiraud, A. M. Wilhelm, and H. Delmas, "Determination of velocity, size and concentration of ultrasonic cavitation bubbles by the phase-Doppler technique," *Chemical Engineering Science*, vol. 56, no. 5, pp. 1831–1840, 2001.

[111] S. Luther, R. Mettin, P. Koch, and W. Lauterborn, "Observation of acoustic cavitation bubbles at 2250 frames per second," *Ultrasonics Sonochemistry*, vol. 8, no. 3, pp. 159–162, 2001.

[112] Z. Guo, A. Jones, N. Li, and S. Germana, "High-speed observation of the effects of ultrasound on liquid mixing and agglomerated crystal breakage processes," *Powder Technology*, vol. 171, no. 3, pp. 146–153, 2007.

[113] I. Tzanakis, G. Lebon, D. G. Eskin, and K. A. Pericleous, "Characterizing the cavitation development and acoustic spectrum in various liquids," *Ultrasonics Sonochemistry*, vol. 34, pp. 651–662, 2017.

[114] H. Monnier, A.-M. Wilhelm, H. Delmas, "Influence of ultrasound on mixing on the molecular scale for water and viscous liquids," *Ultrasonic Sonochemistry*, vol. 6, pp. 67–74, 1999.

[115] J.-C. Fontanier, F. Lortie, J.-F. Gérard and P. Gérard, *Thermoplastic based composites as processed by RTM*. Munich, Germany: Proceedings of the 17th European Conference on Composite Materials, 2016.

[116] J. D. Menczel and R. B. Prime, *Thermal analysis of polymers: Fundamentals and Applications*. Oxford, Great Britain: John Wiley & Sons, Inc, 2009.

[117] R. J. C. Carbas, E. A. S. Marques, A. M. Lopes, L. F .M. da Silva, *Effect of Cure Temperature on the Glass Transition Temperature of an Epoxy Adhesive*. Porto, Portugal: Proceedings of the 15th International Conference on Experimental Mechanics, 2012.

[118] Z. Hua, J. Yang, S. Coulibaly, B. Zhang, "Integration TRIZ with problem-solving tools: A literature review from 1995 to 2006," *International Journal of Business Innovation and Research*, vol. 1, no. 1, pp. 111–128, 2006.

[119] K. Barry, E. Domb, M. S. Slocum, *What Is TRIZ?* [Online] Available: https://triz-journal.com/triz-what-is-triz/. Accessed on: 20170417.

[120] G. S. Altshuller, *The Innovation Algorithm: TRIZ, Systematic Innovation and Technical Creativity*. Worcester, USA: Technical Information Center, 2005.

[121] G. S. Altshuller, *And Suddenly the Inventor Appeared: TRIZ, the Theory of Inventive Problem Solving*. Worcester, USA: Technical Innovation Center, 1994.

[122] G. S. Altshuller *et al., 40 principles: TRIZ keys to innovation*. Worcester, USA: Technical Innovation Center, 2005.

[123] D. Mann, "An Introduction to TRIZ: The Theory of Inventive Problem Solving," *Creativity & Inn Man*, vol. 10, no. 2, pp. 123–125, 2001.

[124] U. Lindemann, *TRIZ Basiskurs*. Munich, Germany: Graduate School MW, Technical University of Munich, 2011.

[125] K. Gadd, *TRIZ for Engineers: Enabling Inventive Problem Solving*. Chichester, Great Britain: John Wiley & Sons, 2011.

[126] Ansys Academic Research, *Help System: Theory Guide*. Release 14.5: Ansys, 2013.

[127] Authorless, *Titan Grade 2: Datasheet.* [Online] Available: http:/www.thyssenkrupp.ch/documents/Titan_Grade_2.pdf. Accessed on: Sep. 18 2017.

[128] Authorless, *Titan Grade 5: Datasheet.* [Online] Available: www.thyssenkrupp.ch/documents/Titan_Grade_5.pdf. Accessed on: Sep. 18 2017.

[129] A. Znidarcic, R. Mettin, and M. Dular, "Modeling cavitation in a rapidly changing pressure field - application to a small ultrasonic horn," (eng), *Ultrasonics Sonochemistry*, vol. 22, pp. 482–492, 2015.

[130] M. K. Schaefer, W. Raffelt, S. Zaremba, and K. Drechsler, "Ultrasonic mixing head for liquid composite molding: Process and material characteristics," *Polymer Composites*, 2017.

[131] G. E. P. Box, N. R. Draper, *Empirical model-building and response surfaces*. New York [etc.], USA: Wiley, 1987.

[132] R. Verseput, *Digging into DOE: Selecting the right central composite Design for response surface methodology applications.* [Online] Available: https://www.qualitydigest.com/june01/html/doe.html. Accessed on: May 02 2017.

[133] S. A. Weissman and N. G. Anderson, "Design of Experiments (DoE) and Process Optimization. A Review of Recent Publications," *Organic Process Research & Development*, vol. 19, no. 11, pp. 1605–1633, 2015.

[134] M. S. E. Kojima, “Characteristics of Fluidborne Noise Generated by Fluid Power Pump: 3rd Report, Discharge Pressure Pulsation of External Gear Pump,” *Bulletin of JSME*, vol. 27, no. 232, pp. 2188–2195, 1984.

[135] Y. Inaguma, “A practical approach for analysis of leakage flow characteristics in hydraulic pumps,” *Proceedings of the Institution of Mechanical Engineers, Part C: Journal of Mechanical Engineering Science*, vol. 227, no. 5, pp. 980–991, 2013.

[136] *Laborgeräte aus Glas - Messzylinder und Mischzylinder, DIN EN ISO 4788*, 2005.

[137] K. Gokul Chandra and D. D. Kale, “Pressure drop for laminar flow of viscoeleastic fluids in static mixers,” *Chemical Engineering Science*, vol. 47, no. 8, pp. 2097–2100, 1992.

[138] I. Tzanakis, G. Lebon, D. G. Eskin, and K. Pericleous, “Investigation of the factors influencing cavitation intensity during the ultrasonic treatment of molten aluminium,” *Materials & Design*, vol. 90, pp. 979–983, 2016.

[139] M. K. Schaefer, *Use of an Ultrasound-Reaction-Chamber for RTM*. Linköping, Sweden: Proceedings of the 27th Sicomp Conference, 2016.

[140] M. K. Schaefer, *Automation of an Ultrasound Mixing Head for Low Pressure Resin Transfer Molding*. Dresden, Germany: Proceedings of the PPS Europe Africa Conference 2017, 2017.

[141] Authorless, *Loctite Rekote 770NC: Data sheet.* [Online] Available: http://na.henkel-adhesives.com/product-search-1554.htm?nodeid=8797750984705. Accessed on: Sep. 18 2017.

[142] Authorless, *Non-crimp E-glass S32EX010-00600-01270-250000: Datasheet.* [Online] Available: www.kompozyty.milar.pl/media/…/S32EX010-00600.pdf. Accessed on: Sep. 18 2017.

[143] K. L. Loewenstein, *The manufacturing technology of continuous glass fibres,* 3rd ed. Amsterdam, Netherlands, New York, USA: Elsevier, 1993.

[144] Q. Govignon, S. Bickerton, and P. A. Kelly, “Simulation of the reinforcement compaction and resin flow during the complete resin infusion process,” *Composites Part A: Applied Science and Manufacturing*, vol. 41, no. 1, pp. 45–57, 2010.

[145] J. Kaminski and B. Alvelid, “Temperature reduction in the cutting zone in water-jet assisted turning,” *Journal of Materials Processing Technology*, vol. 106, no. 1-3, pp. 68–73, 2000.

[146] F. Chen and E. Siores, “The effect of cutting jet variation on striation formation in abrasive water jet cutting,” *International Journal of Machine Tools and Manufacture*, vol. 41, no. 10, pp. 1479–1486, 2001.

[147] J. M. Lawrence, J. Barr, R. Karmakar, and S. G. Advani, “Characterization of preform permeability in the presence of race tracking,” *Composites Part A: Applied Science and Manufacturing*, vol. 35, no. 12, pp. 1393–1405, 2004.

[148] R. Bjekovic and K. Piotrowicz, “Epoxy resin and release agents part I: Inflence of external and internal release agents on the adhesive properties of epoxy resin,” *Istrazivanja i projektovanja za privredu*, vol. 13, no. 1, pp. 45–50, 2015.

[149] G. W. Critchlow, R. E. Litchfield, I. Sutherland, D. B. Grandy, and S. Wilson, “A review and comparative study of release coatings for optimised abhesion in resin transfer moulding applications,” *International Journal of Adhesion and Adhesives*, vol. 26, no. 8, pp. 577–599, 2006.

[150] V. M. Karbhari, “Effect of internal mold release agent on the cure and Effect of internal mold release agent on the cure and property variation in resin transfer molding composites,” *Journal of Materials Science Letters*, vol. 17, no. 24, pp. 2061–2062, 1998.

[151] C. Serré, M. Vayer, and R. Erre, “Behavior of internal mold release agent during BMC Behavior of internal mold release agent during BMC thermosets composites cure and aging,” *Journal of Materials Science Letters*, vol. 20, no. 21, pp. 1989–1991, 2001.

[152] Authorless, *Multi Axial Multi Ply Fabric 90°/0° direction: Data sheet (on request)*.

[153] Authorless, *Multi Axial Multi Ply Fabric +45°/-45° direction: Data sheet (on request)*.

[154] Authorless, *Epikote Resin 05390: Data sheet (on request)*.

[155] L. J. Graham, L. A. Ahlberg, F. Cohen-Tenoudji, B. R. Tittmann, *Processing Resin Matrix Composites Using High Intensity Ultrasound*. Thousand Oaks, USA: Proceedings of the IEEE Ultrasonics Symposium, 1986.

[156] J. Wang and S. Qin, “Study on the thermal and mechanical properties of epoxy–nanoclay composites: The effect of ultrasonic stirring time,” *Materials Letters*, vol. 61, no. 19-20, pp. 4222–4224, 2007.

[157] Q. J. Wang, Y. W. Chung, Ed., *Encyclopedia of Tribology: Nanocomposites*. Boston, USA: Springer US, 2013.

[158] Y. Yang, Z. G. Zhang, E. A. Grulke, W. B. Anderson, and G. Wu, “Heat transfer properties of nanoparticle-in-fluid dispersions (nanofluids) in laminar flow,”

International Journal of Heat and Mass Transfer, vol. 48, no. 6, pp. 1107–1116, 2005.

[159] M. E. Kabir, M. Saha, and S. Jeelani, "Effect of ultrasound sonication in carbon nanofibers/polyurethane foam composite," *Materials Science and Engineering: A*, vol. 459, no. 1-2, pp. 111–116, 2007.

[160] Z. Haddad, C. Abid, H. F. Oztop, and A. Mataoui, "A review on how the researchers prepare their nanofluids," *International Journal of Thermal Sciences*, vol. 76, pp. 168–189, 2014.

[161] Authorless, *Epoxy resin system, EPIKOTE Resin MGS RIMR 135 EPIKURE Curing Agent MGS RIMH 1366: Datasheet (on request)*.

A Appendix

a Experimental Data

Tab. A-1 Amplitudes of the Hielscher sonotrode (HS) and Ultrasonic Mixing Head Sonotrode (UMHS) measured with a Laser Doppler Vibrometer

Sonotrode	Amplitude setting [%]								
	20	30	40	50	60	70	80	90	100
	Amplitude [µm]								
HS	4.99	7.83	10.16	13.25	15.85	18.78	21.54	23.82	26.98
UMHS	13.89	17.71	23.24	30.28	37.00	43.01	49.34	55.58	63.09

Tab. A-2 Power and Frequency at different amplitude settings

Sonotrode	Amplitude setting [%]		
	20	100	100
	Power [W]		Frequency [kHz]
HS	35.0	87.0	19.59
UMHS	34.0	98.0	20.14

Tab. A-3 Position of the material in the data log at the moment of the sample extraction

Mixing head	Unit	P_1	P_2	P_3	P_4	P_5	P_6
UMH	cm³	150.00	145.25	142.75	136.75	130.75	124.75
UMH	cm³	150.00	145.25	141.50	135.50	129.50	123.50
UMH	cm³	150.00	145.25	140.25	134.25	128.25	122.25
SMH	cm³	150.00	150.00	145.00	139.00	133.00	127.00

Tab. A-4 Randomized run order of the DoE approach for the UMH process, factor values, rounded to two decimal figures

Run order	Volume flow [cm³/min]	Amplitude [µm]	Chamber volume [cm³]	Resin temperature [°C]	Counter Pressure [10^5 Pa]
1	50.03	50.00	2.50	23.98	0.00
2	49.90	25.00	5.00	23.97	0.05
3	50.01	25.00	2.50	66.70	0.00
4	15.00	50.00	2.50	60.05	0.00
5	49.99	25.00	5.00	61.05	2.98
6	50.03	50.00	5.00	61.95	0.00
7	49.98	50.00	2.50	62.88	2.97
8	150.06	50.00	5.00	59.82	2.99
9	149.98	25.00	2.50	60.29	2.95
10	149.82	50.00	2.50	25.77	3.00
11	50.00	50.00	5.00	25.50	2.92
12	150.02	25.00	2.50	25.70	0.11
13	100.01	37.50	3.75	26.74	1.42
14	50.02	25.00	2.50	26.10	3.04
15	100.10	37.50	3.75	43.02	1.45
16	99.98	37.50	3.75	42.44	1.45
17	150.05	37.50	3.75	42.00	1.44
18	49.98	37.50	3.75	44.42	1.52
19	99.99	37.50	3.75	42.74	1.51
20	99.98	37.50	3.75	42.30	1.50
21	100.01	50.00	3.75	42.40	1.47
22	100.02	37.50	3.75	62.51	1.46
23	149.96	25.00	5.00	60.30	0.00
24	100.01	37.50	2.50	42.26	1.50
25	100.02	37.50	5.00	42.79	1.51
26	99.96	37.50	3.75	42.39	2.96
27	100.05	37.50	3.75	42.79	0.00
28	99.98	25.00	3.75	42.33	1.47
29	150.03	25.00	5.00	25.90	3.02
30	149.96	50.00	5.00	28.07	0.02

Tab. A-5 Randomized run order of the DoE approach for the SMH process, factor values, rounded to two decimal figures

Run order	Volume flow [cm³/min]	Resin temperature [°C]	Counter pressure [10^5 Pa]
1	50.01	24.40	2.98
2	150.06	25.27	0.00
3	149.97	25.33	2.97
4	150.00	60.59	0.00
5	49.99	63.16	3.03
6	99.97	41.52	0.00
7	100.03	40.96	3.05
8	99.95	41.06	1.51
9	100.05	41.17	1.52
10	149.99	40.85	1.49
11	50.00	41.98	1.51
12	99.92	40.86	1.53
13	99.96	41.45	1.49
14	100.03	60.44	1.38
15	149.96	57.85	2.99
16	49.98	62.14	0.00
17	100.01	26.48	1.51
18	50.01	26.30	0.00

Tab. A-6 Randomized run order of the DoE approach for the UMH process, response values, rounded to two decimal figures

Run order	Pw [W]	ΔT [°C]	Δp [10^5Pa]	$\eta_{initial}$ [Pa s]	t_{gel} [s]	$T_{g\ initial}$ [°C]	ΔH_{res} [J/g]	$T_{g\ final}$ [°C]
1	147.21	26.73	-0.46	0.43	2118.17	-7.64	262.50	95.22
2	81.15	15.46	-0.43	0.09	2310.44	-4.00	198.00	83.95
3	74.43	-3.70	0.00	0.39	2103.94	-7.58	263.40	95.90
4	139.98	1.77	0.00	0.37	2120.46	-9.72	268.20	95.45
5	140.28	12.78	0.20	0.10	2187.45	-5.48	217.20	88.16
6	142.57	7.66	0.00	0.20	2079.94	-5.81	249.10	95.89
7	254.68	38.86	0.33	0.29	1883.59	1.01	162.30	72.41
8	275.03	16.85	0.19	0.15	1960.07	-8.94	231.30	80.74
9	141.25	-0.10	0.12	0.14	1953.48	-4.00	198.00	83.95
10	299.44	22.50	-1.19	0.37	2015.56	-2.72	105.80	45.64
11	265.73	58.40	-0.16	0.07	2120.33	-6.57	220.20	83.90
12	83.02	-0.09	-1.43	0.43	2136.06	-6.56	147.10	51.80
13	166.24	13.39	-0.82	0.72	2009.31	-3.24	163.80	71.56
14	140.97	27.76	-0.20	0.63	2621.01	0.16	158.70	73.62
15	159.27	11.45	0.13	0.10	1928.94	-7.14	188,9	76.11
16	159.25	12.61	-0.03	0.25	1930.85	-5.63	211.50	83.13
17	159.00	8.01	-0.18	0.14	2309.52	-8.18	256.60	95.19
18	159.27	23.11	0.06	0.26	1951.64	-8.99	220.50	75.62
19	161.17	11.58	-0.02	0.35	1920.51	-1.63	200.20	83.46
20	160.70	10.74	-0.01	0.15	1984.80	-5.05	235.30	87.36
21	217.32	20.27	0.05	0.19	1920.87	-17.89	270.10	82.65
22	153.26	5.75	0.16	0.16	2135.37	4.35	174.00	85.28
23	80.40	-2.34	0.00	0.23	2150.03	-6.64	247.00	94.36
24	162.89	14.46	-0.19	0.26	1968.20	-7.73	255.90	93.51
25	164.38	13.45	-0.18	0.48	1937.51	-4.26	222.80	85.60
26	198.60	19.79	-0.14	0.09	2135.61	-7.17	198.80	72.18
27	109.17	6.51	-0.06	0.27	2138.28	-3.07	238.40	93.45
28	113.71	5.54	-0.13	0.12	2071.13	-7.57	229.00	95.46
29	149.83	1.25	-1.79	0.37	5483.83	-7.13	222.50	91.44
30	162.17	8.57	-1.16	0.29	4444.15	-25.24	229.00	71.23

Tab. A-7 Randomized run order of the DoE approach for the SMH process, response values

Run order	ΔT [°C]	Δp [10^5Pa]	$\eta_{initial}$ [Pa s]	t_{gel} [s]	$T_{g\ initial}$ [°C]	ΔH_{res} [J/g]	$T_{g\ final}$ [°C]
1	0.90	-0.56	0.50	2148.03	-20.28	255.60	79.71
2	-0.13	-1.61	0.37	2231.77	-20.72	285.40	90.30
3	-0.13	-1.36	0.11	2000.88	-19.68	306.20	96.30
4	-6.39	-0.06	0.10	2151.37	-25.17	324.50	96.34
5	-8.76	0.01	0.09	2218.85	-14.25	218.60	72.40
6	-2.62	-0.23	0.12	2124.72	-	-	-
7	-1.37	-0.17	0.17	2102.46	-29.16	360.00	96.40
8	-1.31	-0.18	0.36	2090.76	-17.29	229.20	86.01
9	-1.57	-0.09	0.18	2127.24	-15.04	193.30	62.16
10	-1.22	-0.31	0.08	2110.84	-14.50	287.00	92.85
11	-2.28	-0.07	0.10	2098.20	-12.86	206.60	72.04
12	-2.26	-0.18	0.23	2182.31	-8.88	225.90	91.46
13	-1.93	-0.15	0.36	2090.76	-13.94	275.10	95.99
14	-6.84	0.04	0.34	2205.16	-27.53	342.60	95,87
15	-3.80	-0.01	0.08	1952.08	-7.58	191.60	89.44
16	-9.04	0.09	0.65	2133.04	-7.56	273.70	95.32
17	0.22	-0.74	0.58	2045.89	-7.32	244.60	92.57
18	0.10	-0.33	0.50	2093.59	-7.51	225.60	95.98

Tab. A-8 RTM characteristics input values for the prediction of the power values based on the process characteristics (PC),

Injec-tion	$\dot{V}$ [cm³/min]	A [µm]	$V_{Chamber}$ [cm³]	T_{resin} [°C]	p_{mix} [10^5 Pa]	RTM, Pw [W]	PC, Pw [W]
1	49.94	25.00	3.75	48.29	1.45	110.79	112.38
2	49.78	37.50	3.75	46.71	0.91	135.00	136.06
3	50.31	50.00	3.75	51.27	1.06	190.20	187.07
4	50.02	62.50	3.75	46.40	1.03	243.02	245.31
5	100.20	37.50	3.75	43.94	1.68	160.51	166.24
6	100.01	50.00	3.75	40.80	2.08	255.42	241.07
7	99.93	50.00	3.75	42.28	2.11	243.40	241.72
8	100.08	50.00	3.75	42.60	2.31	259.83	248.99
9	99.98	62.50	3.75	42.40	2.27	320.36	322.21
10	150.10	37.50	3.75	39.45	3.19	210.48	213.89
11	150.04	37.50	3.75	39.16	4.02	235.15	231.52
12	150.29	50.00	3.75	38.88	3.04	284.31	285.89
13	149.66	62.50	3.75	38.80	3.64	391.20	398.01
14	50.02	25.00	3.75	46.93	0.30	79.70	85.65
15	50.06	37.50	3.75	45.95	0.28	129.52	114.06
16	49.93	50.00	3.75	48.92	0.25	138.09	151.16
17	50.04	62.50	3.75	46.93	0.28	201.23	203.52
18	100.25	37.50	3.75	42.03	0.34	117.17	120.54
19	99.97	50.00	3.75	44.53	0.29	161.46	160.83
20	100.07	50.00	3.75	41.69	0.34	156.02	164.28
21	99.91	50.00	3.75	41.16	0.33	157.41	164.38
22	99.81	50.00	3.75	41.83	0.33	154.55	163.77
23	100.17	62.50	3.75	42.27	0.32	200.83	217.34
24	150.16	37.50	3.75	36.49	0.40	126.13	126.44
25	149.76	50.00	3.75	39.70	0.35	178.92	170.56
26	150.22	62.50	3.75	39.80	0.36	240.24	228.90

b Data sheets

Tab. A-9 Commercial pure titan grade 2 (excerpt of [127])

Parameter	Value	Unit
Density	4510	g/cm³
Coefficient of the thermal extension	8.9	10^{-6}/°C
Reference temperature		
E-Modulus	1.05	10^{11}Pa
Poisson's ratio	0.36	-
Compression modulus	1.25	10^{11}Pa
Shear modulus	3.8603	10^{10}Pa

Tab. A-10 Commercial pure titan grade 5 (excerpt of [128])

Parameter	Value	Unit
Density	4450	g/cm³
Coefficient of the thermal extension	8.9	10^{-6}/°C
Reference temperature		
E-Modulus	1.14	10^{11}Pa
Poisson's ratio	0.36	-
Compression modulus	1.3571	10^{11}Pa
Shear modulus	4.1912	10^{10}Pa

Fig. A-1 Data sheet of RIMR 135 and RIMH 1366 by Hexion [161]

HEXION™ Specialty Chemicals

Technical Information
Epoxy and Phenolic Resins Division
Epoxy Resins

EPIKOTE™ Resin MGS® RIM 135

EPIKURE™ Curing Agent MGS® RIM H 134 - RIM H 137

Content

Characteristics

Approval	German Lloyd
Application	specially designed for infusion processes (RMT, SCRIMP/VARI) rotor blades for wind turbines, boat and shipbuilding, sports equipment
Operational temperature	-60 °C up to +50 °C (-76 °F up to 122 °F) without heat treatment -60 °C bis +80 °C (-76 °F up to 176 °F) after heat treatment
Processing	at temperatures between 10 °C and 50 °C (50-122 °F) due to the very low mixing viscosity especially suited for infusion, injection and pultrusion
Features	very low viscosity excellent initial curing properties at room temperature pot life from approx. 0,5 hour to approx. 4 hours short curing times at high temperatures
Storage	shelf life of 24 month in originally sealed containers

Am Ostkai 21/22
70327 Stuttgart
Germany
Phone: +49 (0) 711 - 3 89 80 00
Fax: +49 (0) 711 - 3 89 80 011
www.hexionchem.com

May 2008
April, 2009

HEXION™
Specialty Chemicals

Technical Information
Epoxy and Phenolic Resins Division
Epoxy Resins

2.1- 2

EPIKOTE™ Resin MGS® RIM 135

Application

Very low-viscosity laminating resin system with different pot lives for processing of glass, carbon and aramide fibers. Due to its good mechanical properties, this system is suitable for the production of components featuring high static and dynamic loadability.

The range of pot lives is between approx. 0,5 hour and approx. 3 - 4 hours. The parts can be worked and demolded after curing at room temperature. Curing at higher temperatures (up to approx. 80-100 °C, 176-212 °F) is possible, depending on layer thickness and geometry of the parts to be manufactured. The curing times can be reduced to a few minutes by this.

Adding internal parting agents, such as zinc stearate, etc., has proven useful for pultrusion processes. Profiles with good surface qualities are obtained. Depending on profile geometry, mould temperatures in the range of 180-230 °C (356-446 °F) are possible, thus permitting high drawing speeds.

The mixing viscosity is very low, which is especially advantageous for infusion and injection processes. It may be lowered to approx. 150 mPas by heating the resin mass (see diagram). This means that even complicated molded parts with long flow paths can be easily infused. The temperature rise with hardener RIMH 137 remains very low up to a mold temperature of approx. 30 °C, so that even parts of greater thickness can be produced at elevated temperatures.

The infusion resin system does not contain any unreactive components. The raw materials used feature a very low vapor pressure. This permits processing of the material under vacuum even at elevated temperatures (VARIM process). Compatibility problems are not to be expected in combination with UP gelcoats, various paints (e.g. PUR-based), etc. However, comprehensive tests are indispensable.

The relevant industrial safety regulations for the handling of epoxy resins and hardeners and our instructions for safe processing are to be observed.

The resin and hardeners can be stored for at least 12 months in their carefully sealed original containers. The resin and hardeners may crystallize at temperatures below +15 °C (59 °F). The crystallization is visible as a clouding or solidification of the contents of the container. Before processing, the crystallization must be removed by warming up. Slow warming up to approx. 50-60 °C (122-140 °F) in a water bath or oven and stirring or shaking will clarify the contents of the container without any loss of quality. Use only completely transparent products. Before warming up, open containers slightly to permit equalization of pressure. Caution during warm-up! Do not warm up over an open flame! While stirring up use safety equipment (gloves, eyeglasses, respirator).

Am Ostkai 21/22
70327 Stuttgart
Germany
Phone: +49 (0) 711 - 3 89 80 00
Fax: +49 (0) 711 - 3 89 80 011
www.hexionchem.com

April, 2009

HEXION™ Specialty Chemicals

Technical Information
Epoxy and Phenolic Resins Division
Epoxy Resins

2.1- 3

EPIKOTE™ Resin MGS® RIM 135

Specifications

		Infusion resin RIM 135
Density	[g/cm³]	1,13 - 1,17
Viscosity	[mPas]	700 - 1.100
Epoxy equivalent	[g/equivalent]	166 - 185
Epoxy value	[equivalent /100g]	0,54 - 0,60
Refractory index		1,548-1,552

Measuring conditions:
measured at 25 °C / 77 °F

		Hardener RIMH 134	Hardener RIMH 1366	Hardener RIMH 137
Density	[g/cm³]	0,93 - 1,00	0,92 - 0,96	0,93 - 0,98
Viscosity	[mPas]	10 - 80	4 - 25	10 - 50
Amine value	[mg KOH/g]	550 - 700	500 - 625	400 - 600
Refractoy index		1,4900 - 1,5000	1,4525 - 1,4750	1,460 - 1,463

Measuring conditions:
measured at 25 °C / 77 °F

May, 2006

Am Ostkai 21/22
70327 Stuttgart
Germany
Phone: +49 (0) 711 - 3 89 80 00
Fax: +49 (0) 711 - 3 89 80 011
www.hexionchem.com

April, 2009

HEXION™ Specialty Chemicals

Technical Information
Epoxy and Phenolic Resins Division
Epoxy Resins

2.1- 4

EPIKOTE™ Resin MGS® RIM 135

Processing details

	Infusion resin RIM 135	Hardeners RIMH 134-137
Average EP - Value	0,56	-
Average amine equivalent	-	52

Mixing ratios

	Infusion resin RIM 135 : Hardener RIMH 134 - RIMH 137
By weight	100 : 30 ± 2
By volume	100 : 36 ± 2

The specified mixing ratios must be observed as exactly as possible. Adding more or less hardener will not effect a faster or slower reaction - but in incomplete curing which cannot be corrected in any way.
Resin and hardener must be mixed very thoroughly. Mix until no clouding is visible in the mixing container. Pay special attention to the walls and the bottom of the mixing container.

Am Ostkai 21/22
70327 Stuttgart
Germany
Phone: +49 (0) 711 - 3 89 80 00
Fax: +49 (0) 711 - 3 89 80 011
www.hexionchem.com

April, 2009

HEXION™ Specialty Chemicals

Technical Information
Epoxy and Phenolic Resins Division
Epoxy Resins

2.1- 5

EPIKOTE™ Resin MGS® RIM 135

Temperature development

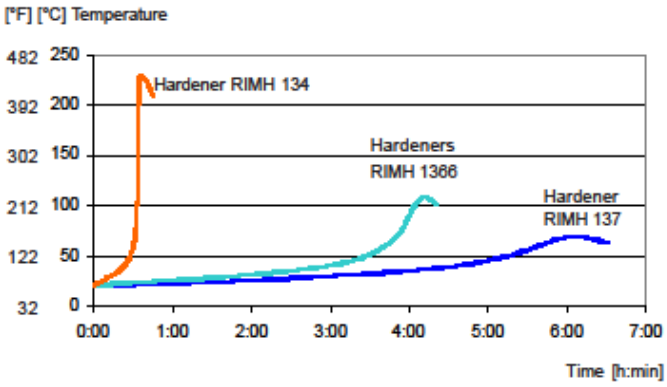

Quantity: 100 g / 20 °C (77 °F)

The optimum processing temperature is in the range between 20 °C and 25 °C (68-77 °F). Higher processing temperatures are possible, but will shorten pot life. A rise in temperature of 10 °C (50 °F) will halve the pot life. Water (for example very high humidity or contained in fillers) causes an acceleration of the resin/hardener reaction. Different temperatures and humidities during processing have no significant effect on the strength of the hardened product.

Do not mix large quantities - particularly of highly reactive systems - at elevated processing temperatures. The heat flow from the mixing container is very low, so the contents will heat up fast because of the dissipating reaction heat (exothermic resin-hardener reaction). This can result in temperatures of more than 200 °C (392 °F) in the mixing container, which may cause smoke-intensive burning of the resin mass.

Am Ostkai 21/22
70327 Stuttgart
Germany
Phone: +49 (0) 711 - 3 89 80 00
Fax: +49 (0) 711 - 3 89 80 011
www.hexionchem.com

April, 2009

HEXION™ Specialty Chemicals

Technical Information
Epoxy and Phenolic Resins Division
Epoxy Resins

2.1- 6

EPIKOTE™ Resin MGS® RIM 135

Viscosity of mixture at different temperatures

Viscosity

Infusion resin RIM 135 with Hardener RIMH 1366

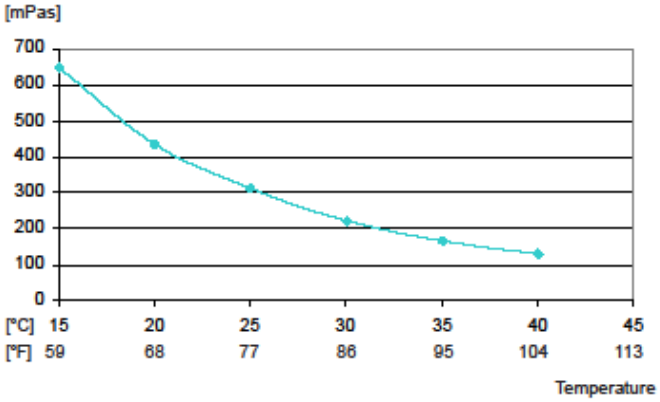

Viscosity development

Infusion resin RIM 135 with Hardener RIMH 1366 and Hardener RIMH 137

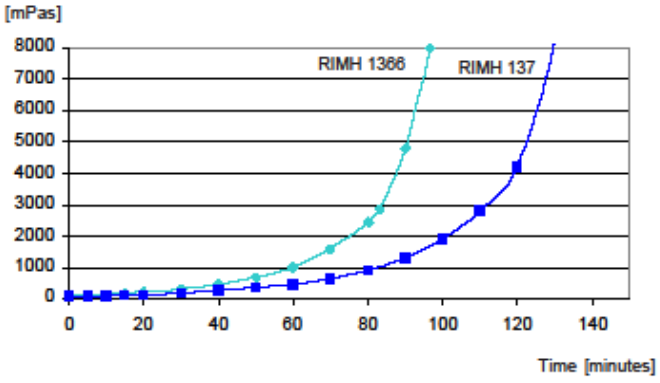

Measuring conditions:
Temperature: 40°C (104 °F); measuring gap 0,2 mm

Am Ostkai 21/22
70327 Stuttgart
Germany
Phone: +49 (0) 711 - 3 89 80 00
Fax: +49 (0) 711 - 3 89 80 011
www.hexionchem.com

April, 2009

HEXION™ Specialty Chemicals

Technical Information
Epoxy and Phenolic Resins Division
Epoxy Resins

2.1- 7

EPIKOTE™ Resin MGS® RIM 135

Development of glass transition temperature (T_g) at 60 °C

T_g Development

Infusion resin RIM 135 with Hardener RIMH 1366

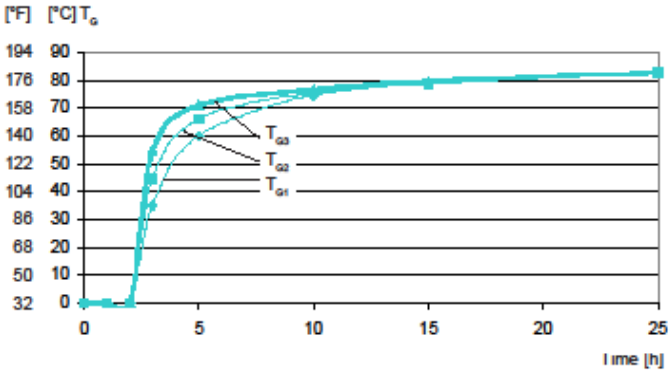

DMA Measuring after heat treatment

DMA

DMA-T_g (peak) tan delta
Infusion resin RIM 135 with Hardener RIMH 1366

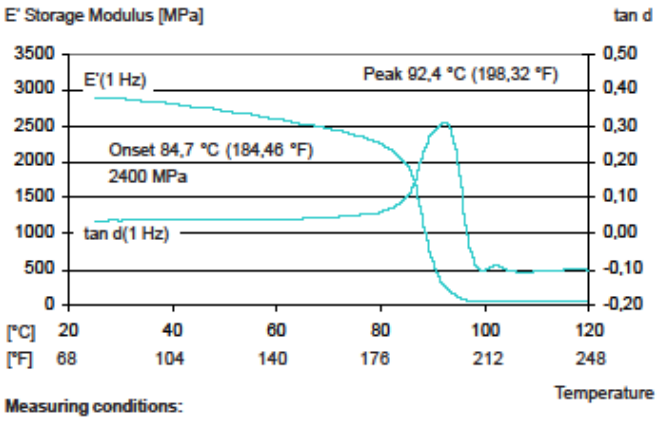

Measuring conditions:
Sample thickness: 2 mm
Heat rate: 2 K/min

Am Ostkai 21/22
70327 Stuttgart
Germany
Phone: +49 (0) 711 - 3 89 80 00
Fax: +49 (0) 711 - 3 89 80 011
www.hexionchem.com

May 2008
April, 2009

HEXION™ Specialty Chemicals

Technical Information
Epoxy and Phenolic Resins Division
Epoxy Resins

2.1- 8

EPIKOTE™ Resin MGS® RIM 135

Mechanical data

Mechanical data of neat resin		
Density	[g/cm³]	1,18 - 1,20
Flexural strength	[N/mm²]	90 - 120
Modulus of elasticity	[kN/mm²]	2,7 - 3,2
Tensile strength	[N/mm²]	60 - 75
Compressive strength	[N/mm²]	80 - 90
Elongation at break	[%]	8-16
Impact strength	[KJ/m²]	70-80
Water absorption at 23 °C	24 h [%] 7 d [%]	0,10 - 0,20 0,20 - 0,50
Fatigue strength under reversed bending stresses acc. to DLR Brunsw.	10 % 90 %	exp. > 1 x 10⁸ exp.> 2 x 10⁸
Curing: 24 h at 23 °C (74 °F) + 15 h at 60 °C (140 °F), partly cured/full cure		
Typical data according to **WL 5.3203 Parts 1 and 2** of the German Aviation Materials Manual.		

Advice:
Mechanical data are typical for the combination of laminating resin RIM 135 with hardener RIMH 137. Data can differ in other applications.

Am Ostkai 21/22
70327 Stuttgart
Germany
Phone: +49 (0) 711 - 3 89 80 00
Fax: +49 (0) 711 - 3 89 80 011
www.hexionchem.com

HEXION™ Specialty Chemicals

Technical Information
Epoxy and Phenolic Resins Division
Epoxy Resins

2.1- 8

EPIKOTE™ Resin MGS® RIM 135

Mechanical data

Mechanical data of neat resin		
Density	[g/cm³]	1,18 - 1,20
Flexural strength	[N/mm²]	90 - 120
Modulus of elasticity	[kN/mm²]	2,7 - 3,2
Tensile strength	[N/mm²]	60 - 75
Compressive strength	[N/mm²]	80 - 90
Elongation at break	[%]	8-16
Impact strength	[KJ/m²]	70-80
Water absorption at 23 °C	24 h [%] 7 d [%]	0,10 - 0,20 0,20 - 0,50
Fatigue strength under reversed bending stresses acc. to DLR Brunsw.	10 % 90 %	exp. > 1 x 10^6 exp.> 2 x 10^6
Curing: 24 h at 23 °C (74 °F) + 15 h at 60 °C (140 °F), partly cured/full cure		
Typical data according to **WL 5.3203 Parts 1 and 2** of the German Aviation Materials Manual.		

Advice:
Mechanical data are typical for the combination of laminating resin RIM 135 with hardener RIMH 137. Data can differ in other applications.

April, 2009

Am Ostkai 21/22
70327 Stuttgart
Germany
Phone: +49 (0) 711 - 3 89 80 00
Fax: +49 (0) 711 - 3 89 80 011
www.hexionchem.com

HEXION™
Specialty Chemicals

Technical Information
Epoxy and Phenolic Resins Division
Epoxy Resins

2.1- 9

EPIKOTE™ Resin MGS® RIM 135

Data of reinforced resin
Static tests in standard climate

Mechanical data

Reinforced with		GRC Glass fibre	CRC Carbon fibre	SRC Aramide fibre
Flexural strength	[N/mm²]	510 - 560	720 - 770	350 - 380
Tensile strength	[N/mm²]	460 - 500	510 - 550	400 - 480
Compressive strength	[N/mm²]	410 - 440	460 - 510	140 - 160
Interlaminar shear strength	[N/mm²]	42 - 46	47 - 55	29 - 34
Modulus of elasticity	[kN/mm²]	20 - 24	40 - 45	16 - 19

GRC samples:
16 layers of glass fabric, 8H satin, 296 g/m² (8.7 oz/sq.yd.), 4 mm (0.16 in) thick
CRC samples:
8 layers of carbon fabric, plain, 200 g/m² (5.9 oz/sq.yd.) 2 mm (0.08 in) thick
SRC samples:
15 layers of aramide fabric, 4H satin, 170 g/m² (5.0 oz/sq.yd.), 4 mm (0.16 in) thick

Fibre content of samples during processing/testing: 40 - 45 vol%
Data calculated for fibre content of 43 vol%

Typical data according to **WL 5.3203 Parts 1 and 2**
of the GERMAN AVIATION MATERIALS MANUAL

Sample preparation
Curing: 24 h at 23 °C (74 °F)
+ 15 h at 80 °C (176 °F)

Am Ostkai 21/22
70327 Stuttgart
Germany
Phone: +49 (0) 711 - 3 89 80 00
Fax: +49 (0) 711 - 3 89 80 011
www.hexionchem.com

Fig. A-2 Data sheet of XB 3538 and XB 3458 by Hunstman [162]

HUNTSMAN
Enriching lives through innovation

Advanced Materials

Resin XU 3508 / Resin XB 3585 / Araldite® LY 564 Hardener XB 3458

COLD TO WARM-CURING EPOXY SYSTEM BASED ON

APPLICATIONS	Industrial composites, composite repair		
PROPERTIES	High reactivity system for composite parts		
PROCESSING	• Wet lay-up • Resin Transfer Moulding		
KEY DATA	**Resin XU 3508**		
	Aspect (visual)	white liquid	
	Viscosity at 25 °C (ISO 12058-1)	11000 - 20000	[mPa.s]
	Density at 25 °C (ISO 1675)	1.15 - 1.2	[g/cm³]
	Flash point (ISO 2719)	200	[°C]
	Storage temperature (see expiry date on original container)	2 - 40	[°C]
	Resin XB 3585		
	Aspect (visual)	clear liquid	
	Viscosity at 25 °C (ISO 12058-1)	6500 - 9000	[mPa.s]
	Colour (Gardner, ISO 4630)	≤ 3	
	Density at 25 °C (ISO 1675)	1.15 - 1.20	[g/cm³]
	Flash point (ISO 2719)	> 200	[°C]
	Storage temperature (see expiry date on original container)	2 - 40	[°C]
	Araldite® LY 564		
	Aspect (visual)	clear liquid	
	Viscosity at 25 °C (ISO 12058-1)	1200 - 1400	[mPa.s]
	Colour (Gardner, ISO 4630)	1 - 2	
	Density at 25 °C (ISO 1675)	1.1 - 1.2	[g/cm³]
	Flash point (ISO 2719)	185	[°C]
	Storage temperature (see expiry date on original container)	2 - 40	[°C]
	Hardener XB 3458		
	Aspect (visual)	clear to slightly yellow / red liquid	
	Viscosity at 25 °C (ISO 12058-1)	190 - 250	[mPa.s]
	Density at 25 °C (ISO 1675)	0.98 - 1.02	[g/cm³]
	Flash point (ISO 2719)	> 102	[°C]
	Storage temperature (see expiry date on original container)	2 - 40	[°C]

HUNTSMAN
Enriching lives through innovation

STORAGE

Provided that Resin XU 3508 / Resin XB 3585 / Araldite® LY 564 and Hardener XB 3458 are stored in a dry place in their original, properly closed containers at the above mentioned storage temperatures they will have the shelf lives indicated on the labels.
Partly emptied containers should be closed immediately after use.
Epoxy Resin XU 3508 or XB 3585 which has crystallized and looks cloudy can be restored to its original state by heating to 60 - 80°C.

PROCESSING DATA

MIX RATIO

Components	*Parts by weight*	*Parts by volume*
Resin XU 3508	100	100
Hardener XB 3458	18	22
Resin XB 3585	100	100
Hardener XB 3458	19	23
Araldite® LY 564	100	100
Hardener XB 3458	20	24

We recommend that the components are weighed with an accurate balance to prevent mixing inaccuracies which can affect the properties of the matrix system. The components should be mixed thoroughly to ensure homogeneity. It is important that the side and the bottom of the vessel are incorporated into the mixing process.
When processing large quantities of mixture the pot life will decrease due to exothermic reaction. It is advisable to divide large mixes into several smaller containers.
For industrial parts production we recommend to use a mixing/dosing device

MIX VISCOSITY

		XU 3508 XB 3458	*XB 3585 XB 3458*	*LY 564 XB 3458*
at 40°C	[mPa.s]	700 - 850	450 - 550	220 - 320
at 60°C	[mPa.s]	320 - 400	100 - 160	50 - 110
at 70°C	[mPa.s]	250 - 290	40 - 70	30 - 60
at 80°C	[mPa.s]	150 - 190	30 - 60	20 - 50

POT LIFE (TECAM 100 G)

		XU 3508 XB 3458	*XB 3585 XB 3458*	*LY 564 XB 3458*
at 23°C	[min]	14 - 18	14 - 18	13 - 17

GEL TIME (HOT PLATE)

		XU 3508 XB 3458	*XB 3585 XB 3458*	*LY 564 XB 3458*
at 40°C	[min]	23 - 30	23 - 30	30 - 37
at 50°C	[min]	12 - 17	12 - 17	16 - 22
at 60°C	[min]	6 - 10	6 - 10	6 - 11
at 70°C	[min]	3 - 7	3 - 7	4 - 8
at 80°C	[min]	2 - 4	2 - 4	2 - 4
at 100°C	[min]	0.5 - 1.5	0.5 - 1.5	0.5 - 1.5

GELATION AT 28°C (IN THIN LAYERS: 0.4-0.7 MM)

		XU 3508 XB 3458	*XB 3585 XB 3458*	*LY 564 XB 3458*
Start	[min]	60 - 80	70 - 90	90 - 100
End	[min]	95 - 125	95 - 125	95 - 125

HUNTSMAN
Enriching lives through innovation

PROPERTIES OF THE CURED, NEAT FORMULATION					
GLASS TRANSITION TEMPERATURE (IEC 1006, DSC, 10 K/MIN)	*Cure:*	T_G	*XU 3508 XB 3458*	*XB 3585 XB 3458*	*LY 564 XB 3458*
	1d 23°C	[°C]	50 - 60	50 - 60	50 - 58
	3d 23°C	[°C]	55 - 65	55 - 65	55 - 63
	7d 23°C	[°C]	60 - 70	60 - 70	58 - 66
	3h 40°C	[°C]	60 - 70	60 - 70	60 - 69
	2h 50°C	[°C]	65 - 75	65 - 75	65 - 73
	1h 60°C	[°C]	73 - 83	75 - 85	70 - 78
	15min 80°C	[°C]	86 - 96	86 - 96	79 - 86
	1h 80°C	[°C]	88 - 98	88 - 98	88 - 96
	3min 100°C	[°C]	96 - 106	96 - 106	90 - 98
	10min 100°C	[°C]	98 - 108	98 - 108	90 - 98
	10min 80°C+20min 100°C	[°C]	100 - 110	100 - 110	92 - 102
	10min 80°C+20min 120°C	[°C]	100 - 110	100 - 110	95 - 105
	10min 80°C+20min 130°C	[°C]	112 - 122	115 - 125	96 - 106
FLEXURAL TEST (ISO 178)	*Cure:*		*XU 3508*	*XB 3585*	*LY 564*
	7d 23°C		*XB 3458*	*XB 3458*	*XB 3458*
	Flexural strength	[MPa]	100 - 110	145 - 155	130 - 145
	Elongation at flexural strength	[%]	3 - 5	4 - 6	3 - 5
	Ultimate strength	[MPa]	100 - 110	120 - 130	125 - 135
	Ultimate elongation	[%]	3 - 5	5 - 7	4 - 7
	Flexural modulus	[MPa]	3450 - 3650	3650 - 3850	3750 - 3950
FRACTURE PROPERTIES BEND NOTCH TEST (PM 258-0/90)	*Cure:*		*XU 3508*	*XB 3585*	*LY 564*
	7d 23°C		*XB 3458*	*XB 3458*	*XB 3458*
	Fracture toughness K_{1C}	[MPa$\sqrt{m}$]	1.30 - 1.60	0.70 - 1.00	0.75 - 1.05
	Fracture energy G_{1C}	[J/m^2]	480 - 580	130 - 150	160 - 200
WATER ABSORPTION	*Cure:*		*XU 3508*	*XB 3585*	*LY 564*
	7d 23°C		*XB 3458*	*XB 3458*	*XB 3458*
	After 24 hours at 23°C	[%]	0.10 - 0.15	0.12 - 0.16	0.18 - 0.22
	After 168 hours at 23°C	[%]	0.40 - 0.50	0.45 - 0.50	0.60 - 0.65
FLEXURAL TEST (ISO 178)	*Cure:*		*XU 3508*	*XB 3585*	*LY 564*
	10min 80°C + 20min 100°C		*XB 3458*	*XB 3458*	*XB 3458*
	Flexural strength	[MPa]	115 - 125	120 - 140	125 - 140
	Elongation at flexural strength	[%]	4 - 6	5 - 6	5 - 6
	Ultimate strength	[MPa]	110 - 120	85 - 100	85 - 100
	Ultimate elongation	[%]	4 - 7	5 - 7	6.5 - 9.0
	Flexural modulus	[MPa]	3050 - 3300	3200 - 3500	3150 - 3350
WATER ABSORPTION	*Cure:*		*XU 3508*	*XB 3585*	*LY 564*
	10min 80°C + 20min 100°C		*XB 3458*	*XB 3458*	*XB 3458*
	After 24 hours at 23°C	[%]	0.10 - 0.15	0.12 - 0.16	0.13 - 0.18
	After 168 hours at 23°C	[%]	0.34 - 0.40	0.35 - 0.40	0.37 - 0.42
FRACTURE PROPERTIES BEND NOTCH TEST (PM 258-0/90)	*Cure:*		*XU 3508*	*XB 3585*	*LY 564*
	10min 80°C + 20min 100°C		*XB 3458*	*XB 3458*	*XB 3458*
	Fracture toughness K_{1C}	[MPa$\sqrt{m}$]	1.20 - 1.35	1.05 - 1.20	1.20 - 1.50
	Fracture energy G_{1C}	[J/m^2]	380 - 500	280 - 325	420 - 520

HUNTSMAN
Enriching lives through innovation

FLEXURAL TEST (ISO 178)	*Cure: 10min 80°C + 120min 120°C*		*XU 3508 XB 3458*	*XB 3585 XB 3458*	*LY 564 XB 3458*
	Flexural strength	[MPa]	110 – 130	115 - 135	115 - 135
	Elongation at flexural strength	[%]	4 - 6	4 - 7	5 - 8
	Ultimate strength	[MPa]	105 - 125	110 - 130	110 - 130
	Ultimate elongation	[%]	4 - 7	5 - 7	6 - 9
	Flexural modulus	[MPa]	3000 - 3300	3100 - 3300	3150 - 3350
FRACTURE PROPERTIES BEND NOTCH TEST (PM 258-0/90)	*Cure: 10min 80°C + 120min 120°C*		*XU 3508 XB 3458*	*XB 3585 XB 3458*	*LY 564 XB 3458*
	Fracture toughness K_{1C}	[MPa√m]	1.10 - 1.25	0.90 - 1.20	1.20 - 1.50
	Fracture energy G_{1C}	[J/m²]	350 - 550	250 - 320	400 - 480
COMPRESSION TEST (ISO 604/85)	*Cure: 10min 80°C+120min 120°C*		*XU 3508 XB 3458*	*XB 3585 XB 3458*	*LY 564 XB 3458*
	Compresion strength	[MPa]	95 - 110	105 - 120	95 - 115
	Elongation at Compression strength	[%]	9 - 12	7 - 10	6 - 9
	Compression modulus	[MPa]	3000 - 3300	3200 - 3600	3200 - 3600
TENSILE TEST (ISO 527)	*Cure: 10min 80°C+120min120°C*		*XU 3508 XB 3458*	*XB 3585 XB 3458*	*LY 564 XB 3458*
	Tensile strength	[MPa]	60 - 80	60 - 80	70 - 90
	Ultimate elongation	[%]	3 - 6	3 - 6	4 - 7
	Tensile modulus	[MPa]	2900 - 3200	3100 - 3400	3000 - 3300

HUNTSMAN
Enriching lives through innovation

HANDLING PRECAUTIONS

Personal hygiene	
Safety precautions at workplace	
protective clothing	yes
gloves	essential
arm protectors	recommended when skin contact likely
goggles/safety glasses	yes
Skin protection	
before starting work	Apply barrier cream to exposed skin
after washing	Apply barrier or nourishing cream
Cleansing of contaminated skin	
	Dab off with absorbent paper, wash with warm water and alkali-free soap, then dry with disposable towels. Do not use solvents
Disposal of spillage	
	Soak up with sawdust or cotton waste and deposit in plastic-lined bin
Ventilation	
of workshop	Renew air 3 to 5 times an hour
of workplaces	Exhaust fans. Operatives should avoid inhaling vapours

FIRST AID

Contamination of the *eyes* by resin, hardener or mix should be treated immediately by flushing with clean, running water for 10 to 15 minutes. A doctor should then be consulted.

Material smeared or splashed on the *skin* should be dabbed off, and the contaminated area then washed and treated with a cleansing cream (see above). A doctor should be consulted in the event of severe irritation or burns. Contaminated clothing should be changed immediately.

Anyone taken ill after *inhaling* vapours should be moved out of doors immediately.

In all cases of doubt call for medical assistance.

HUNTSMAN

Enriching lives through innovation

of the user to evaluate the manufacturing circumstances and the final product under actual end-use requirements and to adequately advise and warn purchasers and users thereof.

Products may be toxic and require special precautions in handling. The user should obtain Safety Data Sheets from Huntsman Advanced Materials containing detailed information on toxicity, together with proper shipping, handling and storage procedures, and should comply with all applicable safety and environmental standards.

Hazards, toxicity and behaviour of the products may differ when used with other materials and are dependent on manufacturing circumstances or other processes. Such hazards, toxicity and behaviour should be determined by the user and made known to handlers, processors and end users.

Except where explicitly agreed otherwise, the sale of products referred to in this publication is subject to the general terms and conditions of sale of Huntsman Advanced Materials LLC or of its affiliated companies including without limitation, Huntsman Advanced Materials (Europe) BVBA, Huntsman Advanced Materials Americas Inc., and Huntsman Advanced Materials (Hong Kong) Ltd.
Huntsman Advanced Materials is an international business unit of Huntsman Corporation. Huntsman Advanced Materials trades through Huntsman affiliated companies in different countries including but not limited to Huntsman Advanced Materials LLC in the USA and Huntsman Advanced Materials (Europe) BVBA in Europe.

Araldite is a registered trademark of Huntsman Corporation or an affiliate thereof.

Main Office :
Huntsman Advanced Materials (Switzerland) GmbH
Kybeckstrasse 200
CH-4057 BASEL
Switzerland
+41 61 299 1111

Fig. A-3 Data sheet of TRAC 06170 and TRAC 06805 by Hexion [163]

HEXION™ **Technical Data Sheet**
Most recent revision date: 3/19/2015

EPIKOTE™ Resin TRAC 06170
(Formerly named TRAC-0031-R)
EPIKURE™ Curing Agent TRAC 06170
(Formerly named EK GCW-RD-639-KW)
HELOXY™ Additive TRAC 06805
(Formerly named HELOXY™ Additive 112)

Product Description

EPIKOTE™ Resin TRAC 06170 is a medium viscous epoxy resin.
EPIKURE™ Curing Agent TRAC 06170 is a low viscous very fast amine hardener.
HELOXY™ Additive TRAC 06805 is a silicone- and wax-free internal mold release agent.

Application Areas/Suggested Uses

Low viscous resin system designed for RTM and LCM applications with excellent wetting and adhesion characteristics on glass-, carbon- or aramid-fibers. Benefits of this system are a very low viscosity during infusion and a fast development of the Glass Transition temperature T_G to above the molding temperature, which allows an easy de-molding, combined with very short cycle times.

Typical suggested uses include but are not limited to mass production of structural automotive parts such as parts of the frame or chassis, floor pans, firewalls, monocoque structure.

Benefits

- Low viscosity during injection.
- Easy to process due to thermo latent behavior:
  - Infusion time easily adjustable by selecting a process temperature (100°C to 145°C)
  - Fast glass transition temperature (T_G) development
  - Short curing cycle (e.g. 4 min at 100°C, or ≈40 sec at 140°C)
- Excellent fiber wetting properties.
- Excellent thermal and mechanical performance.
- Excellent demolding characteristics.

Vaziner Straße 49
47135 Duisburg-Meiderich

Postfach 120552
47125 Duisburg

Germany

www.hexion.com

HEXION™ **Technical Data Sheet**
Most recent revision date: 3/19/2015

Sales Specification

EPIKOTE™ Resin TRAC 06170

Property	Unit	Value	Test Method / Standard
Viscosity at 25°C	mPa·s	9000 ± 1000	DIN 53015 = ISO 12058-1
Color	Gardner	2 max	ISO 4630-1
Color	Hazen	100 max.	ASTM D1209
Refractive index	-	1,572 ± 0,003	DIN 51423-2 = ISO 489

EPIKURE™ Curing Agent TRAC 06170

Property	Unit	Value	Test Method / Standard
Viscosity at 25°C	mPa·s	15 ± 10	DIN 53015 = ISO 12058-1
Refractive Index at 25°C	-	1,495 ± 0,003	DIN 51423-2 = ISO 489

HELOXY™ Additive TRAC 06805

Property	Unit	Value	Test Method
Viscosity at 30°C	mPa·s	750 ± 450	DIN 53015

Typical Properties

EPIKOTE™ Resin TRAC 06170

Property	Unit	Value	Test Method / Standard
Delivery form		Clear liquid	
Density at 20°C	kg/l	1.15 – 1.19	ISO 2811

EPIKURE™ Curing Agent TRAC 06170

Property	Unit	Value	Test Method / Standard
Delivery form		Clear to slightly yellow / brown liquid	
Density at 20°C	kg/l	0,97 ± 0,03	ISO 2811-3

HELOXY™ Additive TRAC 06805

Property	Unit	Value	Test Method
Delivery form		liquid	
Density at 20°C	kg/l	1.01 ± 1.05	DIN 51755
Appearance		yellow/brown	

Vaziner Straße 49
47135 Duisburg-Meiderich
Postfach 120552
47125 Duisburg
Germany
www.hexion.com

HEXION™ **Technical Data Sheet**
Most recent revision date: 3/19/2015

Processing Details

Mixing ratio

EPIKOTE™ Resin TRAC 06170	100	parts by weight
EPIKURE™ Curing Agent TRAC 06170	16	parts by weight
HELOXY™ Additive TRAC 06805	1-2	parts by weight

Mixing tolerance

The maximum allowable mixing tolerance (resin & hardener) is ± 0.5 pbw, but it is particularly important to preserve the recommended mixing ratio as accurately as possible. Incorrect dosing of the hardener is not an appropriate approach to accelerate or retard the reaction; rather it will lead to an incomplete cure. The reaction speed can be properly adjusted by changing the processing temperature, as indicated below. Resin and hardener must be mixed very thoroughly. Mix until no clouding is visible, pay special attention to the walls and the bottom of the mixing container.

Material preheating

To optimize the process a preheating of the components is recommended.

EPIKOTE™ Resin TRAC 06170	60-80	°C
EPIKURE™ Curing Agent TRAC 06170	RT-30	°C
HELOXY™ Additive TRAC 06805	25-30	°C

Vaclmer Straße 49
47135 Duisburg-Meiderich
Postfach 120552
47125 Duisburg
Germany
www.hexion.com

HEXION™ **Technical Data Sheet**
Most recent revision date: 3/19/2015

Processing Temperature and Pot Life
The EPIKOTE™ Resin TRAC 06170 / EPIKURE™ Curing Agent TRAC 06170 system has an infusion time which is easily adjustable by adjusting the process temperature over a relatively wide target range. The system exhibits good processing in the temperature range between 80 and 145 °C, and full curing can typically be achieved in 2 minutes cure at 120°C. Higher processing temperatures are possible but will shorten the pot life. A rise in temperature of 10 °C reduces the pot life by approx. 50%. Different temperatures during processing have no significant effect on the mechanical properties of the hardened product.
Do not mix large quantities at elevated processing temperatures as this can lead to an uncontrolled exothermic reaction where the mixture may heat up very quickly to more than 200 °C in the mixing container.

Processing Data		Unit	Value
Viscosity of the formulation	at 80°C at 100°C at 110°C at 120°C	mPas mPas mPas mPas	41 ± 10 19 ± 10 15 ± 5 11 ± 5
Viscosity development of the formulation after 30s/60s/90s	at 80°C at 100°C at 110°C at 120°C	mPas mPas mPas mPas	49/67/97 37/120/678 95/486/61150 114/65500/>100000
B-time of the formulation (Hot plate)	at 100°C at 110°C at 120°C	s s s	120 ± 30 72 ± 20 45 ± 10
Pot life of the formulation	at 25°C	mm:ss	42:00 ± 05:00 (260°C peak max)

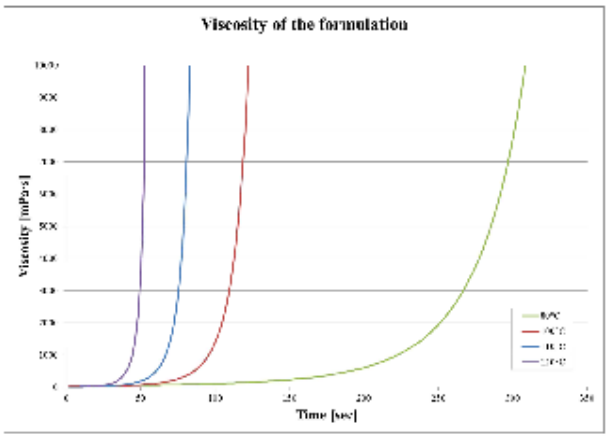

Vaxinor Straße 49
47135 Duisburg-Meiderich

Postfach 120552
47125 Duisburg

Germany

www.hexion.com

HEXION **Technical Data Sheet**
Most recent revision date: 3/19/2015

Typical Properties of the cured, non-reinforced system
Cure cycle: 2min @ 120°C

Property	Unit	Value	Test Method
TG, DSC first run Onset Midpoint	 °C °C	 122 ± 3 124 ± 3	DSC (10K/min) DIN 53445
DMA Onset Peak max	 °C °C	 133 ± 3 140 ± 5	DMA (2K/min) DIN EN 61006
Tensile test @ room temperature Tensile strength Tensile modulus Elongation at break	 MPa MPa %	 74 ± 10 2570 ± 50 7,3 ± 1	DIN EN ISO 527-1
Bending test @ room temperature Flexural strength Flexural modulus	 MPa N/mm²	 100 ± 13 2500 ± 200	DIN EN ISO 178
Fracture toughness at RT (K1C)	MPa.m1/2	0,87 ± 0,03	ISO 17281
Density	g/cm³	1,177 ± 0,003	DIN 53479 A

Safety, Storage & Handling

Please refer to the MSDS for the most current Safety and Handling information.

EPIKOTE™ Resin TRAC 06170 should be stored at room temperature in its carefully sealed original containers. Under these conditions the shelf life is a minimum of three years from date of certification.

EPIKURE™ Curing Agent TRAC 06170 should be stored at room temperature in its carefully sealed original containers, so that moisture is excluded. Under these conditions the shelf life is a minimum of two years from date of certification. Care should be taken to avoid storage environments resulting in moisture contamination. Exposure to moisture will cause an increase in viscosity and reactivity, the degree of increase depending on the amount of moisture, which has been absorbed.

HELOXY™ Additive TRAC 06805 should be stored at room temperature in its carefully sealed original containers, so that moisture is excluded. Under these conditions the shelf life is a minimum of 6 months. HELOXY™ Additive TRAC 06805 should not be stored at temperatures above 30°C. Before use it is necessary to homogenize the material by shaking or stirring.

Occasionally, it is possible that the resin or the hardener crystallize at temperatures below 15°C. The crystallization is visible as a clouding or solidification of the content of the container. Before processing, the crystallization must be removed by warming up. Slow warming up to 50 - 60°C in a water bath or oven and stirring or shaking will clarify the contents in the container without any loss of quality. Use only completely clear products. Before warming up, open containers slightly to permit equalization of pressure. Caution during warm up! Do not warm up over open flame! While stirring up use safety equipment (gloves, eyeglasses, respirator equipment).

Vacziner Straße 49
47135 Duisburg-Meiderich
Postfach 120552
47125 Duisburg
Germany
www.hexion.com

HEXION™ **Technical Data Sheet**
Most recent revision date: 3/19/2015

Contact Information

For further Technical Inquiries on the properties and performance of this matrix system in reinforced composites, please contact us
at our Customer Service Center +1 888 443 9466 / Hexion4information@Hexion.com

Vaxjöner Straße 49
47135 Duisburg-Meiderich

Postfach 120552
47125 Duisburg

Germany

www.hexion.com

B Publications

Journal

[J1] M. K. Schaefer, W. Raffelt, S. Zaremba, and K. Drechsler, “Ultrasonic mixing head for liquid composite molding: Process and material characteristics,” *Polymer Composites*, 2017.

Conferences

[C1] M. K. Schaefer, "Automation of an Ultrasound Mixing Head for Low Pressure Resin Transfer Molding," Proceedings of the PPS Europe Africa Conference 2017, Dresden, Germany, 2017.

[C2] M. K. Schaefer, "Use of an Ultrasound-Reaction-Chamber for RTM," Proceedings of the 27th Sicomp Conference, Linköping, Sweden, 2016

[C3] M. K. Schaefer, S. Zaremba, K. Drechsler, “Comparative Study on Internal and External Release Agents – Evaluation of Process Parameter Variation on Demolding Stresses”, Proceedings of the 20th International Conference on Composite Materials, Copenhagen, Denmark, 2015

C Supervised student work

During my employment at the Institute for Carbon Composites I supervised the following student theses:

[S1] M. Vollmer, Preforming and RTM Injection Studies of a Carbon Composite Tapered Omega-Stiffened Structure: Influence of Preforming-Binder on Part Quality, Diploma Thesis in cooperation with GE, Institute for Carbon Composites, TUM, 2014.

[S2] M. Gößl, Analyse der Verarbeitbarkeit von Trennmitteln im Resin Transfer Molding Prozess, Bachelor's Thesis, Institute for Carbon Composites, TUM, 2014.

[S3] M. Griner, Auslegung eines Durchfluss-Reaktors zur Verarbeitung von Epoxidharzen mit Leistungsultraschall, Bachelor's Thesis, Institute for Carbon Composites, TUM, 2014.

[S4] J. Hornung, Analyse des Materialverhaltens von Epoxidharzen auf den Kavitationseffekt erzeugt durch Ultraschallschwingungen, Bachelor's Thesis, Institute for Carbon Composites, TUM, 2014.

[S5] T. Zimmermann, Einfluss des durch Ultraschall hervorgerufenen Kavitationseffektes auf die Material- und Prozesskennwerte von Mehrkomponentenharzen Bachelor's Thesis, Institute for Carbon Composites, TUM, 2015.

[S6] M. Borgmann, Studie zur Prozessierung und Charakterisierung von Mehrkomponenten-Harzsystemen mit internem Trennmittel, Master's Thesis, Institute for Carbon Composites, TUM, 2015.

[S7] C. Aigner, Simulation der Kavitation durch Ultraschallanregung eines Harzsystems in ANSYS, Semesterarbeit, Institute for Carbon Composites, TUM, 2015.

[S8] A. Dietrich, Konzeptentwicklung zur Automatisierung einer RTM-Injektionsanlage, Master's Thesis, Institute for Carbon Composites, TUM, 2016.

[S9] S. Ehrenreich, Studie zur technischen Verarbeitung von internen Trennmitteln in Resin-Transfer-Molding Prozessen, Semesterarbeit, Institute for Carbon Composites, TUM, 2016.

[S10] M. Ruf, Charakterisierung der Wechselwirkung zwischen werkzeugseitigem Verteilersystem und Faserhalbzeug in Bezug auf die Formevakuierung im RTM Prozess, non public Semesterarbeit in cooperation with BMW, Institute for Carbon Composites, TUM, 2016 locked till 2021.

[S11] Auswirkungen von Leistungsultraschall auf ein Epoxid-Harzsystem für die Anwendung in der Pultrusion, Master's Thesis in cooperation with Fraunhofer IGCV, Institute for Carbon Composites, TUM, 2017.

[S12] S. Wittmann, Konzeptentwicklung, Umsetzung und Inbetriebnahme eines Stand-alone RTM Werkzeug mit Ultraschallmischkop, Bachelor's Thesis, Institute for Carbon Composites, TUM, 2017.

[S13] C. Rauch, Literaturrecherche zum Einfluss der Ultra-schallkavitation auf Harzsysteme: Identifikation von Prozesskennwerten, Bachelor's Thesis, Institute for Carbon Composites, TUM, 2017.

[S14] M. Freudenstein, Konzeptentwicklung, Konstruktion und Evaluierung eines Moduls zur niederfrequenten Schwingungsanregung von Harzsystemen, Bachelor's Thesis, Institute for Carbon Composites, TUM, 2017.

[S15] A. Daxer, Entwicklung eines stabilen Infiltrationsprozesses für eine Rotorkomponente eines Helikopters, non public Bachelor's Thesis in cooperation with Airbus Helicopters, Institute for Carbon Composites, TUM, 2017 locked till 2022.

Parts of the following student theses influenced the thesis at hand: [S2], [S3], [S4], [S5], [S6], [S7], [S8], [S9], [S11], [S12], [S13] and [S14].